

THE UNIVERSITY
of EDINBURGH

This thesis has been submitted in fulfilment of the requirements for a postgraduate degree (e.g. PhD, MPhil, DClinPsychol) at the University of Edinburgh. Please note the following terms and conditions of use:

This work is protected by copyright and other intellectual property rights, which are retained by the thesis author, unless otherwise stated.
A copy can be downloaded for personal non-commercial research or study, without prior permission or charge.
This thesis cannot be reproduced or quoted extensively from without first obtaining permission in writing from the author.
The content must not be changed in any way or sold commercially in any format or medium without the formal permission of the author.
When referring to this work, full bibliographic details including the author, title, awarding institution and date of the thesis must be given.

The Role of MicroRNA-214 in Renal Ischaemia Reperfusion Injury and Fibrosis

Victoria Carmen Banwell

Presented for Doctorate of Philosophy (PhD)

College of Medicine and Veterinary Medicine, University of Edinburgh

Year of Presentation: 2020

Abstract

Organ transplantation is the gold standard treatment of end stage renal failure and has been shown to be superior to dialysis in terms of quality of life and life expectancy. Ischaemia is an inevitable consequence of renal transplantation and in particular, prolonged ischaemia is an independent risk factor for poor short- and long-term graft function and is associated with a higher rate of graft attrition. Chronic allograft damage is characterised by interstitial fibrosis and tubular atrophy and is the leading cause of late graft failure. At present this accounts for 5% of all kidney grafts lost annually and there are no treatments available. MicroRNAs (miRs) are short non-coding single strands of RNA that can inhibit gene expression by post-transcriptional repression or degradation of target mRNAs. MiR synthesis is tightly regulated under physiological conditions but can rapidly become dysregulated in injury. MiRs have been shown to play an important role in native renal disease and in particular miR-214 is associated with renal injury and fibrosis but its role in early injury and transition towards fibrosis remained unclear.

The aim of this project was to investigate the role of miR-214 in early ischaemia reperfusion injury (IRI) and transition towards fibrosis using a murine model of IRI. There are various models of IRI that can be adopted: in this thesis a unilateral model of IRI was adopted in order for the animal to survive beyond the early phase of renal failure. 18 minutes of unilateral renal ischaemia induced significant fibrosis within the kidney after 14 days and peaked at 21 days.

Following characterisation of the model, miR-214 expression from whole kidney tissue was examined at 2, 7, 14, 21 and 28 days to test the hypothesis that miR-214 was associated with early injury and fibrosis following IRI. 18 minutes of IRI resulted in

significant acute kidney injury and upregulation of pro-inflammatory markers. Kidneys demonstrated rapid progression towards fibrosis as assessed by histology and confirmed by upregulation of pro-fibrotic gene expression. Importantly, miR-214 was increased during the early phase of injury and remained elevated at later time points, peaking at 5.5 fold increase in expression at 21 days ($p<0.0001$). Furthermore, miR-214 was upregulated 3.6 fold in $CD3^+$ T-cell populations at 7 days ($p<0.01$) and 15 fold in F4/80hi macrophages at 21 days ($p<0.001$).

Having shown that miR-214 was significantly upregulated at both early injury and later fibrosis, the effect of miR-214 ablation was examined by comparing outcomes of IRI in miR-$214^{-/-}$ and miR-$214^{+/+}$ mice at 2 and 21 days to test the hypothesis that miR-214 blockade was protective against injury. MiR-214 deletion did not result in significant improvement in early injury markers at 2 days however there was a significant reduction in pro-inflammatory gene expression. At 21 days, there was evidence of improved tubular recovery and a 79% reduction in fibrosis on histology along with significant reduction of pro-fibrotic and pro-inflammatory gene expression in miR-$214^{-/-}$ mice. Flow cytometry showed no difference in $CD3^+$ T-cell populations but a significant reduction in $CD4^+$ T-cells from whole kidney tissue in miR-$214^{-/-}$ mice at 21 days potentially suggesting a role of miR-214 in T-cell populations in the kidney.

Lay Summary

The blood supply to a kidney transplant is interrupted when removing it from the donor and implanting it in the recipient and this can be damaging to the kidney, with a risk of scarring. A number of kidney transplants fail due to scarring over the months and years after transplant; the diagnosis is often made late and there are no treatments available. Small RNA molecules are involved in the process of kidney transplant scarring and in particular microRNA-214 (miR-214) has been shown to be involved in kidney scarring in native kidneys. In this project, miR-214 was shown to be associated with early kidney injury following IRI and in the transition towards fibrosis. Removing miR-214 resulted in significant benefit to kidneys after injury suggesting this is a potential novel target to improve kidney transplant health following transplantation.

Declaration

I declare that:

a) this thesis has been composed entirely by myself and that either that the work is my own, or, as a member of a research group, I have made a substantial contribution to the work, such contribution being clearly indicated;

b) that the work has not been submitted for any other degree or professional qualification except as specified, and

c) that any included publications are my own work, except where indicated throughout the thesis and summarised and clearly identified on the declarations page of the thesis.

Signed

Acknowledgements

There are many people who made this possible and without whom I would have given up long ago. First and foremost, I need to thank my husband Dan, without whose unwavering support this would not have been possible. He received the brunt of the highs and lows associated with an inpatient clinician jumping into the deep end of academia.

To my brilliant supervisors, Professor Lorna Marson and Dr Laura Denby. Lorna is my role model and mentor and has always believed in me, even when I didn't believe in myself. Laura, who took me on as a rookie and transformed me into a scientist-a feat that I didn't think was possible at the start of this journey.

Next to all those in the lab who supported me; there are far too many to mention individually but special thanks go to the Denby group past and present, particularly Sarah Finnie, Katie Connor, James O'Sullivan, Ollie Teenan and Andrew Boyd. The wider Baker group were always there to give support, advice and sink the odd tequila at Christmas. Another thank-you must go to the brilliant Carolynn Cairns, the world's best technician and lab encyclopaedia who held my hand through those long FACS days. Thanks also goes to Jeremy Hughes and his group for their support and guidance.

Finally, to my parents whose work ethic taught me perseverance and self-motivation; they are the ones who have invested the most in me throughout the years, thank you too.

Table of Contents

Abstract ..... **ii**

Lay Summary ..... **iv**

Declaration ..... **v**

Acknowledgements ..... **vi**

Table of Contents ..... **vii**

Figures and Tables ..... **xiii**

Abbreviations ..... **xvii**

Chapter 1 : Introduction **1**

1.1 Solid Organ Transplantation 2

1.2 Transplant Immunology 7

1.2.1 The Major Histocompatibility Complex and the Human Leucocyte Antigen System 7

1.3 Clinical Consequences of Ischaemia Reperfusion Injury 9

1.3.1 Delayed Graft Function 9

1.3.2 IRI and acute rejection 11

1.3.3 IRI and chronic allograft damage 12

1.4 Principles of Graft Injury 14

1.4.1 Ischaemia reperfusion injury 14

1.4.2 Adaptive immunity 26

1.4.3 IRI induced fibrosis 29

1.5 Non-coding RNAs 35

1.5.1 Housekeeping ncRNA 36

1.5.2 Regulatory ncRNAs 36

1.5.3 MicroRNA 37

1.5.4 MiRs and Transplantation 40

1.5.5 MicroRNA-214 43

1.6 Models of Renal Ischaemia Reperfusion Injury 53

1.6.1 Bilateral ischaemia reperfusion injury 55

1.6.2 Unilateral ischaemia model without nephrectomy 57

1.6.3 Unilateral ischaemia model with nephrectomy 59

1.6.4 Cold vs warm ischaemia 61

1.7 Aims and Hypotheses 63

Chapter 2: Materials and Methods 64

2.1 General Reagents 65

2.1.1 Dulbecco's Modified Eagle's Medium (DMEM) 65

2.1.2 Complete Roswell Park Memorial Institute Medium (RPMI) 65

2.1.3 Fluorescence Activated Cell Sorting (FACS) buffer 65

2.2 Animals 66

2.3 Surgery 66

2.3.1 Anaesthesia 66

2.3.2 Transplant Model 67

2.3.3 Murine model of ischaemia reperfusion injury 67

2.3.4 Post-operative checks 68

2.4 Kidney Tissue Processing 68

2.5 In situ hybridisation 71

2.6 Histology 71

2.7 Flow cytometric analysis and fluorescence activated cell sorting (FACS) 72

2.7.1 Sample preparation 72

2.7.2 Cell surface staining 73

2.7.3 Transcription factor staining 74

2.7.4 Fluorescence Activated Cell Sorting (FACS) 77

2.8 LEGENDplex™ Assay 78

2.8.1 Preparation of serum samples 78

2.8.2 Assay procedure 79

2.9 In Vitro Models 80

2.10 Immunocytochemistry 80

2.11 Immunofluorescence 81

2.12 RNA Extraction 81

2.12.1 RNA extraction following FACS 82

2.13 Quantitative real-time PCR 82

2.13.1 MiR Expression 83

2.13.2 Gene expression 85

2.14 Human studies/samples 88

2.15 Statistical Analysis 88

Chapter 3: The murine model of chronic allograft damage.....89

3.1 Introduction 90

3.2 Development of the model 91

3.2.1 Donor Nephrectomy Surgery 93

3.2.2 Transplant Recipient Operation 94

3.2.3 Post-operative Care 95

3.3 Discussion 100

Chapter 4 : Characterisation of the murine model of renal ischaemia reperfusion injury 103

4.1 Introduction 104

4.2 Animal model of early renal ischaemia reperfusion injury 105

4.2.1 Surgical technique involved in the murine renal IRI model 106

4.2.2 Bilateral renal ischaemia results in significant renal injury 108

4.2.3 Ischaemia reperfusion injury is associated with increased pro-inflammatory gene expression 112

4.2.4 18 minutes of bilateral ischaemia reperfusion injury is associated with an increase in miR-214 114

4.3 Ischaemia reperfusion as a model of renal fibrosis 116

4.3.1 IRI results in significant kidney fibrosis at 28 days following injury and is dependent on ischaemic time 116

4.3.2 Ischaemia reperfusion results in significant renal injury and increased pro-inflammatory gene expression at 28 days 123

4.3.3 MiR-214 expression is greatest at 28 days following 18 minutes of renal ischaemia reperfusion injury 128

4.4 Discussion 130

Chapter 5 : The role of miR-214 in ischaemia reperfusion injury ... 135

5.1 Introduction 136

5.2 Characterising kidney injury as a result of 18 minutes of IRI over 28 days 137

5.2.1 Significant changes in the IRI kidney weight occur in keeping with early inflammatory infiltration and later development of fibrosis 137

5.2.2 Unilateral ischaemia reperfusion injury results in significant and progressive renal injury and fibrosis. 140

5.2.3 18 minutes of unilateral IRI results in elevation of pro-inflammatory gene expression at all time points 149

5.2.4 $CD3^+$ cells are present at 2 days following injury 153

5.2.5 Unilateral ischaemia reperfusion injury results in upregulation of profibrotic gene expression as early as 2 days 155

5.3 Time course of changes in miR-214 expression following 18 minutes of unilateral renal ischaemia reperfusion injury 157

5.3.1 MiR-214 is upregulated at all time points following 18 minutes of unilateral renal ischaemia reperfusion injury 157

5.3.2 MiR expression in the contralateral kidney 161

5.3.3 MiR-214 is present in injured tubules and the interstitium in the early phase of injury 162

5.3.4 MiR-214 is expressed by multiple cell types following IRI 164

5.3.5 MiR expression in splenocytes of mice undergoing unilateral IRI 169

5.4 MiR-214 and mechanism of injury 170

5.4.1 MiR-214 expression in polarized M1 and M2 macrophages 170

5.4.2 MiR-214 expression in an *in vitro* model of murine tubular epithelial cell injury 171

5.4.3 MiR-214 expression in an *in vitro* model of rat renal fibroblasts 176

5.5 The effect of miR-214 deletion on early injury and fibrosis 180

5.5.1 Phenotypic differences when comparing miR-214$^{-/-}$ and miR-214$^{+/+}$ mice .. 180

5.5.2 The effect of miR-214$^{-/-}$ on outcome at 2 days following IRI 184

5.5.3 The effect of miR-214$^{-/-}$ on outcomes at 21 days following IRI 193

5.5.4 Mechanism of miR-214$^{-/-}$ protection in the kidney following IRI 204

5.6 Discussion 213

Chapter 6: Final discussion 219

6.1 Discussion 220

6.2 Strengths and limitations of the study 223

6.3 Future directions 226

References 229

Appendices 257

Appendix 1: Funding received 257

Appendix 2: Presentations and Prizes 258

Appendix 3: Surgical instruments and consumables 259

Figures and Tables

Figures

Chapter 1

Figure 1.1 Annual UK Kidney transplant activity 4

Figure 1.2 Total kidney transplants per year grouped by donor 5

Figure 1.3 Immune response to IRI 14

Figure 1.4 IRI induced renal fibrosis 31

Figure 1.5 MiR biogenesis 39

Figure 1.6 Schematic representation of hsa-miR-214 44

Figure 1.7 Actions of miR-214 in T cells 49

Chapter 2

Figure 2.1: Diagram of segments taken during kidney dissection 70

Chapter 3

Figure 3.1 Captured images of murine renal transplantation 92

Figure 3.2 Murine transplant post-operative monitoring sheet 96

Figure 3.3 Anastomotic times 97

Figure 3.4 Diagram of modifications to the arterial anastomotic technique 99

Chapter 4

Figure 4.1 Murine model of renal ischaemia reperfusion injury 107

Figure 4.2 Assessment of functional injury following IRI 109

Figure 4.3 Structural injury following bilateral IRI 111

Figure 4.4 Gene expression following IRI 113

Figure 4.5 MiR expression of whole kidneys following IRI 114

Figure 4.6 Comparison of kidney weights in unilateral IRI at 28 days 118

Figure 4.7 Pro-fibrotic gene expression in unilateral IRI at 28 days 121

Figure 4.8 Quantification of fibrosis at 28 days 122

Figure 4.9 KIM-1 gene expression in unilateral IRI at 28 days 124

Figure 4.10 Haematoxylin and eosin stains of unilateral IRI at 28 days 125

Figure 4.11 Inflammatory gene expression panel 127

Figure 4.12 MiR expression of kidneys 129

Chapter 5

Figure 5.1 Comparison of kidney weights from timecourse 138

Figure 5.2 Comparison of weights of experimental (right) kidney vs contralateral (left) kidney during timcourse 139

Figure 5.3 Structural injury at 2 days following 18 minutes of IRI compared to sham 141

Figure 5.4 Structural injury at 7 days following 18 minutes of IRI compared to sham 143

Figure 5.5 Structural injury at 14 and 21 days following 18 minutes unilateral IRI 144

Figure 5.6 Fibrosis following 18 minutes unilateral IRI 146

Figure 5.7 Quantification of fibrosis following 18 minutes unilateral renal IRI 147

Figure 5.8 KIM-1 gene expression following 18 minutes unilateral renal IRI 148

Figure 5.9 Cytokine gene expression following 18 minutes unilateral renal IRI 150

Figure 5.10 CD3e and CD68 gene expression 152

Figure 5.11 Representative immunohistochemistry staining for CD3e at 2 days 154

Figure 5.12 Pro-fibrotic gene expression following 18 minutes unilateral renal IRI 156

Figure 5.13 MiR-214 expression following 18 minutes unilateral renal IRI 158

Figure 5.14 MiR-21 expression 159

Figure 5.15 MiR-29c expression 160

Figure 5.16 In situ hybridisation of miR-214 expression 163

Figure 5.17 MiR-214 expression from whole kidney tissue for FACS 165

Figure 5.18 Gene expression validating the IRI model 166

Figure 5.19 MiR-214 expression from FACS sorted cells 168

Figure 5.20 MiR-214 expression from spleens 169

Figure 5.21 MiR-214 expression in polarized ex vivo human monocytes 171

Figure 5.22 NRK-52E stimulated with TGF-β 173

Figure 5.23 Validation of NRK-52E model of renal injury 174

Figure 5.24 MiR expression in an NRK-52E model of renal injury 175

Figure 5.25 NRK-49F stimulated with TGF-β 177

Figure 5.26 Validation of NRK-49F model of renal injury 178

Figure 5.27 MiR expression in an NRK-49F model of renal injury 179

Figure 5.28 MiR-214 expression at 2 and 21 days 181

Figure 5.29 Pre-operative and post-operative mean body weight 182

Figure 5.30 Pre-operative and post-operative mean percentage change in body weight 183

Figure 5.31 Comparison of kidney weights from miR-214$^{-/-}$ and miR-214$^{+/+}$ at 2 days 184

Figure 5.32 Structural injury at 2 days in miR-214$^{+/+}$ and miR-214$^{-/-}$ mice 186

Figure 5.33 KIM-1 expression at 2 days in miR-214$^{+/+}$ or miR-214$^{-/-}$ mice 187

Figure 5.34 Pro-inflammatory expression at 2 days in miR-214$^{+/+}$ or miR-214$^{-/-}$ mice 189

Figure 5.35 CD3 and CD68 expression at 2 days in miR-214$^{+/+}$ or miR-214$^{-/-}$ mice 191

Figure 5.36 Serum cytokine expression at 2 days in miR-214$^{+/+}$ or miR-214$^{-/-}$ mice 192

Figure 5.37 KIM-1 expression at 21 days in miR-214$^{+/+}$ or miR-214$^{-/-}$ mice 193

Figure 5.38 Structural injury at 2 days in miR-214$^{+/+}$ and miR-214$^{-/-}$ mice 194

Figure 5.39 Inflammatory cytokine gene expression at 21 days in miR-214$^{+/+}$ or miR-214$^{-/-}$ mice 196

Figure 5.40 Serum cytokine expression at 2 days in miR-214$^{+/+}$ or miR-214$^{-/-}$ mice 197

Figure 5.41 Comparison of kidney weights from miR-214$^{-/-}$ and miR-214$^{+/+}$ mice 198

Figure 5.42 Comparison of weights of experimental (right) kidney vs contralateral (left) kidney 199

Figure 5.43 Fibrosis in miR-214$^{+/+}$ and miR-214$^{-/-}$ mice at 21 days 201

Figure 5.44 Pro-fibrotic gene expression in miR-214$^{+/+}$ and miR-214$^{-/-}$ mice at 21 days 202

Figure 5.45 PTEN gene expression in miR-214$^{+/+}$ and miR-214$^{-/-}$ mice at 21 daysg 203

Figure 5.46 T cell populations from kidneys of male miR-214$^{+/+}$ and miR-214$^{-/-}$ mice at 2 days 205

Figure 5.47 T cell populations from kidneys of male miR-214$^{+/+}$ and miR-214$^{-/-}$ mice at 21 days 206

Figure 5.48 T cell populations from spleens of male miR-214$^{+/+}$ and miR-214$^{-/-}$ mice at 2 days 208

Figure 5.49 T cell populations from spleens of male miR-214$^{+/+}$ and miR-214$^{-/-}$ at mice 21 days 209

Figure 5.50 CD4^{+} T cell populations from spleens of miR-214$^{+/+}$ and miR-214$^{-/-}$ mice at 2 days 211

Figure 5.51 CD4^{+} T cell populations from spleens of miR-214$^{+/+}$ and miR-214$^{-/-}$ mice a 21 days 212

Tables

Table 2-1 Antibodies used for extracellular T-cell panel in flow cytometry 75

Table 2-2 Antibodies used for T-cell intracellular transcription factor panel 76

Table 2-3 Antibodies used for FACS staining kidney cells following IRI 78

Table 2-4 Taqman probes used for examination of miR expression 84

Table 2-5 Taqman probes used for examining gene expression 86

Appendices

Table A1-1 Funding received for PhD 257

Table A3-1 Surgical Instruments used in mouse models 259

Table A3-2 Sutures used in mouse models 260

Table A3-3: Consumables used in mouse models 260

Abbreviations

ADP	Adenosine diphosphate
ADPKD	Autosomal dominant polycystic kidney disease
AGE	Advanced glycation end products
AKI	Acute kidney injury
α-SMA	Alpha-smooth muscle actin
ALK	Activins receptor like kinase
APC	Antigen presenting cell
AR	Acute rejection
ATF3	Activating transcription factor 3
ATN	Acute tubular necrosis
ATP	Adenosine triphosphate
$A_{2A}R$	Adenosine 2A receptor
BAX	Bcl-2-associatied X
Bcl-2	B-cell lymphoma 2
BSA	Bovine serum albumin
CAD	Chronic allograft damage

CD	Cluster of differentiation
cDNA	Complementary DNA
CIT	Cold ischaemia time
CKD	Chronic kidney disease
CTLA4	Cytotoxic T lymphocyte-associated protein 4
DAMPS	Danger associated molecular patterns
DAPI	4',6-diamidino-2-phenylindole
DBD	Donation after brainstem death
DC	Dendritic cell
DCD	Donation after circulatory death
DGF	Delayed graft function
DMS	N, N-dimethylsphingosine
DNA	Deoxyribonucleic acid
DNM3OS	DNM3 opposite strand
ECM	Extracellular matrix
eGFR	Estimated glomerular filtration rate
ELISA	Enzyme linked immunosorbent assay
EMT	Epithelial-mesenchymal transition

eNOS	Endothelial nitric oxide synthase
ER	Oestrogen receptor
ERK	Extracellular-signal-regulated kinase
ESRD	End-stage renal disease
ESRF	End-stage renal failure
FACS	Fluorescence-activated cell sorting
FCS	Foetal calf serum
GFP	Green fluorescent protein
GFR	Glomerular filtration rate
GSK-3β	Glycogen synthase kinase 3 beta
HA	Heme arginate
H&E	Haematoxylin and eosin
Her2	Herceptin 2 receptor
HIF-1	Hypoxia-inducible factor-1
HLA	Human leucocyte antigen
HMGB-1	High-mobility group B-1
HO-1	Heme oxygenase-1
HSP	Heat-shock protein

ICC	Immunocytochemistry
IFN	Interferon
IFTA	Interstitial fibrosis and tubular atrophy
IgAN	IgA nephropathy
IL	Interleukin
iNOS	Inducible nitric oxide synthase
IP	Intraperitoneal
IRI	Ischaemia reperfusion injury
ISH	In situ hybridisation
IV	Intravenous
JNK	c-Jun N-terminal kinase
KIM-1	Kidney injury marker-1
KO	Knockout
LD	Living donor
LTL	Lotus tetragonolobus lectin
MAPK	Mitogen-activated protein kinase
MHC	Major histocompatibility complex
MiR	MicroRNA

MiR-RT	MicroRNA reverse transcription
MMP	Matrix metalloproteinase
MRE	Magnetic resonance elastography
MRI	Magnetic resonance imaging
mRNA	Messenger ribonucleic acid
NF-κβ	Nuclear factor-κβ
NLR	Nod-like receptor
NMP	Normothermic machine perfusion
NO	Nitric oxide
NRP	Normothermic regional perfusion
OSOM	Outer stripe of the outer medulla
PAH	Pulmonary arterial hypertension
PAMPS	Pathogen associated molecular pattern
PBMC	Peripheral blood mononuclear cell
PBS	Phosphate buffered saline
PCR	Picrosirius red staining
PDGF-β	Platelet derived growth factor beta
PDGFR-β	Platelet derived growth factor receptor beta

PFA	Paraformaldehyde
PI3K	Phosphoinositide-3-kinase–protein kinase
PPARδ	Peroxisome proliferator-activated receptor δ
PR	Progesterone receptor
PRR	Pattern recognition receptor
PTEC	Proximal tubular epithelial cell
PTEN	Phosphatase and tensin homolog
qRT-PCR	Real-time quantitative polymerase chain reaction
RAGE	Receptor for advanced glycation products
RISC	RNA-induced silencing complex
ROS	Reactive oxygen species
RPM	Revolutions per minute
RVH	Right ventricular hypertrophy
SC	Subcutaneous
SRF	Serum response factor
TCR	T cell receptor
TCMR	T cell mediated rejection
TEC	Tubular epithelial cell

TGF-β	Transforming growth factor-beta
TIM-1	T cell immunoglobulin and mucin domain-containing protein-1
TIMP	Tissue inhibitor of metalloproteinase
TLR	Toll-like receptor
TNF	Tumour necrosis factor
Treg	Regulatory T cells
UTR	Untranslated region
UUO	Unilateral ureteric obstruction
VEGF	Vascular endothelial growth factor
WT	Wildtype

Chapter 1: Introduction

There is increasing pressure to develop novel therapies following kidney transplantation as the transplant community pushes the boundaries of what is considered to be an acceptable organ for transplantation in order to meet the increasing demands for kidneys. Pharmacological advancement has failed to keep up with changes in practice and, as a consequence, long term graft survival has plateaued. The resulting clinical predicament needs to be addressed urgently so that longevity of graft function is improved upon. This introduction will give an overview of kidney transplant practices, the role of ischaemia reperfusion injury in early and late allograft injury, followed by an overview of microRNAs and their pharmacological potential in relation to renal transplantation.

1.1 Solid Organ Transplantation

Kidney transplantation is seen as the gold standard treatment for suitable candidates with end-stage renal failure and has been shown to be superior to dialysis in significantly improving mortality, quality of life, and productivity[1]. In general outcomes have greatly improved over the last 30 years; analysis of graft survival in transplants performed in the USA between 1988 and 1996 showed a dramatic increase in the half-life of both living and cadaveric donor kidneys (12.7 to 21.6 year and 7.9 to 13.8 years respectively)[2]. However, 4% of grafts are still lost annually despite improvements in patient selection, graft monitoring and immunosuppression therapy[3]. Whilst short-term graft and patient survival remain excellent following renal transplantation, long-term graft outcomes are limited by chronic allograft damage (CAD)[4] which is the leading cause of late graft failure[5]. CAD results from continuing exposure of the graft to immunogenic and non-immunogenic insults leading to a final common pathway of fibrosis. Currently, there are no specific pharmacological

interventions for patients diagnosed with CAD; therapeutic options include modulation of immunosuppression and treatment of concurrent infections and other comorbidities. The lifespan of a kidney graft is approximately 10-15 years, depending on the type of donor graft, with the best results in patients receiving organs from living donors and poorest from donation after circulatory death (DCD), with donation after brainstem death (DBD) lying in between.

The transplant community faces a considerable clinical challenge in meeting the growing demand for organ transplantation. Historically, kidney transplantation was dependent on organs from young healthy DBD donors who typically died from catastrophic intra-cranial trauma. However, as demand for organ transplantation increased with a simultaneous decrease in traumatic death, there is a disproportionate number of patients waiting for a kidney transplant. In the financial year 2018-2019, there were approximately 5000 patients waiting for a kidney transplant, and just over 4100 transplants were performed that year (**Figure 1.1**).

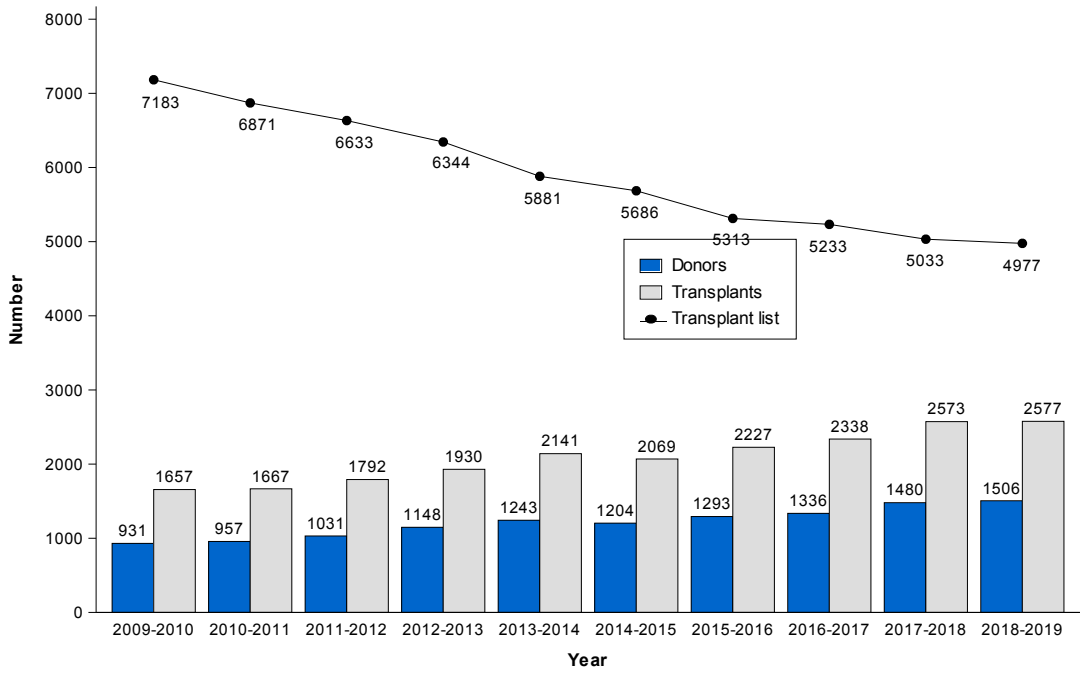

Figure 1.1 Annual UK Kidney transplant activity representing patients on the waiting list, number of transplants performed and number of donors. Source Kidney Activity 2018/2019, NHS Blood and Transplant.

In order to address this disparity between demand and supply, there has been a drive to utilise alternative strategies to increase the donor pool. The biggest shift in practice has been an increasing reliance on organs from donor after circulatory death (DCD) together with organs from older donors, with potential concurrent co-morbidities; the so called 'marginal' donor, later renamed as 'expanded criteria donor' (**Figure 1.2**). Results from longitudinal studies demonstrate poorer long-term graft and patient survival from marginal donors[6–8] when compared to standard criteria donors but, despite this, outcome remains superior to continuing dialysis[9].

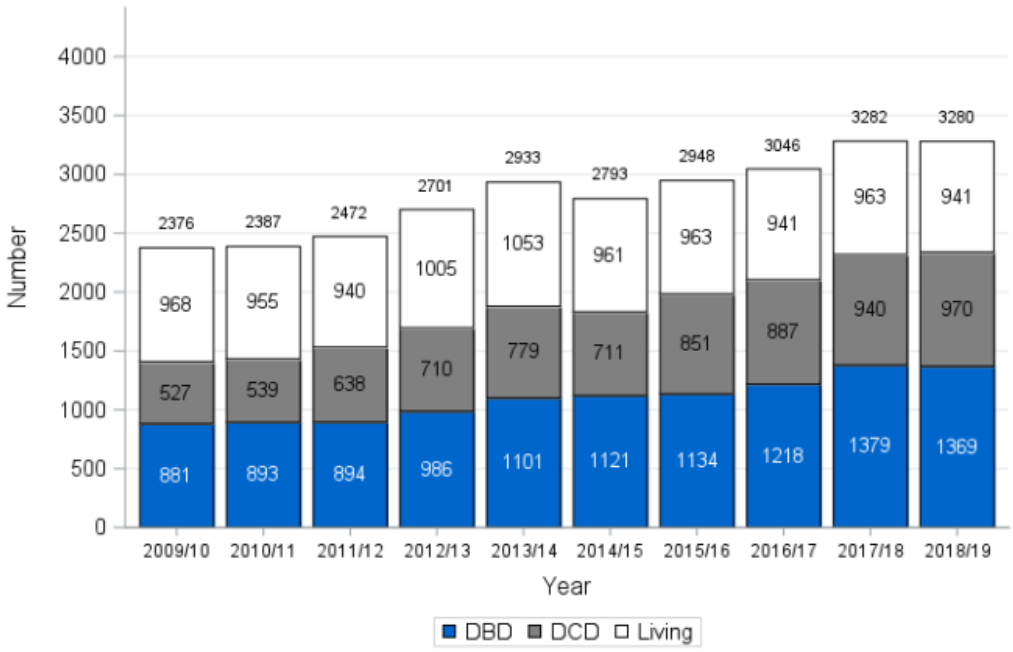

Figure 1.2 Total kidney transplants per year grouped by donor. Source: Annual Report of Kidney Transplantation 2018/2019, NHS Bloods and Transplant. DBD-donation after brainstem death; DCD-donation after circulatory death; living-living donor.

There are several factors that influence the outcome of organs from DCD donors; a major factor is length of warm ischaemia time which is more prolonged during DCD retrieval, particularly if there is a period of sustained hypotension and organ hypoperfusion. Recently, the focus has been on improving organs from these donors by using *ex-vivo* perfusion. This aims to partially reverse the damage inflicted on the organ by sustained ischaemia, potentially allowing transplantation of previously un-usable organs[10,11], and further examination of the results of this technique have shown an improvement of kidney injury markers following prolonged perfusion in human kidneys[12]. Multiple studies in porcine models have also demonstrated functional improvement with reduced creatinine in pigs undergoing transplantation with DCD grafts that had undergone prolonged normothermic perfusion[13]. In addition, *ex vivo*

perfusion has other benefits; firstly, it can potentially be performed whilst the organ is in transit and secondly it provides a platform for perfusion of pharmacological agents to the graft before implantation. At present a large multicentre trial comparing machine perfusion with standard cold storage is taking place in the UK[14]. An alternative perfusion method involves reperfusion *in situ* during multi-organ retrieval by means of normothermic regional perfusion (NRP); although the primary intent of this was to reduce ischaemic cholangiopathy following liver transplantation, recent evidence has shown an additional kidney-related benefit where rates of DGF went from 35% to 14.8% in transplanted grafts[15].

Other strategies include pharmacological pre-conditioning in the recipient. The HOT study used heme-arginate (HA) to induce the protective enzyme heme oxygenase-1 (HO-1) or placebo (saline) in patients receiving deceased donor grafts[16]. Results showed there was significant up-regulation of HO-1 in renal tissue and macrophages. A large multi-centre trial (HOT2) is currently recruiting in the UK which aims to determine whether there is a significant reduction in rates of delayed graft function (DGF) in patients receiving HA compared with placebo.

Along with advancements in deceased donor organ optimisation, there has been a concurrent increase in living donation kidney transplantation within the UK. Grafts from living donors have superior long-term function and patient survival and can be more readily performed pre-emptively, i.e. before the recipient commences dialysis. The planned approach also allows the recipient to undergo pre-operative systemic treatment which is required for ABO incompatible grafts or for patients who are highly sensitised. There has been a recent trend towards increasing this service, particularly as more altruistic donors come forward, allowing complex multi-step paired donation across the UK, through the National Living Kidney Sharing Scheme, which is

particularly beneficial in patients who are highly sensitised to donor specific antibodies.

1.2 Transplant Immunology

The first long-term functioning kidney transplant was performed between identical twins in Boston in 1954 by Joseph Murray who was later awarded the Nobel prize for medicine[17]. Sir Michael Woodruff performed the first kidney transplant in the UK at the Edinburgh Royal Infirmary between twins which continued to work until the death of the patient 6 years later of an unrelated condition. Early success of transplants between non-identical patients was hampered by high graft attrition until the immunological basis of transplant rejection was understood and immunosuppression introduced to clinical practice in the early 1960s. One of the major developments in transplantation involved understanding the immunological response to non-self proteins and thus graft rejection, first described by Peter Medawar in an experimental rabbit model in the 1940s[17].

1.2.1 The Major Histocompatibility Complex and the Human Leucocyte Antigen System

All nucleated cells express proteins that enable the body to recognise 'self' and 'non-self' called the major histocompatibility complex (MHC). Their function is to present small fragments of either endogenous or exogenous protein to T-lymphocytes; on presentation of non-self antigen, an immune response is initiated. In humans, the MHC codes the human leucocyte antigen (HLA) system of surface molecules, which act as both a stimulus and target of the immunological response. HLA antigens are

divided into class I and class II molecules, with the distribution being dependent on their function. The vast majority of nucleated cells constitutively express class I molecules on their cell surface and are able to present peptides derived from cytoplasmic material, including viral pathogens, to circulating immune cells. Class II molecules are expressed by cells that are able to process endosomal material and are thus limited to cells that are able to process exogenous material; these include dendritic cells (DC), macrophages and B-lymphocytes. Class II expression can also be induced on endothelial and epithelial cells during an inflammatory response by TNF-alpha and other pro-inflammatory cytokines.

The HLA system encodes a highly conserved but polymorphic region of approximately 250 genes located on the short arm of chromosome 6. Approximately 30% of the genes within the HLA system code for proteins associated with immune function and therefore are integral in transplant immunity. Class I peptides include the HLA-A, HLA-B and HLA-C antigens, formed by a combination of three polymorphic alpha heavy chain molecules, and a β2 microglobulin chain to stabilise the antigen (encoded on chromosome 15). The structure is folded to produce a peptide-binding area of approximately 8-10 amino acids containing endogenous protein processed within the cell that circulating T cells recognise as 'self'. The main antigens that make up class II molecules are HLA-DR, HLA-DQ and HLA-DP. These are formed by α and β chain heterodimers that bind to produce a peptide binding area slightly larger than class I molecules (10-20 amino acids), with the capacity to bind exogenous protein which render them to be recognised by circulating T cells as 'non-self', and thus initiate an immune response.

The HLA system is highly polymorphic as each individual inherits one co-dominant HLA allele encoding each of the class I and class II molecules from each parent.

Therefore, most exogenous peptides will be recognised by T lymphocytes, and although this presents a significant survival advantage within a species, it brings immunological challenges within transplantation.

1.3 Clinical Consequences of Ischaemia Reperfusion Injury

Ischaemia reperfusion injury (IRI) is an inevitable consequence of organ transplantation and results in activation of cellular, biochemical and vascular factors resulting in local and systemic inflammatory responses. IRI is initiated in the donor before organ retrieval takes place; this can be due to functional ischaemia prior to donation after circulatory death where systolic blood pressure fluctuates and falls below 50mmHg before cardiac asystole; or following donation after brainstem death where a catecholamine release occurs within the donor causing sudden changes in peripheral vascular resistance, reduced systolic blood pressure and therefore ischaemia. During the retrieval process organs are subjected to varying degrees of warm ischaemia before being rapidly cooled and exposed to cold ischaemia for storage and transportation. Subsequent reperfusion triggers a non-specific inflammatory event in the graft, resulting in an injurious state that can ultimately affect graft outcome[18].

1.3.1 Delayed Graft Function

The clinical consequences of IRI are organ specific; however, following renal transplantation, ischaemia results in DGF, defined as the failure of the graft to function sufficiently after transplantation, necessitating dialysis within the first week following

surgery. The reported risk of DGF varies within the literature but is reported to be up to 54% in some studies[19]. The differences worldwide can be partially explained by heterogeneity between studies but also because of differences in the definition of DGF amongst authors[20]. However, the incidence of DGF is lower in living donors where reported rates are between 4-10% and higher following deceased donation, affecting approximately 25% of transplants[21]. A key difference between these types of donor is the length of cold ischaemia time (CIT); typically, following deceased organ donation, the logistics of transportation between centres after retrieval adds hours to the transplant process, whereas in live donation, CIT is usually below 3 hours when performed in the same centre. Fundamentally, clinical evidence supports the idea that longer ischaemia times are detrimental to the graft, as prolonged cold ischaemia is an independent risk factor for DGF[22–27].

Evidence also shows that DGF results in poorer short term and long-term graft survival in both deceased donation[19,23,25,28,29] and living donation[30,31]. Evidence from these studies suggest a potential cold ischaemia 'threshold'; Barba *et al* showed significant difference in risk of DGF when grafts were subjected to >18 hours CIT and increased by 10% with every hour beyond this. Similarly, Quiroga *et al* showed that CIT impacted on DGF with CIT greater than 21 hours[25]. Interestingly, Kayler *et al* showed that in extended criteria donor kidneys, CIT did not independently impact graft outcomes but that there was a significantly higher risk of DGF in those with longer CIT[26].

Evidence of the impact of CIT on living donation suggests that the risk of DGF is not completely abrogated as Krishnan *et a*l demonstrated a hazard ratio of 1.3 with CIT greater than 4 hours which increased to 1.93 in grafts from donors over 50 years of age[30]. Similarly, Redfield *et a*l demonstrated that those that had a CIT of greater than 12 hours had an increased risk of DGF and increased risk of graft loss at 5 years

(65% in patients with DGF compared to 85% in those without)[31]. The increased CIT in this study was secondary to transport between centres, and this should be considered in complex paired living donor exchanges.

Other researchers have disputed that DGF independently impacts on long-term graft survival but suggest that it is a predictor of poorer graft outcomes only when associated with acute rejection (AR)[22,32–34]. Troppmann *et al* suggested that the observed effect of DGF on graft outcomes might actually be due to undiagnosed acute rejection during episodes of DGF[32]. Other studies have shown that unrecognised acute rejection significantly reduces long term graft survival[35], necessitating the requirement for biopsy for diagnosis as kidney dysfunction will be unreliable in differentiating AR from DGF.

Notwithstanding the disparity in evidence surrounding the impact of DGF on graft survival, the clinical significance of these studies show that even short periods of CIT can significantly impact short and long-term function. It also highlights that risk factors for DGF are multifactorial, but that CIT and DGF are closely interlinked.

1.3.2 IRI and acute rejection

T cell mediated rejection (TCMR) occurs in approximately 20% of recipients and is defined by immune cell infiltrates comprising T cells, macrophages and B cells. TCMR is also known as acute rejection (AR) and has been shown to adversely affect long term graft survival[22,36].

The severity of IRI is thought to drive alloimmunity by triggering the innate immune response on reperfusion thus priming the adaptive immune response in the graft. Therefore, it would stand to reason that IRI would be a causal factor in AR[37] and may

explain why Bryan *et al* demonstrated increased HLA class I antibody production after acute rejection in patients with prolonged CIT[38]. Despite this, the clinical impact of CIT on acute rejection and graft loss has been inconsistent in the literature[19,22,24,27,39–41]. A retrospective study by Kayler *et al* of approximately 14,000 ECD grafts showed no link between acute rejection and CIT in ECD grafts[26]. In another much larger retrospective cohort study of 64,000 deceased donor transplants (including 14% ECD grafts), investigators showed a CIT of greater than 24 hours resulted in a relative risk of AR of 1.13 and increased risk of graft loss. In the latter study, the authors also demonstrated a significant reduction in the incidence of AR in older age groups in keeping with dampened immune response in older recipients. When comparing studies, the mean recipient age and mean CIT were similar (age 55.5±12.6 vs 51±13; CIT >24 vs 23.3±9.1 hours respectively) suggesting that the lack of effect of CIT on AR in ECD grafts could be due to the relatively less severe impact of CIT in these kidneys rather than a dampened response seen in older recipients.

1.3.3 IRI and chronic allograft damage

There is an increasing body of evidence in native renal disease to suggest an association between acute kidney injury (AKI) and the development of chronic kidney disease (CKD)[42,43]. Although there are fundamental differences between native renal fibrosis and transplant associated CAD, ischaemic injury is a common feature of both disease entities and is essential in triggering a cascade of deleterious molecular pathways. Evidence from the transplant community favours this as multiple studies have found that prolonged CIT is a predictor of short[24,44] and long-term graft survival, and importantly this is independent of DGF[20,23–25,28,29,45].

CAD is defined by the Banff criteria as 'interstitial fibrosis and tubular atrophy (IFTA) of non-specific aetiology' and is a defined entity separate from 'chronic rejection'[46]. As described above, prolonged ischaemia predisposes the recipient to DGF and triggers an alloimmune response, both of which increase the risk of acute rejection and predispose the graft to CAD[21]. Clinically, CAD can present as worsening renal function[47], however an increase in creatinine is often a late sign, once significant loss of renal mass has already occurred.

Major risk factors for developing CAD include ischaemia, episodes of acute rejection[48], delayed graft function, hypertension and calcineurin inhibitor toxicity[49]. Early detection of CAD and prompt management of any potential risk factors are critical in maintaining organ function, as Nankivell *et al* showed in protocol biopsies, mild CAD is found as early as 3 months and is present in over 90% of biopsies at one year and once present is progressive[47]. Other studies have confirmed that the presence of either acute rejection or acute tubular necrosis on histology was strongly associated with risk of developing CAD[50–52], and that CAD occurring in combination with subclinical rejection was associated with poorer outcomes than presence of CAD alone[53].

Clinical evidence has shown that despite a reduction in the number of episodes of acute rejection with improved immunosuppression regimens, there has been no significant improvement in long-term graft fibrosis and clinical outcomes. Evidence from both these studies highlights that the deleterious effects of ischaemia impact the graft well beyond the early and reparative phases of injury, triggering a cascade of pathways resulting in an environment of continual immunological insult leading to a final common pathway of fibrosis. This is confirmed by studies in native renal disease where multiple insults beyond the initial ischaemic injury result in the progression of fibrosis.

1.4 Principles of Graft Injury

1.4.1 Ischaemia reperfusion injury

Figure 1.3 highlights key cell populations involved in the inflammatory process following IRI. Several immune cells are present within the normal kidney but following ischaemia and tubular injury, there is activation of the innate immune response and recruitment of cells to the interstitium in response to cytokines and chemokines released from TEC and immune cells.

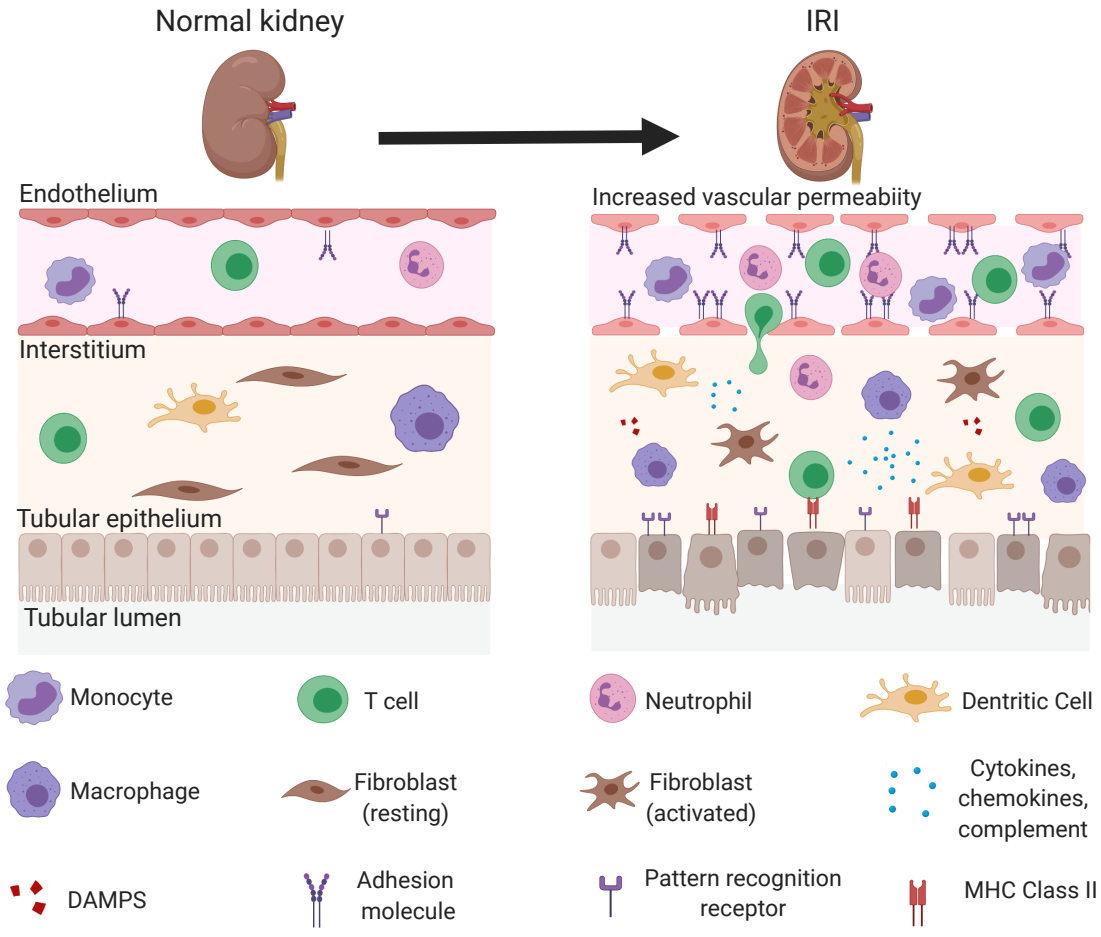

Figure 1.3 Immune response to IRI. Schematic diagram highlighting the main immune response following IRI. Made with BioRender.

4.2.1.1 The role of oxidative stress in IRI

Oxidative stress is caused by the relative abundance of reactive oxygen species (ROS) due to increased production and reduced clearance of ROS by tissues in response to stress. ROS play important physiological roles (for example in cell signalling) and are the product of oxygen metabolism in the mitochondria. However following insults such as prolonged ischaemia, oxygen depletion in the mitochondria disrupts oxidative phosphorylation resulting in impaired ATP synthesis and failure of ATP dependent cellular processes[54]. ATP depletion leads to influx of sodium, water and intracellular calcium overload[55]. In addition to mitochondrial dysfunction, hypoxia impairs the action of antioxidant enzymes including glutathione peroxidase, catalase and superoxide dismutase[56]. On reperfusion, increased oxygen availability results in a rapid increase in ROS due to increased production and impaired actions of the antioxidant systems[56]. In addition, the enzyme NAPDH oxidase is activated by IRI; NAPDH oxidase catalyses superoxide free radical production by transferring one electron from NAPDH to oxygen[57]. ROS cause damage to lipids, proteins and DNA resulting in apoptosis and cell death.

The role of oxidative stress in post-renal transplant outcomes has been suggested by correlation studies where there is an increased incidence of poorer functional outcomes in patients with markers of oxidative stress. For example, patients with increased levels of malondialdehyde (MDA)- a marker of oxidative stress- on day one post-transplant, were at greater risk of DGF compared to those with normal levels. In addition, higher levels of MDA predicted poorer renal function at 1-year[58]. Another study examining the association between polymorphism in a subunit of NADPH oxidase $p22^{phox}$ (C242T) involved in maintaining its stabilisation and thus activation under hypoxic conditions, demonstrated an association between $p22^{phox}$ C242T polymorphism and DGF in transplant recipients[59].

In a cross-sectional study by Antolini *et al*, there was an inverse correlation between markers of oxidative stress and creatinine clearance up to 3 months after transplant[60]. Levels of most markers normalised to control levels once renal function had improved and remained lower than patients on haemodialysis demonstrating that clearance of ROS was restored with remission of renal failure.

Studies have examined the role of pre-conditioning in an attempt to attenuate the effect of IRI. Pre-clinical studies in rats have shown that pre-conditioning with flavonoids and linoleic acid improve outcomes following IRI[61,62]. Outcomes included a reduction in biochemical injury markers and upregulation in antioxidant activity and a reduction in MDA. Another group examined the effects of atorvastatin and N-acetylcysteine (NAC) in rat IRI[63]. Both atorvastatin and NAC have known anti-inflammatory and antioxidant properties. Both treatments given as either single agents or in combination resulted in an increase in antioxidant activity and reduction in biochemical markers of renal dysfunction. A randomised controll trial using NAC in deceased renal transplant recipients showed improved renal function and reduced rates of DGF in those given NAC compared to controls[64]. Another trial examining the effect of spironolactone after living donor kidney transplantation showed no difference in clinical parameters but a reduction in urinary antioxidant mediators suggesting a subclinical protective effect[65].

1.4.1.1 Inflammation and the innate immune response

The innate immune response to transplantation provides an effective first line defence to tissue damage. Initiation occurs during ischaemia and is triggered prior to donation as the result of haemodynamic dysfunction and functional warm ischaemia in the

donor. The response continues during cold storage and is amplified on reperfusion, further propagating the immune response, resulting in sterile inflammation.

Loss of cell membrane integrity activates a stress response releasing so called 'danger signals' which comprise of ROS as well as damage-associated molecular patterns (DAMPS), including extra-cellular adenosine triphosphate (ATP), heat-shock proteins (HSP) and high-mobility group B-1 (HMGB-1) proteins resulting in cytokine and chemokine release[66].

1.4.1.2 Tubular injury

The outer medulla of the kidney is primarily made up of tubular epithelial cells (TEC). Under normal physiological conditions, the outer medulla has a lower oxygen tension than the cortex[67] making it more prone to hypoxic injury during ischaemia. During the ischaemic phase of IRI, hypoxia results in vascular endothelial dysfunction, reduced nitric oxide (NO) production and an imbalance of local mediators acting on vascular smooth muscle cells resulting in prolonged vasoconstriction due to impaired vasodilatation[68]. On reperfusion, blood flow is primarily restored to the cortex in order to re-establish glomerular filtration. Within the medulla, blood flow is further impaired by occlusion of the microvasculature because of increased endothelial-leucocyte binding via increased expression of ICAM-1 in response to TNF-α[69], and localised oedema caused by disruption of endothelial cell-cell interactions and microvascular permeability[70]. A combination of hypoperfusion and vascular congestion results in an almost 'no-flow' state[71], meaning that the ischaemic insult has the potential to alter regional blood flow and exacerbate tubular epithelial injury beyond the initial reperfusion phase[72,73]. This has been demonstrated in human and animal studies where blood flow within the medulla is reduced to 40-50% of physiological levels[72]

and functional MRI has shown that a reduction in medullary perfusion can last up to 7 days after injury[74].

Vascular permeability leads to increased transmigration of the host innate immune cells recruited to the graft, initiating an early inflammatory response to tissue damage. TEC necrosis results in release of DAMPS, which are recognised by a group of receptors called pattern recognition receptors (PRR), most commonly involving Toll-like receptors (TLR)[75,76]. TLRs are a family of highly conserved transmembrane receptors that, once activated, initiate a pro-inflammatory response by release of chemokines, which attract inflammatory cells such as macrophages and neutrophils to the graft. Activation of TLR by DAMPS (except TLR3) engages the MyD88 pathway resulting in activation of the transcription factor NF-κB and secretion of pro-inflammatory mediators including IL-6, IL-1β, TNF-α and CCL2[77].

In addition, surviving TECs play an active role in promoting inflammation by generating pro-inflammatory cytokines such as CCL5 (RANTES), CCL2 (MCP-1), IL-8, TGF-β, IL-6, IL-1β and TNF-α as well as upregulation of increasing constitutively expressed TLR2 and TLR4[78]. Indeed, upregulation of TLR4 has been shown to be particularly important in promoting inflammation in IRI as kidneys from deceased donors had increased expression of TLR4 compared to living donors[79]. Murine experiments have demonstrated the importance of TLR activation and signal transduction via MyD88 pathway as $TLR4^{-/-}$ and $MyD88^{-/-}$ mice are protected from IRI by a reduction in macrophages and neutrophil infiltration as well attenuated levels of pro-inflammatory cytokine and chemokine expression[80]. Pharmacological inhibition of MyD88 has recently been shown to ameliorate injury and improve survival in mice following IRI[81].

TECs are also involved in promoting alloimmunity via MHC-class II presentation and expression of co-stimulatory ligands: CD154 interacts with CD40 found on $CD4^+$ T lymphocytes, and B7-1 and B72 interact with CD28 which is required for general T cell activation in combination with CD3[82]. The interaction of TECs and T cells leads to activation of MAPK pathway and subsequent production of MCP-1, CCL5 and IL-8. TLR activation also results in dendritic cell maturation, upregulation of antigen presenting capacity and thus proliferation of Th1 cell required for alloimmunity[83].

1.4.1.3 The role of complement

Complement is part of the soluble arm of the innate immune system and is comprised of a series of proteases that are sequentially activated in response to injury. As part of the inflammatory response, there is concurrent activation of the complement system, cascading to produce the membrane attack complex involving components C5b-C9, which is inserted into the host cell membrane, disrupting it and resulting in allograft renal tubule toxicity[84]. Release of DAMPS from damaged cells further propagates the immune response to IRI.

In the kidney, TECs along with resident innate immune cells express receptors for C3a and C5a[85]. Animals studies have shown that mice deficient in either C5aR or a combination of C3aR/C5aR are protected from IRI as shown by a reduction in renal failure at 24 hours[86]. Evidence from human studies has shown C3d deposition in kidneys with ATN[87], and activation may affect short term graft outcome as was demonstrated in a clinical study of 53 donor kidneys, in which there was significant upregulation of complement gene expression (C2, C3, C4, C6) in kidneys from deceased donors compared to living donors. In addition, complement levels from biopsies at the time of implantation highly correlated with rates of DGF[88].

1.4.1.4 Role of inflammatory cells

1.4.1.4.1 Neutrophils, macrophages and dendritic cells

Neutrophils are rapidly recruited to the graft in response to chemokine secretion after injury by interaction of endothelial ICAM-1 and integrins on neutrophils, aided by increased vascular permeability of damaged peritubular capillaries. Neutrophils act to clear cellular debris by either direct phagocytosis or enzymatic degradation of damaged cells in response to PRR engagement by DAMPS and, in doing so, release ROS, myeloperoxidase and cytokines into the environment, thus promoting inflammation and further aggravating kidney injury[89]. Evidence from experimental models has demonstrated that blocking ICAM-1 results in reduction of neutrophil recruitment and protection of the kidney after ischaemia[90]. Neutrophils can also be beneficial in the resolution of inflammation by promoting the secretion of the anti-inflammatory mediator IL-10.

Macrophages are the dominant innate immune cell following injury and play a pivotal role in both propagating the inflammatory response in early injury and regeneration during the later repair phase[91]. The diverse action of macrophages in injury is highlighted by macrophage depletion studies where, although beneficial in early injury, this resulted in poor tubular regeneration and proliferation thus impairing functional recovery[92]. During early injury, the numbers of macrophages are boosted by recruitment of circulating monocytes to the graft. Macrophages possess multiple PRR, including TLRs and NOD-like receptors (NLR) resulting in production of IL-1β and IL-8 on engagement of DAMPS; this further promotes recruitment and activation of neutrophils via upregulation of I-CAM on endothelial cells. Macrophages also

secrete the cytokine TNF-α which can add to tissue damage by promoting cellular necroptosis and inflammation by concomitant release of DAMPS, as well as T-cell activation, angiogenesis and secretion of metalloproteinases.

Macrophages can adopt a variety of phenotypes depending on the cytokine milieu in the local environment. Traditionally, macrophages are described as classically (M1) or alternatively activated macrophages (M2) depending on their surface markers and phenotypic characteristics in response to *in vitro* stimuli. This traditional classification represents a gross over-simplification of macrophage behaviour given their function and plasticity *in vivo*[91]. Macrophages are important in tissue repair as well as inflammation and the traditionally labelled alternatively-activated macrophages are polarised under the influence of IL-4, IL-13, IL-10 and glucocorticoid hormones[82]. Macrophages involved in tissue repair secrete IL-10 and TGF-β, which act to dampen inflammation and the immune response but as a consequence, may promote fibrosis.

Dendritic cells (DCs) play an important role in interacting with the innate immune response via their capacity as antigen presenting cells (APC). Immature tissue DCs become activated in response to DAMPS and once mature, express both class I and class II MHC antigens[93]. Following transplantation, DCs migrate out of the organ into the recipient's lymphoid tissues where they interact with the host innate immune system, stimulating host immune response by production of pro-inflammatory cytokines and co-stimulatory molecules required for T cell activation.

Both DCs and macrophages have antigen presenting capacity and play an important role in the bridge between innate and adaptive immunity and this is discussed in more detail below.

1.4.1.4.2 T lymphocytes

T cells are prominent in the inflammatory cell population after ischaemic acute kidney injury[94] and are detected within several hours of injury in experimental models [95,96].

The T cell family comprises of multiple subsets with different characteristics and effector roles. A common feature of all T cells is the expression of the CD3 ligand ($CD3^+$) and T cell receptor (TCR). There are two main functional arms of the T cell family; $CD4^+$also known as T helper cells (Th) and $CD8^+$cells, or cytotoxic T cells. $CD4^+$ lymphocytes are further subdivided according to their transcription factor and cytokine profile into Th1, Th2, Th17 and regulatory T cells (Tregs) that become polarised from naïve T cells by various factors present in the inflammatory milieu such as cytokines and co-stimulation by other immune cells. The subsets of $CD4^+$ lymphocytes can be broadly divided into two categories based on effector actions; Th1 and Th17 lymphocytes promote inflammation whereas Tregs and to a lesser extent Th2 have suppressor actions. Experimental studies have suggested diverging roles of different T cell subsets demonstrating that certain populations promote injury whilst others are protective.

The traditional function of T cells following kidney transplantation is in the primary arm of the adaptive immune system. They play an integral role at the interface with the innate immune response via recognition of donor material presented on MHC I cells and MHC II APCs (macrophages, DCs and B calls) and tubular epithelial cells expressing MHC II under the influence of TNF-α. Activation and expansion of T cells in this capacity takes approximately 2-4 days. Evidence from animal and human studies of AKI and IRI have challenged the traditional immunological model, demonstrating that T cells are rapidly recruited to the graft and play a role in the early mediation of inflammation alongside members of the innate cellular family[97].

Early evidence of the role of T cells in IRI was initially performed in mice following liver ischaemia. Mice deficient in T cells (athymic *nu/nu* mice) were protected from IRI following warm ischaemia, which was reversed on adoptive transfer of wild-type (WT) T cells[98]. In addition, other authors demonstrated this was also true after cold ischaemia, and that pre-treatment with IL-10 improved outcomes[99]. Mechanistic studies showed that lymphocytes are important in mediating TNF-α-induced endothelial cell adhesion molecule expression, thereby exerting some of their effects by increased leucocyte binding in non-renal tissues[100]. Similar results have been seen in other organ systems subjected to IRI including in heart and cerebral ischaemia models where depletion of T cells resulted in smaller infarct volumes compared to WT mice primarily due to the function of $CD4^+$ T cells[101].

1.4.1.4.2.1 T cells involved in promoting injury

The majority of evidence in multiple organ systems has shown that $CD4^+$ lymphocytes are the main instigators of injury following IRI. Rabb *et al* showed that T cells are involved in mediating injury in the kidney as mice deficient in $CD4^+$ and $CD8^+$ cells had reduced functional and structural impairment[102]. The same group examined this in more detail in experiments using a combination of $CD4^{-/-}$, $CD8^{-/-}$ and *nu/nu* mice and found that, similar to the hepatic IRI model, injury was ameliorated in *nu/nu* and $CD4^{-/-}$ mice but not the $CD8^{-/-}$ group compared to WT controls. This finding was confirmed on adoptive transfer of $CD4^+$ but *not* $CD8^+$ cells from WT mice into *nu/nu* mice[103]. Pharmacological blockade of $CD4^+$ lymphocytes but not $CD8^+$ lymphocytes also resulted in significant reduction of injury following ischaemia[104]. These experiments also suggest T cells play a direct role independent of neutrophil and macrophage recruitment as in the latter study, there was no significant change in neutrophil or macrophage infiltration on repletion of T-cells[105]. The authors commented that these results were dependent on a much more aggressive treatment

strategy than that required to prevent experimental allograft rejection, and as such is not feasible to translate to a clinical setting.

Of the $CD4^+$ lymphocyte subsets, Th1 cells have been implicated as the main promotors of inflammation. Th1 cells are polarised into effector cells by IL-2 and IL-12 and are identified by the production interferon-gamma (IFN-γ), IL-2 and TNF. In addition, IFN-γ produced by $CD8^+$ cells and macrophages can further promote Th1 differentiation. Evidence has shown that reconstitution of RAG deficient mice with IFN-γ knockout $CD4^+$ T cells resulted in significantly reduced ischaemia-related injury than wild-type following renal IRI[106], demonstrating the importance of IFN-γ in T cell activation in response to injury.

1.4.1.4.2.2 Protective T cells

There has been increasing interest in the role of Tregs particularly in transplant immunology because of their role in graft tolerance, which is defined as stable graft function in the absence of immunosuppression[107]. Tregs help promote resolution of inflammation by suppressing pro-inflammatory mediators and subsequent immune cells responses[97].

Early evidence of the role of Tregs in protecting the kidney from IRI was shown in several papers where blockade of Tregs by anti-CD25 antibody potentiated injury and resulted in increased abundance of inflammatory cells[108–110]. In order to protect kidneys from IRI, secretion of the anti-inflammatory mediator IL-10, and expression of A_{2A} receptor on the surface of Tregs are required[111].

Tregs can potentiate benefit by clonal expansion of intrinsic populations or adoptive transfer; the latter has been performed previously in humans and so has potential therapeutic benefit. Expansion of intrinsic Tregs was performed by Kim *et al* who

showed that expansion of Tregs by blocking IL-2 also protects the kidney from injury and importantly prevents fibrosis at 28 days[112]. Alternatively, mesenchymal stems cells have been shown to interact and induce Tregs to reduce pro-inflammatory mediators following renal IRI[113].

Pharmacological recruitment of Tregs following renal IRI was shown by Lai *et al* who utilised N, N-dimethylsphingosine (DMS)[114] which inhibits sphingosine kinase, a key component in an intracellular pathway involved in determining T cell phenotype and recirculation[115]. Evidence has shown that knocking out sphingosine-1-phosphate-a derivative of sphingosine kinase-results in suppression of T cell responses with a concurrent rise in thymic-derived Tregs[116]. In keeping with these results, treatment with DMS resulted in significant expansion of Tregs and attenuation of injury following IRI.

Both expansion of Tregs and/or adoptive transfer offer potential therapeutic benefit in the context of renal IRI and transplantation.

1.4.1.4.3 B cells

B cells play multiple complex roles in the immune response from their ability to present antigens via MHC class II receptors and stimulate T cell responses, to the production of antibodies to donor antigens resulting in antibody mediated rejection, and immune regulation[117]. The role of B cells in the immune response is best demonstrated in episodes of hyperacute rejection[118] where pre-formed antibodies react with the graft, resulting in complement activation, thrombosis and graft infarction. This would have previously occurred in HLA transplants but is now a rare event after introduction of the cytotoxicity crossmatch assay[119,120].

B cells play a key role in modulating immune responses by production of cytokines including IFNγ, IL-12, IL-13 and IL-4[121]. B cell depletion has been shown to be advantageous in reducing pro-inflammatory cytokines and chemokines in a murine model of renal transplantation which conferred protection against developing CAD[122]. Non-specific deletion of B cells in human renal transplantation demonstrated a significant increase in episodes of AR demonstrating the complex role of B cells in graft immunology[123].

1.4.2 Adaptive immunity

1.4.2.1 Alloantigen recognition

Antigen presenting cells are at the interface between the innate and adaptive immune systems and provide a pivotal link that drives allorecognition following renal transplantation. This interaction is enabled via several pathways; direct, indirect and semi-direct. The direct pathway involves recipient T cell recognition of donor cells presenting MHC I or donor antigen presenting cells expressing class II major histocompatibility complex (MHC II) receptors. The indirect pathway involves recognition of donor antigens processed and presented by the recipient's APCs. The semi-direct pathway involves the capacity of DCs to exchange intact MHC-peptide complexes from other DC via cell-to-cell contact or exosome vesicles and present them to alloreactive T-cells[124–126].

MHC I cells are typically recognised by circulating $CD8^+$ cytotoxic T cells that bind with the donor cell. Dendritic cells are activated as described above by recognition of DAMPS by TLR and engulf material via endocytosis[66]. The antigenic material is then processed by the cell and presented to $CD4^+$ cells via MHC II loading. Similarly,

macrophages present antigens after phagocytosing material and B cells bind soluble antigens via their surface receptors.

T cell activation requires three key signals for activation; the first signal comprises binding of MHC loaded antigen to the T cell receptor (TCR) present on all T cells which is stabilised by binding of either $CD4^+$ or $CD8^+$ surface proteins to the MHC molecule. A secondary co-stimulatory signal is required through interaction of CD28 on the surface of T cells with either CD80 or CD86 found on APC or either CD70 or CD137 for cytotoxic T cell activation. This induces IL-2 which is the main stimulatory cytokine responsible for T cell activation. The final signal comes from cytokines, which polarise T cells into different subpopulations for example Th1 requires Il-12, whereas Th2 require IL-4.

1.4.2.2 The alloimmune response following IRI

There is a body of clinical evidence demonstrating a causal relationship between length of ischaemia, acute rejection and long-term graft outcomes, leading academics to postulate that the severity of ischaemia directly impacts upon the alloimmune response by intensifying inflammation and amplifying the innate immune response. Cells from the myeloid and lymphoid lineages play critical roles at the interface of the innate and adaptive responses; one of the most important is recognition of antigen by $CD4^+$ lymphocytes on APCs which are activated on recognition of DAMPS released in response to tissue damage.

Evidence of the role of enhanced innate immune response and acute rejection has been shown in multiple pre-clinical models of transplantation. Evidence from a partial liver transplant model showed that exaggerated macrophage infiltration in the graft

resulted in accelerated acute rejection and poorer outcomes[127]. Goldstein *et al* also highlighted the importance of innate cells in rejection as blocking TLRs, which are found on macrophages, neutrophils and DC, or the intracellular MyD88 pathway, resulted in improved survival of mismatched skin transplants[83]. Similarly following lung transplantation, enhanced neutrophil recruitment in the graft in response to ischaemia and the subsequent interaction with APC (mainly DCs) resulted in upregulation of MHC Class II expression and expansion of T cell colonies under the influence of IFN-γ[128].

Whilst this demonstrates a relationship between intensity of innate response and severity of acute rejection, direct evidence of the impact of length of ischaemia and acute rejection has been shown in a rat mismatched skin graft model, where ischaemia >18 hours resulted in an increase in CXCR3 expressing lymphocyte infiltration at 5 days and was associated with poorer long-term graft survival[129]. These findings were confirmed in a renal transplant rejection model, where blocking CXCR3 in combination with CCR5 using the antagonist TAK resulted in reduced macrophage and lymphocyte ($CD4^+$) accumulation in the graft and improved survival[130]. Prolonged ischaemia also induces Fc-receptor expression on innate immune cells, which on activation mediates vasculopathy irrespective of antibody specificity and independent of T cell response[131]. Transplanting MHC mismatched hearts into complement C3-deficient mice resulted in longer graft survival and reduced cytokine/chemokine expression and associated infiltration and expansion of infiltrating IFN-γ secreting T cells[132].

Recently, Uehara *et al* has examined the impact of ischaemia in a cardiac transplant model and found that prolonged graft ischaemia >8 hours resulted in increased $CD8^+$ infiltration and that $CD4^+$ lymphocytes are critical to the alloimmune response.

Interestingly, simply blocking T cell activity did not entirely recover the negative effects of prolonged ischaemia but a combination of T cell costimulation blockade with CTLA4 antibody and anti-IL-6 conferred improved survival even in a completely MHC mismatched graft[133]. In contrast, other authors have shown that endogenous $CD8^+$ memory cells may be responsible for accelerated acute rejection after prolonged ischaemia in a cardiac transplant model as $CD4^+$ T cell depletion did not impact on rejection[134]. The authors of the previous study postulated that the disparities seen in their results might be due to differences in donor vs recipient T cell populations where donor specific $CD8^+$ lymphocytes rely on presence of $CD4^+$ lymphocytes to develop into effector cells[133].

Both direct and indirect evidence of the role of ischaemia in alloimmunity show the complex mechanisms initiated by IRI involving cellular and humoral response and the interaction between the innate and adaptive interface. Ischaemia activates multiple pathways that drive alloimmunity and can result in acute rejection.

1.4.3 IRI induced fibrosis

The link between inflammation and fibrosis has long been established, however it is evident that the mechanism(s) behind this relationship remain complex. It is clear that non-resolving inflammation results in a vicious and relentless cycle of ongoing tissue damage and fibrosis. Evidence from native renal disease suggests multiple mechanisms are involved in the ischaemic AKI to CKD transition involving maladaptive repair pathways and progression to fibrosis. **Figure 1.4** below highlights the transition towards fibrosis following IRI. The histological appearances of progressive CAD in sequential biopsies can be described as having two distinct phases involving early tubulointerstitial damage followed by a later phase of

microvascular and glomerular injury involving worsening arteriolar hyalinosis and ischaemic glomerulosclerosis[135].

Initiation of fibrosis occurs due to continuous tissue damage as a result of non-immunological and immunological insults to the graft. IRI plays a pivotal role in priming the innate and subsequently the adaptive immune systems ultimately resulting in infiltration of the interstitium and mesangium with leucocytes, and thus promoting ongoing inflammation by secreting cytokines and chemokines into the environment. There is clear evidence that T cells, macrophages and dendritic cells have a role in renal fibrosis and contribute to ongoing injury by acting on resident interstitial cells within the kidney[136]. Evidence from the pre-clinical model of unilateral ureteric obstruction (UUO) has demonstrated significant increase in $CD4^+$ populations associated with fibrosis[137] and showed that a subset of $CD4^+$ T cells are implicated as restoration of Th2 cells restores fibrosis in BALB/c *nu/nu* mice following UUO[138]. Likewise, macrophages are well-known contributors of fibrosis. Transition of macrophages from pro-inflammatory M1 to the anti-inflammatory M2 phenotype occurs during the reparative phase, with populations peaking after the initial inflammatory response[139]. M2 macrophages act to resolve injury and promote repair by secreting IL-10 and TGF-β; however evidence has suggested a strong correlation of macrophages expressing CD206 or CD163 with renal fibrosis in human disease and pre-clinical models of renal injury[91], suggesting a potential maladaptive role in fibrosis which is most likely mediated via ongoing cytokine section acting on renal precursor cells within the interstitium.

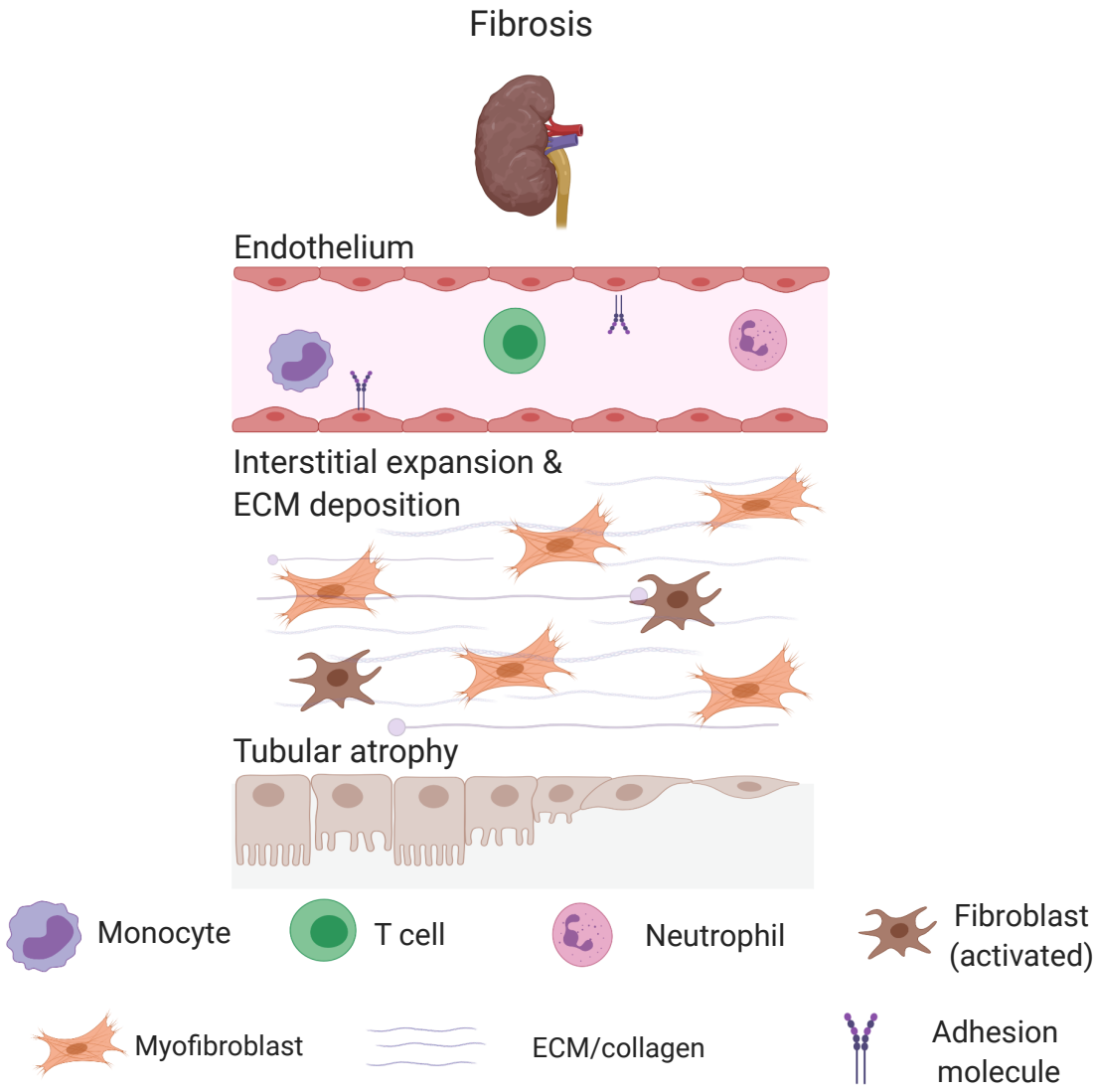

Figure 1.4 IRI induced renal fibrosis. Schematic of the effects of IRI on renal fibrosis. Made with BioRender.

TECs can regenerate form surviving cells to form a functioning nephron after dedifferentiation, migration and redifferentiation[140] under the influence of secreted growth factors and cytokines[78]. However, following injury tubular repair is frequently incomplete; some TECs can remain undifferentiated and, despite being growth arrested, release pro-fibrotic peptides into the interstitium promoting fibrosis via ERK-MAPK, JNK-MAPK and TGF-β pathways and resulting in upregulation of TGF-β and PDGF-β expression[141]. In some pre-clinical models of ischaemic injury, areas of

interstitial fibrosis are in direct contact with atrophic tubules expressing PDGFR-β but not differentiated tubules that do not express PDGFR-β, suggesting atrophic tubules could be promoting fibrosis through secretion of PDGF-β in a paracrine fashion[142].

In response to humoral factors produced by regenerating tubules and leucocytes, interstitial precursor cells, predominantly tissue resident fibroblasts and pericytes, differentiate into myofibroblasts that act to produce extracellular matrix including collagens, elastins, fibronectins, and proteoglycans resulting in interstitial fibrosis[143]. Differentiation of myofibroblasts is integral in renal fibrosis and the origin of cell type outwith tissue resident fibroblasts and pericytes remains controversial: whilst there is evidence that tubular cells dedifferentiate and act to produce a pro-inflammatory and pro-fibrotic secretome during cell cycle arrest, their role in epithelial to mesenchymal transition (EMT) and differentiation into myofibroblasts remains under debate[144].

The relative contribution of different cell populations to the myofibroblast pool remains controversial. There is evidence that fibroblasts and pericytes are the main sources of myofibroblasts, which are characterised by α-SMA expression, normally expressed by vascular smooth muscle cells, thereby making it 'non-exclusive' as a myofibroblast activation marker[136]. In addition, not all myofibroblasts express α-SMA at all times as demonstrated in a collagen I α1-green fluorescent protein reporter (GFP) mouse where the majority of cells were dual positive however a population were persistently negative for α-SMA but positive for GFP and vice versa[145].

Under physiological conditions, fibroblasts reside in the interstitium, which is defined as the space between the epithelial basement membrane and capillaries[146], and are responsible for the production and turnover of extracellular matrix (ECM) as well as homeostasis via communication with epithelial, endothelial and circulating cells[147]. They are characterised by their morphological spindle-like appearance, by expression

of markers PDGFR-β[148,149], CD73 (also known as ecto-5'-nucleotidase) and production of erythropoietin[150]. Following activation by cytokines, fibroblasts differentiate into myofibroblasts and contribute to interstitial expansion by producing ECM components. The relative contribution of fibroblasts to the myofibroblast pool differs between researchers. Le Bleu *et al* showed that proliferating tissue resident fibroblasts contribute 50% of the total number of myofibroblasts after injury[151] whereas Asada *et al* demonstrated that >90% of myofibroblasts where traced from tissue resident fibroblasts[152]. The former study also showed that only 5% of myofibroblasts where from EMT.

Similarly, Humphreys *et al* demonstrated that pericytes significantly contribute to myofibroblast population in a murine model of UUO[153]. Pericytes connect tubules and capillaries via dendritic-like processes and function to maintain capillary endothelial integrity in response to VEGF signalling between endothelial cells and pericytes[154]. Pericytes, like fibroblasts, express PDGFR-β which can often make differentiating between the two populations difficult. Following injury, there is dissociation of pericytes from capillaries in response to disruption in VEGF pathways, resulting in transformation of pericytes to myofibroblasts under the influence of PDGFR-β, resulting in expansion of the interstitium and loss of endothelial integrity. Capillary destabilisation in addition to interstitial expansion results in capillary regression, rarefaction and subsequent interstitial hypoxia[155].

Whatever the origin of the differentiated myofibroblast, expansion of the ECM occurs under the influence of pro-fibrogenic mediators, including TGF-β1, angiotensin II, CTGT and FGF2. BMP7 and hepatocyte growth factor act as anti-fibrotic mediators via antagonism of TGF-β1 pathway. Synthesis of ECM proteins is therefore dependent on the balance of pro-fibrogenic and anti-fibrogenic mediators that

regulate the transcription factors required for transcription of collagens and laminin proteins. TGF-β is a key modulator of fibrosis, acting via canonical SMAD-dependent pathway following TGF-β1 engagement with kinase receptors including activins-receptor like kinase (ALK) 1 and ALK 5; and non-canonical SMAD-independent pathways including MAPK, NK-kB and Ras/Rho pathways, resulting in upregulation of pro-fibrotic gene expression[135,156,157]. Initially, in the early stages of fibrosis, deposition of fibronectin in combination with procollagens forms a loose scaffolding for fibrillar collagens to adhere to. This is closely followed by upregulation and deposition of collagens I and III in the interstitium and later collagen IV which is primarily deposited in the tubular basement membrane, leading to the characteristic finding of a thickened tubular basement membrane on histology[158]. Together with the proteoglycans biglycan and decorin, collagens and fibronectin regulate the ECM assembly[159]. Eventually, the ECM is stiffened by biochemical crosslinking induced by transglutaminases[160], which renders it resistant to proteolysis[161]. At this point, the architecture of the kidney parenchyma is distorted resulting in functional impairment[162].

Evidence has shown that components of the ECM can modulate cellular activity, mediated by a family of transmembrane receptors called integrins. This provides a mechanical and biochemical interaction between the ECM and cells which bind ligands including collagens, fibronectin and laminins resulting in modulation of the adjacent cellular population. Some authors suggest that this interaction is fundamental in integrating various fibrogenic signals required for ECM production and assembly as many pro-fibrotic cytokines are known to induce the production of integrins[136]. Selective knock-out of integrin subunits has been beneficial in renal injury following UUO and protects against renal, lung and liver fibrosis in animal models[163]; this can be replicated pharmacologically using antagonists to integrins present on

myofibroblasts[164]. Conversely, the proteoglycans biglycan and decorin can promote healing and tissue repair by blocking TGF-β1 signaling and inducing autophagy in macrophages via TLR4[165].

The medulla is particularly predisposed to injury from ischaemia as it is normally hypoxic under physiological conditions. Expansion of the interstitium with oedema, inflammatory cell infiltrates and later extracellular matrix deposition is particularly damaging as it widens the space between damaged tubules and capillaries, thereby reducing oxygen availability and exacerbating the hypoxic state. The evidence supports that this 'pathological' hypoxia persists beyond IRI as fibrosis develops[166]. Overall this results in a persistent or chronic hypoxia whereby the metabolic demands of the TECs cannot be met due to a combination of massive interstitial expansion, hypoxia and microvascular rarefaction, which further hinders tubular repair[141] and promotes tubular cell apoptosis and necrosis[167]. Ultimately, this results in the pathological finding of interstitial fibrosis and tubular atrophy, leaving the kidney scarred, shrunken and functionally impaired.

1.5 Non-coding RNAs

When the human genome was sequenced in the early 21st century, up to 98% of what was thought of as 'junk' DNA was actually transcribed[168]. These transcripts that did not encode protein and are known as ncRNA[169]; subsequent research has shown they are integral to regulating biological functions under physiological and pathological conditions. ncRNA can be classified into housekeeping or regulatory ncRNA based on their function; housekeeping ncRNA are ubiquitously expressed in all cells and

regulate cellular function whereas regulatory ncRNA regulate gene function at transcriptional and post-transcriptional levels.

1.5.1 Housekeeping ncRNA

This group of ncRNAs include small nuclear RNA (snRNA), small nucleolar RNA (snoRNA), ribosomal RNA (rRNA), telomerase RNAs (TERC) and transfer RNAs (tRNA). Because of their function, they are abundant in the cellular environment[170]; up to 80% of cellular RNA is estimated to be rRNA, 15% tRNA and 5% all other RNA including protein coding RNA and other ncRNA. Both rRNA and tRNA are essential in translation of RNA into protein, snRNA in RNA splicing and snoRNA in in RNA modification[168,170]. Research has shown that cleavage of tRNA can transform a housekeeping ncRNA into a regulatory ncRNA; for example, tRNA-derived fragments (tRFs) have been shown to be involved in translational inhibition[171].

1.5.2 Regulatory ncRNAs

Regulatory ncRNA can be subdivided depending on the length of the transcript. Small ncRNA (sncRNA) are classed as having less than 200 nucleotides whereas long ncRNA (lncRNA) greater than 200 nucleotides long.

LncRNA can be divided further by their location with respect to protein-coding genes[172] or according to their regulatory function on DNA[173]. Using the first classification, long intergenic ncRNA (lincRNAs) are transcribed from the intergenic region whereas long intronic lncRNA are transcribed from the introns of protein coding genes. Sense lncRNAs are only transcribed from sense strands whereas anti-sense

lncRNA are transcribed from the antisense strand and can overlap exonic and intronic material. Bidirectional lncRNAs are localised in the proximity of a coding transcript on the opposite strand. When defining lncRNAs according to function and regulatory effect on DNA, they can be divided into cis-acting lncRNA or trans-acting lncRNA that act on genes in close proximity or at a distance.

Circular of circRNA are another class of ncRNA that can range from 100 to 10 000 nucleotides in length[174]. They are by definition closed loop structures that are the result of splicing events. They are derived from exons, introns and even the untranslated region (UTR). Like many ncRNA they play important roles in regulating RNA splicing and transcription[175] and can act as sponges of short ncRNA including microRNAs[176].

Small ncRNA comprises of ncRNA that are fewer than 200 nucleotides in length. MicroRNA (miRs) and short interfering RNA (siRNA) make up the majority of this group. SiRNA are short double stranded segments of RNA usually between 20-25 nucleotides in length. They can silence mRNA through binding to the RNA-induced silencing complex and are thus important in RNA interference pathways. Whereas miRs can inhibit multiple gene targets, siRNA can only inhibit one gene by binding to a single gene location. Researchers have exploited this in loss of function studies and are using it to develop novel therapies in cancer treatment[177].

1.5.3 MicroRNA

MicroRNAs (miRs) are short non-coding single strands of RNA (18-22 bases) that can inhibit gene expression by post-transcriptional repression or degradation of target messenger RNA (mRNA). MicroRNAs are transcribed and processed as a primary

transcript (pri-miR), which contain either a single miRNA stem loop or multiple stem loops encoding a cluster of different miRNAs. The pri-miR is processed by Drosha- an RNAse III enzyme found within the nucleus- and DiGeorge syndrome critical region 8 (DGCR8) to a pre-miR transcript. Following translocation to the cytoplasm, the pre-miR undergoes further cleavage by Dicer, a cytoplasmic RNase III enzyme, which cleaves the loop of the hairpin to generate a double stranded miR. This double stranded mature miR is loaded onto an AGO protein to form the RNA-induced silencing complex (pre-RISC)[178]. Once bound, the passenger strand is removed to form mature RISC and the complex binds to specific complementary regions in the 3' UTR region of the target messenger RNA (mRNA) resulting in reduced functional mRNA and thus protein translation. One miR has the potential to silence multiple genes by disrupting the translation of numerous different mRNA strands, thus making them an attractive and powerful target to investigate in the role of different disease states.

Since their discovery in 1993, research has demonstrated miRs play a fundamental role in normal physiology, as knockout of Dicer is embryonically lethal. It is estimated that over 2000 miRs are encoded in the human genome and 60% of genes are targeted by miRs[179]. Almost all human cells express miRs and under normal physiological conditions, their biogenesis is under strict control. However, in disease, dysregulation of miR expression has a significant effect on downstream gene expression. This has led to an abundance of research examining their role in different disease states with the aim of finding novel targets and treatments.

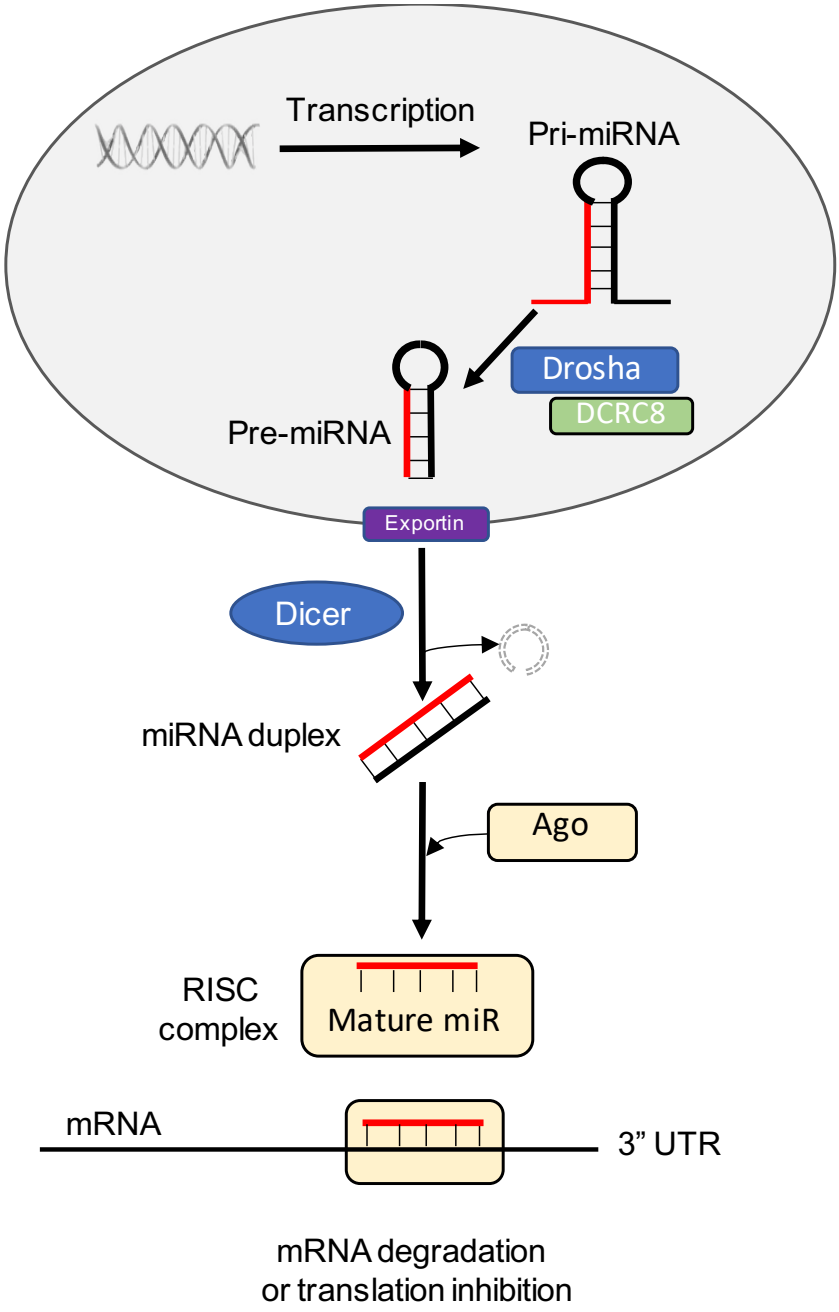

Figure 1.5 MiR biogenesis. Schematic of miR biogenesis from transcription to mature miRNA. DCRC8 DiGeorge syndrome critical region 8; RISC complex RNA induced silencing complex; UTR untranslated region.

1.5.4 MiRs and Transplantation

There is increasing evidence that miRs play an important role in the pathogenesis of renal transplantation disorders and may serve as potential biomarkers of graft outcomes.

1.5.4.1 IRI

A review by Fan *et al* in 2016 showed there were 120 differentially expressed miRs following experimental IRI in the literature[180]. The number of miRs shown to be dysregulated following renal injury demonstrates the complexity of their role in regulating target genes in renal physiology and pathophysiology.

The integral role of miRs in renal IRI has been demonstrated in multiple studies, particularly by Wei *et al* who showed the protective effect of selective Dicer-knockout in proximal renal tubules of mice undergoing IRI[181]. Selective knockout mice demonstrated superior outcomes in terms of renal function and survival compared to wildtype controls thus demonstrating the pathogenic role of miRs following IRI.

Subsequent studies have shown dysregulation of miRs in response to IRI. In one of the first studies in the kidney, Godwin *et al* used microarray to show upregulation of miRs -20a, -21, -146a, -187, -192, -194, -199a, -214 and -805 in mice undergoing 24 minutes of unilateral IRI compared to controls[182]. Shapiro *et al* took this further by examining miR expression profiles in lymphocyte depleted mice and showed that alteration in miR expression profile was independent of lymphocytes following IRI[183]. Another study showed that miR-146a targets TLR-4 signal transduction pathways promoting inflammation resulting in NF-$\kappa\beta$ transcription and upregulation of pro-inflammatory mediators[184].

MiR-24 has been shown to be important in regulating multiple targets following IRI including heme oxygenase-1 (HO-1), which is known to be protective in multiple *in vivo* models of renal IRI[185,186]. MiR-24 is upregulated in both mouse models and human transplant recipients and ablation is protective in murine model of IRI[187].

Several miRs have organ specific effects, for example, miR-494 appears to be deleterious in renal IRI but protective following cardiac ischaemia reperfusion. Following renal ischaemia, miR-494 targets activating transcription factor 3 (ATF3) which induces inflammation and renal injury in mice[188]. However, following cardiac IRI, miR-494 is downregulated immediately post injury and restoration of miR-494 levels is protective against IRI[189]. This evidence demonstrates that miRs play different roles between organ systems and have different targets within cells.

MiR-494 is increased in the urine of rodents following IRI and is detected prior to creatinine changes and so may be a more sensitive means of detecting injury following ischaemia[188].

As described previously, IRI is a major contributor to DGF. Khalid *et al* showed a panel of 6 miRs predictive of DGF following renal transplantation with an Area Under the Curve of 0.75 for the panel[190]. Interestingly, the group demonstrated that the panel of miRs was superior in sensitivity compared to individual miRs.

One study has examined the role of miRs in post-transplant AKI and demonstrated that miR-182 is significantly elevated[191]. Subsequent investigation by the same group revealed that inhibition of miR-182 resulted in significantly less injury in a preclinical model of IRI[192]. Interestingly, the paper also showed that miR-182 can be inhibited by an anti-sense oligonucleotide during normothermic machine perfusion of pig kidneys demonstrating the potential therapeutic benefit of a combination of anti-miR strategies and machine perfusion.

1.5.4.2 Acute rejection

In contrast to the evidence regarding miRs in IRI, the majority of evidence surrounding miRs in acute rejection is derived from transplant patient samples. Murine models of transplantation are technically challenging and thus there are very few pre-clinical studies.

Evidence from such studies have shown differential expression of miRs in acute rejection. Lorenzen *et al* found that miR-210 is a marker of acute T cell rejection in urine from renal transplant recipients[193]. It is downregulated during periods of acute rejection and normalised following administration of anti-rejection therapies. Downregulation of miR-210 also predicted poorer graft function at one year compared to patients with stable function and no evidence of acute rejection.

Anglicheau *et al* first demonstrated differential expression of miRs -142, -155 and -233 in both biopsy samples and in circulating mononuclear cells cultured from these patients *ex-vivo* (total sample size of 9 patients with rejection and 17 control samples)[194].

Sui *et al* examined the miRNA-mRNA integration in three patient samples with proven rejection compared to controls[195]. The group found 5 transcription factors that were activated in AR associated with 12 miRs. In another paper by the same group miRs -320 and -324 were validated in separate biopsy samples using qRT-PCR.

In a much larger cohort of 65 samples, Wilfingseder *et al* demonstrated a different miR signature that could discriminate between IRI and AR[196]. In summary, the pathways associated with AR were predominantly inflammatory whereas those observed in IRI were involved in apoptosis, angiogenesis and pathways associated with TGF-β signalling.

1.5.4.3 Chronic allograft damage

Other patient studies have examined miR expression in tissue from renal transplant recipients with or without interstitial fibrosis and tubular atrophy[197]. One group examined miRs in multiple patient samples and found 5 differentially expressed miRs in patients with or without histological evidence of CAD which were validated using qRT-PCR[198]. They took this further in a later study and showed that three specific miRs were upregulated in biopsy samples and paired urine taken from patients with IFTA; results were then validated in a larger independent group. These miRs were miR-142-3p, miR-204 and miR-211. The authors concluded that they had described a characteristic miRNA signature for CAD that correlated tissue and urine[199]. Again, these studies examine the role of miRs as biomarkers; few studies have examined their mechanism of action in pre-clinical models of transplantation.

Both Ben-Dov *et al* and Glowacki *et al* demonstrated significant upregulation of miR-21 in patients with evidence of IFTA in kidney biopsies[200] and serum[201]. In a pre-clinical study, Schauerte *et al* demonstrated significant upregulation of miR-21 in a murine model of renal transplantation and therapeutic silencing of miR-21 using an anti-sense oligonucleotide conferred significant protection from fibrosis[202].

1.5.5 MicroRNA-214

MicroRNA-214 (miR-214) is a 21-nucleotide miR that is highly conserved across species. In humans and mice, it is encoded within Dynamin-3 (*DNM3*) gene on Chromosome 1. It is transcribed alongside miR-199a (known as miR-199-214 cluster) to form a 7.9kbp long non-coding RNA primary transcript called *DNM3os* which is transcribed on the opposite strand to *DNM3*. *DMN3os* is processed to produce miR-

214-3p, its passenger strand miR-214-5p (or miR-214*), miR-199-3p and miR-199-5p[203] (**Figure 1.6**).

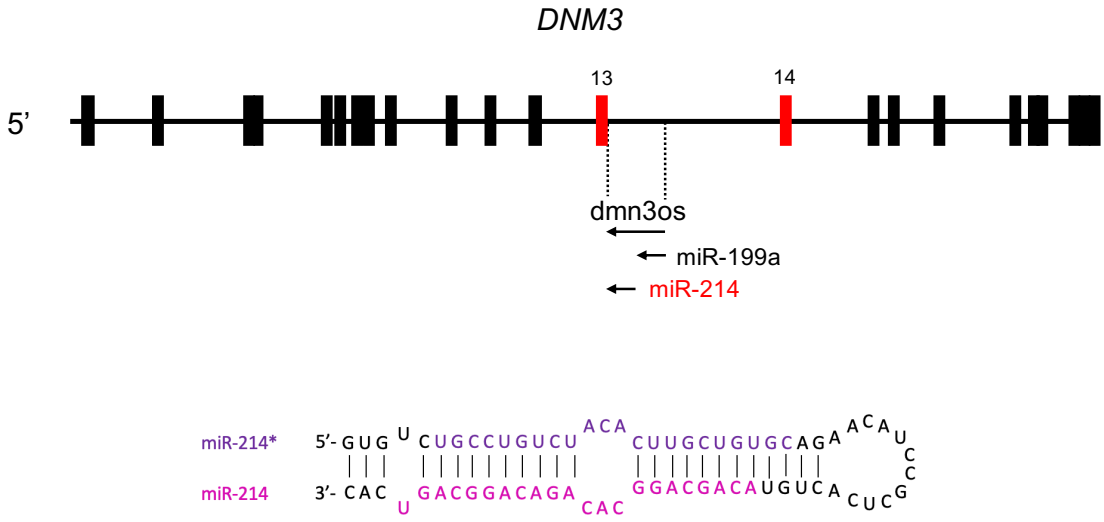

Figure 1.6 Schematic representation of the genetic location of human hsa-miR-214 and its hairpin structure. MiR-214 is transcribed along with miR-199a as part of the lncRNA DNM3os on the opposite strand of intron 14 of the dnm3 gene. Hairpin structure adapted from miRbase.

Evidence shows that expression of DMN3os transcript is under the control of the transcription factor TWIST-1 during murine development by binding to an Ebox motif found within the promoter[204]. MiR-214 is most highly expressed at E12.5 and is found specifically within the mouse cerebellum, midbrain, nasal processes and limb buds[205]. The DMN3os promoter contains multiple binding sites for transcription factors including ebox site, CAG repeats and CArG element allowing HIF-1[206], TWIST-1[205],

STAT3[206], serum response factor (SRF)[207] and ATF4[208,209] to bind under different physiological and pathophysiological conditions.

MiR-214 has been implicated in the pathogenesis of renal fibrosis and is upregulated following renal IRI. Its role in early injury has not been fully established and given that there is increasing evidence to suggest miR-214 has been shown modulates immune responses, miR-214 is an attractive target to investigate in renal IRI and fibrosis.

1.5.5.1 MiR-214 and Inflammation

There is evidence to suggest that miR-214 plays a role in modulation of leucocytes in response to injury. Studies have implicated a pro-inflammatory role in both macrophages and T cells, as well as inflammatory disorders such as ulcerative colitis.

Polytarchou *et al* demonstrated significant upregulation of miR-214 in patients with active colitis and expression correlated with clinical disease severity[206]. Mechanistic studies demonstrated phosphatase and tensin homolog (PTEN) as its potential target, postulating that its inhibition is involved in promoting inflammation by increased NF-κβ activity. Longstanding inflammation in colitis is associated with an increased risk of colorectal cancer and miR-214 was upregulated in mice with colitis-associated colon cancer thus demonstrating its potential in mediating the transition from inflammation to malignancy.

1.5.5.1.1 MiR-214 and macrophages

PTEN has also been implicated as a target of miR-214 in an *ex vivo* model of monocytes from patients with CKD where there was a 140-fold increase in miR-214 expression compared to healthy controls. Interestingly, miR-214 acted to promote inflammation by preventing apoptosis in monocytes activated by advanced glycation end products (AGEs) binding to the PRR receptor RAGE (receptor for advanced glycation products)[210].

Other evidence suggesting a role for miR-214 in macrophage activity and promotion of inflammation has been suggested by Zhao *et al* who showed that miR-214 acts to inhibit adenosine A_{2A} receptor ($A_{2A}R$) in bone marrow derived macrophages in an *in vivo* model of acute lung injury[211]. $A_{2A}R$ is an ubiquitously expressed receptor that, on activation, modulates anti-inflammatory responses. Activation of $A_{2A}R$ results in a corresponding downregulation of miR-214 whereas activation of the NF-$\kappa\beta$ pathway results in increased transcription of miR-214 by binding to its promoter resulting in enhanced miR-214 transcription.

Conversely, miR-214 may play a role in dampening the immune response in autosomal dominant polycystic kidney disease (ADPKD). Recently, miR-214 was shown to be upregulated in multiple models of ADPKD by pro-inflammatory pathway involving TLR4, and deletion of miR-214 resulted in significant increase in cyst growth. The mechanism behind this involved increased expression of M2 markers and accumulation of mannose receptor 1-positive macrophages ($MRC1^+$) around cysts whilst there was no change in expression markers of M1 macrophages, T cells or fibroblasts[212].

1.5.5.1.2 MiR-214 and T-cells

MiRs are critical to immune modulation and are required for T cell development in the thymus, lineage differentiation and homeostasis. Dicer knockout in thymic lymphocytes or Treg specific ablation results in phenotypic changes typical of autoimmune disease in mice displaying inflammatory pathology of visceral and thoracic organs due to reduced Treg numbers[213] or due to loss of suppressor function *in vivo*[214].

There have been multiple studies examining miR-214 in T cells in the context of pro-inflammatory, autoimmune and malignant conditions. Jindra *et al* showed that miR-214 is significantly upregulated in activated T cells and expression has been shown to be upregulated in both $CD4^+$ and $CD8^+$ subtypes in an *ex vivo* $CD3^+$ mouse model[215]. Furthermore, they demonstrated miR-214 significantly increases proliferation that is dependent on presence of the TCR co-stimulatory molecule CD28 by targeting PTEN. The PI3K pathway is critical to T cell activation and it stands to reason that downregulation of its inhibitor would result in increased T cell activation.

Within the $CD4^+$ lineage, miR-214 has also been shown to be differentially expressed when comparing conventional $CD4^+$ T cells and Tregs and, unlike the evidence above, was preferentially upregulated in the Treg population[216]. Another group showed that miR-214 acts to expand Treg population in malignancy which is potentially mediated via macrovesicles containing miR-214 secreted by cancer cells[217]. Again, PTEN was implicated as a target and was found to be significantly reduced in Tregs.

Tregs act as suppressor, which are beneficial in resolving inflammation but may promote tumour growth and malignancy by modulating the immune response, and are increased during tumorigenesis. The PI3K/AKT pathway is common in activation

and expansion of multiple T cell lineage subsets[218] and therefore the role of miR-214 in T cells is likely to be dependent on the context of the disease and local environment.

In clinical studies, miR-214 has been shown to be both upregulated and downregulated in line with differential T cell expression in autoimmune diseases and may be involved with balance of T cell differentiation and homeostasis. In one study, active multiple sclerosis lesions were associated with miR-214 upregulation[219].

In asthma, miR-214 was significant upregulated in patients with active disease and correlated with increased Th2 expression compared to increased Th1 expression in controls. MiR-214 was found to inhibit Runx3 which is a transcription factor involved in thymic T cell development and important in affecting the Th1/Th2 balance[220,221]. Th2 T cells have been implicated in mediating early injury in IRI and promoting renal fibrosis and this evidence could suggest miR-214 has a role in Th2 cell modulation. **Figure 1.7** depicts the role of miR-214 in T-cells.

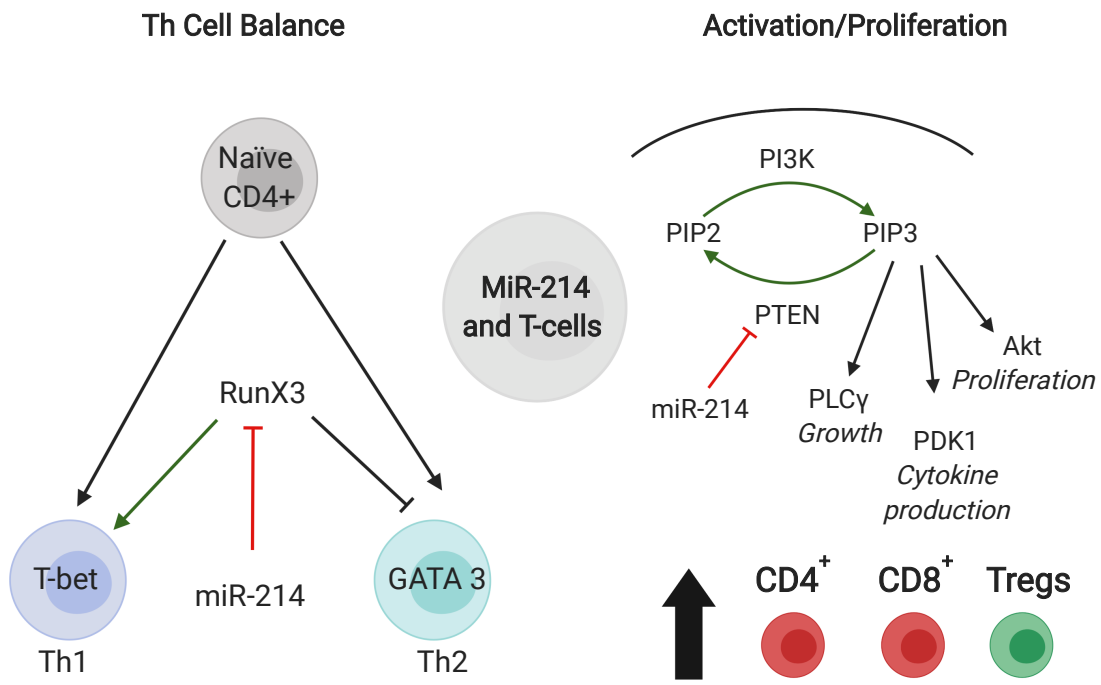

Figure 1.7 Actions of miR-214 in T cells. MiR-214 plays different roles in T cell activation and proliferation by targeting PTEN and shapes T helper cell balance in asthma by targeting RunX3. Made using BioRender.

1.5.5.2 MiR-214 in native renal disease and fibrosis

MiR-214 has mainly been studied in the context of renal fibrosis and is commonly thought of as a pro-fibrotic miR or 'fibroMir'. Expressed at low levels in normal physiological conditions, it is significantly upregulated following renal injury. Denby *et al* demonstrated an upregulation of miRs -214 and -21 in multiple *in vivo* models of renal injury and fibrosis including UUO, a salt sensitive hypertensive rat and a murine model of glomerulonephritis[222]. In an *in vitro* TGF-β induced injury model in tubular endothelial and mesangial cells, there was concurrent upregulation of these miRs and pro-fibrotic gene expression, suggesting that miR-214 was acting on multiple cell types within the kidney to promote fibrosis. Knocking out miR-214 and -21 protected the kidney from fibrosis following UUO, with the greatest protection seen in the miR-

214 knockout group where there was a 93% reduction in fibrosis compared to controls[223]. Pharmacological blockade using subcutaneous anti-miR-214 oligonucleotide conferred significant reduction in fibrosis (83%) and importantly, pharmacokinetics showed that anti-miR-214 was primarily distributed in the kidney, therefore reducing the risk of potential systemic side effects.

Mechanistic studies from these experiments have highlighted two important features of miR-214; firstly, unlike miR-21, it is independent of TGF-β *in vivo* and secondly, under pathological conditions, miR-214 is pro-apoptotic, targeting the anti-apoptotic mediator gankyrin encoded on *PSMD10*. Tubular cell apoptosis is integral to tubular atrophy in chronic kidney disease, and in situ hybridisation of kidney tissue from patients with CKD showed that expression of miR-214 was predominantly localised to damaged tubules, suggesting that miR-214 potentially promotes tubular injury.

Its role in apoptosis has recently been confirmed by Bai *et al* who demonstrated that conditional proximal tubular knockout of miR-214 decreased apoptosis through a reduction in mitochondrial dysfunction, conferring protection from fibrosis by de-repression of mitochondrial genes *mt-Nd4l* and *mt-Nd6*. The authors had previously shown that miR-214 was upregulated in hypoxic injury through the TWIST-1 pathway and postulated that miR-214 acts as a mitochondrial DNA regulator in proximal tubular cells[224,225]. Controversially, the same authors stated that miR-214 promotes tubular EMT; however its role in promoting fibrosis might be secondary to differentiation of resident fibroblasts via secretion of pro-fibrotic cytokines whilst in a cell arrested state as described above[224].

Other groups have also demonstrated miR-214 is upregulated in renal injury and fibrosis[225–227]. Wang *et al* showed that miR-214 is upregulated in an *in vivo* model of diabetic nephropathy, which primarily models significant mesangial cell hypertrophy,

and targets PTEN[226]. PTEN antagonises the PI3K/AKT/mTOR pathway by opposing the action of PI3K which converts PIP2 to PIP3. The PI3K/AKT/mTOR pathway is important in several cellular processes including cell growth survival; inhibition of PTEN by miR-214 in this context resulted in mesangial cell hypertrophy which is a key to the pathogenesis of diabetic nephropathy. Other groups have shown that PTEN inhibition is involved in hypertrophy in cardiomyocytes[228] however not skeletal muscle [229], suggesting that the phenotypic results of PTEN dysregulation is cell type specific.

In salt sensitive hypertensive rats, miR-214 was upregulated compared to insensitive rats and renal inhibition of miR-214 using anti-miR-214 delivered to the medulla significantly improved hypertension and albuminuria and was associated with a reduction in pro-inflammatory and pro-fibrotic gene expression in the renal medulla[227]. The authors also showed that miR-214 acted to inhibit eNOS which is important for maintaining vascular tone.

MiR-214 is upregulated in early injury in response to IRI. Godwin *et al* showed miR-214 upregulation 72 hours following 26 minutes ischaemia in mice undergoing unilateral IRI[182] and Zhu *et al* showed miR-214 was upregulated in a rat model of IRI where animals were subjected to 30 minutes of bilateral ischaemia and in an *in vitro* model of rat renal tubular cell hypoxia[230]. The authors of the latter study showed that pharmacological overexpression of miR-214 inhibited apoptosis in both models and protected against injury quantified by a reduction in urinary KIM-1 and biochemical injury markers including serum creatinine and urea. Luciferase assay identified DDK3 as a target which is a negative regulator of the WNT/β-catenin pathway. Inhibition of the pathway results in ubiquitination and degradation of E-Cadherin adaptor protein β-catenin leading to loss of cell to cell adhesion. Whilst this study is suggesting an

opposing role for miR-214 in renal injury to the evidence above, it is contradictory to the evidence published by multiple independent groups and should be interpreted with caution. However, the protective role is in keeping with evidence from some cardiac models where miR-214 appears to be protective against fibrosis.

Interestingly, evidence from lung fibrosis models have similarly implicated miR-214 in promoting the β-catenin pathway by suppression of GSK-3β which acts to inhibit β-catenin accumulation and nuclear translocation[231]. In contrast to the beneficial results described by Zhu *et al*, this leads to upregulation of pro-fibrotic gene expression and differentiation of fibroblasts to myofibroblasts required for fibrosis. There is evidence to show interplay between TGF-β1 and the WNT/β-catenin canonical pathway, thereby promoting myofibroblast differentiation via multiple pathways involving GSK-3β. Moreover, over-expression of WNT/β-catenin has been observed in kidney fibrosis and this, together with the results from this study, demonstrate a potential of miR-214 in kidney myofibroblast differentiation and fibrosis. In addition, the authors demonstrated that inhibition of DNM3OS protected mice against lung fibrosis. DNM3OS encodes miR-214, miR-199a-5p and miR-199-3p. The authors did show that miR-199a-5p inhibition was protective in this model but did not examine miR-214 inhibition strategies.

Finally, there may be a role for miR-214 as a biomarker of renal injury. In a retrospective analysis of patients with IgA nephropathy, expression of miR-214 from kidney biopsies was associated with poorer long-term outcome[232]. It is also associated with a worse clinical score of IgAN, thus demonstrating a potential role in differentiating severity and progression of disease.

1.5.5.3 MiR-214 and cardiac disease

There is conflicting evidence concerning the role of miR-214 in cardiac disease and cardiac fibrosis where some studies suggest miR-214 is protective whilst others show miR-214 ablation is protective. Aurora *et al* demonstrated that knocking-out miR-214 was deleterious in cardiac fibrosis following ischaemia reperfusion injury[233] by de-repression of cardiac sodium/calcium exchanger 1 (NCX-1), allowing increased calcium influx into the cardiac myocyte and promoting cell death. It has also been shown to be upregulated in mice with pulmonary arterial hypertension (PAH), and deletion resulted in exacerbated right ventricular hypertrophy (RVH) in response to hypoxia[234]. Interestingly, there was significant sex variation where miR-214 deletion had no effect on PAH in female mice but resulted in progression of RVH in males.

On the other hand, miR-214 has been shown to be a marker of cardiac stress in ventricular hypertrophy and progression to heart failure[235,236] with evidence that miR-214 inhibition exerts protective effects by de-repression of PPARδ and restoration of fatty acid metabolism[237]. These conflicting results could be explained by miR-214 targeting different pathways in different cell types in the right and left cardiac systems conferring both beneficial and deleterious effect dependent on the injury and pathways involved.

1.6 Models of Renal Ischaemia Reperfusion Injury

Renal ischaemia reperfusion injury is important in the pathogenesis of early and late renal transplant complications and is a common cause of acute kidney injury in native kidney disease. In turn, AKI is a well-known risk factor for development of CKD, which can potentially progress to ESRD. Therefore, modelling IRI is important in aiding our

understanding of the complex pathways and mechanisms triggered by ischaemia and subsequent reperfusion in both these settings.

Much attention has been paid to the role of ischaemia in the transition from AKI to CKD, as experimental evidence demonstrates that the ischaemic event triggers an innate immune response that promotes inflammation and results in maladaptive repair mechanisms that facilitate fibrosis. Animal models play a crucial role in aiding our understanding of these complex pathways and mechanisms in the expectation of discovering novel therapeutic targets.

Animal models were first used in the 1960s and have been refined for use in small animals which was first described in the 1990s with the introduction of the mouse model of AKI[238]. There are multiple *in vivo* models of IRI that commonly utilise rodents (rats and mice) primarily because of the relatively low cost associated with rodent experiments compared to large animal studies, and the ability to introduce genetic variations allowing a greater understanding of the role of specific mechanisms *in vivo*. However, one disadvantage of the rodent model is the variation in results due to different experimental murine strains which may introduce a degree of disparity between studies. Given the relatively low complexity of the procedure and associated costs, the murine model allows high throughput studies and remains a popular model for studying renal disease.

The IRI model offers considerable versatility despite the low complexity of the procedure and is beneficial in modelling the effects of IRI in AKI and transition to fibrosis which are relevant to both native renal disease and transplantation. Important considerations include the length of ischaemia which impacts upon the severity of injury, whether the injury is unilateral or bilateral, and, in the case of unilateral injury, whether the contralateral or uninjured kidney is removed and if so, timing of the

nephrectomy. All of these factors impact on experimental outcomes and introduce experimental limitations that determine which model is best to investigate early and late features of IRI and are therefore essential considerations to factor into an experimental plan.

1.6.1 Bilateral ischaemia reperfusion injury

Bilateral IRI affects the total renal mass and results in significant biochemical and functional renal injury resulting in a rise in serum urea and creatinine and histological evidence of acute tubular necrosis. The bilateral model of ischaemia is a popular model of human AKI where disruption of blood supply typically affects both kidneys simultaneously. One important factor that impacts on outcome is length of ischaemia as longer ischaemia results in a more significant injury. Typically, injury is scored histologically by assessing the degree of ATN in the outer stripe of the outer medulla[239]. The ATN score is calculated as the percentage of necrotic tubules present within a magnified field after staining with H&E. Injury as scored by the degree of ATN can be ranked from mild to severe depending on the degree of necrosis according to the Jablonski scale first published in 1983[240]. This group showed that rats with 30 minutes of ischaemia had structural evidence of necrosis with no significant increase in biochemical markers of renal dysfunction and therefore suggested a scoring system ranging from 0-4 which ranks injury according to percentage of ATN where 0 is equivalent to no necrosis; 1 ranges from 1-25%; 2 from 26-50%, 3 from 51-75% and 4 represents >75%. Where a score of 0 is no injury, 1-2 represent mild injury, 3 is moderate and 4 is severe.

The length of ischaemia that determines the severity of ATN varies between studies and may be explained by differences between mouse strains and /or operator

technique; for example, some groups recommend bilateral flank incisions[241,242] whereas others utilise a laparotomy[238]. Whilst bilateral flank incisions avoid mobilising the intestines and heat loss from the peritoneal cavity, a laparotomy is quicker as both kidneys are accessed via the same incision, reducing the operative time. Other differences in technique include variation in anaesthesia, analgesia and post-operative care. However, even after taking this into consideration, in general 18-20 minutes ischaemia would be considered mild, and often there is return of normal renal function and reverse of histological damage within a week of injury. Ischaemia of around 30 minutes or more would induce a severe injury resulting in a high proportion of death from renal failure in experimental animals after 48-72 hours surgery[243].

Whilst this is a robust model for human AKI, there are experimental limitations that confine its use to studying the early phase of injury because of the fine balance between complete reversal of injury due to too short ischaemia resulting in mild ATN and inducing fatal renal failure secondary to severe ATN, which in humans can be overcome with renal replacement therapy.

Notwithstanding these limitations, some studies have investigated the long-term outcomes of bilateral IRI and have shown almost complete reversal of injury within 2 weeks of ischaemia. Spurgeon *et al* induced 60 minutes of bilateral renal ischaemia in a rat model and followed up the outcomes for 40 weeks[244]. Despite an 80% reduction in glomerular filtration rate, renal function returned to normal after 16 days and, over the following 40 weeks, rats only lost 10% glomerular filtration compared to controls demonstrating no significant functional decline in renal function. There was however evidence of capillary rarefaction alongside tubular atrophy and interstitial fibrosis on histology. Therefore, other variations of this model can be utilised to investigate the consequences of severe ischaemic insult on long term renal function.

1.6.2 Unilateral ischaemia model without nephrectomy

Unilateral ischaemia without nephrectomy is primarily used to model the effects of hypoxia on the kidney beyond the early phase of injury. The unilateral injury model was first established in 1954 by Kolestsky who demonstrated severe injury following unilateral ischaemia in rats and since then has been further characterised in multiple rodent studies[245]. Again, as with the bilateral model, increasing ischaemia of a single kidney has been shown to increase the severity of injury and result in greater renal atrophy and poorer function as shown by a significant reduction in inulin clearance, urine output and glomerular blood flow in rats subjected to 60 minutes ischaemia up to 8 weeks after injury[246–248]. The remaining non-injured kidney supports the injured kidney, so the impact of renal dysfunction is limited, thus allowing the animal to survive beyond the first 48-72 hours. The result is that the injured kidney becomes fibrotic as shown by increased collagen deposition in kidney sections and upregulation of fibrotic gene markers whilst the uninjured kidney compensates by increasing its renal mass[249,250].

The pathophysiology of renal injury when normal renal mass is left *in situ* is primarily due to alterations in blood flow and subsequent haemodynamic changes in the kidney post-injury. Presence of the normal kidney exacerbates the injury by prolonging vasoconstriction on the outer medulla as blood flow is diverted to the uninjured kidney. The subsequent reduction in glomerular filtration worsens the glomerular debris and cast formation because of decreased glomerular washout. This had previously been demonstrated in studies from the 1970s and 1980s using a micro-puncture technique where the operator cannulated a single tubule and measured tubular flow rate by injecting a labelled perfusate. This technique yielded interesting data however is technically challenging and may have resulted in significant variation in results due to back flow of fluid[248]. Recently, advances in functional imaging-in particular MRI-mean

that the effects of ischaemia can be visualised and quantified in real time and more importantly *in vivo*, and, as it is non-invasive, changes in renal morphology can be assessed multiple times in the same animal over the period of the experiment. Another advantage is that MRI can assess the function of the whole kidney and, in particular, the relationship between the cortex, outer medulla and inner medulla. Studies by Hueper *et al* have demonstrated that decreased perfusion 7 days after severe injury as assessed by arterial spin labelling correlated with decreased renal mass at 28 days[251]. The same group also showed that increased T1 enhancement and T2 relaxation times of the OSOM, which are indicative of tissue oedema secondary to increased capillary permeability, were predictive of renal fibrosis and increased inflammatory cell infiltrate as assessed by histology[74,252,253]. Interestingly, these functional MRI studies have shown variation between mouse strains as 35-45 minutes of unilateral ischaemia resulted in greater renal perfusion impairment in 129/Sv mice when compared to C57Bl/6 mice.

Haemodynamic factors act to prolong the 'no flow' phenomenon and potentially intensify subsequent injury and impair recovery. At the level of the transcriptome, hypoxia triggers downstream mechanisms including pro-inflammatory gene expression resulting in upregulation of chemokines and cytokines such as IL-1, TNF-α, IL-6, IL-10 as well as MHC class II expression on tubular epithelial cells[73,82]. The subsequent inflammatory response results in ongoing deleterious pathway activation ultimately leading to activation of pro-fibrotic pathways. Both Zager *et al* and Le Chef *et al* demonstrated that 18-30 minutes of renal ischaemia leads to significant pro-inflammatory and pro-fibrotic changes up to 12 weeks following injury[249,250].

A limitation of this method is the inability to easily assess function after injury as the presence of the contralateral kidney will impact serum GFR and urinary biomarkers of injury. Whilst there are several methods to assess functional status of the kidney,

they inevitably involve nephrectomy of the contralateral kidney and are usually end-point events. For example, inulin clearance of the affected kidney could be measured following nephrectomy of the contralateral kidney, however this is time consuming and may impact on time critical outcomes such as flow cytometry. Other methods include ureteric catheterisation allowing functional assessment of the individual kidneys however this method is limited to rat, dog or pig models and as such, would not be suitable for murine studies which make up a considerable proportion of the experimental population[250].

Despite the disadvantages of the technique, it has been demonstrated to be a robust model of AKI to CKD transition and will be continued to be used to examine the effects of ischaemia beyond the early phase of injury.

1.6.3 Unilateral ischaemia model with nephrectomy

Performing unilateral ischaemia with concurrent nephrectomy can serve multiple research objectives. Firstly, the contralateral kidney can be removed at the time of unilateral injury and can be used as a control to model AKI without the need for sham[239]. This is particularly beneficial when administering pre-surgical treatments or drugs as demonstrated by Ferenbach *et al*, who successfully upregulated heme-oxgenase-1 (HO-1) by administering heme arginate 24 hours before surgery and using the right kidney as suitable control material[254]. Again, this model is best suited for examining the early phase of IRI as animals will inevitably develop renal dysfunction that may hinder recovery beyond the early phase of injury and therefore is more applicable to studying the effects of IRI in renal transplantation than native renal disease. Interestingly, this group demonstrated moderate recovery of renal function at 7 days post-surgery even in the face of severe functional and structural

injury, suggesting that either they overestimated injury or contralateral nephrectomy is potentially beneficial to the recovery of the remaining kidney.

The protective effect of a contralateral nephrectomy was first observed by in the 1980s after researchers observed that nephrectomy of the non-injured kidney diminished functional and structural injury following unilateral IRI[255]. Jablonski *et al* demonstrated renoprotection when the nephrectomy was performed up to 7 days after injury; however, when delayed until day 14 there was evidence of significant fibrosis in the affected kidney suggesting that presence of the uninjured kidney impaired recovery[256]. Further evidence to support the protective effect of unilateral nephrectomy on transient ischaemia has been shown in multiple subsequent studies demonstrating that it acts as a pre-conditioning stimulus. Importantly, this protective mechanism is independent of compensatory hypertrophy of the remaining kidney as it is also observed when the contralateral nephrectomy is performed prior to the ischaemic insult[256,257].

As with other models of renal IRI, the outcome of the post-ischaemic recovery phase is dependent on acute shifts in renal blood flow. Following unilateral nephrectomy, the immediate vasoconstrictive phase in the injured kidney is limited as renal blood flow is conserved resulting in a reduction of vasoconstrictor mediators acting on the endothelium[258,259]. This has been shown to alter humoral responses including reducing renin activity and altering renal sodium handling[260]. There is recovery of the tubular epithelial cells[261] resulting in elongation of tubules by up to 70% in rats[262]. At a transcriptional level, there are significant changes in genomic response within hours of nephrectomy including suppression of genes involved in growth inhibition and apoptosis in keeping with a 'pro-hypertrophic' signalling state[263]. Consequently, there is a drive towards a compensatory increase in nephron size and function under the control of various growth factors including growth hormone and IGF-1[264–266].

Recently, there has been interest in the significance of variation in regional perfusion within the kidney rather than total renal blood flow following injury. Newer non-invasive techniques including functional MRI can monitor regional perfusion longitudinally over time *in vivo*. One group showed there was significantly increased perfusion in the medulla of male rats that were subjected to 37 minutes ischaemia and contralateral nephrectomy compared to rats that underwent ischaemia without nephrectomy[267]. Histology demonstrated that rats that underwent nephrectomy had significantly less fibrosis in the ischaemic kidney. This is in keeping with previous evidence that the renoprotective effects of unilateral nephrectomy on post-ischaemic outcomes is likely to be due to increased medullary perfusion resulting in a dampened inflammatory response to injury.

1.6.4 Cold vs warm ischaemia

Hypothermic conditions can affect the outcome of renal ischaemia and has been shown to be protective in reducing the metabolic demands during the ischaemic period[268]. In light of this, human organs are preserved in ice-cold solution as standard procedure during the organ retrieval process and can be stored for hours before successful implantation to allow for the logistics of transportation between donor and recipient centres[269]. Normothermic or warm ischaemia is thought to be more detrimental than cold ischaemia because of cellular membrane disruption[270] and production of oxygen free radicals[268,271] although this now being questioned in clinical transplantation, with evidence of benefit of normothermic organ perfusion prior to transplantation, particularly in liver transplantation [272–275].

In animal studies, several groups have demonstrated the effect of body temperature on outcomes following renal IRI[242,276–279]. Delbridge *et al* showed that hypothermic

conditions resulted in significant attenuation of renal injury following 45 minutes of renal ischaemia in a rat model whereas hyperthermic (39.7°C) animals had a non-recoverable renal failure and normothermic animals recovered renal function by day 3[242]. Early work by Zagar *et al* showed that continuing mild hypothermia into the reperfusion phase offered additive protection against renal failure but the effect was no longer observed beyond 60 minutes of reperfusion[277].

Le Clef *et al* showed that hypothermia protected the kidney against fibrosis in a unilateral model of IRI in mice[250]. Mice underwent IRI and were sustained at 34°C and compared to outcomes in normothermic mice. There was significantly less fibrosis in the hypothermic animals as quantified by increased renal mass compared to normothermic controls, lower deposition of collagen 1 and significantly reduced expression of pro-fibrotic gene expression. There was no significant reduction in KIM-1 expression between hypothermic and normothermic groups suggesting that hypothermia does not prevent tubular injury but potentially dampens the subsequent inflammatory response.

1.7 Aims and Hypotheses

The aim of this thesis is to undertake mechanistic studies investigating the role of miR-214 in fibrosis related to renal ischaemia reperfusion injury.

Based on this aim, the hypotheses are as follows:

1. Expression of miR-214 increases following renal IRI and is associated with subsequent fibrosis.
2. Blockade of miR-214 expression ameliorates renal injury following IRI.

Chapter 2: Materials and Methods

2.1 General Reagents

All reagents were purchased from Sigma-Aldrich unless otherwise stated.

2.1.1 Dulbecco's Modified Eagle's Medium (DMEM)

Dulbecco's Modified Eagle's Medium (Sigma-Aldrich) supplemented with 100 U/ml penicillin and 100μg/ml streptomycin (Gibco) and 10% heat-inactivated fetal calf serum (FCS) (Gibco). Serum free media contained the above with the exception of 0.2% FCS (Gibco).

2.1.2 Complete Roswell Park Memorial Institute Medium (RPMI)

Roswell Park Memorial Institute Medium (RPMI) medium containing HEPES (Gibco) supplemented with 2mM L-glutamine, 100 U/ml penicillin and 100μg/ml streptomycin (Gibco) and 10% fetal calf serum (Gibco).

2.1.3 Fluorescence Activated Cell Sorting (FACS) buffer

PBS was supplemented with 2% FCS (Gibco) and 1% 0.1M EDTA.

2.2 Animals

Male C57Bl/6 mice were purchased from Charles River laboratories and were between 8-10 weeks of age. Male BM12 mice and transgenic strains (miR-214$^{-/-}$) were bred in-house. MiR-214 mice were bred from miR-214 heterozygotes (miR-214$^{+/-}$) and litter mate controls were used for knockout experiments. Animals used in the transplant model experiments were housed individually post-operatively; those used for ischaemia-reperfusion were housed in groups. All mice were kept at a 12hr light/dark cycle and had free access to water and food. All experiments were performed under UK Home Office Personal and Project Licences and were approved by the University of Edinburgh Veterinary Services under PPL numbers 60/4375 and P1F59E89D.

2.3 Surgery

2.3.1 Anaesthesia

General anaesthesia was achieved using either intraperitoneal injection or inhalation agents. All animals were maintained at normothermia throughout experiments using specialised animal surgical mats set at 37°C.

Intraperitoneal anaesthesia was achieved by injecting a mixture of 1.8mg ketamine (Vetalar, Zoetis Ltd) and 25ug medetomidine (Domitor, Vet Quinol Ltd) for a 25g mouse. These agents were diluted as follows to make a 5ml mixture: 0.36ml ketamine at 100mg/ml; 0.5ml medetomidine at 1mg/ml and 4.14mls water. A total of 250μl was injected into each mouse.

Inhalation general anaesthesia was achieved using inhalation agents (isoflurane, Abott Labratories Ltd) in accordance with the local veterinary protocols. Induction of anaesthesia was achieved using a mixture of 4% isoflurane and 1L/min oxygen and maintained using 1.5%-2% isoflurane and 1L/min oxygen (recommended for 25g mouse).

All recoverable animals were given 0.1mg/kg buprenorphine (Vetergesic, Reckitt Benckiser Healthcare Ltd) analgesia at induction of anaesthesia and 24 hours later. For a 25g mouse, 2.5μg was administered in a 50μl subcutaneous injection by diluting 100μl buprenorphine at 0.3mg/ml in 900μl sterile water.

2.3.2 Transplant Model

The murine model of chronic allograft damage involves transplantation of the left kidney of a male BM12 into a male C57BL/6 mouse; characterized by a single class II mismatch this results in the development of interstitial fibrosis and tubular atrophy over the course of 8-12 weeks following surgery. Isograft controls involve transplanting male C57BL/6 into male C57BL/6 mice. All mice were aged between 8-12 weeks of age. The procedure is described in more detail in **Chapter 3.2.**

2.3.3 Murine model of ischaemia reperfusion injury

Male C57Bl/6 mice were anaesthetised using inhalation anaesthesia and buprenorphine administered subcutaneously as described above. Throughout surgery, normothermia was maintained at 37°C using specialised heat mats. The technical aspects of the model are described in more detail in **Chapter 4.2.1**.

(Interfocus, Linton, UK, list of instruments and consumables are outlined in Appendix 3).

Animals received 1ml saline on completion of the procedure and placed in a recovery chamber set at 28°C for 24 hours. Mice received a further dose of buprenorphine day one post-operatively.

2.3.4 Post-operative checks

Animals were checked twice a day for signs of distress for the first 72 hours in accordance with unit protocols; mice were referred for veterinary examination if deemed appropriate. All mice were weighed daily for the first 72 hours and given supplementary mashed food in the floor of their cage if required. Beyond the first 72 hours, animals were weighed twice a week until the end of the experiment.

Animals were culled via schedule one method if they sustained a weight loss >20%.

2.4 Kidney Tissue Processing

At the termination of an experiment mice were culled under isoflurane terminal anaesthesia and confirmed using cervical dislocation. The abdomen and chest were opened allowing access to the heart for cardiac puncture. Blood was obtained via direct puncture of the left ventricle. The right atrium was cut open and 5ml saline infused via a left ventricular puncture in order to flush the kidneys prior to removal. The kidneys were then carefully dissected free from surrounding tissue and harvested. Each kidney was meticulously prepared by cutting the hilar vessels flush

with the kidney to remove the renal vascular pedicle and ureter and weighed individually. Thereafter, each kidney was divided into four or six segments depending on the experiment; the first was preserved in zinc fixative and the second segment into 10% formalin. Both segments were fixed for 24 hours before being placed into 70% ethanol and subsequently mounted in paraffin to produce zinc or formalin fixed parafiin embedded blocks (ZFPB or FFPE) for immunohistochemistry (ZFPB) and histological purposes (FFPE). Segments three and four were further cut in half for RNA and protein and snap frozen in dry ice before being stored at -80°C. If further segments were required for experimental reasons, the kidney was divided further and segments five and six were used for Legendplex assay and flow cytometry. **Figure 2.1** shows how kidney tissue was cut for analysis depending on segments required for experimental protocols. Blood was allowed to clot for at least 30 minutes and serum was separated off by centrifuging whole blood at 3000g for 10 minutes at 4°C and stored at -80°C.

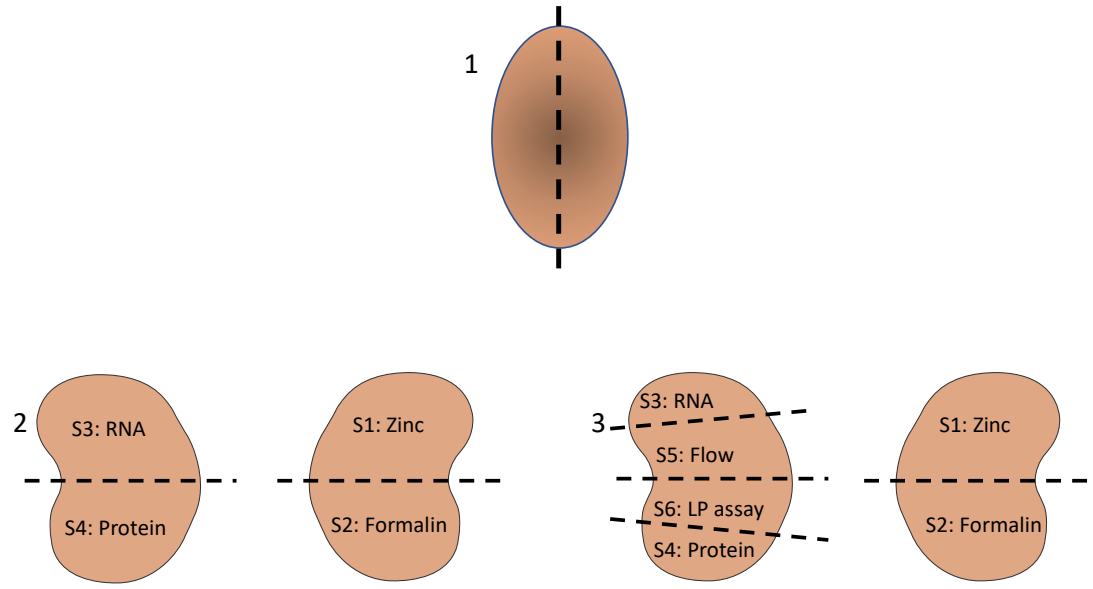

Figure 0.1: Diagram of segments taken during kidney dissection. 1 Whole kidney prior to dissection, dotted line represents the sagittal plane along which the kidney is initially cut into two halves; 2 standard four segment dissection; 3 extended dissection including segments for flow cytometry and legendplex assay.

2.5 In situ hybridisation

FFPE blocks were cut into 3μm sections, deparaffinised and rehydrated with decreasing concentrations of alcohol. Slides were washed and incubated with proteinase K for 30 minutes at 37°C before being prehybridised in hybridisation buffer in a humidified chamber at 60°C for an hour before applying 5' 3' DIG-labeled-214 (Exiqon, Denmark) probe to each slide (final concentration 40nM). The slides were incubated at 60°C overnight before undergoing stringency washing in 1x and 0.2x saline sodium citrate (SSC) and PBS. The sections were then blocked with blocking buffer (0.5% blocking reagent, 10% goat serum, 0.1% tween and 1x PBS) for an hour and incubated with 1:500 anti-Dig-AP Fab (Roche, UK) overnight in humidified chamber at 4°C. Slides were washed with PBS-T and AP buffer. BM Purple solution was added to each section and incubated at room temperature in the dark. Once colour staining was confirmed, the reaction was stopped using PBS-T washes and slides were mounted with aqueous mounting solution.

2.6 Histology

FFPE sections were cut into 3μm sections. Haematoxylin and eosin (H&E) staining was then performed according to laboratory protocol. Sections were deparaffinised with xylene and rehydrated in increasing gradient concentrations of alcohol followed by distilled water. Sections were then stained in haematoxylin for 5 minutes and washed for a further minute. Slides were differentiated in 1% acid alcohol for 30 seconds, washed in tap water then placed in Scott's tap water for 30 seconds. Slides were washed again and counterstained in eosin solution for 5-10 seconds. Finally,

slides were dehydrated in decreasing concentrations of alcohol, cleared in xylene and mounted with coverslips.

Picrosirius red staining was performed after sections were deparaffinised and rehydrated. Slides were washed and stained with Sirius red staining (ab150681, Abcam) and incubated in the dark for 60 minutes. Slides were rinsed twice with acetic acid solution, dehydrated with 100% ethanol dips and mounted.

2.7 Flow cytometric analysis and fluorescence activated cell sorting (FACS)

2.7.1 Sample preparation

Samples from perfused kidneys were weighed and digested using digestion buffer consisting of 4mls of the following per sample: Collagenase 2 (0.425mg/ml, Sigma), Collagenase D (0.625mg/ml), Dispase (1mg/ml, Gibco) and DNase (30μg/ml) for 30 mins at 37°C. Kidneys were then homogenised in gentleMACS tubes using gentleMACS dissociator and filtered using 100μm, 70μm and 40μm sieves. Finally, red cells were lysed using red cell lysing buffer (Sigma) for one minute, washed and spun before being disrupted using MACS tubes. Each sample was resuspended in 300μl FACS buffer.

Spleens were prepared by mashing samples through a 100μm sieve into 10ml ice-cold PBS and spun at 2000rpm for 5 minutes at 4°C. The pellet was resuspended in 1ml 1x cell lysis buffer for 2 minutes, 9mls PBS was added to the sample and spun for a further 5 minutes at 2000rpm at 4°C. The pellet was resuspended in 3mls FACS

buffer and counted using trypan blue to assess cell viability. In total $2x10^6$ cells were plated in round bottomed 96 well plates in a total volume of 200μl per well.

2.7.2 Cell surface staining

To prevent non-specific antigen binding, samples were incubated with 50μl polyclonal IgG for 20 minutes at 4°C. FACS antibodies were diluted to a final concentration in 50μl FACS buffer and incubated with samples in the dark for 30 minutes at 4°C. Single stain controls were used by adding 1μl antibody to 50μl Ultracomp ebeads™ (Invitrogen) compensation beads. Following incubation, cells were washed twice with 150μl FACS buffer and resuspended in 350μl FACS buffer for acquisition. All antibodies are listed in **Table 2.1** below.

Fluorescence minus one (FMO) controls were used by adding all but one antibody to a fluorochrome panel. Both kidney and splenic samples were incubated with antibody and treated as above.

All stained controls were performed by adding all antibodies to spleen and kidney samples and washing as above. Kidney and spleen unstained controls were also plated and washed using FACS buffer as above.

DAPI (1:1000) was added to samples immediately prior to acquisition to assess cell viability.

2.7.3 Transcription factor staining

Samples were plated and incubated with IgG blocking antibody as described above. Cell viability was assessed by adding 50μl of Zombie™ (Biolegend) live/dead stain at 1:100 for 20 minutes at room temperature. Cell were washed using 150μl FACS buffer. Cell surface antibodies were diluted to an appropriate concentration and 50μl of antibody added to each sample and incubated for 30 minutes at 4°C in the dark. Following incubation, samples were fixed using 150μl fixation/permeabilization buffer (eBioscience) and incubated at 4°C for an hour. All antibodies used are listed in **Table 2.2** below.

Intracellular antibodies were diluted to final concentration in permeabilisation buffer and 50μl added to each sample for 30 minutes at room temperature. Cells were washed and spun twice using 150μl permeabilisation buffer and finally resuspended in 350μl FACS buffer for acquisition.

Acquisition was performed using BD Biosciences LSR Fortessa flow cytometry and analysed using FlowJo software (Tree Star).

Table 2-1 Antibodies used for extracellular T-cell panel in flow cytometry

Antigen	Fluorochrome	Clone	Manufacturer	Final Concentration
CD3	AF700	17A2	Biolegend	1:100
CD4	FITC	GK1.5	Biolegend	1:75
CD8	PerCP/Cy5.5	53-6.7	Biolegend	1:100
PDI	PE	29F.1A12	Biolegend	1:100
CD44	eFlour® 450	IM7	eBioscience™	1:150
CD62L	Pe/Cy7	MEL-14	Biolegend	1:100

Table 2-2 Antibodies used for T-cell intracellular transcription factor panel

Antigen	Fluorochrome	Clone	Manufacturer	Final Concentration
CD3	AF700	17A2	Biolegend	1:200
CD4	FITC	GK1.5	Biolegend	1:200
CD8	BUV395	53-6.7	BD Horizon	1:200
Foxp3	BV 421™	MF-14	Biolegend	1:150
GATA	AlexaFlour® 488	16E10A23	Biolegend	1:150
TBET	PerCP/Cy5.5	4B10	Biolegend	1:150
RORγT	PE	B2D	eBioscience™	1:150

2.7.4 Fluorescence Activated Cell Sorting (FACS)

Kidney tissue was digested, filtered and underwent red cell lysis as described above. Following plating, kidney specimens were blocked using 75μl of rat anti-mouse CD16/CD32 (BD Biosciences) at a concentration of 1:50 and incubated for 20 minutes at 4°C. 75μl of antibody mastermix was then added to the cells at twice normal concentration and further incubated for 30 minutes at 4°C in the dark. The cells were then washed with 120-150μl FACS buffer and spun a total of three times. Finally, cells were resuspended in 1ml FACS buffer for sorting. Controls included all-stained and unstained, FMO and single stains on Ultracomp ebeads™ (Invitrogen) with the exception of LTL fluorescein which was stained using cells. DAPI 1:1000 was added just prior to acquisition.

All antibodies used are listed in **Table 2.3** below.

Table 2-3 Antibodies used for FACS staining kidney cells following IRI

Antigen	Fluorochrome	Clone	Manufacturer	Final Concentration
CD3	AF700	17A2	Biolegend	1:100
CD45	APC	30-F11	BD Bioscience	1:100
F4/80	PE Cy7	BM8	eBioscience	1:100
LTL	FITC		Vector	1:100
PDGFRβ	PE	APB5	Biolegend	1:50

2.8 LEGENDplex™ Assay

2.8.1 Preparation of serum samples

Blood was obtained following cardiac puncture and allowed to clot at room temperature for at least 30 minutes before being centrifuged at 3000g for 10 minutes at 4°C. The serum was removed and aliquoted into new eppendorfs before being immediately frozen at 80°C.

2.8.2 Assay procedure

Standard samples were prepared by sequential dilutions of the lyophilized Mouse Inflammation Standard and assay buffer cocktail as per manufacturer's instructions. 25μl of each standard was added to 75μl of assay buffer resulting in a 1:4 serial dilution.

Samples were diluted two-fold with assay buffer to give a final volume of 60μl. Beads and antibodies were also diluted two-fold.

The assay was performed using a 96-well V-bottom plate and samples run in duplicate. 25μl of standard solution was added to control wells and 25μl assay buffer to all other sample wells. Following dilution, 25μl of sample was added to the assay buffer. Finally, 25μl diluted beads mixture was added to each well after being vortexed for 30 seconds to resuspend the beads. The plate was sealed and incubated on a shaker at 800rpm in the dark for two hours at room temperature. After incubation, the plate was spun at 250g, washed with 200μl washing buffer per well and shaken at 800rpm for 1 minute and the process was repeated. 25μl diluted antibody mixture was added to each well (including those with standard solution) and incubated whilst shaking at 800rpm in the dark at room temperature. Then 25μl of SA-PE buffer was added to each well before being incubated for a further 30 minutes at room temperature. Finally, the wells were washed and spun with 200μl washing buffer before being resuspended in 150μl washing buffer for acquisition. Samples were run on BD FACSArray™ and data analysed using LEGENDplex™ Data Analysis software.

2.9 In Vitro Models

TGF-β *In Vitro* model of renal fibrosis.

Cultured rat renal fibroblasts (NRK 49F) and renal epithelial cells (NRK 52E) were seeded in 6 wells plates at $8x10^4$ in complete DMEM and cultured at 37°C degrees and 5% CO_2.

After 24 hours cells were serum starved with DMEM supplemented with 0.2% fetal calf serum and penicillin-streptomycin for 48 hours. Cells were treated daily with 10ng/mL TGF-β (R&D Systems, Minnesota). Total RNA was extracted at 72 and 96 hours (n=3 complete). Control was same volume 0.2% DMEM.

2.10 Immunocytochemistry

Cells were plated on 13mm glass coverslips in 6 well plates and stimulated with TGF-β as described above. Following treatment for 96 hours, cells were fixed with 4% paraformaldehyde for 20 minutes at room temperature, washed twice with PBS, permeabilised in PBS-Tween (PBS-T, 0.1%) for 10 minutes and blocked with 20% heat inactivated goat serum in PBS-T. Primary antibody against α-SMA (1:100, Abcam), E-cadherin (NRK 52E only, 1:1000 Biosciences) and PDGFRβ (NRK 49F only, 1:100) in 20% rabbit serum diluted in PBS-Tween (0.1%) were applied to the cells; same species IgG was used as negative control. The coverslips were incubated in the dark at 4°C overnight. Coverslips were then washed in PBS and secondary antibody applied using goat anti-mouse Alexa Fluro 488 or goat anti-rabbit Alexa Fluro 488.

2.11 Immunofluorescence

Zinc fixed sections were cut to 3μm, deparaffinised and rehydrated. Antigen retrieval was performed by immersing sections in boiling 0.01M sodium citrate buffer (pH6) for 10 minutes. Slides were then washed in PBS-T and blocked with PBS-T containing 20% goat serum for 30 minutes. Slides were incubated with 1:100 primary antibody to CD3e (abcam) in PBS-T diluted with 20% goat serum overnight at 4°C. Same concentration rabbit IgG was used as control. The following day, sections were washed and incubated with goat anti-rabbit Alexa Fluro 488 1:500 in PBS (Life Technologies) in the dark for an hour at room temperature. Finally, slides were washed and mounted using 4',6-diamidino-2-phenylindole Prolong Gold mounting media (DAPI, Life Sciences).

2.12 RNA Extraction

Total RNA was extracted using miReasy kit (Qiagen, Germany) as per manufacturer's instructions. Tissue was lysed using 700μl Qiazol and homogenised with steal beads (Qiagen, Germany) using Tissue Lyser II (Qiagen) for 1 minute. Cell samples were lysed using 700μl Qiazol and homogenized by vortexing for 30-60 seconds.

Samples were centrifuged at 12 000g for 15 minutes at 4°C and the clear aqueous phase was pipetted off and mixed with 550μl 100% ethanol. The mixture was placed through the miReasy column and washed with 700μl RWT buffer provided. Each sample was treated with DNase 1 (Qiagen) for 15 minutes at room temperature to remove genomic contamination. The columns were washed twice with 500μl RPE buffer and dried. 35μl RNase free water was passed through each column twice to

make to the final RNA concentration. RNA was quantified using Nanodrop and diluted to produce 200ng-1000ng cDNA and 2ng/μl for miR reverse transcription.

For T-cell ex vivo experiments, the miReasy microkit (Qiagen) was used because of low concentrations of RNA from these cells. Up to $1x10^6$ cells were used per column and protocol was followed as above with the exception of an additional wash with 80% ethanol after the second RPE wash. RNA was extracted in a total of 14μl per sample.

For human serum samples, RNA was extracted from 200μl serum following manufacturer's instructions using miR-39 from *C. Elegans* as a spike in control.

2.12.1 RNA extraction following FACS

Following FACS, cells sorted into 350μl RLT buffer at room temperature. RNA was extracted using RNeasy micro kit which has been amended for miR extraction. Briefly, cells were homogenized by vortexing for 10 seconds, the lysate pipetted onto a gDNA Eliminator spin column and centrifuged at 10,000g for 30 seconds. The gDNA column was discarded and 1.5 times volume pure ethanol was added to the lysate and placed on a RNeasy MinElute column. The column was spun at 10,000g for a further 30 seconds, 700μl RWT buffer was added and the extraction continued as per standard RNA extraction for miRs.

2.13 Quantitative real-time PCR

All primers and probes were purchased from Applied biosystems. All qrt-PCR was performed in duplicate in 384-well plates using QuantStudio™ 5 Real-Time PCR

system (Applied Biosystems™). Results were calculated using $2^{-\Delta\Delta CT}$ method and normalised to species specific control miR or GAPDH for gene expression.

2.13.1 MiR Expression

Following RNA extraction and dilution to 2ng/μl, miR expression was quantified using RT-PCR, according to laboratory protocol. Briefly, miR-reverse transcription involved addition of the following solutions in the quantities shown below (per sample run):

DNTPS 100nM 0.075μl; Multiscribe 0.5μl; 10x RT buffer 0.75μl; RNAse inhibitor 0.095μl; RNase free water 2.08μl; primer (5x RT) 1.5μl.

Up to 7.5ng of RNA was then added to the mastermix and run on thermocycler to produce miR-RT product. Specific Taqman probes were used for RT-PCR by combining the following; Taqman mastermix 5μl per sample, water 3.1μl per sample and primer (20x) was combined with 1.4μl miR-RT product.

Each reaction was amplified in duplicate and results calculated using $2^{-\Delta\Delta CT}$ method and normalised to species specific control (human RNU48, rat U87, mouse U6). MiR primer sequences are listed in **Table 2.4.**

MiR expression in human serum samples was assessed by using 200μl serum and miR-39 used as a spike in control.

Table 2-4 Taqman probes used for examination of miR expression

MicroRNA (miR)	Species	Taqman Assay ID
hsa-miR-214-3p	Human/mouse	002306
hsa-miR-214-3p	Rat	000517
hsa-miR-21-5p	Human/mouse/rat	000397
hsa-miR-29c-3p	Human/mouse/rat	000587
hsa-miR-199a-5p	Human/mouse/rat	000498
hsa-miR-199a-3p	Human/mouse/rat	002304
U6 snRNA	Mouse	001973
U87	Rat	001712
cel-miR-39-3p	Human	000200

2.13.2 Gene expression

cDNA was prepared from RNA diluted to lowest concentration of RNA extracted for each cell line or serum RNA concentration to a maximum concentration of 200ng/μl. cDNA was prepared by loading up to 1000ng/μl RNA per reaction and run on thermocycler.

Specific gene expression primers in **Table 2.5** listed below were used for PCR quantification of gene expression. Each reaction was normalised to species specific GAPDH as endogenous control.

Table 2-5 Taqman probes used for examining gene expression

Gene	Species	Taqman Code
Acta2	Mouse	Mm00725412_s1
Ccl2	Mouse	Mm00441242_m1
CD68	Mouse	Mm03047343_m1
Col1a1	Mouse	Mm00801666_g1
Col3a1	Mouse	Mm01254476_m1
Col4a1	Mouse	Mm01210125_m1
GAPDH	Mouse	Mm999999915_g1
Havcr1	Mouse	Mm00506686_m1
CD3e	Mouse	Mm00599684_g1
IL10	Mouse	Mm00439616_m1
IL-1β	Mouse	Mm01336186_m1

Gene	Species	Taqman Code
IL-6	Mouse	Mm00446190_m1
PDGFR-β	Mouse	Mm00735546_m1
PTEN	Mouse	Mm00477208_m1
TNF	Mouse	Mm00443258_m1
BCL2	Mouse	Mm00477631_m1
BAX	Mouse	Mm00432051_m1
GAPDH	Rat	Rn01462662_g1
Col1a	Rat	Rn01463848_m1
Col3a	Rat	Rn01437681_m1
Cdh1	Rat	Rn00580109_m1
Acta	Rat	Rn01426628_g1

2.14 Human studies/samples

Patients with renal grafts undergoing clinically indicated biopsies more than three months post-transplantation were recruited to this study registered at the University of Edinburgh, no 18/SS/0053. Serum and urine samples for miR-214 expression were obtained prior to biopsy and correlated with presence and severity of fibrosis.

2.15 Statistical Analysis

All statistical analyses were performed using Graphpad Prism 8.0e (Graphpad Prism, Inc). Data was tested for normality and for comparison of two groups that matched parametric data requirements, a two tailed unpaired t-test was used. For three or more groups where groups were compared to one control group, a one-way ANOVA with a Dunnett's test for multiple comparisons was used. For experiments with three groups or more and with multiple comparisons between groups, a one-way Anova was used with Tukey's correction for multiple comparisons. A statistical probability <0.05 was considered significant. Significance is depicted as follows: *$p<0.05$, **$p<0.01$, ***$p<0.001$, ****$p<0.0001$.

Chapter 3: The murine model of chronic allograft damage

3.1 Introduction

The murine model of renal chronic allograft damage was developed Lorna Marson and has been fully validated in the literature[280]. It involves transplantation of a donor kidney from a C57bl/6^{BM12} mouse into a C57bl/6NCrl recipient, resulting in a single class II mismatch and the typical histological appearance of interstitial fibrosis and tubular atrophy in keeping with chronic allograft damage over an 8-12 week period following transplantation. Similarly, Win et al demonstrated histological appearance of chronic vasculopathy in a cardiac transplantation model using the same strain combination[281]. The model of renal transplantation has previously been used by our group to demonstrate a potential role for galectin 3[282] and intrarenal B cells[122] in the pathogenesis of CAD.

A murine model of renal transplantation was first described in 1973 by Skoskiewicz et al[283]. The advantage of the murine model is that commonly bred strains can be utilised to model various transplant disease states, and multiple research groups have successfully performed murine renal transplantation to model acute rejection, antibody mediated rejection, T-cell related changes and interstitial fibrosis and tubular atrophy[202,284]. Several authors have described the technical aspects of the procedure including pre-operative and post-operative care to increase survival following surgery. The technique used by our group has been adapted over time to ensure a reproducible model established for the purposes of our research[280] .

3.2 Development of the model

Murine transplantation is a technically challenging model, requiring advanced microsurgical skills and acquisition of knowledge regarding best murine peri-operative care, recovery techniques and general animal husbandry. Great time and care were taken in developing microsurgical technique and in particular developing efficiency of speed and movement to reduce the amount of time taken to perform the vascular anastomoses, thus reducing the period of kidney ischaemia and overall operative time. The technique described previously has been slightly adapted to suit personal preference.

Figure 3.1 describes the critical steps involved in the donor and recipient procedures. The development of chronic allograft damage involves transplantation of the left kidney from a male C57bl/6^{BM12} mouse into a male C57bl/6NCrl recipient; isograft transplants from a male C57bl/6NCrl into a recipient of the same strain acted as controls. It is important to note that the model is not transplant dependent and the recipient's left kidney is left *in situ* to allow the animal to recover without renal impairment.

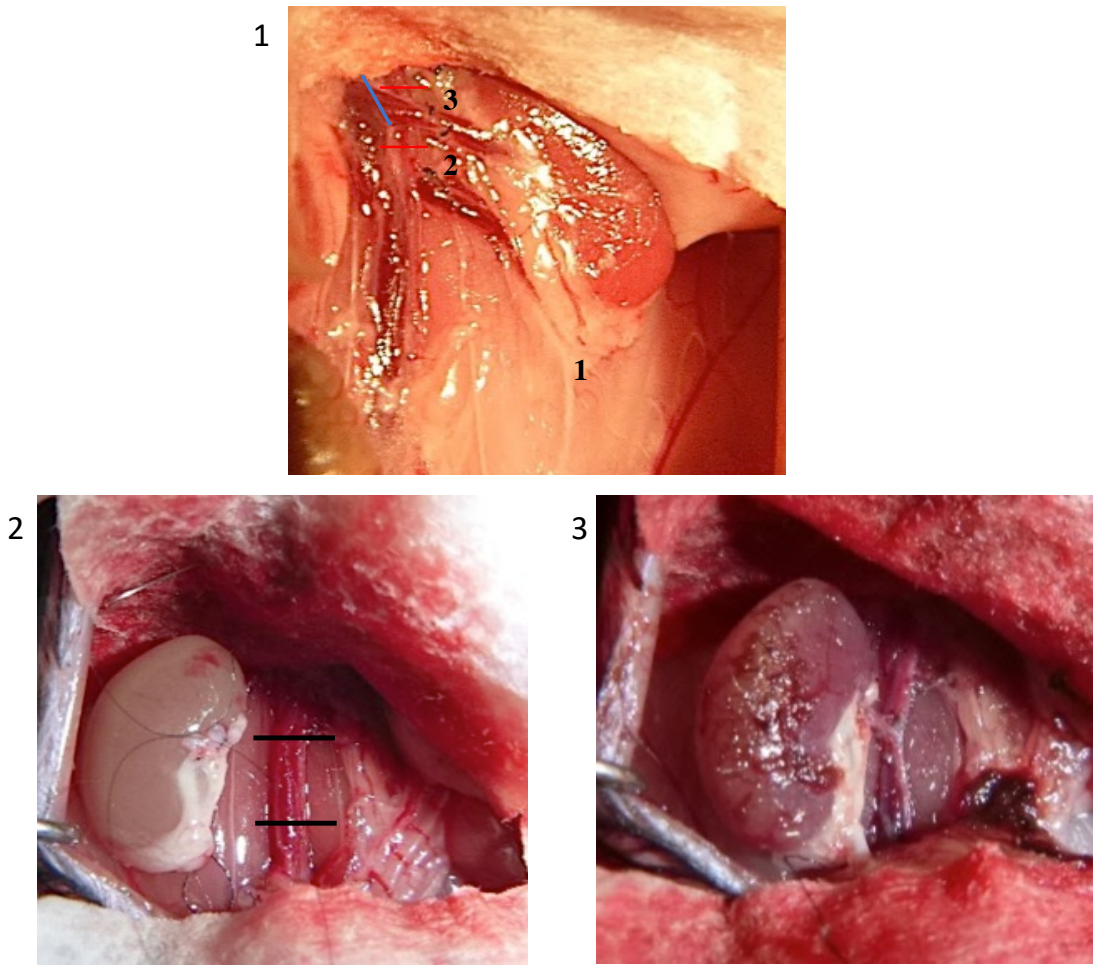

Figure 3.1 Captured images of murine renal transplantation. **1**. Donor kidney in situ: Divided ureter close to the bladder (1). Dissected and divided gonadal (2) and adrenal (3) veins. The left renal vein is divided at the junction with the vena cava (blue line), and the aorta divided above and below the left renal artery (red line); **2**. Recipient preparation prior to implantation: The clamps are placed across the vena cava and aorta (black line). The donor vein is anastomosed onto the vena cava and the donor aortic patch onto the recipient aorta; **3**. The transplanted kidney immediately following reperfusion: The clamps are removed; the transplanted kidney is reperfused and as a result changes colour. Following the vascular anastomosis, the ureter is anastomosed to the bladder. using a three-point fixture technique**.**

3.2.1 Donor Nephrectomy Surgery

Donor animals were anaethestised by using intraperitoneal anaesthetic agents as described in **Chapter 2.3.1** and given 1ml of normal saline subcutaneously before the procedure. The abdomen was shaved, and skin prepared using chlorhexidine solution (Animal Care Ltd). A laparotomy incision was made, and the bowel retracted to the animal's right. The left ureter was divided close to the bladder. The adrenal and gonadal veins are ligated at the junction of the left renal vein. The infra-renal aorta and vena cava were dissected sufficiently to be able to pass a tie around the proximal infra-renal aorta and around the distal aorta and vena cava. The supra-renal aorta was also cleared of tissue to allow placement of a tie. Once tied, the left kidney was isolated from the arterial system. Particular attention was paid to haemostasis throughout the procedure to minimise blood loss.

Just prior to removing the left kidney, 5 units of heparin was administered via intravenous injection (5 units in 500μl injected via penile vein). Once sufficient time was allowed for circulation of the heparin, the distal vena cava and aorta, and proximal aorta were tied off, isolating the kidney from the arterial system. The infra-renal aorta was injected with 1ml of University of Wiscosin Solution (Belzer, UW), replacing the blood volume in the isolated kidney. Immediately following this, the left renal vein was transected at its junction with the vena cava, the proximal aorta was divided leaving a tie in place, and the distal aorta divided leaving the proximal aorta untied for the arterial anastomosis.

The mouse is immediately terminated by cervical dislocation. The kidney is then dissected from any remaining intra-abdominal attachments and placed in ice-cold solution.

3.2.2 Transplant Recipient Operation

The recipient mouse was anaesthetized using inhalation agents (isoflurane, Abott Labratories Ltd) in accordance with the local veterinary protocols as described in **Chapter 2.3.1**. Induction of the recipient animal was performed whilst the donor kidney was prepared for transplantation, reducing the cold ischaemia time before implantation. Prior to surgery, animals received 1ml saline and 50μl buprenorphine analgesia via subcutaneous injection.

The animal was anaesthetized as described above, the abdomen shaved, and skin prepared using chlorhexidine. The abdomen was opened via a laparotomy incision and the right nephrectomy performed by ligating and transecting the right renal vascular pedicle and the distal ureter. The vena cava and abdominal aorta were dissected clear of tissue and tributaries tied off to prevent back-bleeding during the anastomosis. 5000 units of heparin were administered via the posterior penile vein and the VC and aorta were clamped after sufficient time was given for circulation. The VC was opened in a longitudinal manner, flushed and an end-to-side continuous anastomosis between the donor renal vein and recipient VC was performed using double ended 10.0 nylon suture (Ethicon, New Jersey). A small aortic patch was excised from the recipient's anterior aorta, flushed with heparinised saline and an-end-to-side anastomosis was performed between the donor's distal aorta and recipient aorta using 10.0 nylon (Ethicon, New Jersey). Once the anastomoses were completed, the vascular clamps were removed and bleeding controlled with Surgicel (Ethicon, USA). Next, the bladder was identified and both lateral walls were opened with a 21-gauge needle and the donor ureter pulled through into the bladder. The ureter was then fixed to the bladder wall using three-point interrupted suture fixation technique and the defect closed with an interrupted 10.0 nylon suture (Ethicon, New Jersey).

On completion of the transplant, the abdominal linea alba is closed with continuous 5.0 polyamine (Vicryl Rapide, Ethicon, New Jersey) and the skin approximated with clips.

The animal received 1ml bolus of saline via subcutaneous injection. The animal was then placed in a warm box at 28-30°C for 24-48 hours post-operatively.

3.2.3 Post-operative Care

Recovered animals were checked at four hours post-operatively; any mouse in distress or that had not recovered sufficiently was culled. A post-operative checklist for the transplant model was utilised and is shown in **Figure 3.2**.

Post-Operative Monitoring **Date:**

Procedure: Renal Transplant

Mouse number+strain Combination	DATE	TIME	INITIAL	COMMENTS	RED FLAGS (letters see below)

Mouse to be monitored at

- 1 hour post-op
- 4 hours post-op
- Day 1 at 0800 & 1700
- Day 2 to 7 at 0800 and additionally if any cause for concern

Red flag codes

A: Muscle rigidity, lack of muscle tone
B: Dehydration/Skin tenting/sunken eyes
C: Twitching, trembling, tremor
D: Vocalisation (rare)
E: Redness/swelling around surgical site
F: Increased salivation
G: Increased/decreased movement
H: Unkempt appearance (erected, matted or dull haircoat)
I: Abnormal posture or positioning (e.g. head-pressing, hunched back)
J: Decreased food or water consumption
K: Weight loss
L: Self imposed isolation or hiding
M: Self-mutilation or gnawing at limbs
N: Rapid breathing, opened mouth breathing or abnormal breathing
O: Limb swelling

Score 3 or more or limb paralysis >12 hours, cull mouse and contact the responsible person

Figure 3.2 Murine transplant post-operative monitoring sheet

Development of the model requires a significant learning curve, first of all training on cadavers and refining basic techniques before moving into live animals. During this period, animals were either culled routinely by cervical dislocation at the end of the procedure if there was prolonged anastomotic time or following a significant intra-operative complication that would compromise recovery or survival. The initial anastomotic times were consistently over 60 minutes however this was reduced this to a mean of 24 minutes for the last 30 procedures as shown in **Figure 3.3**. The survival rate for the animals also increased with experience and reduced operating times. In total 57 complete procedures were performed in live animals corresponding to approximately 200 hours operating on this model.

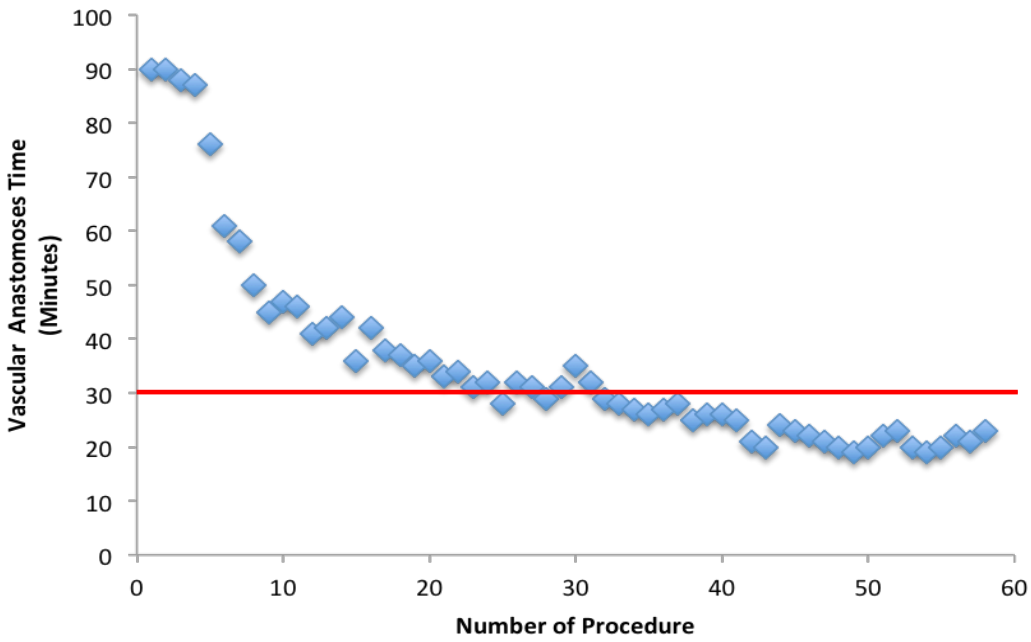

Figure 3.3 Anastomotic times. Graph demonstrating anastomotic times in minutes for each live procedure of the transplant murine model performed. The red line indicates 30 minutes; vascular anastomotic time below 30 minutes is considered sufficient to achieve perfusion of the transplanted kidney with minimal hind limb paralysis secondary to vascular thrombosis or spinal ischaemia.

A significant complication of clamping the aorta includes hind limb paralysis, either from thrombosis of the distal aorta or spinal ischaemia. Rates of hind-limb paralysis in this model are normally <3% with an overall survival rate of >70% of those animals that survive beyond the initial 48-hour recovery phase. Despite improvements in reducing the anastomotic time, hind limb paralysis occurred in 90% of recovered animals.

As part of the protocol, mice were given 5 units of heparin via the penile vein to reduce the risk of thrombi developing whilst the vascular clamps were in place. This is standard practice in most vascular operations performed in humans where there is a balance of risk between vascular thrombosis and bleeding. In this model, there can be significant bleeding after completion of the anastomosis, affecting recovery and which can be fatal if the animal has already suffered from substantial bleeding as part of the recipient preparation. One step that was taken to reduce the rate of hind-limb paralysis was to titrate the dose of heparin incrementally from 5 to 7 units. In animals given 6 units, there was no difference in the rates of hind limb paralysis and in animals given 7 units, it was evident this resulted in more bleeding and in termination of the procedure.

Another significant step taken to overcome hind-limb paralysis was adjusting the approach to the anastomosis after seeking advice from supervisors and previous students who had performed the model. The most significant change was in the anastomotic technique; previously the renal artery was harvested in continuity with the donor aorta and the anastomosis was performed between the proximal end of the aorta to the recipient aorta. The technique was modified to one using an aortic patch containing the renal artery, where the donor aorta is cut longitudinally along its length (**Figure 3.4**). This technique is potentially advantageous in that the size of the patch could be adjusted after removing the donor kidney and there was as wider aortic

lumen after completion of the anastomosis. It was critical that the sutures were not tied too tight on completion of the anastomosis as this could result in narrowing of the aortic lumen thereby increasing the risk of distal aortic thrombosis. The clamps were released immediately prior to completion of the anastomosis to flush out any thrombi that may have formed as. Overall, these changes resulted in a discernable increase in perfused kidneys.

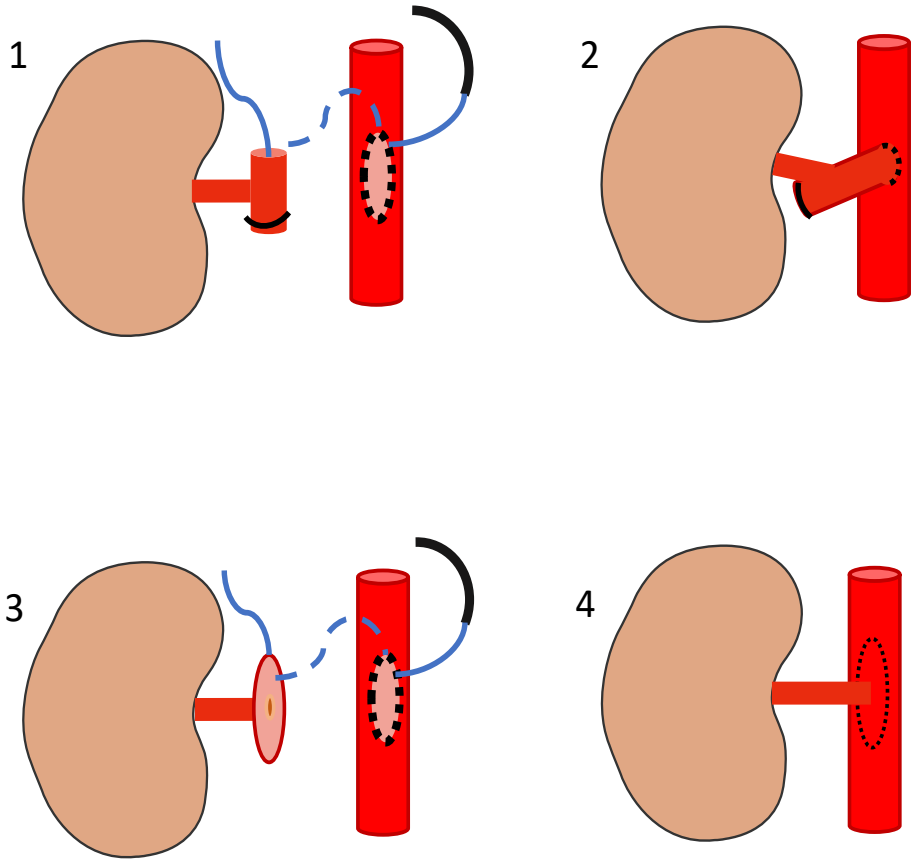

Figure 3.4 Diagram of modifications to the arterial anastomotic technique. **1-2** represent an end-to-side anastomosis of the proximal donor aorta to recipient aorta using continuous suture, the renal artery is in continuity and the distal aorta is tied off with 9.0 vicryl; **3-4** show modified technique using an aortic patch with the renal artery in continuity, which is anastomosed to the recipient aorta using continuous suture.

The mice used were aged between 8-12 weeks, the rationale for this being that younger animals are too small to allow for an adequate vascular anastomosis and older animals have increased adiposity making the procedure more difficult, particularly with regards to fine dissection and thus increase risk of bleeding. During the development of the model, animals at either end of this age range were used to discern if this had any effect on outcome. Unfortunately, this was not the case and there was no difference in outcomes between younger and older mice.

After approximately 60 procedures on live animals there was no improvement in the model over a 12-month period. At this point, it was evident that there was little time left to perform all the planned transplant experiments and therefore after careful consideration of time constraints, a decision was made to utilise a different model and opted to use a model of renal ischaemia reperfusion injury. This model is beneficial in that it can be used to interrogate the role of miR-214 at multiple time points after injury including acute renal injury and its effects on fibrosis. The ischaemia reperfusion injury model is described in more detail in **Chapter 4**.

3.3 Discussion

The murine model of chronic allograft damage is technically very challenging, and despite spending approximately 200 hours performing the model, few animals survived beyond the first 4 hours post-operatively. Martins et al demonstrated that this murine transplant requires a large learning curve and competency in this model is usually achieved after 40 procedures[285]. After 57 transplant procedures were performed there was demonstration of the 'learning curve' as anastomosis times improved and more animals survived following surgery. It stands to reason that with

increasing technical complexity, the demand on the operator is greater and there is a significant chance of encountering problems that can affect the outcome of the procedure, whether this is poor graft perfusion, hind-limb paralysis or death. Here this was confounded by having to perform both donor and recipient procedures independently, which may have prolonged the time taken to become competent in the model, particularly when considering the vascular anastomosis which is critical to the success of a transplant. Performing the model independently also added extra time between procedures where the kidney was not perfused and may have impacted on vascular perfusion in the graft, particularly where there was sub-optimal perfusion of the donor kidney *in situ* prior to its retrieval.

As described above, the main issue encountered with the model was hind limb paralysis. Hind limb paralysis is most commonly secondary to either vascular thrombosis or spinal cord ischaemia due to prolonged vascular clamping to allow venous and arterial anastomosis. As part of the learning curve, there was a significant decrease in anastomosis times with increasing operative experience; in the last 30 procedures the mean anastomosis time was 24 minutes. The literature shows that anastomotic times less than 35 minutes are associated with improved survival in this model, where the rates of hind limb paralysis are minimal[284,286]. Therefore, the most likely cause of hind-limb paralysis in animals where the anastomosis was less than 30 minutes was mostly likely to be due to vascular thrombosis rather than spinal cord ischaemia.

Several steps were taken to overcome hind limb paralysis, the most critical of which involved modification of the arterial anastomosis. The original model developed by Lorna Marson used an end-to-side donor to recipient aorto-aortic anastomosis with the renal artery in continuation with the donor aorta. This can be challenging as the donor aorta could be difficult to handle without damaging the vascular endothelium,

which is to be avoided in preventing thrombosis in the graft. Modifying the technique involved changing the anastomosis so the donor renal artery was on an aortic patch which was anastomosed to the recipient aorta. This technique was also utilised by Tse et al who published the model describing the modified technique which is more representative of the 'Carrell patch' utilised in human renal transplantation[280]. Following this modification, there was a discernable increase in perfused donor kidneys, however this may have contributed to potential 'steal syndrome', where flow to the hind limbs was sacrificed because of increased flow through the transplanted kidney thus resulting in hind-limb hypoperfusion. The technical modifications are reflective what is used in human renal transplantation and other vascular surgery operations. Particular care was also taken in handling tissues and avoid damaging the vascular endothelium, flushing the aorta and ensuring sutures are not tied too tight.

Given time, another consideration would be to utilise a rat model, which may be technically easier given their larger size. Other groups have published successful transplants in a rat model and one group quoted an 87% survival rate at two weeks post procedure. Like the mouse model, anastomotic times of less than 30 minutes are critical to success[287,288].

The problem of hind-limb paralysis was approached systematically and modified multiple aspects of the procedure. The most likely explanation to account for a high rate of hind-limb paralysis is likely to be due to a combination of factors that may have given time been overcome in order to achieve a reproducible model. This model encompasses a significant learning curve and as an independent operator the increased surgical time resulted in a longer period before competency was achieved which may represent a significant contributory factor to the model not succeeding within a reasonable timeframe.

Chapter 4: Characterisation of the murine model of renal ischaemia reperfusion injury

4.1 Introduction

Following on from the difficulties of establishing the murine model of chronic allograft damage, a decision was made to utilise a model of renal ischaemia reperfusion injury. Ischaemia reperfusion injury (IRI) is relevant to solid organ transplantation as every graft is subjected to a period of cold and warm ischaemia prior to reperfusion. In kidney transplantation, severe or prolonged ischaemia can negatively affect long-term outcome and increases the risk of DGF and acute rejection[23,29,30]. The pathogenesis as described in the introduction is complex but essentially results in activation of the innate and adaptive immune systems in response to acute injury. The reparative response can be maladaptive because of ongoing inflammation within the interstitium leading to upregulation of TGF-β expression, myofibroblast differentiation and extracellular matrix deposition[82,139,289]. Expansion of the interstitium results in a vicious cycle of ongoing hypoxia, inflammation and TGF-β upregulation exacerbating the maladaptive response[290,291]. Ultimately this results in interstitial fibrosis and tubular atrophy[136].

Modelling IRI is therefore beneficial in furthering our understanding of its pathogenesis and dissecting the effects of ischaemia on individual cells and key mediators. Importantly, IRI can be used to model early injury and progression towards fibrosis, which is useful when attempting to decipher the role of a particular mediator in disease progression and lends itself to cover the scope of this project.

The aim of this chapter is to characterise a suitable model of renal IRI in order to determine whether miR-214 has a role both early injury and later fibrosis. This model will be used to test the hypothesis that miR-214 is upregulated in early injury and later fibrosis following renal IRI.

4.2 Animal model of early renal ischaemia reperfusion injury

Our group has experience in using a murine model to successfully model IRI in the acute post-injury phase and as a method of inducing renal fibrosis[239]. Animal morbidity is low and there is an expected survival rate of >90%. The severity of injury in early IRI is assessed using functional and structural parameters such as biochemical analysis of serum urea and creatinine and quantification of acute tubular necrosis (ATN) using histological techniques.

Ischaemia reperfusion injury severity is nominally defined as mild, moderate and severe and can be adjusted by increasing ischaemia times and/or clamping one or both kidneys. Animals subjected to bilateral ischaemia inevitably develop renal failure that can hinder recovery beyond the early phase of inflammation and lead to significant mortality. This however can be avoided by utilising a unilateral occlusion model, which is particularly beneficial in studying the effects of IRI on renal fibrosis without the deleterious effects of significant renal failure.

IRI has been used in many different species to model renal injury but common *in vivo* models include mouse, rat and pig. MiR-214 is conserved across species so technically any of these models can be used in this project. Given previous experience in the mouse transplant model and the group's experience of murine renal IRI, a decision was made to utilise a mouse of renal ischaemia reperfusion injury using 8-10 week old male C57BL/6 mice.

4.2.1 Surgical technique involved in the murine renal IRI model

The animal was anaesthetised by inhalation and given analgesia as described in **Chapter 2.3.1.** The mouse was placed on a specialised heating mat that maintained temperature of 37°C using thermostatic control and measuring the animal's body temperature via a rectal thermometer. After shaving and cleaning the abdomen with chlorhexidine, the abdomen was opened via a midline laparotomy, and the intestines carefully retracted to the animal's left. The liver was gently retracted upwards to reveal the right renal pedicle and the renal vessels were dissected free of surrounding tissue. The pedicle was clamped, taking care to avoid damaging surrounding tissue-particularly the peripheral nerve running immediately behind the renal pedicle-or clamping the adrenal vessels. The intestines were then gently replaced to the animal's right and the left renal pedicle dissected free of the surrounding tissues distal to the adrenal and gonadal veins which are tributaries of the left renal vein. The left renal pedicle was then clamped, again taking care to avoid damaging surrounding tissue and intestines returned to anatomical position; a sterile gauze swab was placed over the animal to reduce heat loss during the renal ischaemia time. Successful ischaemia is characterised by a change in colour of the kidney; immediately following clamping the kidney is pale but becomes a deep purple with increasing ischaemia. Clamps were removed after a specified time and the kidney is reperfused and subsequently returns to normal colour. On completion of the procedure, the abdominal wall closed with 5.0 Vicryl Rapide (Ethicon, New Jersey) and skin opposed with surgical clips (Interfocus, Linton, UK).

In unilateral procedures, only the right renal pedicle was clamped; this decision was made because the left renal vein has multiple tributaries making it slightly more difficult to clamp than the right. If there was suboptimal ischaemia demonstrated by patchy colour changes or poor reperfusion on release of the clamp, the animal was

terminated immediately by cervical dislocation under anaesthesia. Sham operated animals underwent the same procedure with exception of clamping the renal pedicle(s). All animals received the same post-operative care and were weighed regularly. **Figure 4.1** demonstrates the key technical steps involved in the model.

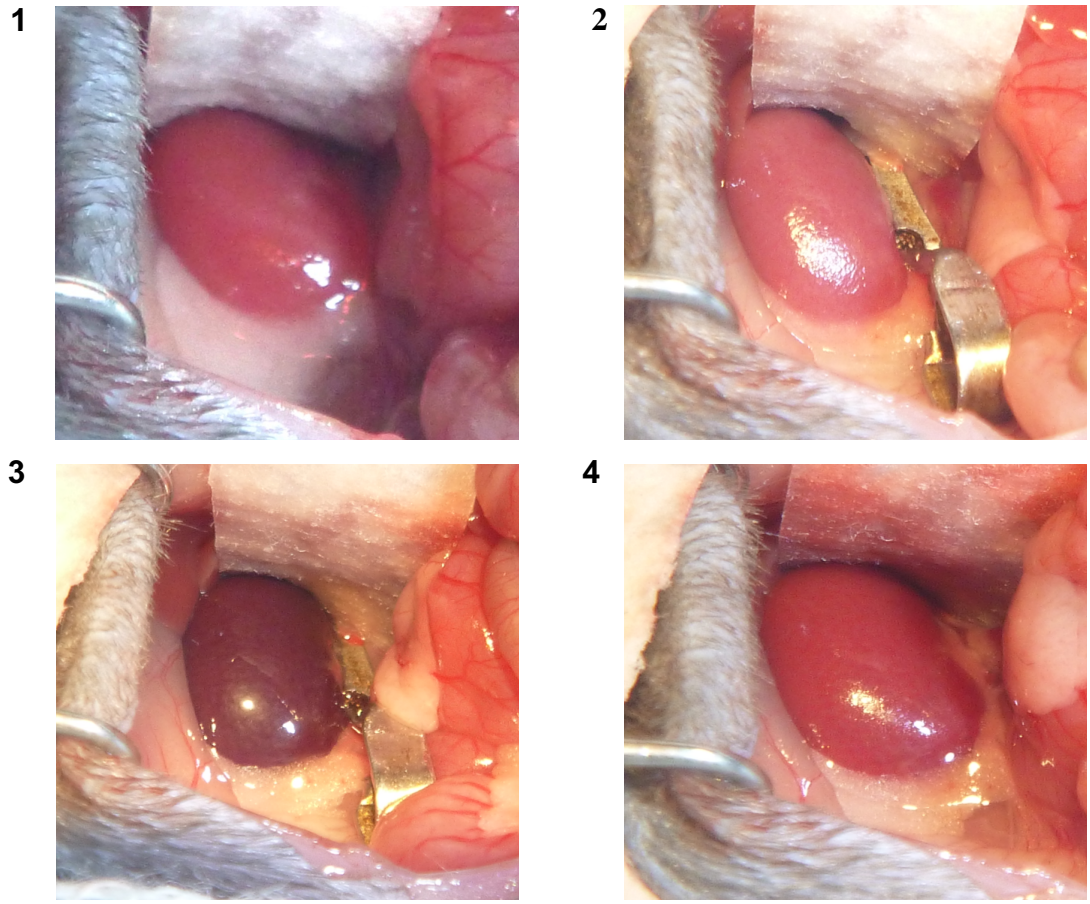

Figure 4.1 Murine model of renal ischaemia reperfusion injury (right kidney). **1**: A laparotomy is performed, the bowels retracted to the animal's left and liver upwards to reveal the right kidney. The renal pedicle (including the renal artery and vein) are dissected free of surrounding tissue. **2**: Vascular clamp is applied to the renal pedicle, note the kidney is paler than the pre-ischaemic kidney pictured in A. **3:** Right kidney following 18 minutes of ischaemia 4: right kidney immediately following release of the vascular clamp.

Beyond the length of ischaemia, other technical aspects of this procedure can alter outcomes. Groups have shown that the temperature of an animal during the procedure significantly affects the transcriptome and therefore functional outcomes. Le Chef et al showed that performing a unilateral procedure in hypothermic conditions down to 32°C resulted in renal protection compared to normothermic conditions[250] and other authors have commented on the variability of results after significant changes in their operating environment resulted in cooler ambient temperatures[242,278]. In the model used here, all animals were warmed in specialised mats which encompassed the mouse and maintained normothermia by thermostatic control to avoid variability in the results.

4.2.2 Bilateral renal ischaemia results in significant renal injury

As a proof of concept experiment, a bilateral model of IRI was utilised where both kidneys were rendered ischaemic for 18 minutes and animals culled at 48 hours. Evidence from the literature has demonstrated that miR-214 was upregulated early following renal IRI in mice[182]; the primary aim of this experiment was to reproduce these findings and therefore examine whether the model was suitable to be used to test the hypothesis that miR-214 contributes to acute injury and inflammation following IRI. Its role in early injury has not been examined and thus there is a potential novel role in renal injury and inflammation.

Animals subjected to 18 minutes of bilateral renal ischaemia had a significantly higher mean serum creatinine compared to sham operated controls (mean 129 μmol/l vs 18 μmol/l respectively, $p=0.026$) and serum urea (42.6mmol/l vs 8.3mmol/l respectively, $p<0.001$, **Figure 4.2**), demonstrating a significant biochemical renal injury in this

model. There was some variation in serum creatinine between animals suggesting that some results were suboptimal, potentially due to a degree of learning curve associated with the model. In particular, there may be variation in renal vascular anatomy that wasn't appreciated at the time of surgery or a delay in clamping the second kidney meaning there was a period where one kidney maintained perfusion, thereby reducing overall ischaemia time.

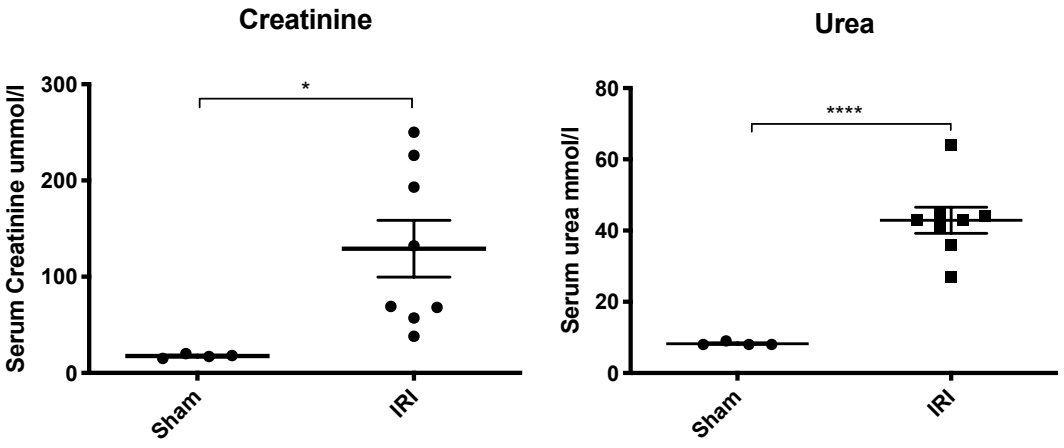

Figure 4.2 Assessment of functional injury following IRI. Male C57Bl/6 mice were subjected to 18 minutes of bilateral IRI and culled at 48 hours. Comparison of serum creatinine (left) and urea (right) in animals subjected to IRI (n=8) and sham operated controls (n=4) at 48 hours following injury. Line indicates mean ± SEM each group. * $p<0.05$ ****$p<0.0001$, Student's t-test

Structural integrity was assessed using a historical scoring system of acute tubular necrosis (ATN) within the outer medulla of each kidney; this area is particularly injured in this model as it is susceptible to hypoxia. Paraffin sections were stained with Haemotoxylin and Eosin (H&E) and scored on 8 non-overlapping field views of the outer medulla captured at 400x magnification. Tubules were scored as either healthy or necrotic based on morphological appearances and ATN was scored as the percentage of necrotic tubules present within the medulla of each kidney.

Sham kidneys had a normal tubular structure within the outer medullary stripe. Healthy tubules are defined as intact with uniform cells forming a lumen with an intact brush border (**Figure 4.3 top panel**). Kidneys subjected to ischaemia demonstrated a significant increase in necrotic tubules defined as tubules that have lost their normal structural integrity (**Figure 4.3 bottom panel**). Necrotic tubules exhibit disruption of the brush border, significant cell loss and abnormal cell morphology; often the lumen appears haemorrhagic or filled with cellular debris known as casts.

Quantification of ATN showed a significantly greater ATN score in animals subjected to ischaemia versus sham animals (mean necrotic tubules 67.41% ± 4.266 vs 2.250% ± 1.315 respectively, $p<0.0001$, **Figure 4.3, B**) representing a moderate model of ischaemia in these animals.

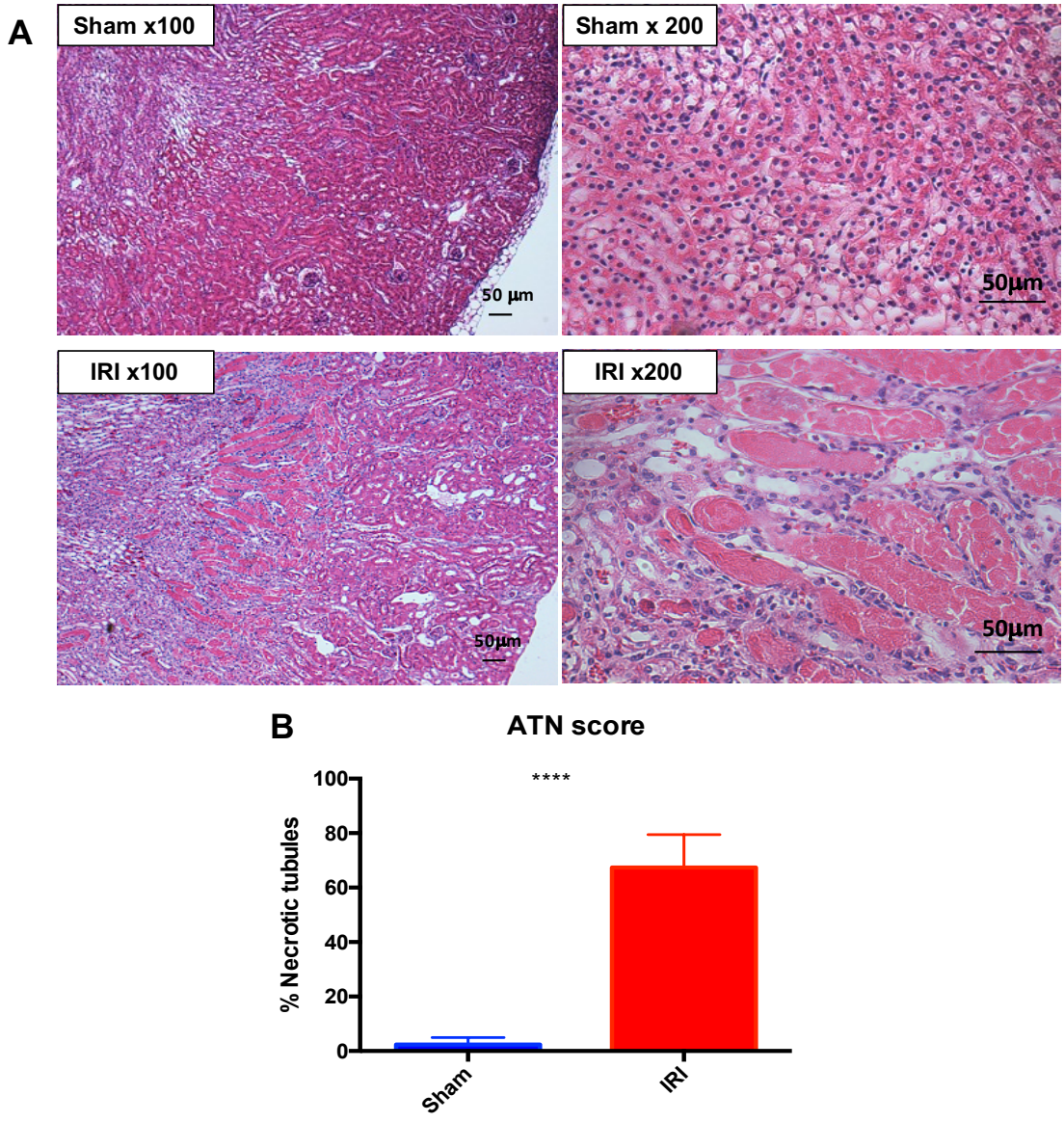

Figure 4.3 Structural injury following bilateral IRI. Male C57Bl/6 mice were subjected to 18 minutes of bilateral IRI (n=8) or sham laparotomy (n=4) and culled at 48 hours. Haemotoxylin and eosin stains of a sham kidney (top panel, left x100 magnification, top right x200 magnification) and kidney 48 hours following 18 minutes of ischaemia (bottom panel, left x100 magnification, right x200 magnification); B Quantification of ATN in IRI (n=8) vs sham (n=4), represented as mean ± SEM, Student's t-test **** p<0.0001

4.2.3 Ischaemia reperfusion injury is associated with increased pro-inflammatory gene expression

A panel of genes was chosen based on characterisation of acute kidney injury secondary to IRI[82]. Amongst these was a well-known mediator of kidney tubular injury, KIM-1, which is not expressed in healthy tubules but is upregulated shortly after injury. This showed the greatest increase in expression compared to sham operated controls where there was an 80.2-fold increase compared to controls (normalised to GAPDH, $p<0.0001$, Student's t-test).

There was also significant increase in pro-inflammatory cytokines; the greatest increase was seen in the gene coding for MCP-1 with an 8.8-fold increase in expression. There was also significant upregulation of of TNF-α (RQ 7.5, $p<0.0001$), IL-6 (3.2-fold, $p=0.04$) and IL-1β (2.4-fold, $p=0.025$). The anti-inflammatory mediator IL-10 was also upregulated compared to controls, by 2.5-fold ($p=0.01$), and, given the fact that other mediators were expressed at greater levels, this would suggest a potent pro-inflammatory state.

Bcl-2 and Bcl-2 associated X (BAX) are well known regulators of apoptosis; Bcl-2 acts an inhibitor to the pro-apoptotic mediator BAX. There was a significant increase in the ratio of BAX:Bcl-2, (1.9, $p<0.01$ Student's t-test) suggesting that cells were driven towards apoptosis as well as necrosis in response to hypoxic injury. This is in keeping with the literature where other groups have shown that apoptosis contributes to dysfunction following IRI particularly as renal TEC are highly susceptible to apoptosis[292].

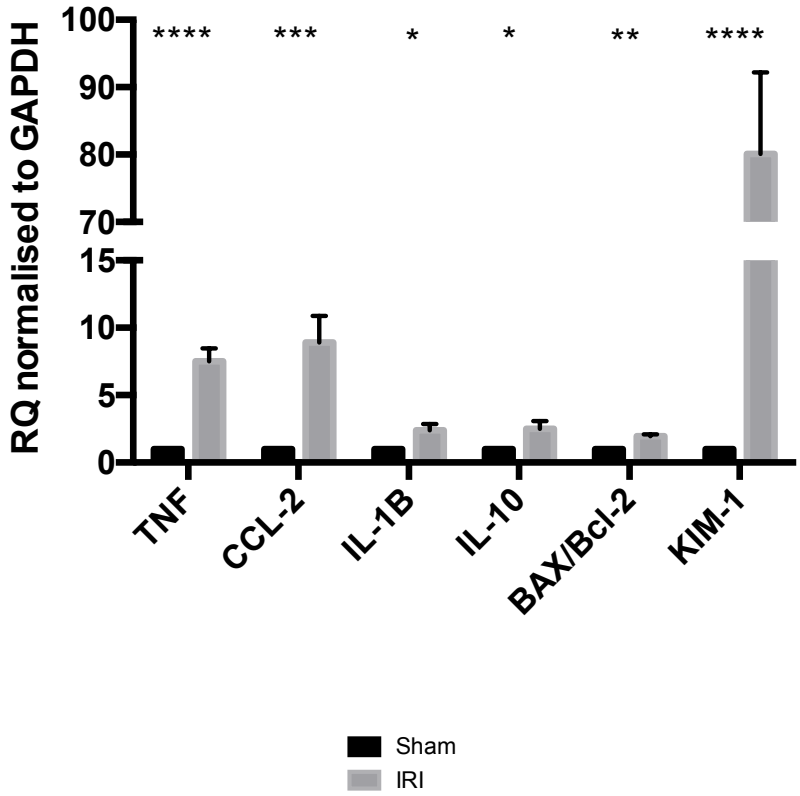

Figure 4.4 Gene expression following IRI. Male 8-10 week old C57Bl/6 mice subjected to bilateral renal ischaemia for 18 minutes and culled at 48 hours (n=8) compared to shams (n=4). Gene expression quantified from total kidney RNA and normalised to GAPDH. * $p<0.05$, ** $p<0.01$ *** $p<0.001$, **** $p<0.0001$. Student's t-test.

4.2.4 18 minutes of bilateral ischaemia reperfusion injury is associated with an increase in miR-214

Following renal injury, there was a 3.3-fold increase in miR-214 expression and 2.9-fold increase in miR-21 expression at 48 hours compared to sham operated controls (both $p<0.0001$). This is a novel finding as no group has demonstrated upregulation at such an early time point. Interestingly, the increase in miR-214 was greater than miR-21 at this time point. There was no significant difference in miR-29c expression compared to controls.

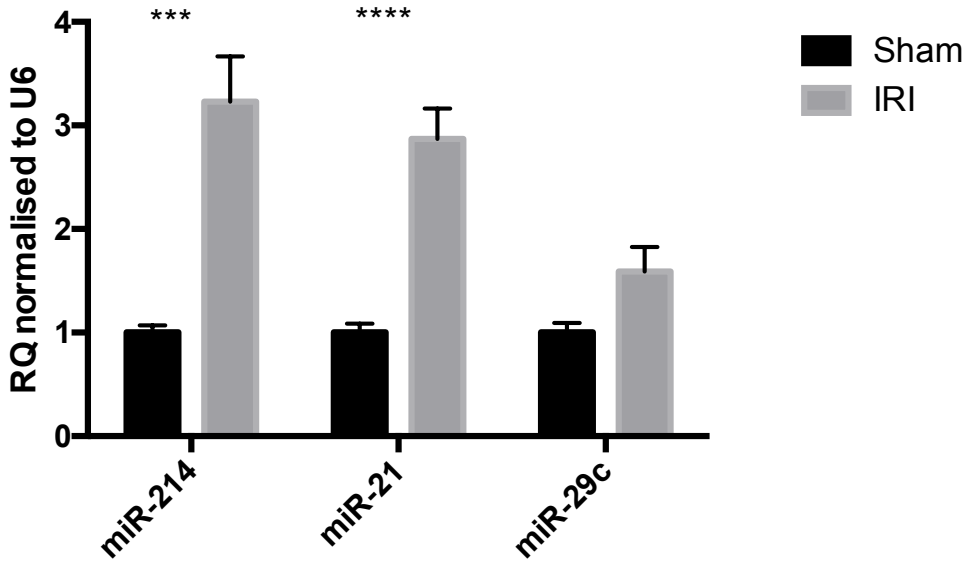

Figure 4.5 MiR expression of whole kidneys following IRI. Male 8-10 week old C57Bl/6 mice subjected to bilateral renal ischaemia for 18 minutes (n=8) culled at 48 hours and compared to sham (n=4). RNA extracted from whole kidneys, miRNA reverse transcription performed, and miRNA expression determined by Taqman qRT-PCR using specific miRNA primers. Data was normalised to U6. *** $p<0.001$, **** $p<0.0001$, Student's t-test

These results signify that this is a suitable model of IRI as 18 minutes of bilateral renal ischaemia caused a severe biochemical and structural injury; importantly, miR-214 is upregulated as early as 48 hours indicating that this model is valid to test the hypotheses. There are several benefits of adopting this model following these results; firstly, it is relevant to transplantation; secondly, multiple experiments can be performed in a relatively short space of time with no significant complications resulting in early termination of the experiment; and thirdly, the role of miR-214 can be elucidated at different stages of injury other than fibrosis. Following these considerations, a decision was made to adopt this model for all future *in vivo* experiments.

4.3 Ischaemia reperfusion as a model of renal fibrosis

After demonstrating early upregulation of miR-214 in response to bilateral IRI, the next step was to demonstrate that renal IRI would result in fibrosis. Developing a suitable fibrosis model would be used to interrogate the role of miR-214 in experiments described in **Chapter 5**. In the bilateral IRI model it was evident that some animals would not survive to 28 days following injury due to severe renal failure. At 48 hours post-injury, mean animal weight had decreased 20% from pre-operative weight and biochemical analysis demonstrated a significant increase in creatinine and urea in keeping with a severe functional injury. In order to perform a time-course analysis of miR-214 examining early injury and the transition towards fibrosis, a suitable IRI model needed to be characterised that had minimal impact on animal morbidity whilst ensuring that enough tissue could be recovered to perform adequate assessment of fibrosis. Therefore, a quantification experiment was performed where animals were subjected to various periods of unilateral IRI to avoid the deleterious effects of renal failure and enable animals to survive to 28 days.

After reviewing the literature regarding suitable length of ischaemia for a unilateral IRI model, fibrosis was quantified after 12 (n=7), 15 (n=7) and 18 minutes (n=8) of unilateral ischaemia and compared outcomes to sham operated controls (n=4) at 28 days.

4.3.1 IRI results in significant kidney fibrosis at 28 days following injury and is dependent on ischaemic time

Mice were subjected to unilateral ischaemia by clamping the right renal pedicle for 12, 15 and 18 minutes (n=7/8 per groups) as described in the methods section. Sham

operated controls (n=4) were subjected to the same procedure as experimental animals with the exception of renal pedicle clamping. Animals were recovered and sacrificed at 28 days.

Results demonstrate a significant reduction in adjusted renal weight following 15 and 18 minutes unilateral ischaemia compared to the right kidneys of sham operated controls ($p<0.01$ and $p<0.0001$ respectively, one-way Anova with Dunnett's adjustment, **Figure 4.6, A**). There was no significant difference in renal weight between 12 minutes of ischaemia and sham operated controls. When comparing the weight of kidneys subjected to ischaemia (right) and the contralateral kidney (left), there was a significant difference in weight in all groups demonstrating a reduction in functioning renal mass presumably due to fibrosis. There was also a compensatory increase in the weight of the contralateral kidney with greater differences observed with longer ischaemia times (**Figure 4.6, B)**. This is commonly observed in a unilateral renal fibrosis model where the contralateral kidney compensates for a functional decline in renal function, which justifies the use of sham animals in these experiments, as the unaffected kidney is not a suitable control in this model.

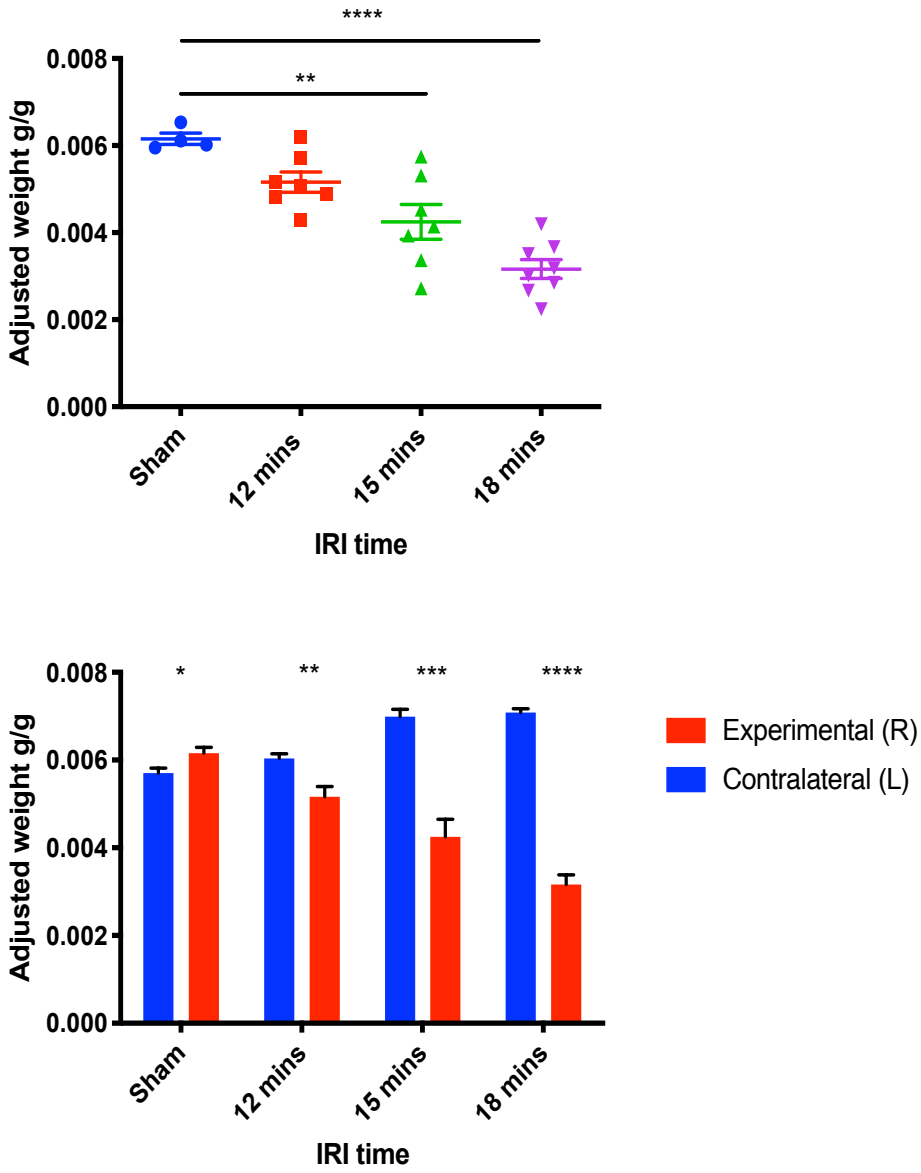

Figure 4.6 Comparison of kidney weights from experimental animals undergoing 12 (n=7), 15 (n=7) or 18 (n=8) minutes unilateral renal ischaemia reperfusion injury versus sham (n=4) and culled at 28 days. **A** Graph comparing experimental (right) kidney weights for each group; **B** Graph comparing the weights of experimental (right) and contralateral (left) kidney in each group. Kidneys adjusted for body weight g/g. Lines and bars represent mean +/-SEM *p<0.05, **p<0.01, ***p<0.001 ****p<0.0001, Top graph, one-way Anova with Dunnett's adjustment; bottom graph paired t-test comparing kidneys in the same group.

Assessment of pro-fibrotic gene expression show there was significant upregulation of pro-fibrotic gene expression in all groups compared to sham operated controls and, as might be expected, there was a step wise increase in expression of these genes with increasing length of ischaemia (**Figure 4.7**). With 18 minutes of ischaemia, there was a 40-fold increase in collagen 1a expression ($p<0.0001$), 32-fold increase in collagen 3 expression ($p<0.0001$), 3.2-fold increase in collagen 4a ($p<0.01$), 6.4-fold increase in α-SMA ($p<0.0001$) and 4-fold increase in PDGFR-β ($p<0.01$, one way Anova with Dunnett's adjustment for multiple comparisons test).

Similarly there was elevation in the 15-minute group, with a 14-fold increase in *Col1a* expression ($p<0.0001$), 13-fold in *Col3a* expression ($p<0.0001$), 2.9-fold in *Col4a* ($p<0.05$), 4-fold in α-SMA gene expression ($p<0.001$) and 3.2-fold in *PDGFR-β* ($p<0.01$, all one way Anova, Dunnett's multiple comparisons test).

Following 12 minutes of ischaemia there was only a modest upregulation in both collagens 1a and 3a ($p<0.01$) and 2-fold increase in α-SMA ($p<0.05$, one-way Anova with Dunnett's multiple comparisons test). There was however no significant difference in *Col4a* or *PDGFR-β* expression.

Collagen deposition was assessed by staining 3μm paraffin embedded section with Picrosirius red and quantified using Image pro-plus. There is evidence of collagen deposition in all experimental groups as demonstrated in **Figure 4.8**. Collagen is mainly deposited in the cortex as expected in fibrosis however there also appears to be increased staining in the medulla. Although not typical of other renal injury models, medullary injury and fibrosis are not unexpected following IRI as the medulla undergoes significant hypoxia, tubular injury and inflammation.

Quantification of fibrosis using image Pro-plus also confirms findings from qRT-PCR

where the greatest increase in collagen deposition is in the 18-minute group compared to control. Surprisingly, despite significant increase in pro-fibrotic gene expression, there was no significant difference in collagen deposition compared to sham after 15 minutes of ischaemia. There was also no significant difference when comparing the 12-minute group to the sham group.

These findings show that 18 minutes of ischaemia results in significant fibrosis in a unilateral model of renal IRI at 28 days as demonstrated by significant upregulation of pro-fibrotic gene expression and quantified by fibrosis scoring on histology.

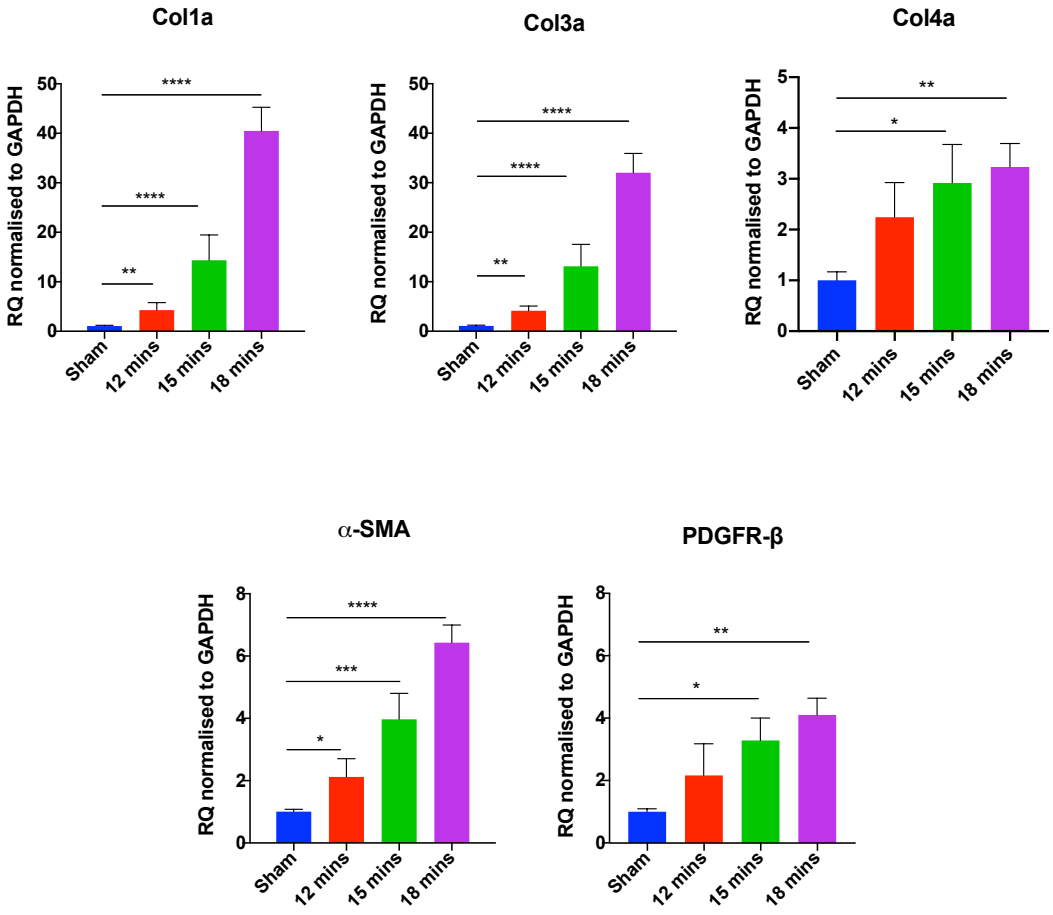

Figure 4.7 Pro-fibrotic gene expression of kidneys from 8-10 week old C57bl/6 mice subjected to unilateral renal ischaemia for 12 (n=7), 15 (n=7) and 18 (n=8) minutes compared to sham operated controls (n=4). Gene expression quantified from total kidney RNA. cDNA synthesized and expression determined by Taqman qRT-PCR using specific gene primers and normalised to GAPDH. Bars represent mean RQ + RQ max; * p<0.05, **p<0.01 ***p<0.001 **** p<0.001. One-way Anova with Dunnett's adjustment for multiple comparisons.

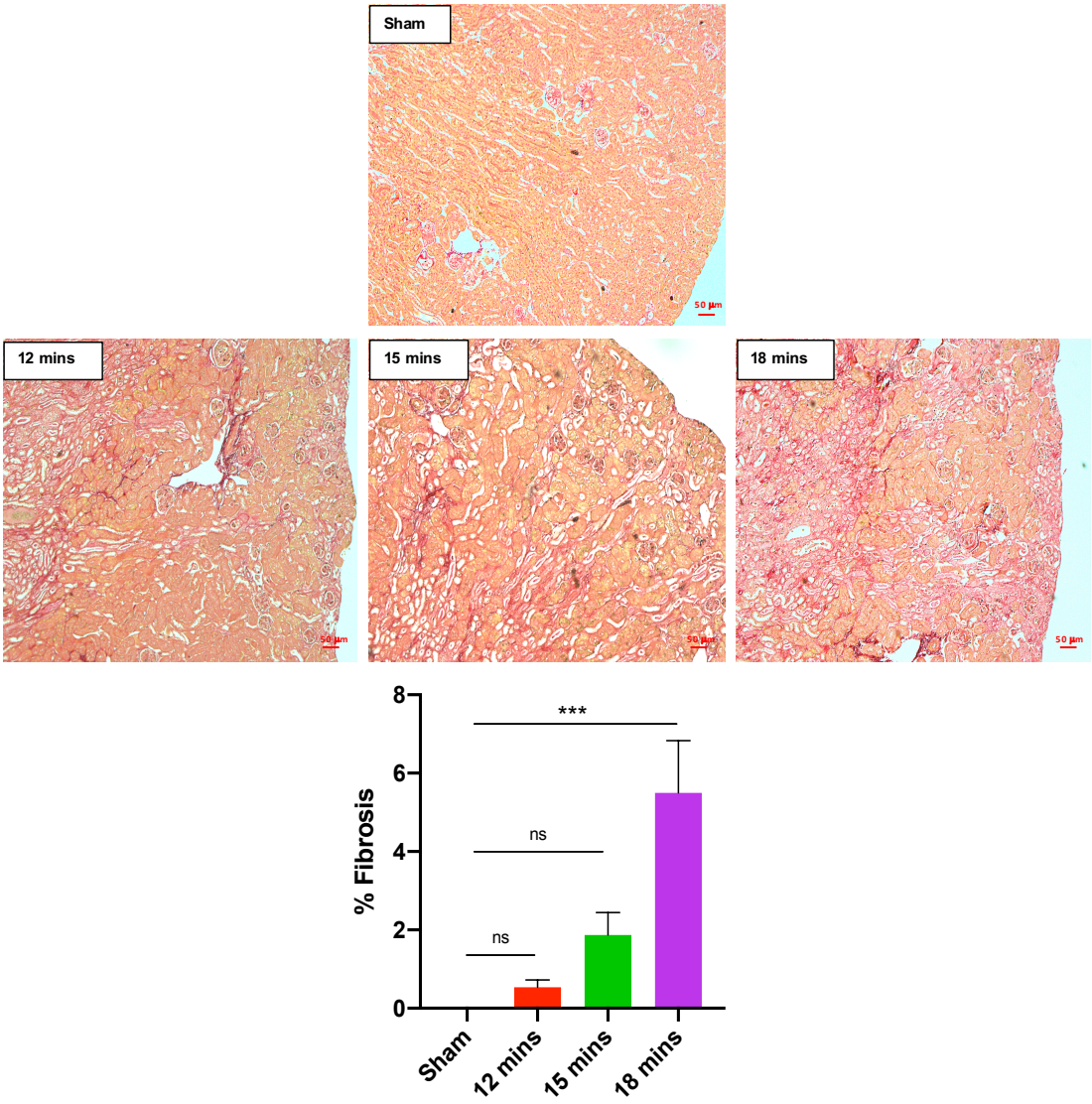

Figure 4.8 Quantification of fibrosis at 28 days. A Formalin fixed and paraffin embedded kidney sections of male C57bl/6 mice subjected to unilateral renal IRI and culled at 28 days. 3µm sections stained with Picrosirius red, images taken at 100x and represent sham (n=4), 12 minutes (n=7), 15 minutes (n=8) or 18 minutes (n=8) ischaemia; **B** Quantification of fibrosis using Image Pro-Plus in blinded manner. Bars represent mean +SEM **** $p<0.0001$, One way Anova with Dunnett's adjustment for multiple comparisons**.**

4.3.2 Ischaemia reperfusion results in significant renal injury and increased pro-inflammatory gene expression at 28 days

Renal injury was assessed by qrt-PCR for KIM-1 mRNA and Hematoxylin and Eosin staining of 3μm sections of paraffin embedded sections.

KIM-1 mRNA was significantly elevated at all time points compared to sham and, as was observed in the markers of fibrosis, severity of injury increased with longer ischaemic time and reached a maximum of 221-fold increase in expression following 18 minutes ischaemia (**Figure 4.9**, $p<0.0001$, one-way Anova). KIM-1 is primarily described as an acute injury marker however other groups have shown it to be raised in fibrosis. Thus, the observed upregulation in this study is in keeping with published results and suggests an ongoing injurious state within the kidney.

In addition to raised KIM-1 expression, sections stained with Haematotoxylin and Eosin (H&E) showed cellular expansion of the cortical interstitium, massive tubular atrophy and debris/casts within the remaining tubules. There is evidence of peri-glomerular sclerosis following 18 minutes ischaemia. This is in contrast to the findings in animals culled after 48 hours where injury was confined to the outer stripe of the outer medulla demonstrating the impact of ischaemia on surrounding structures (**Figure 4.10**).

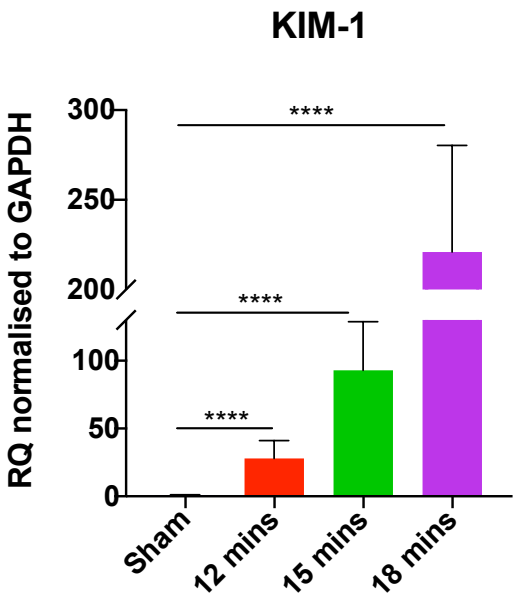

Figure 4.9 KIM-1 gene expression of kidneys from 8-10 week old C57bl/6 mice subjected to unilateral renal ischaemia for 12 (n=7), 15 (n=7) and 18 (n=8) minutes compared to sham operated controls (n=4). Gene expression quantified from total kidney RNA. cDNA synthesised and expression determined by Taqman qRT-PCR using specific gene primers and normalised to GAPDH. Bars represent mean RQ + RQ max; **** $p<0.001$. One-way Anova with Dunnett's adjustment for multiple comparisons.

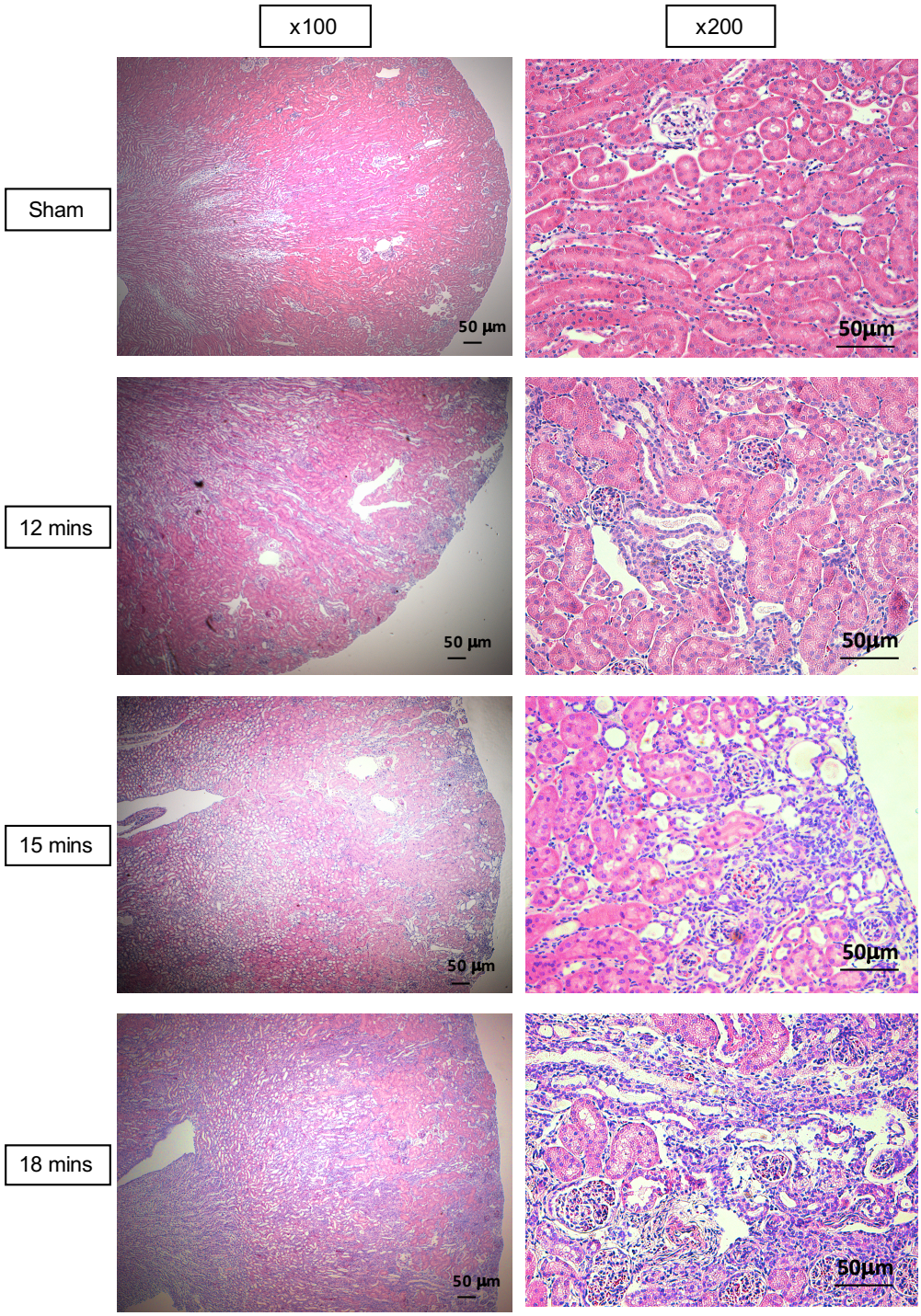

Figure 4.10 Haematoxylin and eosin stains of formalin fixed and paraffin embedded kidney sections from male C57bl/6 mice subjected unilateral renal IRI and culled at 28 days. Images taken at 100x and 200x magnification and represent sham, 12 minutes, 15 minutes or 18 minutes ischaemia.

As there was significant upregulation of pro-inflammatory cytokine and chemokine gene expression in the early phase of injury, and evidence of fibrosis with ongoing injury, the same genes were examined at 28 days. There was marked increase in pro-inflammatory genes in all groups suggesting an ongoing pro-inflammatory state in the context of renal fibrosis (**Figure 4.11**). As with pro-fibrotic gene expression, the greatest increase in expression was seen with longer ischaemia times compared to shams. The most significant increase was in TNF-α after 18 minutes of ischaemia where expression was increased 51-fold versus sham. IL-1β was elevated 22- fold, and IL-6 10-fold in this group. The anti-inflammatory mediator IL-10 was also significantly upregulated at 7-fold however given its modest increase compared to the pro-inflammatory mediators, it would suggest a drive towards ongoing inflammation rather than inhibition and resolution. This was also true for the 15-minute group but less so in the 12-minute group.

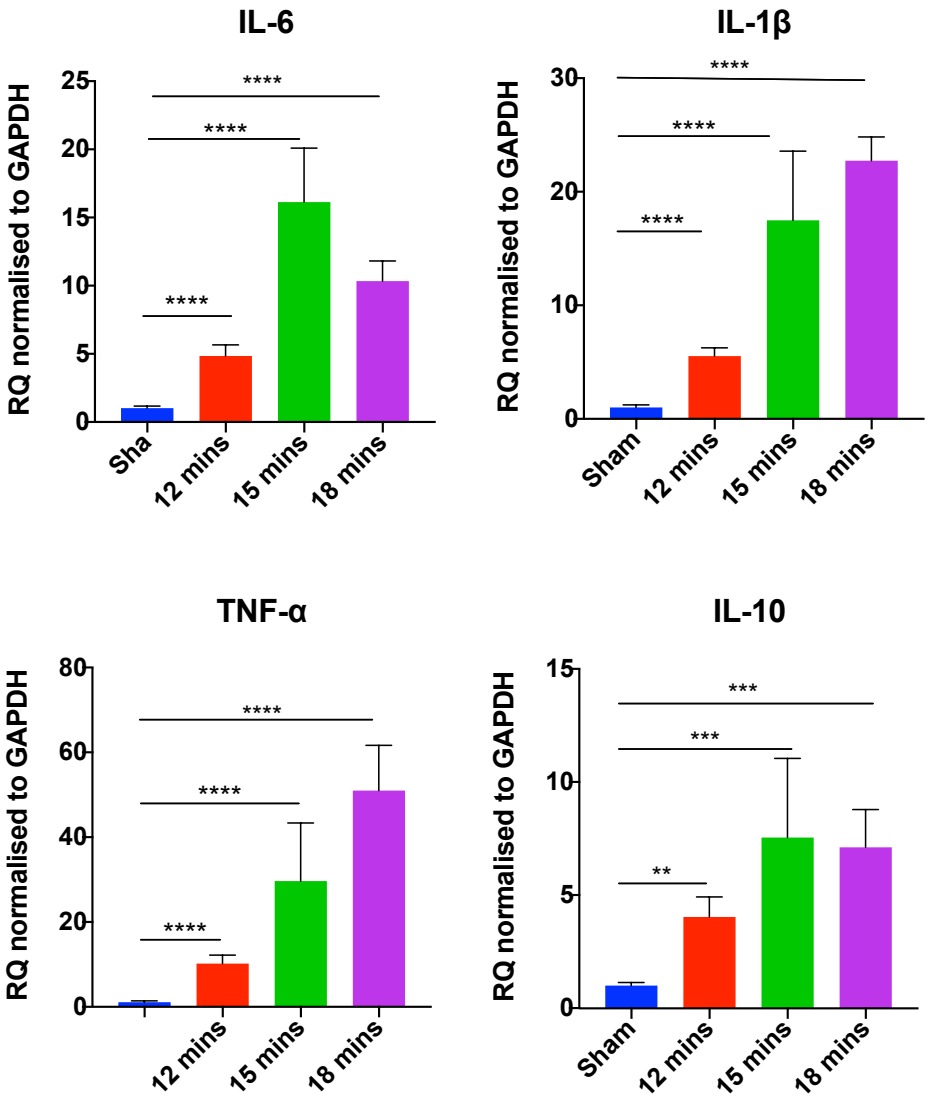

Figure 4.11 Inflammatory gene expression panel. 8-10 week old C57Bl/6 mice subjected to unilateral renal ischaemia for 12 (n=7), 15 (n=7) and 18 (n=8) minutes compared to sham operated controls (n=4). Gene expression quantified from total kidney RNA. cDNA synthesized and expression determined by Taqman qRT-PCR using specific gene primers and normalised to GAPDH. Bars represent mean RQ + RQ max * $p<0.05$, **$p<0.01$ ***$p<0.001$ **** $p<0.001$. One-way Anova with Dunnett's adjustment for multiple comparisons.

4.3.3 MiR-214 expression is greatest at 28 days following 18 minutes of renal ischaemia reperfusion injury

MIR-214 and miR-21 and well known pro-fibrotic miRs and have been shown to be upregulated in multiple pre-clinical models of kidney fibrosis. Importantly, miR-214 has been shown to be increased in an IRI induced model of fibrosis and at greater levels then miR-21[293].

Results show there is a significant increase in miR-214 tissue levels following both 15 and 18 minutes of renal ischaemia in this model at 28 days (**Figure 4.12**). Again, the greatest increase was seen in the 18-minute group with over 4-fold increase in expression compared to shams ($p<0.01$); following 15 minutes of ischaemia there was a 3.8-fold increase in expression ($p<0.01$, one-way Anova with Dunnett's multiple comparisons test). There was no significant difference in expression following 12 minutes of ischaemia.

MiR-21 expression was only significantly up-regulated following 18 minutes of ischaemia and less than miR-214 (2.8-fold increase, $p<0.05$ one-way Anova with Dunnett's multiple comparisons test). There was no significant increase in either the 12- or 15-minute groups.

Although there was no significant difference in miR-29c levels in any experimental group, there was a decrease in expression as would be expected as miR-29c is usually downregulated in fibrosis.

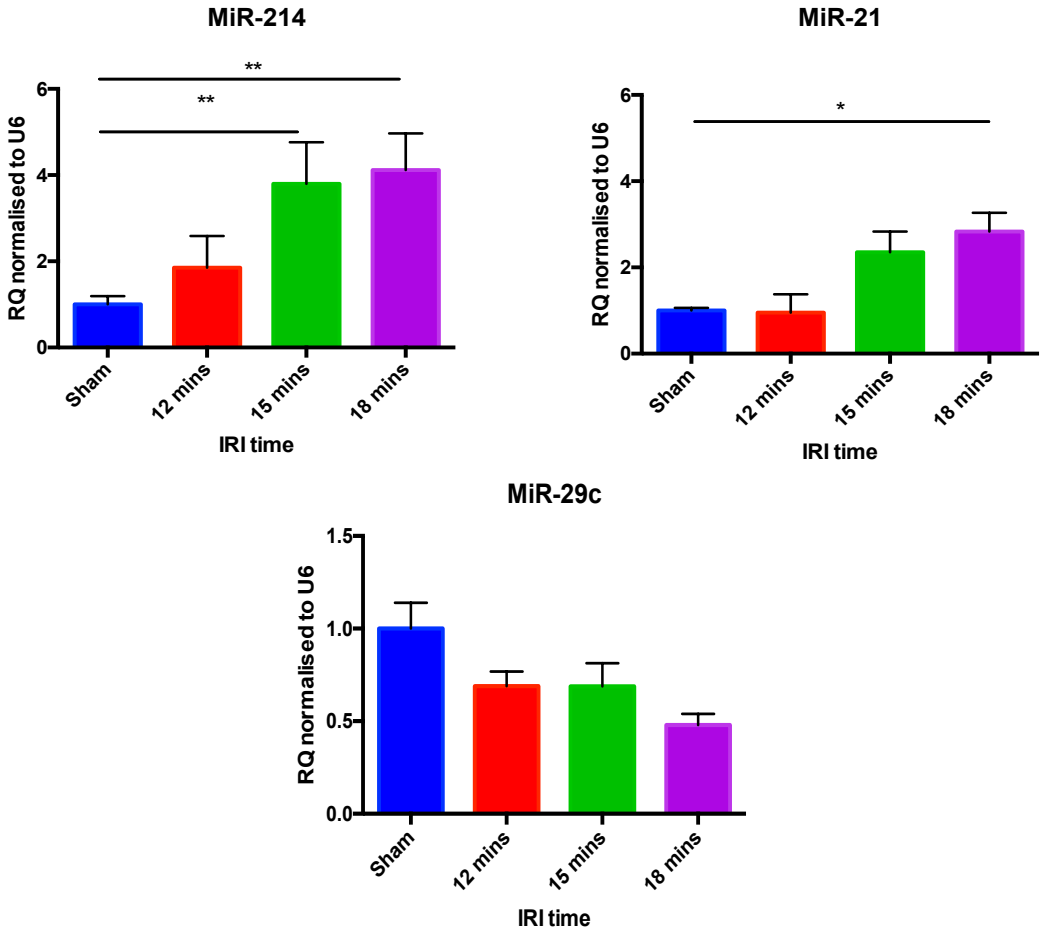

Figure 4.12 MiR expression of kidneys. 8-10-week-old C57Bl/6 mice subjected to unilateral renal ischaemia for 12 (n=7), 15 (n=7) and 18 (n=8) minutes compared to sham operated controls (n=4). MiR expression quantified from total kidney RNA. reverse transcription performed, and expression determined by Taqman qRT-PCR using specific miR primers. Data and normalised to U6. Bars represent mean RQ + RQ max *p<0.05 **p<0.01 ***p<0.001 **** p<0.001. One-way Anova with Dunnett's adjustment.

These results demonstrate 18 minutes of ischaemia induces significant fibrosis as quantified by histology and upregulation of profibrotic gene expression at mRNA level. Whilst miR-214 was significantly upregulated after 15 minutes and 18 minutes of ischaemia, miR-21 was only significantly increased in the 18-minute group despite being previously demonstrated to be upregulated on early injury and fibrosis. Therefore, given these findings a decision was made to utilise 18 minutes of unilateral renal ischaemia for all future experiments.

4.4 Discussion

Having had significant problems achieving a reliable model of murine transplantation, a decision was made to change model and perform renal ischaemia reperfusion injury. As a pilot study, 18 minutes of bilateral ischaemia resulted in significant renal injury as assessed using functional outcomes demonstrating successful modelling of IRI. Results also demonstrated that 18 minutes of unilateral ischaemia resulted in a robust model of fibrosis where there was enough recoverable renal mass to assess multiple endpoints.

Various models of renal ischaemia reperfusion injury have been adopted; however not all are suitable to model the progression of early injury to fibrosis. Bilateral renal ischaemia results in significantly increased urea and creatinine which are diagnostic of renal failure, and, as such, is a good model to replicate human acute kidney injury. However, inducing significant renal failure imposes experimental limitations on the model beyond the early phase of injury. Several groups have demonstrated that, after 40 minutes of bilateral ischaemia in rats, at 4 weeks post injury the serum creatinine had returned to normal despite histological evidence of tubulointerstitial capillary

dropout, suggesting the injury is too mild to allow progression towards fibrosis[244]. This finding has been replicated in mice where ischaemia of less than 18 minutes can result in recovery of the animal and reversal of the functional injury. As demonstrated here, inducing a severe injury, as quantified by acute tubular necrosis, results in significant renal failure which would hamper any chance of recovery beyond the early phase; animals lost 20% body weight and many of the mice would not have survived beyond 48 hours. Therefore, the bilateral IRI model is a suitable model for AKI and should be reserved for studying the early phase of IRI[294].

Here, the unilateral model provides several advantages by confining the injury to one kidney, firstly it reduces the systemic insult to the mouse and secondly it allows longer ischaemia times (up to 120 minutes has been reported)[246,247]. Careful consideration needs to be given when using this model, which include length of ischaemia and whether the contralateral kidney is excised or not (and if so the timing of the nephrectomy). When considering the latter point, evidence has shown that in the presence of normal renal tissue, the ischaemic insult to the injured kidney is exacerbated because of prolonged vasoconstriction in the immediate post-ischaemic period, thereby accelerating the progression fibrosis in the injured kidney[247,295]. As the injured kidney becomes more fibrotic, the contralateral kidney hypertrophies to compensate for the functional decline of the injured kidney and this process was reflected when comparing kidney weights from the injured and uninjured kidneys, which was most markedly different following 18 minutes of ischaemia.

Length of ischaemia is fundamental in determining the severity of kidney injury and significant early renal injury was seen after 18 minutes of bilateral ischaemia and progression to fibrosis following 18-minutes of unilateral ischaemia. These results are supported by 67% of tubules being scored as necrotic (ATN) in the outer medulla of stained kidney sections and an accompanying 80-fold increase in KIM-1

expression, representing significant tubular injury. Evidence that tubular injury was still ongoing after 28 days is suggested by both raised mRNA levels of KIM-1 in all groups, peaking at 221-fold increase following 18 minutes of ischaemia, and histological evidence of tubular atrophy, interstial expansion and cortical fibrosis, both of which suggest no functional recovery and ongoing injury at this time point. KIM-1 is typically described as maker of acute tubular injury[296] however it has also been shown to be raised in allograft and native kidney fibrosis[297–300]. Furthermore, KIM-1 may be involved in promoting fibrosis by secretion of MCP-1 resulting in macrophage recruitment; Humphreys et al showed that mice with mutant KIM-1 were protected against fibrosis following unilateral ureteric obstruction (UUO)[301]. As might be expected, the extent of injury on histology was more severe with longer ischaemia times. This finding has been replicated in the literature; however other groups showed that 18 minutes only conferred a modest fibrosis response and longer times of 26-30 minutes were preferable. Given that there was significant fibrosis after only 18 minutes of ischaemia in our hands confirms the importance of assessing injury and developing the model as an individual researcher. Differences in strains of animals and technical parts of the model may explain the variability in results in the literature[250].

Early activation of the pro-inflammatory pathways was demonstrated with 18 minutes of bilateral ischaemia at 48 hours with significant upregulation of pro-inflammatory markers, including IL-6, TNF-α, IL-1β and the anti-inflammatory mediator IL-10. Some authors have described ischaemia reperfusion injury as primarily an inflammatory disorder generating pro-inflammatory mediators from damaged tubule cells[302], as proximal tubular cells are known to release these pro-inflammatory mediators in response to injury[82,289]. The expression of pro-inflammatory genes was sustained following 28 days in all groups suggesting a prolonged and ongoing pro-

inflammatory state. This demonstrates that even after what could be considered mild to moderate ischaemia, the ischaemic insult sets up a cascade of pro-inflammatory pathways that persist well beyond the early phase of injury, and ultimately lead to fibrosis. These results have been replicated by other authors who have demonstrated that early injury results in ongoing evidence of inflammation well beyond the initial phase when renal tissue shows evidence of significant fibrosis[249]. Stroo et al have also shown that chemokine expression continues to increase after the initial injury and peaks during the reparative phase confirming ongoing activation of pro-inflammatory pathways[303]. Inflammation and fibrosis are intricately linked[43,289,304] and here it has been demonstrated that unilateral renal ischaemia reperfusion injury is a robust model of acute kidney injury to fibrosis progression.

In addition to this, miR-214 was elevated in early injury and fibrosis. MiR-214 has previously been demonstrated to be upregulated in murine IRI but only after 72 hours[182] and has never been shown to be raised as early as 48 hours. Its role in early injury is therefore unknown and may represent a novel target in this context and will be explored in **Chapter 5**. It has, however, been shown to be upregulated in other renal models of injury and has previously been described as a pro-fibrotic miR[222,223,225]. As expected, it was upregulated at 28 days, and again there was a positive correlation between length of ischaemia and expression, peaking in the 18-minute group. MiR-21 is an abundantly expressed miR that is readily upregulated in multiple models of renal injury and has shown to be highly expressed following early IRI and fibrosis[293,305,306]. After 48 hours of bilateral injury, there was only a modest increase in miR-21 and it was only upregulated following 18 minutes of ischaemia at 28 days. The higher expression of miR-214 than miR-21 in both early injury and later fibrosis means that miR-214 is a valid target to pursue in future experiments and may be more relevant than miR-21 in ischaemic kidney injury.

There was no significant difference in miR-29c expression after 48 hours, which is expected at such an early time point as miR-29c is a regulator of collagen expression[307]. Results from other groups have shown that members of the miR-29 family are ordinarily downregulated in renal fibrosis[307–309]; however, although there was a downward trend in miR-29c expression at 28 days, this was not significant.

Together, these results demonstrate several key points that are integral to the rest of this project; firstly, the murine renal IRI model can be adopted to investigate the role of miR-214 in ischaemia induced fibrosis; secondly that this model can be used to interrogate miR-214 in different phases of injury including early inflammation, repair and later fibrosis. Importantly, no group has examined the its role in early injury and represents a potential novel mechanism in renal injury.

Chapter 5: The role of miR-214 in ischaemia reperfusion injury

5.1 Introduction

Having first sought to characterise IRI induced renal fibrosis, the next aim was to elucidate the potential role of miR-214 in different stages of injury, using the unilateral IRI model to perform a time-course analysis of its expression during early inflammation, through the reparative phase and fibrosis. In **Chapter 4**, miR-214 was shown to be upregulated in early and late injury. Two key experiments will be outlined in this chapter that test the hypotheses that miR-214 is upregulated during IRI and fibrosis and that knocking out miR-214 protects the kidney from injury.

MiR-214 has previously been investigated by our group in the context of renal fibrosis[222,310]; inhibition by either pharmacological blockade or genetic knockdown resulted in protection against injury following unilateral ureteric obstruction. The precise mechanism behind its role in injury remains unclear; there is evidence to suggest that, when overexpressed in fibroblasts *in vitro*, there is myofibroblast differentiation and expression of pro-fibrotic gene expression. Evidence also suggests that miR-214 contributes to immune cell regulation, which is relevant in the context of renal transplantation. MiR-214 is expressed in activated T cells ($CD4^+$ and $CD8^+$)[215] and is upregulated 140 fold in an *ex vivo* model of activated monocytes in patients with CKD[210]. A recent publication from Nosalski et al data shows that miR-214 regulates $CD3^+$ cells in perivascular fibrosis[311], and data from our group shows that miR-214 is expressed in infiltrating leucocytes in kidney biopsy specimens of patients with diabetic nephropathy[312]. Therefore, there is a potential role for miR-214 in the early phase of injury following IRI which to date has not been investigated.

5.2 Characterising kidney injury as a result of 18 minutes of unilateral IRI over 28 days

This section examines the effect of 18 minutes of injury at different time points post - injury from as early as 2 days to the development of fibrosis at 28 days.

5.2.1 Significant changes in the IRI kidney weight occur in keeping with early inflammatory infiltration and later development of fibrosis

The experimental (right) kidney and contralateral (left) kidneys were weighed immediately following sacrifice and adjusted for body weight. Results show there was a significant increase in experimental kidney weight at 2 days when compared to both the corresponding (right) kidney of the sham operated controls (**Figure 5.1**) and to the contralateral uninjured (left) kidney (**Figure 5.2**) which is likely to reflect post-injury oedema and significant inflammatory infiltrate. When comparing weights at 7 days, the experimental kidney weight had returned to a similar weight of the time operated sham and there was no significant difference between the injured and uninjured kidneys. Beyond 7 days however, there was a significant stepwise reduction in the IRI kidney weight compared to sham right kidney at 14 and 21 days with little difference in weights between 21 and 28 days, suggesting the kidney was already significantly fibrosed by day 21 (**Figure 5.1**). Following 14 days the reduction in weight of the injured kidney was accompanied by an increase in the contralateral kidney weight demonstrating a compensatory expansion in renal mass and potential filtration capacity of the uninjured kidney in this model (**Figure 5.2**).

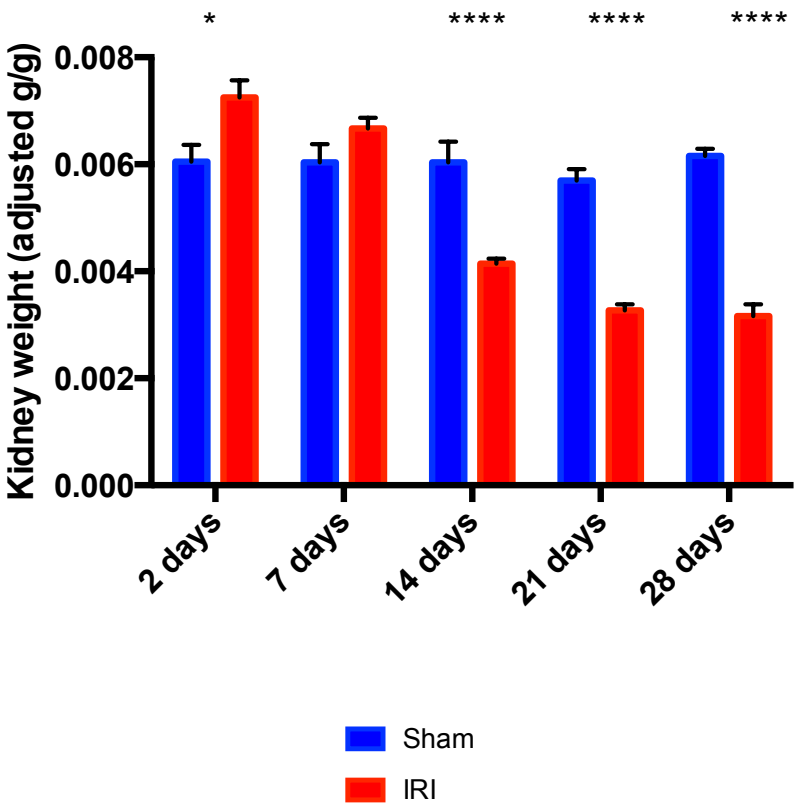

Figure 5.1 Comparison of kidney weights from animals undergoing IRI vs sham. The right kidney from animals undergoing 18 minutes unilateral IRI (n=7/8 per group) is compared against time-matched sham-operated controls (n=4 per group). Kidney weight adjusted for body weight g/g. Bars represent group mean + SEM *p<0.05, **p<0.01, ***p<0.001, ****p<0.0001, Student's t-test

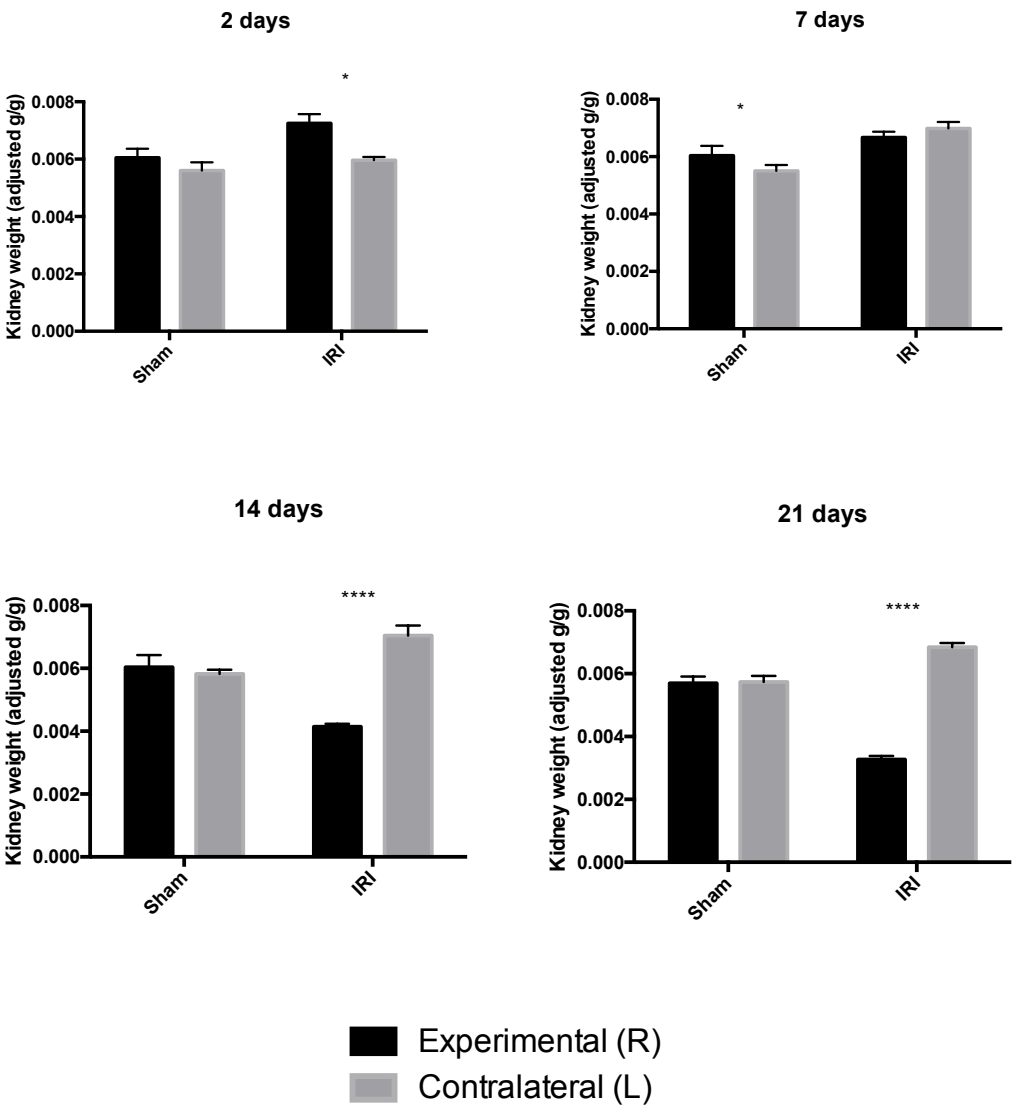

Figure 5.2 Comparison of weights of experimental (right) kidney vs contralateral (left) kidney. Male C57bl/6 mice ether underwent 18 minutes unilateral IRI (right kidney, n=7/8 per group) or sham laparotomy as control (n=4 per group) and sacrificed at 2, 7, 14 and 21 days. Kidney weight adjusted for body weight g/g. Bars represent group mean + SEM *p<0.05, **p<0.01, ***p<0.001, ****p<0.0001 Paired t-test

5.2.2 Unilateral ischaemia reperfusion injury results in significant and progressive renal injury and fibrosis.

As previously demonstrated in **Chapter 4,** using the model of 18 minutes of bilateral renal IRI, 18 minutes of unilateral IRI also resulted in significant early injury, demonstrated by significant structural changes on histology and tubular injury within the outer stripe of the outer medulla (OSOM). Pathological features include significant disruption of the normal architecture of this region with tubular necrosis as well as luminal casts and debris within damaged tubules resulting from cessation of urine production and reduction of tubular debris washout (**Figure 5.3**). Quantification of injury showed 67.3% of tubules were deemed to be necrotic. In the contralateral uninjured kidney, there was a mean 1.6% rate of acute tubular necrosis which is similar to what is seen in sham kidneys demonstrating that structural injury was confined to the kidney undergoing ischaemia.

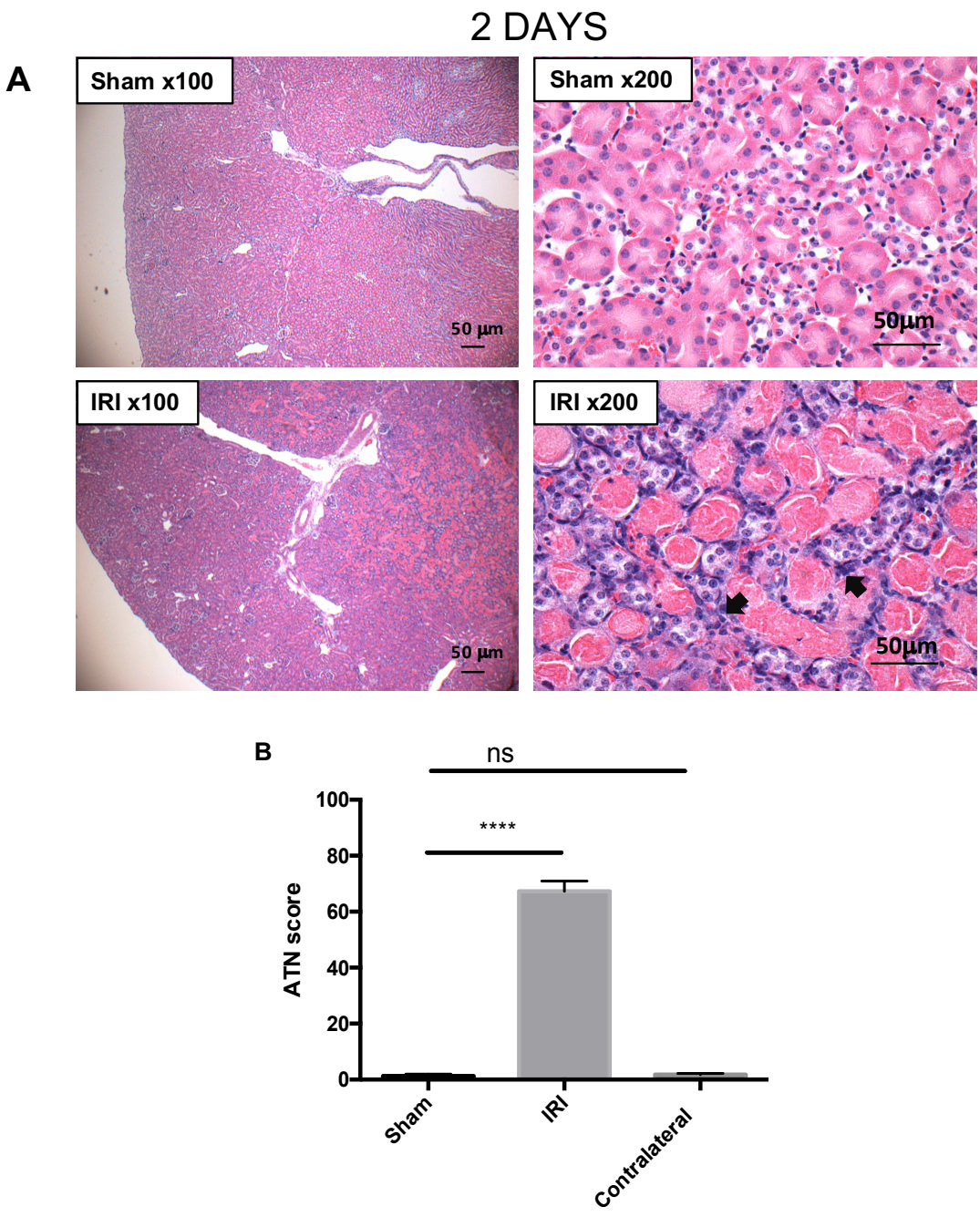

Figure 5.3 Structural injury at 2 days following 18 minutes of IRI compared to sham. Male C57Bl/6 mice either underwent 18 minutes of unilateral IRI (n=8) or sham laparotomy (n=4) and sacrificed at 2 days **A** Haemotoxylin and eosin stains of a sham kidney (top panel and IRI kidney (bottom); **B** Quantification of ATN in IRI kidneys (n=8), contralateral kidneys (n=8) and sham (n=4), represented as mean ± SEM, One way Anova with Dunnett's adjustment **** p<0.0001

At 7 days, there is evidence of increased cellularity in the interstitial space between tubules shown by black arrows in **Figure 5.4**, potentially representing an increase in infiltrating inflammatory cells in response to injury. The kidney remained grossly abnormal; however, there was evidence of fewer necrotic tubules suggesting that the kidney was undergoing repair in response to injury. This was supported by a reduction in ATN with 22.6% of tubules in the OSOM deemed to be necrotic at this time point.

As injury progressed beyond the early phase, no structural recovery was seen on histology as suggested by increasing acellular expansion of the interstitial space and gradual tubular atrophy by 21 days post injury (**Figure 5.5**).

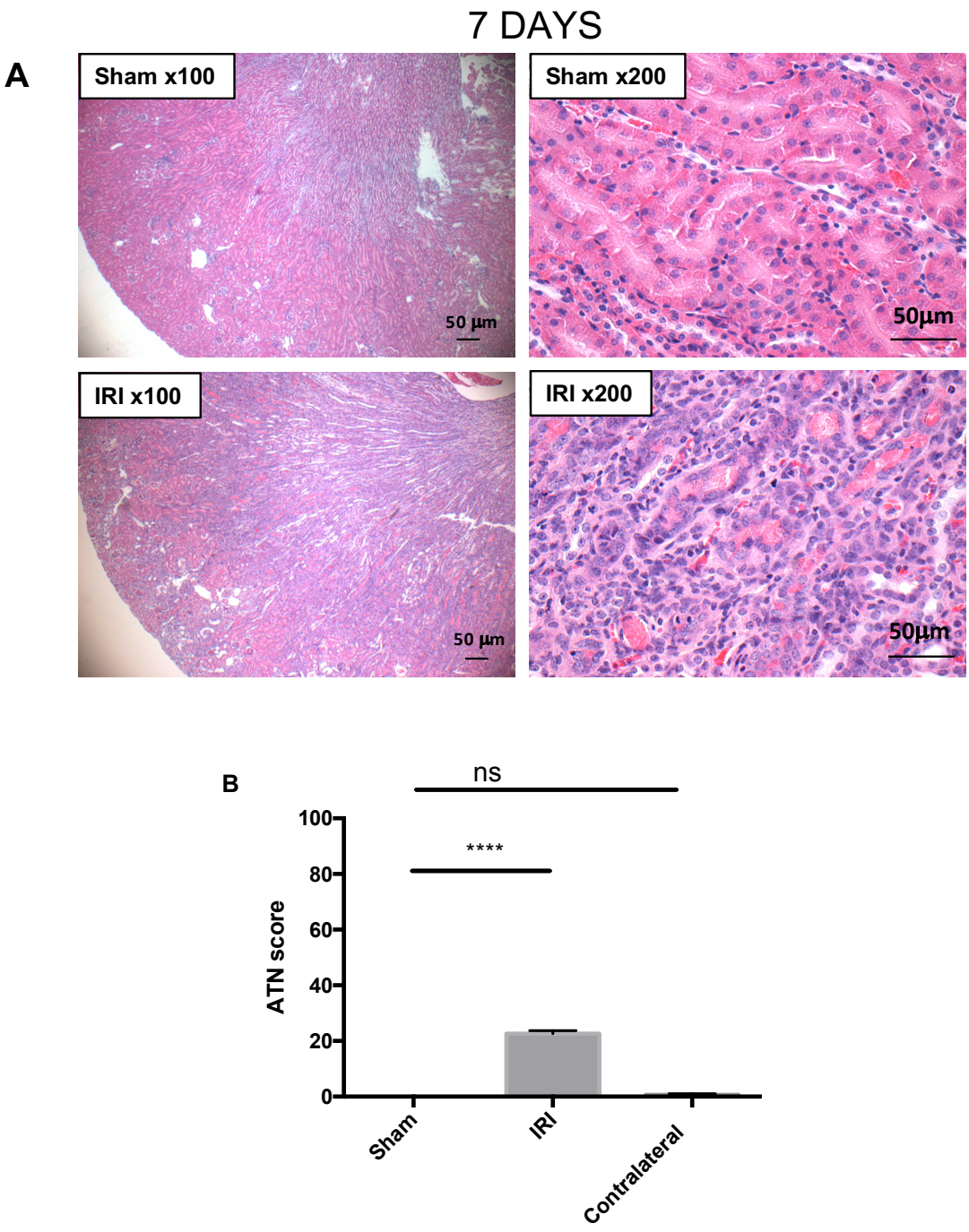

Figure 5.4 Structural injury at 7 days following 18 minutes of IRI compared to sham. Male C57Bl/6 mice either underwent 18 minutes of unilateral IRI (n=8) or sham laparotomy (n=4) and sacrificed at 7 days **A** Haemotoxylin and eosin stains of a sham kidney (top panel and IRI kidney (bottom); **B** Quantification of ATN in IRI kidneys (n=8), contralateral kidneys (n=8) and sham (n=4), represented as mean ± SEM, One way Anova with Dunnett's adjustment **** p<0.0001.

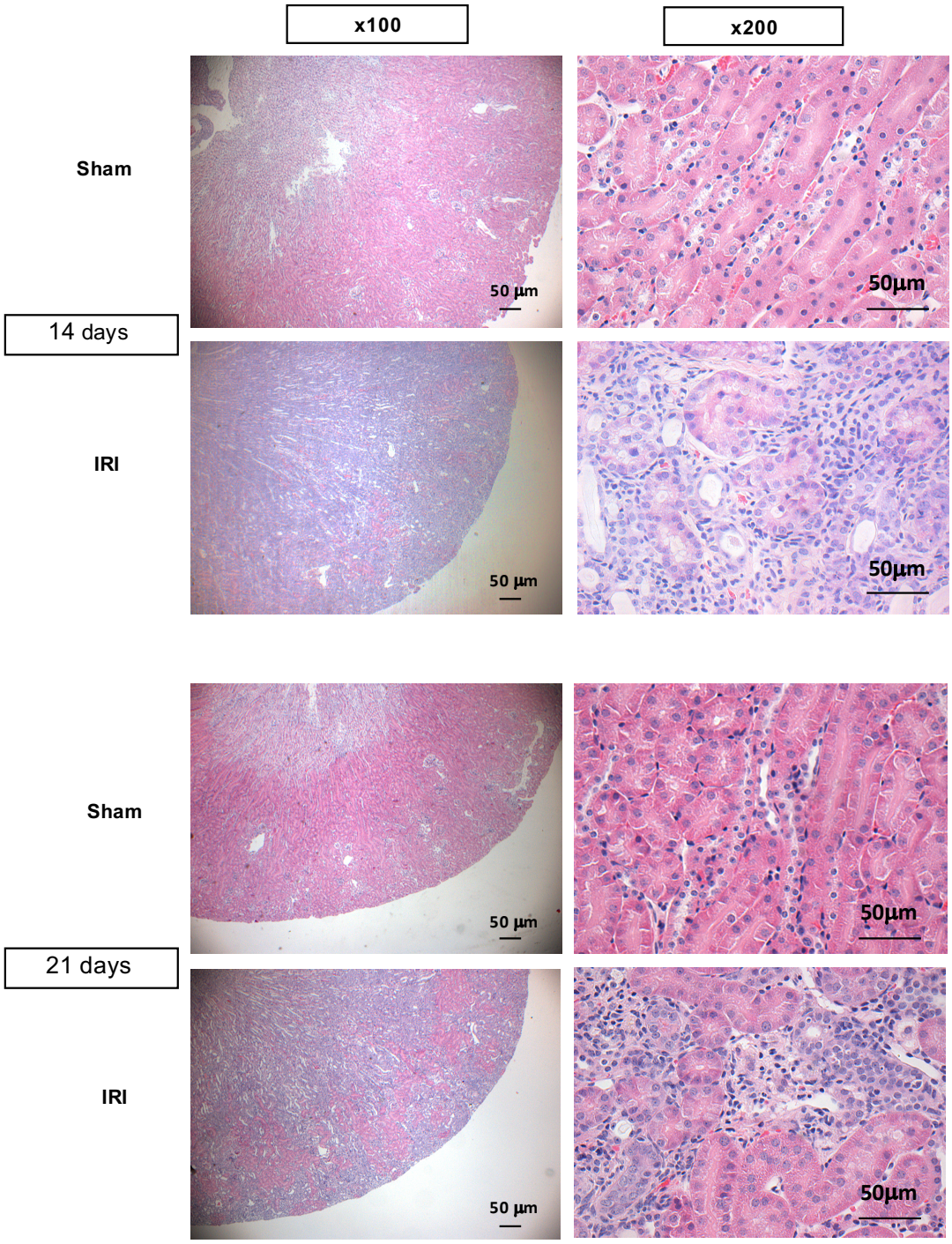

Figure 5.5 Structural injury at 14 and 21 days following 18 minutes unilateral ischaemia reperfusion injury. Male C57bl/6 mice underwent 18 minutes IRI (n=7/8) or sham laparotomy (n=4) and were sacrificed at 14 and 21 days. Formalin fixed and paraffin embedded kidney were cut into 3µm sections. Top: Haemotoxylin and eosin stains kidney sections 14 days post injury at 100x magnification and 200x magnification. Bottom: Haemotoxylin and eosin stains of kidney sections 21 days

Picrosirius red staining demonstrated marked collagen deposition from 14 days onwards in keeping with significant fibrosis. Quantification of cortical fibrosis showed that 3.2% of the cortex was fibrosed at 14 days and there was a significant increase to 7.4% by day 21 (**Figure 5.7,** $p<0.05$, one-way ANOVA with Tukey's post-hoc test).

There was significant upregulation of KIM-1 at all time points which is consistent with histological findings of significant tubular injury (**Figure 5.8**). KIM-1 mRNA peaked at day 7 days when there was an 859-fold increase in expression (compared to time-matched control, $p<0.00001$, one-way ANOVA with Tukey's post-hoc test). Expression remained persistently elevated at 14 days with a 452-fold increase compared to shams; however, by day 21 expression had fallen to 230-fold and remained static at 221-fold increase at day 28 (compared to time-matched sham-operated controls, $p<0.0001$ at all time points, one-way ANOVA with Tukey's post-hoc test).

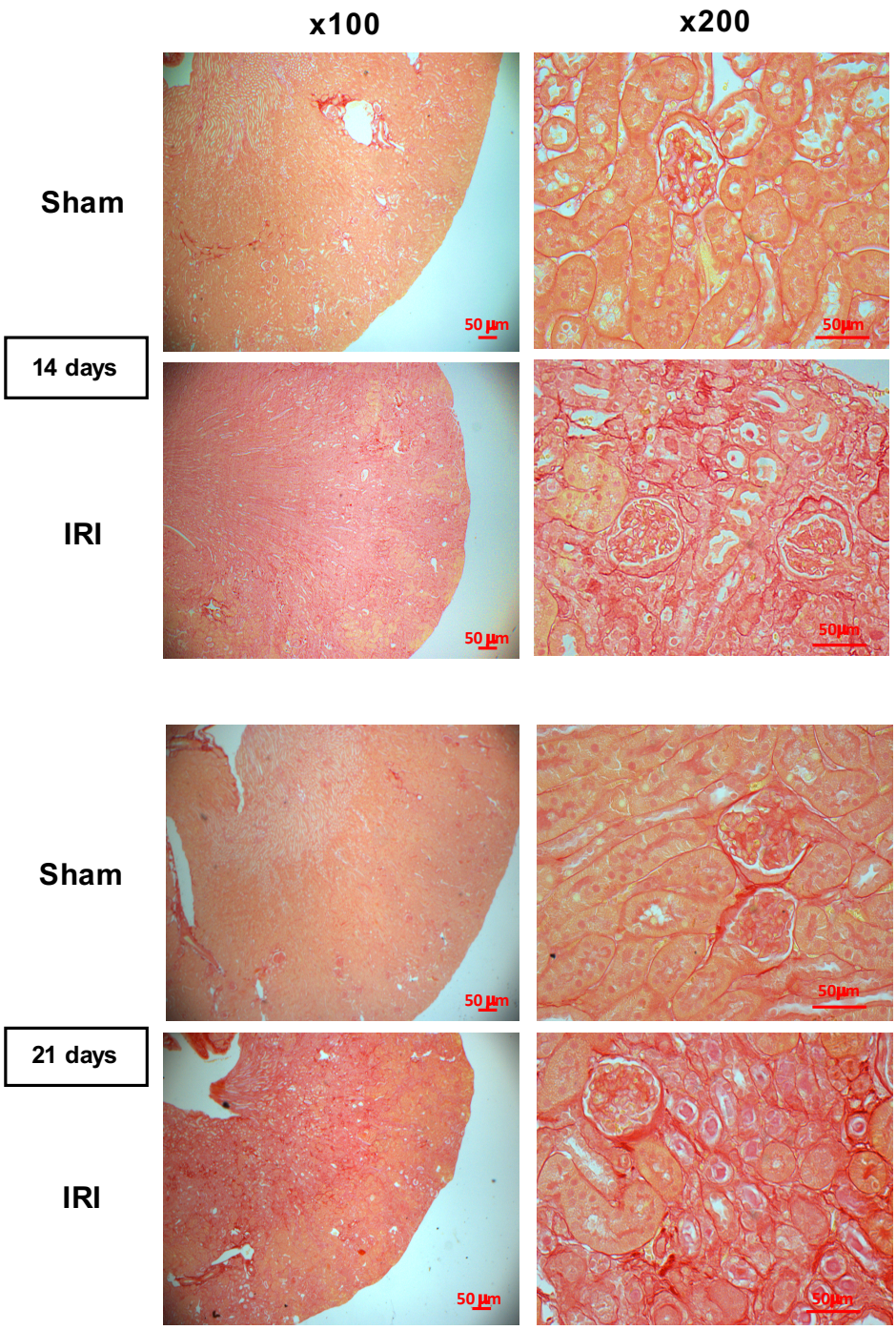

Figure 5.6 Fibrosis following 18 minutes unilateral ischaemia reperfusion injury. Male C57bl/6 mice underwent 18 minutes (n=7/8) IRI or sham laparotomy (n=4) and were sacrificed at 14 and 21 days. Formalin fixed and paraffin embedded kidney were cut into 3µm sections. Picrosirius red stain of sham kidneys and IRI kidneys 14 (top) days (top) and 21 days (bottom) post injury at 100x magnification and 200x magnification.

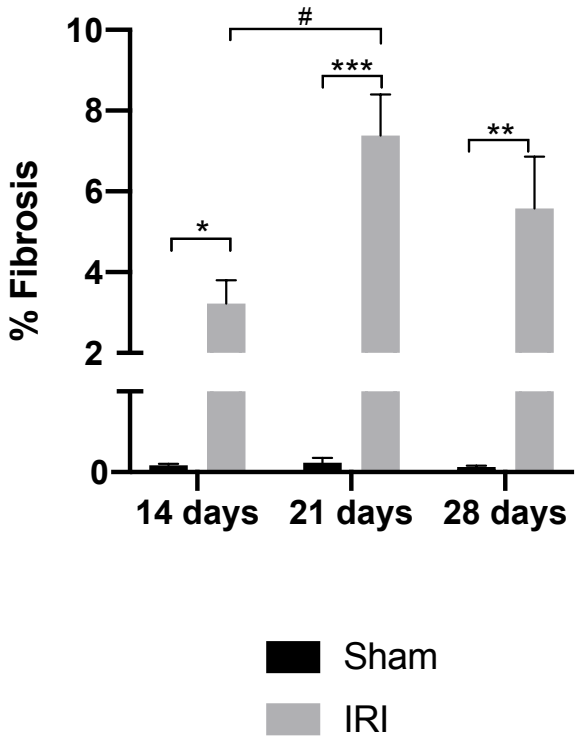

Figure 5.7 Quantification of fibrosis following 18 minutes unilateral renal IRI. Male C57bl/6 mice underwent 18 minutes IRI (n=7/8 per group) or sham laparotomy (n=4) and were sacrificed at 14-, 21- and 28-days post injury. Fibrosis was quantified from picrosirius red stained sections using Image Pro-Plus in blinded manner. Bars represent mean +SEM; *p<0.05, ** p<0.01, ***p<0.001 when comparing sham to IRI; #p<0.05 when comparing IRI groups. One-way ANOVA with Tukey's post-hoc test.

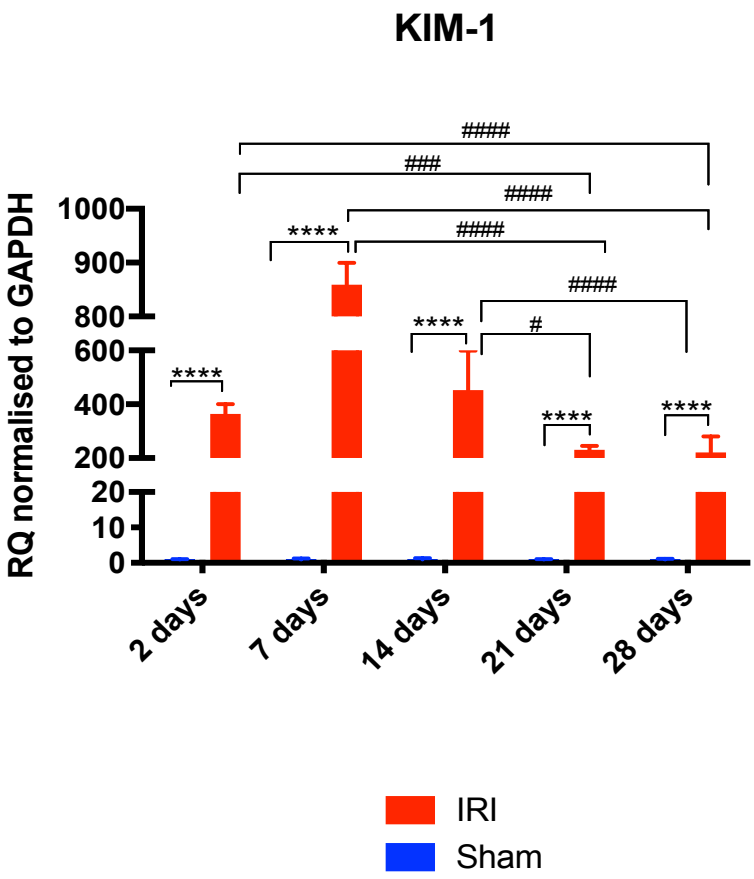

Figure 5.8 KIM-1 gene expression. Male C57bl/6 mice were subjected to 18 minutes unilateral renal IRI and culled at 2, 7, 14, 21 and 28 days (n=7/8) minutes compared to sham operated controls (n=4). Gene expression quantified from total kidney RNA. cDNA synthesised and expression determined by Taqman qRT-PCR using specific gene primers and normalised to GAPDH. Bars represent mean RQ + RQ max; Bars represent mean +SEM; ****p<0.0001 when comparing sham to IRI, # p<0.05 ### p<0.001, #### p<0.0001 when comparing IRI groups. One-way ANOVA with Tukey's post-hoc test.

5.2.3 18 minutes of unilateral IRI results in elevation of pro-inflammatory gene expression at all time points

The expression of the pro-inflammatory genes IL-1β, IL-6 and TNF-α and the anti-inflammatory mediator IL-10 were measured. **Figure 5.9** shows there was significant upregulation of pro-inflammatory genes at day 2 as expected, however expression continued to increase well beyond the immediate phase of injury. Expression of IL-1β and IL-6 were increased at all time points compared to controls; with the greatest increase in expression of both cytokines at 7 days, 24-fold and 42-fold increase respectively ($p<0.001$, one-way ANOVA with Tukey's post-hoc test). This was also reflected in expression of the anti-inflammatory mediator IL-10 which peaked at 7 days with an almost 70-fold increase in expression suggesting a significant inflammatory response at this time point in keeping with the increased cellularity seen on histology. Although IL-10 remained significantly elevated beyond 7 days, there was a sharp decrease in expression by 14 days at around an 8-fold upregulation which remained static at time points beyond this. There was a concurrent decrease in IL-6 expression from 42-fold at 7 days to 15-fold at 14 days, and, although all inflammatory gene expression remained upregulated, suggesting ongoing inflammation throughout all phases of injury, the relative reduction in expression of IL-6 and IL-10 suggests a potential dampening of the immediate immune response as injury progresses towards fibrosis.

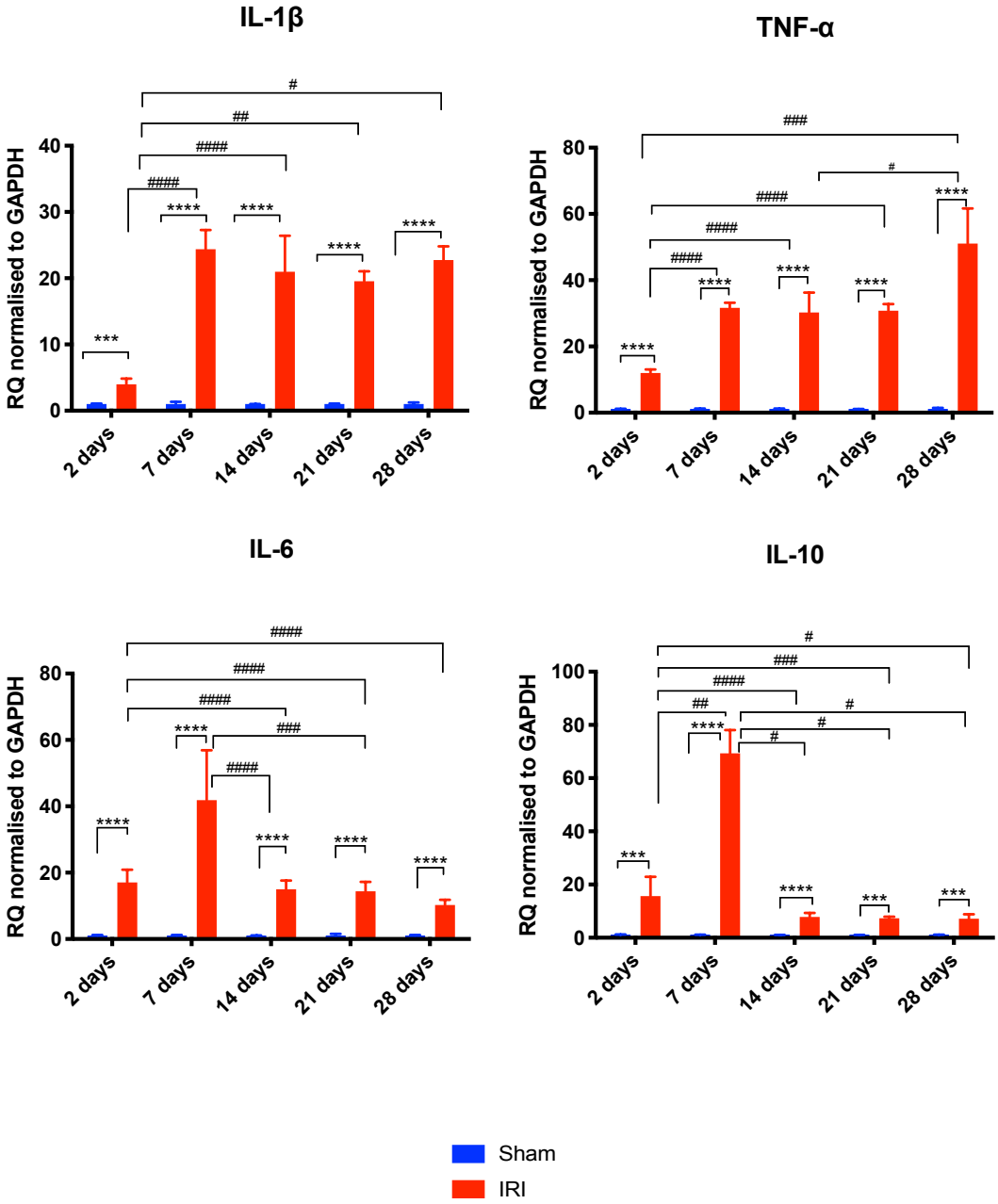

Figure 5.9 Cytokine gene expression. Male C57bl/6 mice were subjected to 18 minutes unilateral renal IRI and culled at 2, 7, 14, 21 and 28 days (n=7/8) minutes compared to sham operated controls (n=4). Gene expression quantified from total kidney RNA, cDNA synthesised and expression determined by Taqman qRT-PCR using specific gene primers and normalised to GAPDH. Bars represent mean RQ + RQ max; *** p<0.001, **** p<0.0001 when comparing sham to IRI, # p<0.05 ### p<0.001, #### p<0.0001 when comparing IRI groups. One-way ANOVA with Tukey's post-hoc test.

CD68, which is highly expressed by monocytes and macrophages, was significantly elevated at all time points. Expression was greatest at 14 days with a 44-fold increase in levels compared to shams and this remained at elevated 27- and 39-fold increase at 21 and 28 days respectively (**Figure 5.10**, both $p<0.0001$, one-way ANOVA with Tukey's post-hoc test). Ongoing elevation at all time points suggests that macrophages are important in all phases of injury.

There was also significant upregulation of CD3e expression, with the greatest increase observed at 28 days with a 40-fold upregulation in levels compared to controls (**Figure 5.10** $p<0.0001$, one-way ANOVA with Tukey's post-hoc test). Whilst there was no difference in expression at 2 days, there was a significant increase at all other time points. $CD3^+$ populations are a heterogenous family of immune cells and evidence from the literature suggests that clonal expansion of T cells in response to injury can take 48-72 hours[182] and this may explain why CD3 expression is not significant at mRNA level at 2 days.

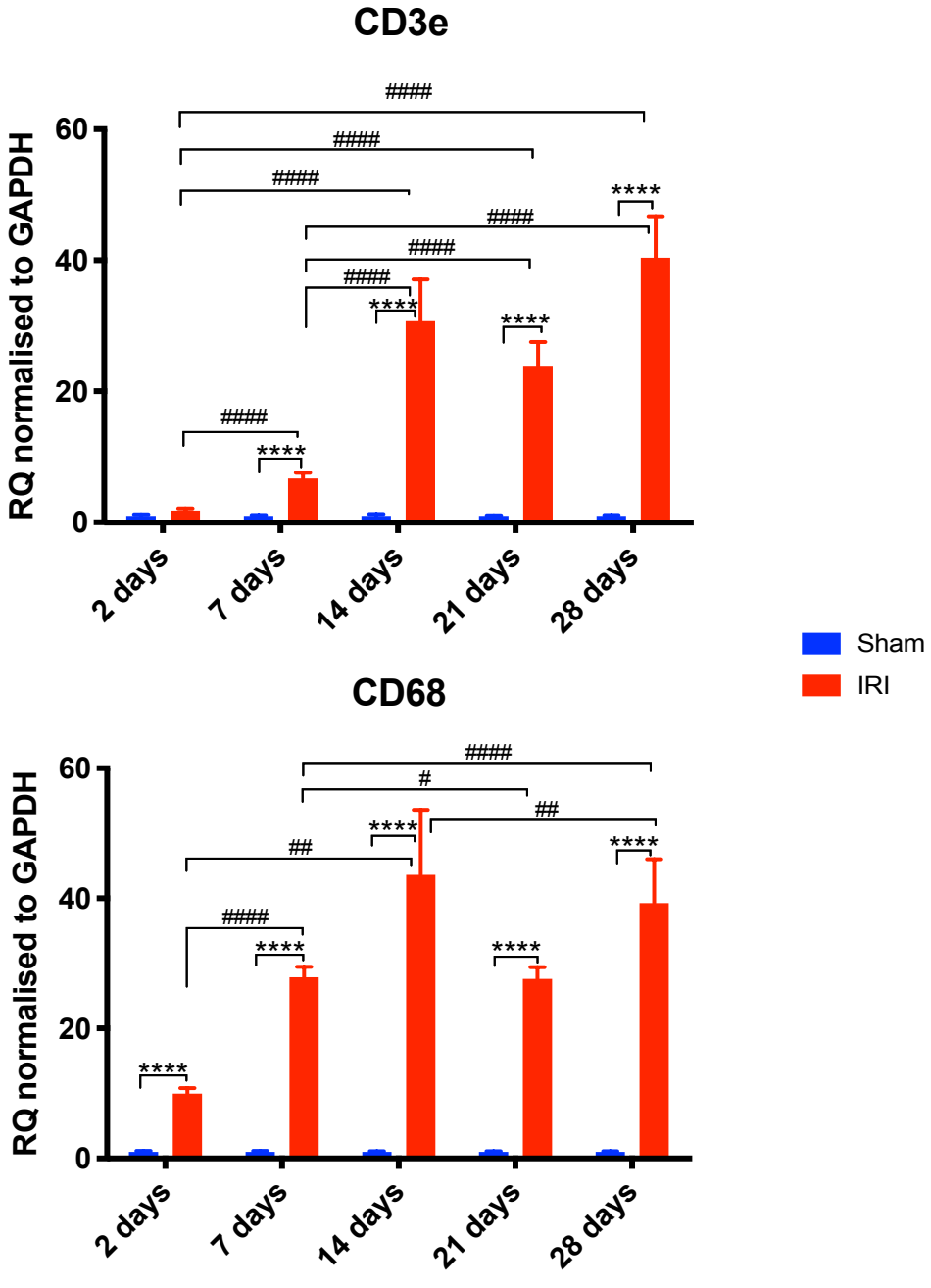

Figure 5.10 CD3e and CD68 gene expression. Male C57bl/6 mice were subjected to 18 minutes unilateral renal IRI and culled at 2, 7, 14, 21 and 28 days (n=7/8) minutes compared to sham operated controls (n=4). Gene expression quantified from total kidney RNA. cDNA synthesised and expression determined by Taqman qRT-PCR using specific gene primers and normalised to GAPDH. Bars represent mean RQ + RQ max; **** p<0.0001 when comparing sham to IRI, # p<0.05 ### p<0.001, #### p<0.0001 when comparing IRI groups. One-way ANOVA with Tukey's post-hoc test.

5.2.4 $CD3^+$ cells are present at 2 days following injury

Immunofluorescent staining for $CD3^+$ T cells revealed evidence of staining at 2 days (**Figure 5.11,** red arrows) which may represent tissue specific T cells at such an early stage of injury. These areas were concentrated around tubules in keeping with evidence that $CD4^+$cells (a subset of $CD3^+$ cells) can interact with damaged tubular epithelial cells via antigen presenting cell capacity in response to IRI. There was no evidence of CD3e staining in sham sections as areas that look positive for CD3e were also present on the autofluorescence sections.

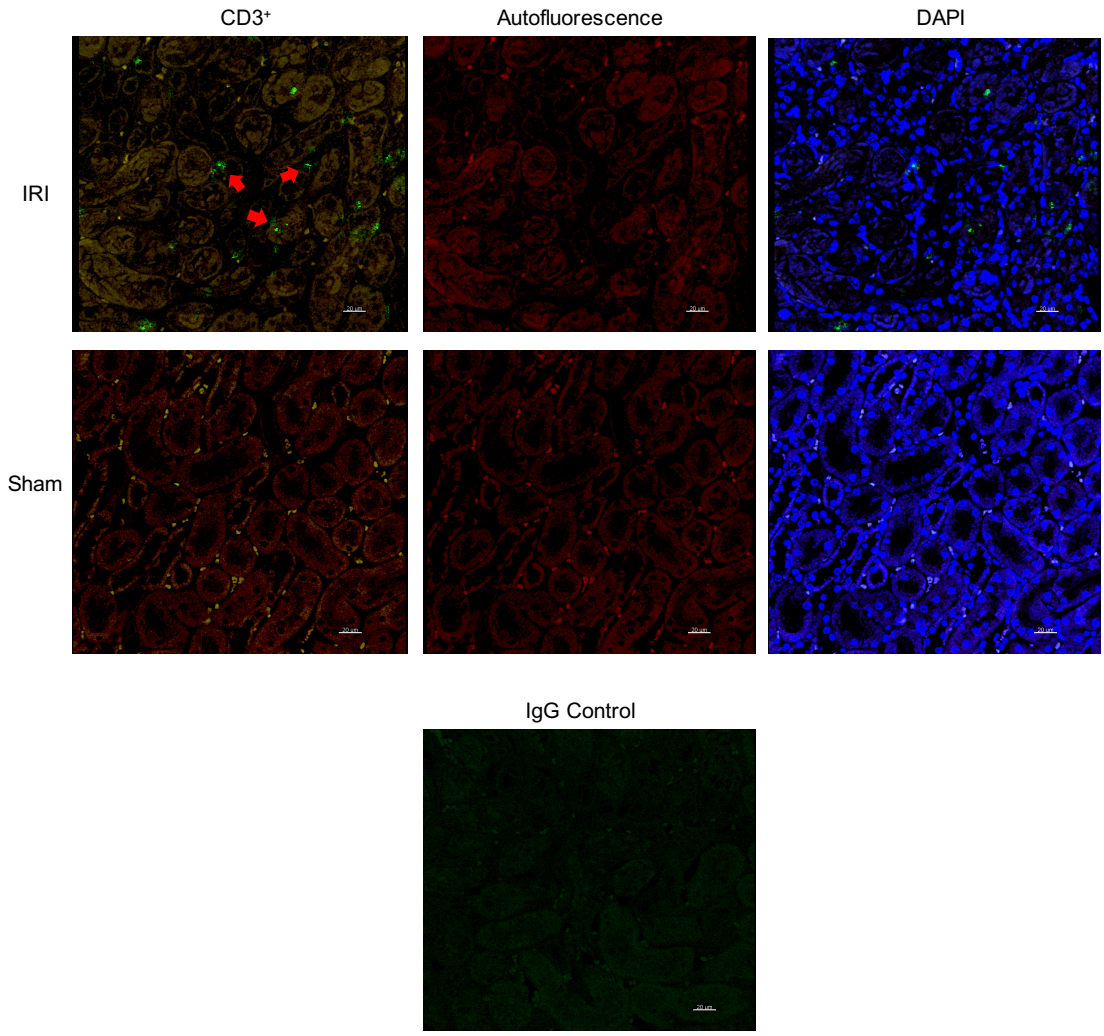

Figure 5.11 Representative immunohistochemistry staining for CD3e at 2 days. Male C57bl/6 mice were subjected to 18 minutes unilateral renal IRI and culled at 2 days (n=8) and compared to sham operated controls (n=4). Zinc fixed and paraffin embedded 3μm sections were cut and stained with CD3e primary antibody and AlexaFluro-488 secondary antibody. Red arrows demonstrate $CD3^+$ staining.

5.2.5 Unilateral ischaemia reperfusion injury results in upregulation of profibrotic gene expression as early as 2 days

There was upregulation of pro-fibrotic gene expression at all times points following injury as demonstrated in **Figure 5.12**. Interestingly, there was a 22- and 23-fold increase in *col1a* and *col3a* respectively as early as 2 days which is in keeping with findings in the literature where elevation of pro-fibrotic gene expression is observed before histological evidence of collagen deposition[313]. *Col3a* expression subsequently increased to 69-fold at 7 days whereas *Col1a* was highest at 14 days with a 57-fold increase in expression. Like *col3a*, expression of *PDGFR-β*, a surface marker of activated fibroblasts, was also greatest at 7 days. These results suggest that there is significant overlap in peak expression of pro-inflammatory and pro-fibrotic genes between 7-14 days after injury demonstrating the transition between inflammation and fibrosis in this model. Beyond this, sustained upregulation of pro-fibrotic genes was in keeping with progressive collagen deposition and fibrosis as demonstrated on picrosirius red staining.

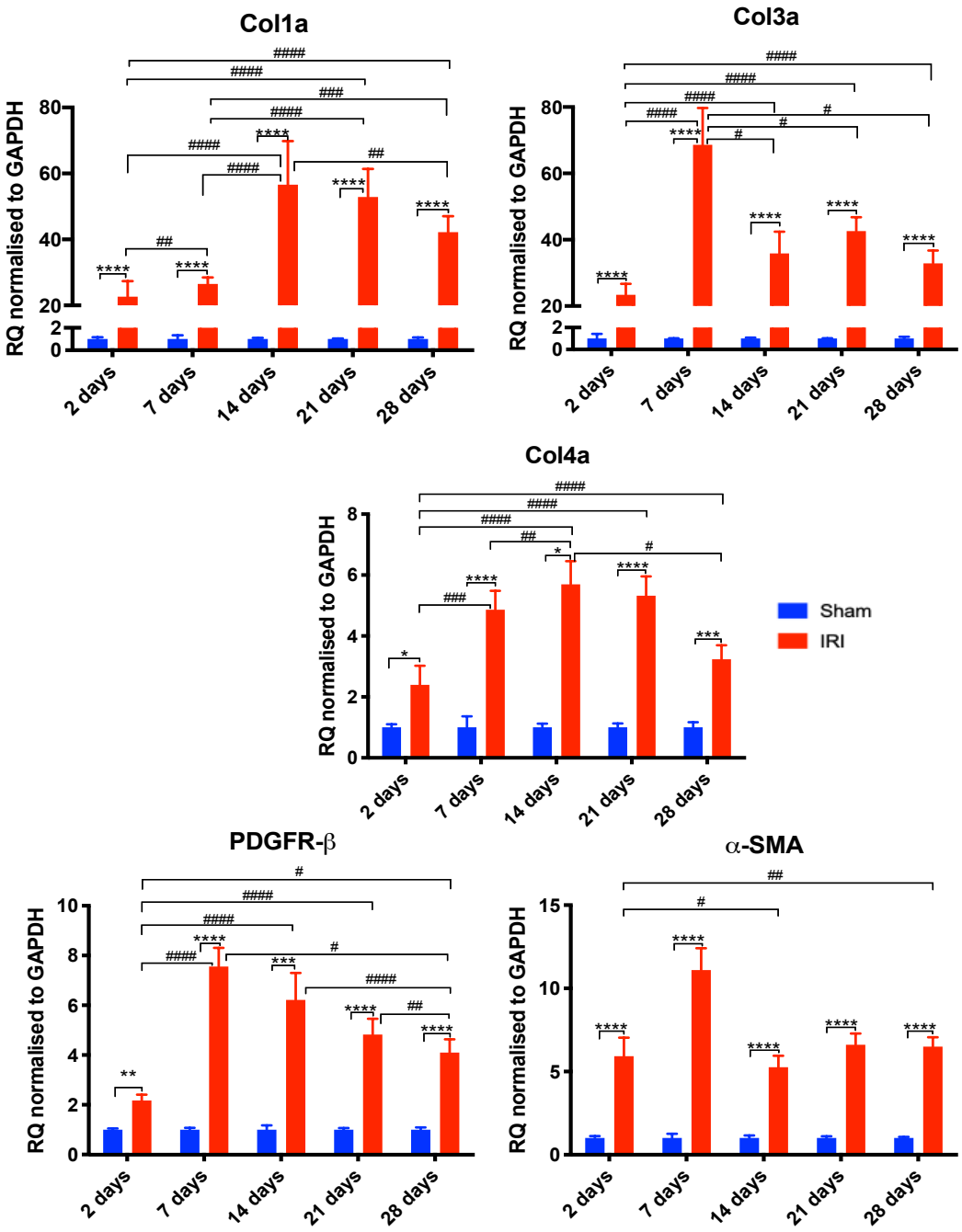

Figure 5.12 Pro-fibrotic gene expression. Male C57bl/6 mice were subjected to 18 minutes unilateral renal IRI and culled at 2, 7, 14, 21 and 28 days (n=7/8) minutes compared to shams(n=4). Gene expression quantified from total kidney RNA, cDNA synthesised and expression determined by Taqman qRT-PCR using specific gene primers and normalised to GAPDH. Bars represent mean RQ + RQ max; **p<0.01*** p<0.001 **** p<0.0001 when comparing sham to IRI, # p<0.05 ### p<0.001, #### p<0.0001 when comparing IRI groups. One-way ANOVA with Tukey's post-hoc test.

5.3 Time course of changes in miR-214 expression following 18 minutes of unilateral renal ischaemia reperfusion injury

5.3.1 MiR-214 is upregulated at all time points following 18 minutes of unilateral renal ischaemia reperfusion injury

In order to follow up the finding of early upregulation, miR-214 expression was examined at various times following injury to determine whether it remained upregulated at different stages of injury and fibrosis.

Figure 5.13 demonstrates that miR-214 is significantly upregulated in the early phase of injury in the ischaemic kidney with 1.6-fold increase at 2 days ($p<0.05$) which increased to 3.1-fold increase by 7 days ($p<0.001$, one-way Anova with Dunnett's adjustment). Expression continued to increase in a step wise manner and peaked at 21 days when there was histological evidence of significant fibrosis (4.3-fold increase at 14 days, 5.5-fold increase at 21 days, 4.1-fold increase at 28 days, all one-way ANOVA with Dunnett's adjustment).

MiR-214 was also more highly expressed in this model compared to miR-21 at all time points except 7 days where miR-21 was increased 4.4-fold compared to 3.1 for miR-214. MiR-21 has been shown to be upregulated in renal injury by multiple groups in early injury and fibrosis. Interestingly, there was no significant difference in miR-21 expression at 2 day as might be expected from previous studies[314] (**Figure 5.14**). There was however upregulation of miR-21 at 7 days (4.4-fold increase $p<0.0001$); 14 days (3.7-fold increase, $p=0.0007$); 21 days (3.4-fold increase, $p=0.001$) and 28 days (2.8-fold increase, $p=0.006$; all groups all one-way ANOVA with Dunnett's adjustment.

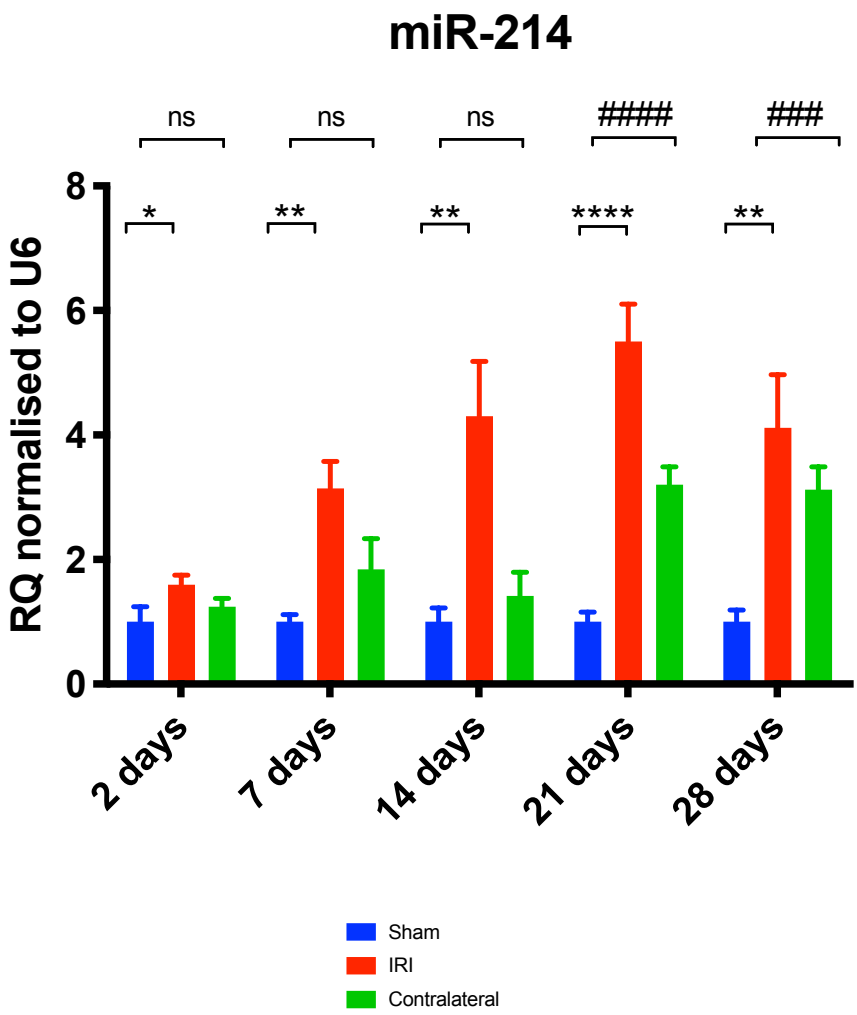

Figure 5.13 MiR-214 expression. Male C57bl/6 mice were subjected to 18 minutes unilateral renal IRI and culled at 2, 7, 14, 21 and 28 days (n=7/8) minutes compared to sham operated controls (n=4). MiR expression quantified from total kidney RNA, reverse transcription performed, and expression determined by Taqman qRT-PCR using specific miR primers. Data and normalised to U6. Bars represent mean RQ + RQ max **p<0.01, **** p<0.001 comparing IRI kidney vs sham; ### p<0.001 #### p<0.0001 comparing contralateral kidney to sham. One-way Anova with Dunnett's adjustment.

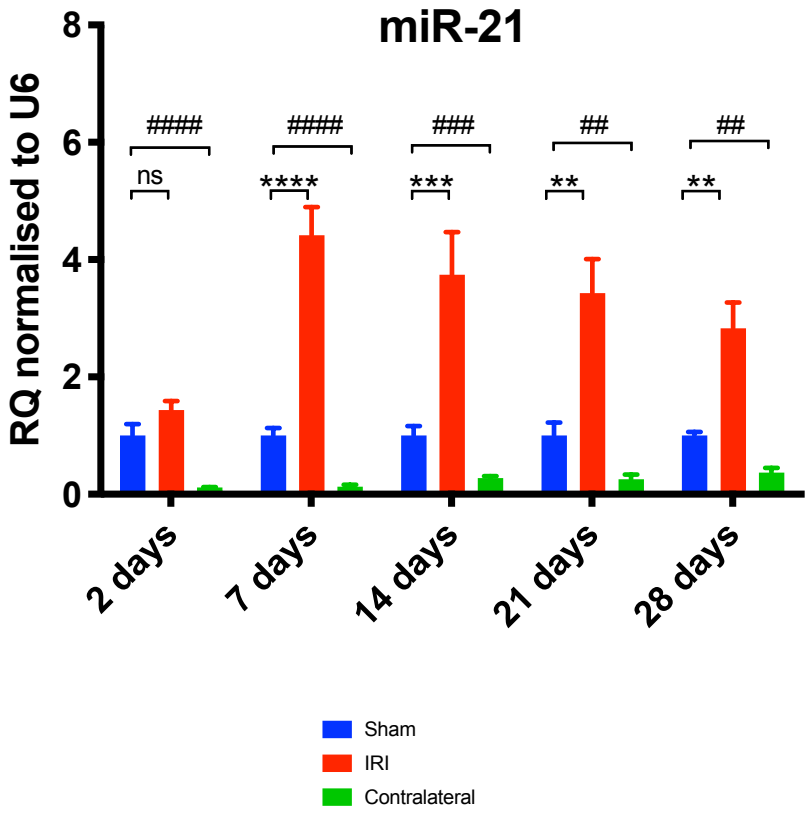

Figure 5.14 MiR-21 expression. Male C57bl/6 mice were subjected to 18 minutes unilateral renal IRI and culled at 2, 7, 14, 21 and 28 days (n=7/8) minutes compared to sham operated controls (n=4). MiR expression quantified from total kidney RNA. reverse transcription performed, and expression determined by Taqman qRT-PCR using specific miR primers. Data and normalised to U6. Bars represent mean RQ + RQ max **p<0.01, ***p<0.001 ****p<0.0001 comparing IRI kidney vs sham; ## p<0.01 ### p<0.001 #### p<0.0001 comparing contralateral kidney to sham. One-way Anova with Dunnett's adjustment.

Expression of miR-29c typically decreases following injury and has been shown to be downregulated in renal fibrosis. **Figure 5.15** demonstrates miR-29c expression across all time points. As might be expected, there is no significant difference in expression at 2 days however there is significant downregulation at 7 and 21 days ($p<0.05$ and $p<0.0001$ respectively, one-way ANOVA with Dunnett's adjustment).

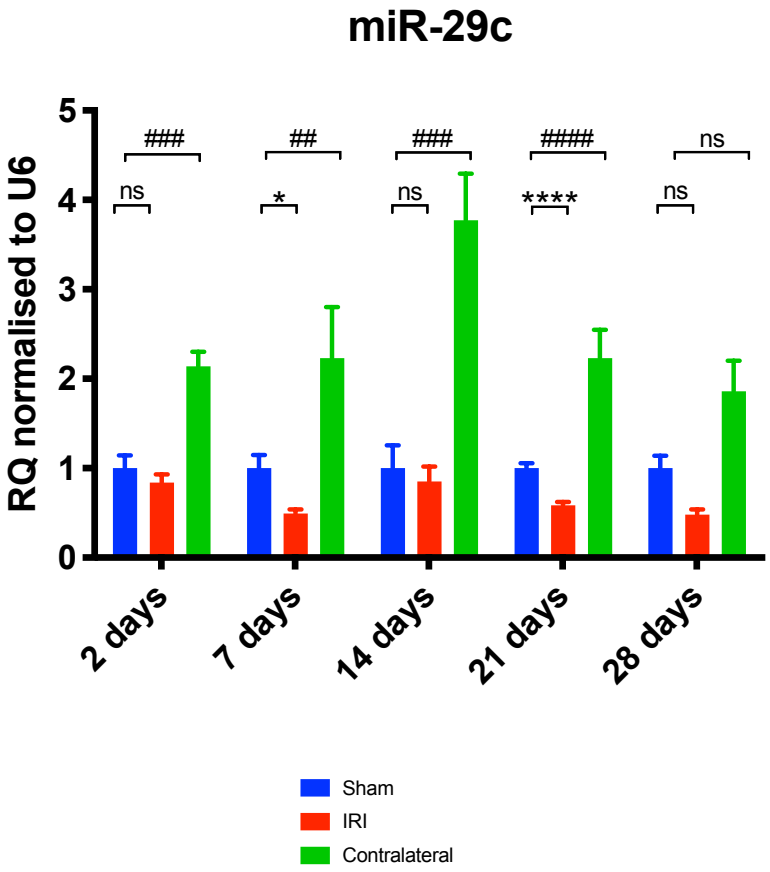

Figure 5.15 MiR-29c expression. Male C57bl/6 mice subjected to unilateral renal IRI and culled at 2, 7, 14, 21 and 28 days (n=7/8) minutes compared to sham operated controls (n=4). MiR expression quantified from total kidney RNA, reverse transcription performed, and expression determined by Taqman qRT-PCR using specific miR primers. Data and normalised to U6. Bars represent mean RQ + RQ max *p<0.05, **** p<0.001 comparing IRI kidney to sham; ##p<0.01, ### p<0.001 #### p<0.0001 comparing contralateral kidney to sham. One-way Anova with Dunnett's adjustment.

5.3.2 MiR expression in the contralateral kidney

MiR expression was examined in the contralateral kidney which undergoes compensatory hypertrophy in response to injury. Although the uninjured kidney appeared macroscopically normal throughout the time-course, the sequalae of combined haemodynamic changes and systemic inflammation may result in an altered transcriptome.

MiR-214 was upregulated in the contralateral kidney at 21 and 28 days, with a 3.2 ($p<0.0001$) and 3.1-fold ($p<0.001$) increase in expression respectively, (both one-way Anova with Dunnett's adjustment, compared to time-matched controls, **Figure 5.13**). There was no upregulation of miR-214 at any earlier time points in the experiment. The increase in miR-214 is contrary to what is seen in the expression of renal miR-21 which was significantly downregulated compared to sham operated controls at all timepoints following injury (**Figure 5.14**). The greatest decrease was demonstrated at 2 days (89% reduction in expression, $p<.0001$) but by 28 days, expression had increased marginally compared to the early time point but expression was still downregulated by 66% compared to time-matched controls.

MiR-29c expression was significantly upregulated at all time points following injury except at 28 days where there was no significant difference in expression compared to time-matched controls (**Figure 5.15**). The greatest change was seen at 14 days when there was a 3.7- fold increase in expression ($p<0.001$) before decreasing to a 2-fold increase at 21 days ($p<0.0001$).

Downregulation of miR-21 and upregulation of miR-29c are the opposite of what was observed in the injured kidney. MiR-21 is usually upregulated in renal injury and is associated with ischaemia reperfusion injury and fibrosis[182]; knocking miR-21 down protects the kidney from injury in multiple *in vivo* models[182,201]. MiR-29c however is

typically downregulated in renal fibrosis and upregulation results in repression of pro-fibrotic gene expression including *col3a*, *col4a* and *MMP2 in vitro*[222,223]. The results here demonstrate an altered transcriptome, possibly reflecting a protective state following injury where the uninjured kidney is undergoing hyperfiltration to compensate for the injured kidney. It is unclear why miR-214 would be upregulated when miRs -21 and 29c are demonstrating reciprocal expression, however this may suggest that, after a significant period of compensatory hyperfiltration, there is a subtle injury to the kidney.

5.3.3 MiR-214 is present in injured tubules and the interstitium in the early phase of injury

Having demonstrated that miR-214 was significantly upregulated in early injury, in situ hybridisation was performed in order to localise its expression using 3' 5' Dig-LNA probe for miR-214 on formalin fixed and paraffin embedded kidney tissue (**Figure 5.16**). It demonstrates that miR-214 is expressed under physiological conditions in kidneys from sham-operated animals, particularly within the nucleus of tubular epithelial cells. At 2 days following injury, there is loss of staining around necrotic tubules suggesting these tubules are dead. There is also staining in the remaining damaged tubules and interstitium, potentially from infiltrating inflammatory cells.

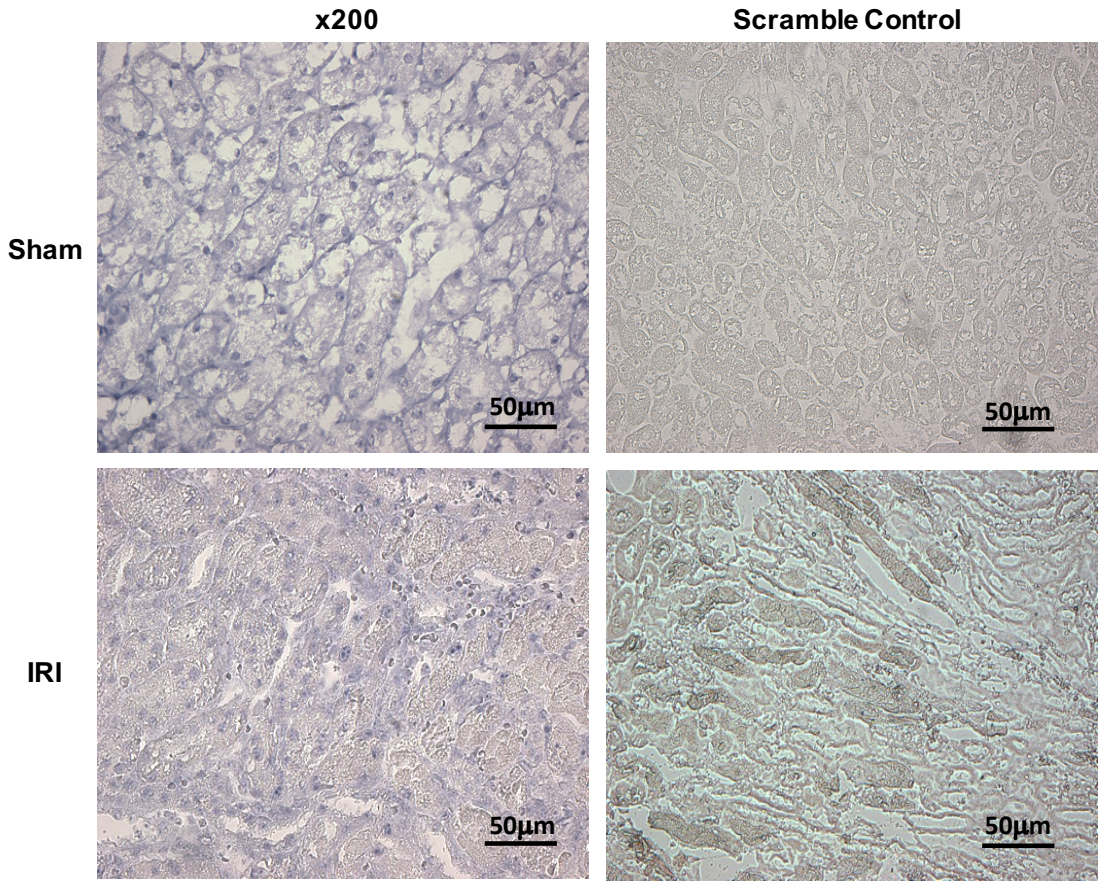

Figure 5.16 In situ hybridisation of miR-214 expression. Formalin fixed and paraffin embedded kidneys were cut into 3µm sections and stained using Dig-LNA probe for miR-214. Pictures are of representative examples demonstrating the outer medulla of the kidney following either sham laparotomy or 18 minutes IRI. All sections demonstrate the outer stripe of the outer medulla. **Top** sham kidney at 200x magnification and scramble control of sham kidney 100x magnification; **bottom** miR-214 expression following IRI at 200x magnification and scramble control of IRI kidney at 200x magnification.

5.3.4 MiR-214 is expressed by multiple cell types following IRI

In a separate experiment, male C57bl/6 mice underwent 18 minutes of unilateral IRI (n=4) or sham laparotomy (n=3) and were sacrificed at 2, 7 and 21 days and FACS sorted for $CD3^+$ cells (CD45+, CD3+), macrophages (CD45+, $F4/80^{hi}$), proximal tubular cells (CD45-, CD31- LTL+) and fibroblasts (CD45- CD31- PDGFRβ+) in order to interrogate which cells expressed miR-214 following injury as data so far is representative of whole kidney tissue.

As expected, there was significant upregulation of miR-214 at all time points from whole kidney tissue, replicating previous results of an overall increase in expression following injury (**Figure 5.17**).

There was a concurrent increase in KIM-1 as well as pro-inflammatory and pro-fibrotic gene expression thus demonstrating induction of injury at the level of the transcriptome previously observed (**Figure 5.18**).

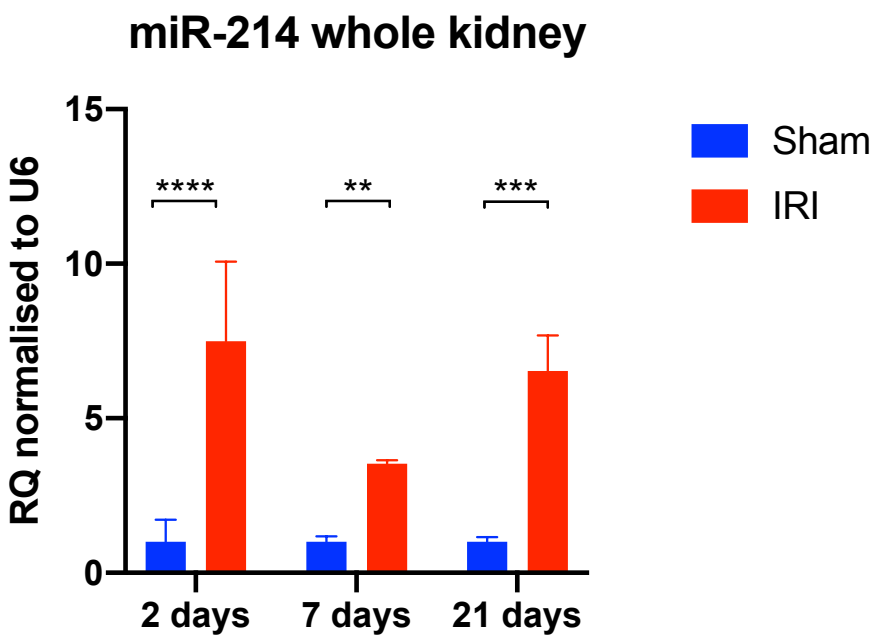

Figure 5.17 MiR-214 expression from whole kidney. Male C57bl/6 mice were subjected to 18 minutes unilateral renal IRI and culled at 2, 7, and 21 days (n=3/4) compared to sham operated controls (n=4). MiR expression quantified from total kidney RNA, reverse transcription performed, and expression determined by Taqman qRT-PCR using specific miR primers. Data and normalised to U6. Bars represent mean RQ + RQ max **p<0.01, **** p<0.001. One way ANOVA with Tukey's adjustment.

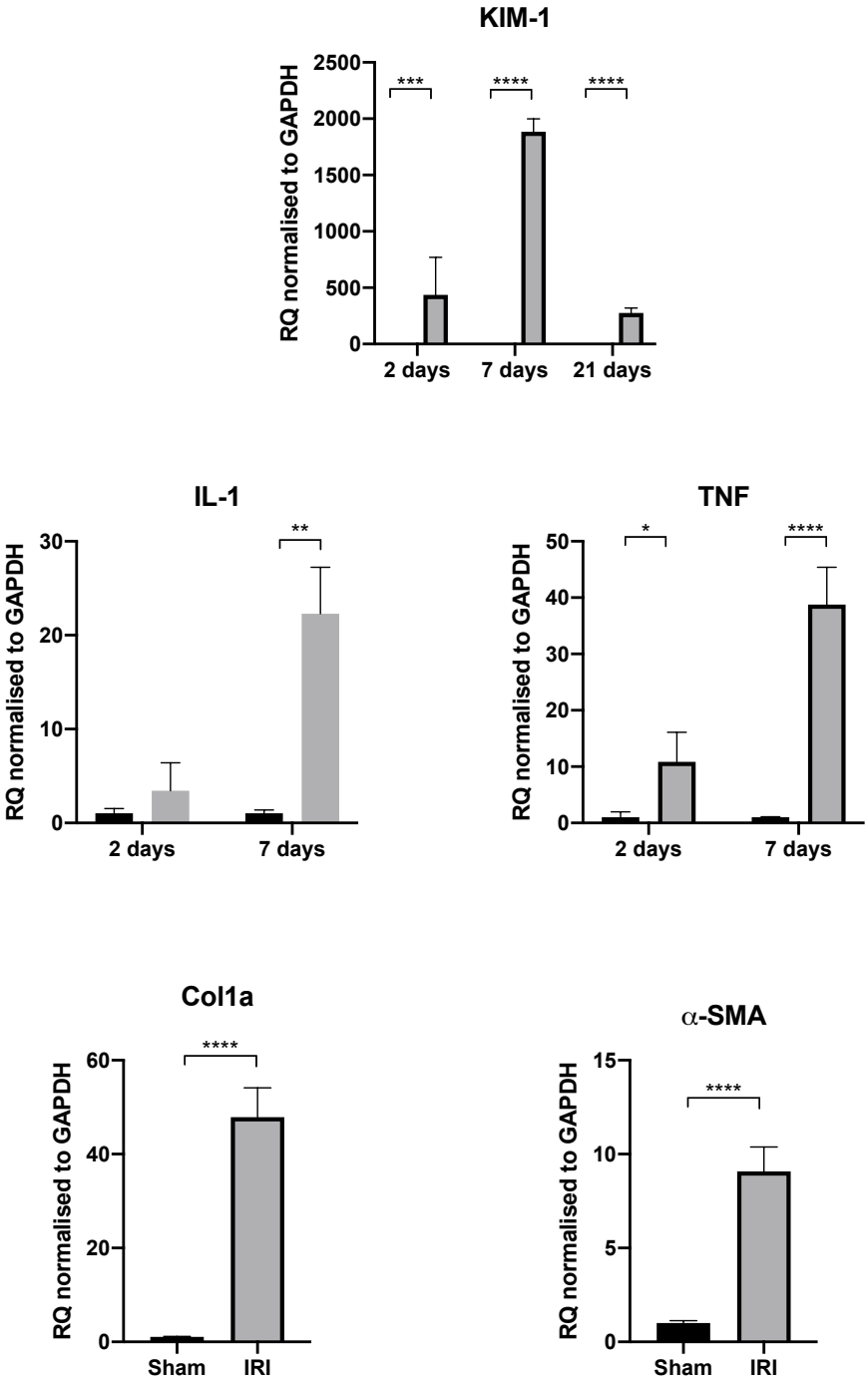

Figure 5.18 Gene expression validating the IRI model. Male C57bl/6 mice were subjected to 18 minutes unilateral renal IRI and culled at 2, 7, and 21 days (n=3/4) minutes compared to sham operated controls (n=4). Gene expression quantified from total kidney RNA. cDNA synthesised and expression determined by Taqman qRT-PCR using specific gene primers and normalised to GAPDH. Bars represent mean RQ + RQ max; **p<0.01, ***p<0.001, **** p<0.0001. Student's t-test.

Analysis of the single populations of FACS sorted cells revealed there was significant upregulation of miR-214 in $CD3^+$ cells at 7 days with a 3.6-fold increase in expression compared to shams (**Figure 5.19**, $p<0.01$, Student's t-test). MiR-214 has been previously shown to be upregulated in T cells subsets; however, this is the first evidence of direct involvement of miR-214 upregulation in T cells within the kidney following injury and as such is a novel finding. MiR-214 was upregulated in $F4/80^{hi}$ macrophages at all times points and was greatest at 21 days when there was a 15-fold increase compared to shams, corresponding to the time of significant fibrosis. Macrophages are a key innate immune cell involved with both propagation and repair of injury and upregulation of miR-214 at all time points suggests that it potentially plays an important role in macrophages.

Acute tubular necrosis and subsequent repair are hallmarks of injury following ischaemia and reperfusion. There was significant upregulation of miR-214 from proximal tubular cells at 2 days where levels were raised 5.5-fold compared to shams and at 21 days, with a 7.4-fold increase, demonstrating that miR-214 may play a potential role in early tubular injury which has been previously described by Denby et al[315]. MiR-214 was also increased in PDGFR-β-positive cells at both 7 and 21 days (15.7 and 6.5-fold increase in expression respectively) in keeping with activation of fibroblasts during transition from early injury to fibrosis. Overall, these results demonstrate that miR-214 arises from multiple cell types in both early injury and transition towards fibrosis.

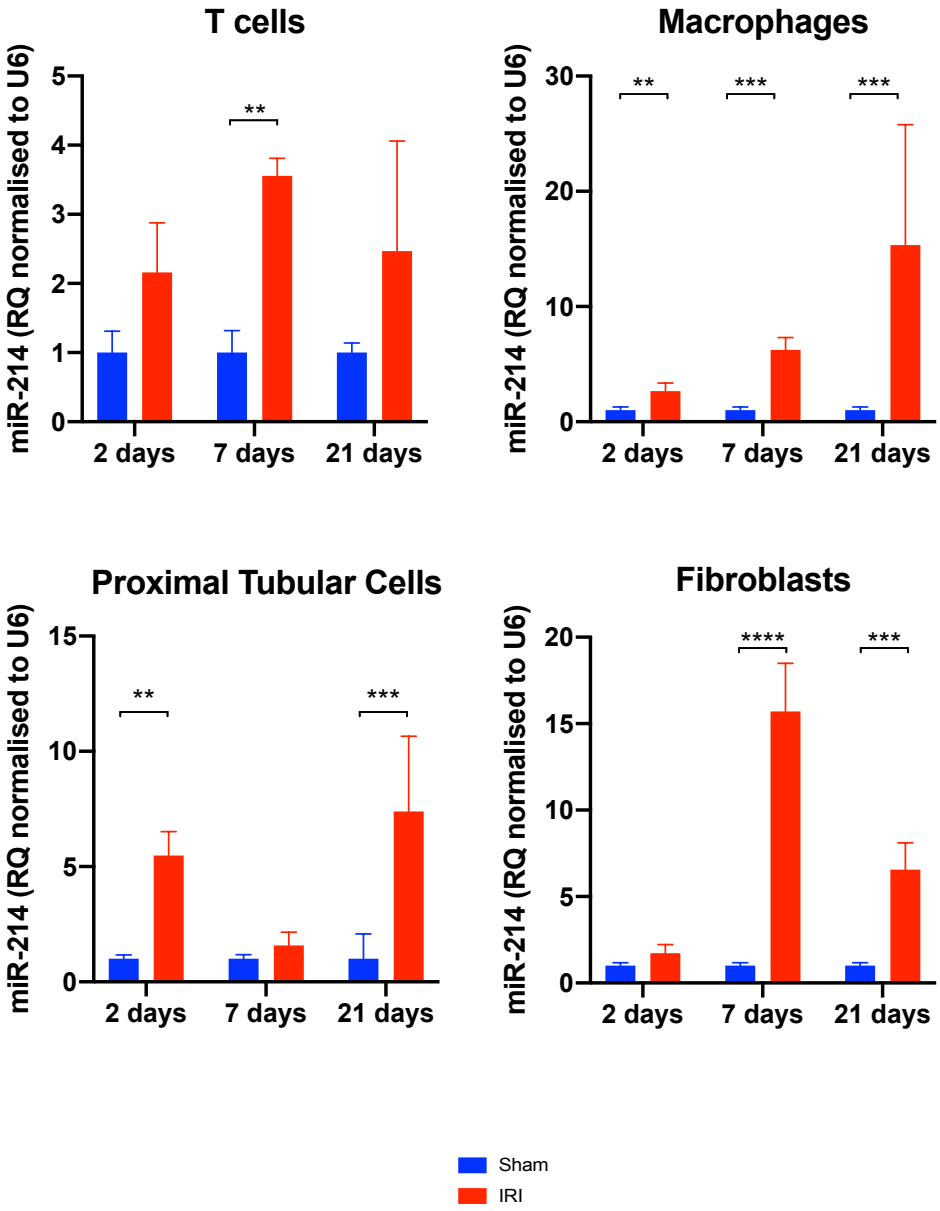

Figure 5.19 MiR-214 expression from FACS sorted cells. Male C57bl/6 mice were subjected to 18 minutes unilateral renal IRI and culled at 2, 7, and 21 days (n=3/4) minutes compared to sham operated controls (n=4). MiR expression quantified from individual cell RNA, reverse transcription performed, and expression determined by Taqman qRT-PCR using specific miR primers. Data and normalised to U6. Bars represent mean RQ + RQ max **p<0.01, **** p<0.001. Student's t-test to time matched controls.

5.3.5 MiR expression in splenocytes of mice undergoing unilateral IRI

Given that miR-214 was significantly upregulated in $CD3^+$ cells at 7 days following IRI, miR-214 expression was examined in spleens from mice undergoing IRI. There was no significant change in expression of miR-214 compared to controls at any time point suggesting that miR-214 expression is potentially arising from kidney specific immune cells (**Figure 5.20**).

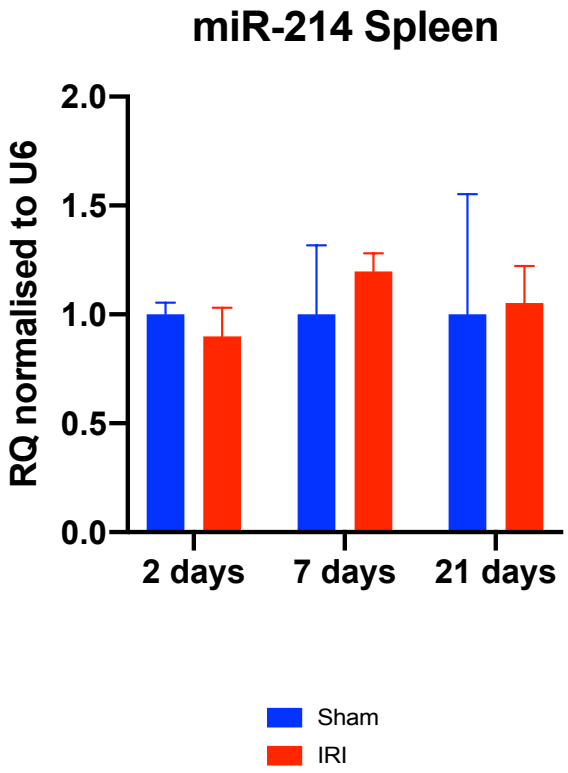

Figure 5.20 MiR-214 expression from spleens. Male C57bl/6 mice were subjected to 18 minutes unilateral renal IRI and culled at 2, 7, and 21 days (n=3/4) compared to sham operated controls (n=4). MiR expression quantified from whole spleens, reverse transcription performed, and expression determined by Taqman qRT-PCR using specific miR primers. Data and normalised to U6. Bars represent mean RQ + RQ max, one way ANOVA with Tukey's adjustment.

5.4 MiR-214 and mechanism of injury

5.4.1 MiR-214 expression in polarized M1 and M2 macrophages

To examine the relative expression of miR-214 in M1 and M2 macrophages, an *ex-vivo* model of activated macrophages from human donors cultured from PBMCs and stimulated with a combination of IFN-γ and LPS for a M1 phenotype or IL-13 and IL-4 for a M2 phenotype was adopted (RNA was taken from an experiment performed by Katie Connor). Results show no significant change in miR-214 expression in either M1 or M2 macrophages (**Figure 5.21**) which is in contrast to results from FACs sorted murine F4/80 cell populations where miR-214 was significantly upregulated at 2, 7 and 21 days. This could represent different cell populations whereby the FACS sorted $F4/80^{hi-}$population were tissue resident as opposed derived from a bone marrow lineage.

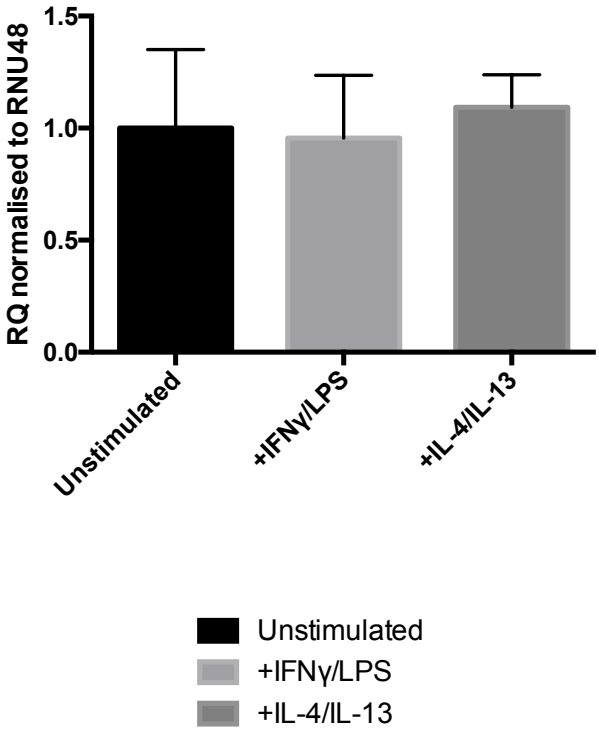

Figure 5.21 MiR-214 expression in polarized ex vivo human monocytes. Human monocytes were cultured ex vivo and stimulated with a combination of either IFNy and LPS or IL-4 and IL-13. MiR expression was quantified using reverse transcription and expression determined by Taqman qRT-PCR using specific miR primers. Data normalised to RNU48. Bars represent mean RQ + RQ max. One way Anova with Dunnett's adjustment n=4 per group.

5.4.2 MiR-214 expression in an *in vitro* model of murine tubular epithelial cell injury

In order to further interrogate the role of miR-214 in tubular injury, rat renal tubular epithelial cells (NRK 52E) were stimulated with TGF-β for either 72 or 96 hours and compared to time matched controls. TGF-β is a well described potent mediator of renal fibrosis and as such has been shown to induce injury *in vitro*[222,310].

Bright-light views of the cells show alterations in cellular architecture following 72 and 96 hours of stimulation. Alongside this, immunocytochemical analysis of α-SMA demonstrates increased staining compared to unstimulated controls in keeping with tubular cell de-differentiation (**Figure 5.22**). Assessment of gene expression was used to examine pro-fibrotic gene expression to order to further validate the model. There was a 4-fold and 9-fold increase in expression of collagen 1 at 72 and 96 hours compared to unstimulated controls ($p<0.01$ and $p<0.0001$ respectively, Student's t-test) and concurrent significant downregulation of E-cadherin at both time points (**Figure 5.23**). These results further demonstrate successful induction of injury, as E-cadherin is key to cell-to-cell adhesion and loss of expression represents cellular de-differentiation which is seen *in vivo* in response to renal injury.

Results show that miR-214 was significantly upregulated at 96 hours as previously described by the group ($p<0.05$, Student's t-test, **Figure 5.24**) thus showing that miR-214 may mediate injury in tubular epithelial cells. There was significant upregulation of miR-21 at both 72 and 96 hours ($p<0.05$, Student's t-test, n=3 complete). MiR-21 has been shown to be upregulated in multiple models of renal injury which were included to further validate this model.

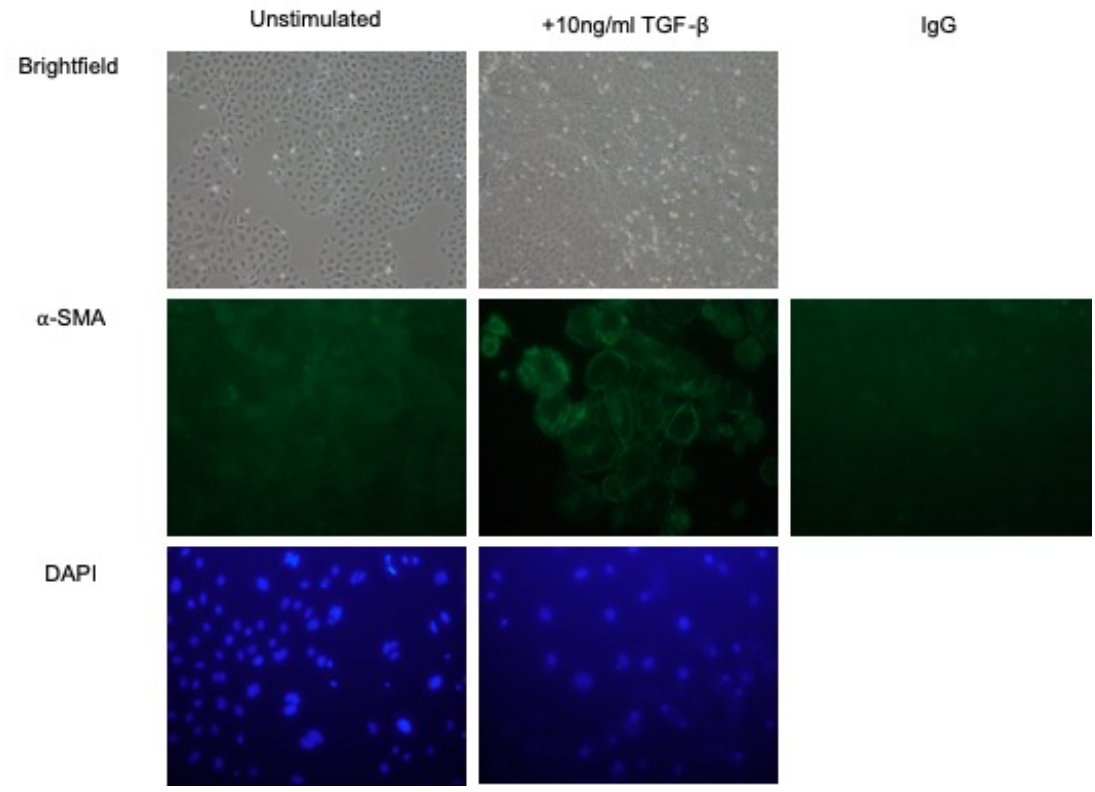

Figure 5.22 NRK-52E stimulated with TGF-β. Representative pictures of rat renal epithelial (NRK-52E) cells stimulated with TGF-β and stained for α-SMA. Species specific IgG used as control.

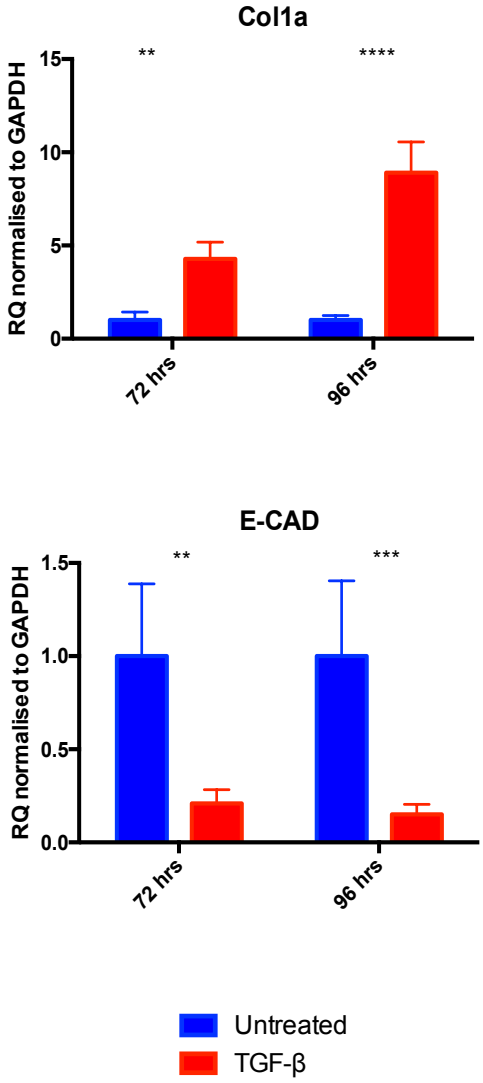

Figure 5.23 Validation of NRK-52E model of renal injury. Rat tubular epithelial cells were stimulated with 10ng/ml TGF-β and RNA extracted at 72 and 96 hours and gene expression quantified. cDNA synthesised and expression determined by Taqman qRT-PCR using specific gene primers and normalised to species specific GAPDH. Bars represent mean RQ + RQ max; **p<0.01, ***p<0.001, **** p<0.0001. Student's t-test comparing time matched unstimulated controls, n=3.

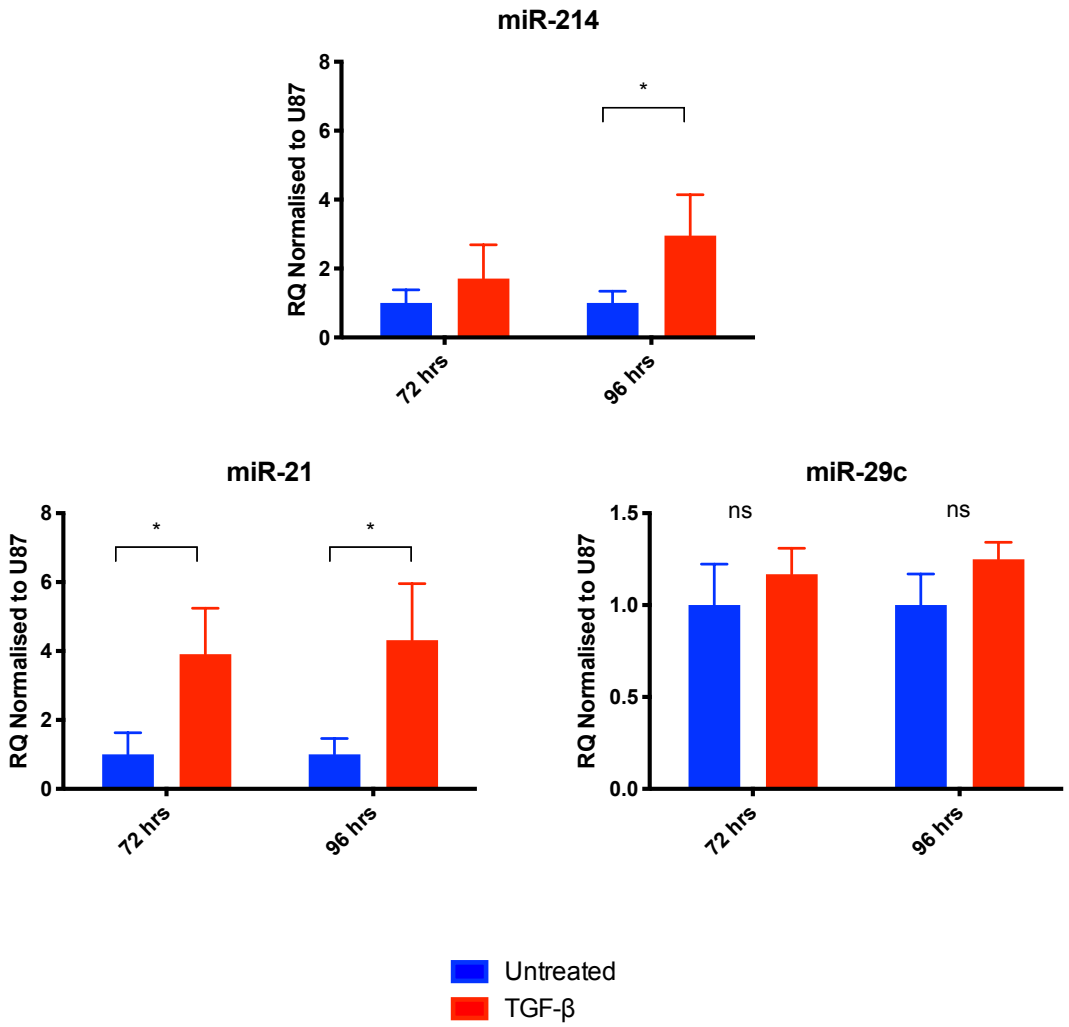

Figure 5.24 MiR expression in an NRK-52E model of renal injury. Rat tubular epithelial cells were stimulated with 10ng/ml TGF-β and RNA extracted at 72 and 96 hours and gene expression quantified. MiR expression was quantified using reverse transcription and expression determined by Taqman qRT-PCR using specific miR primers. Data normalised to U87. Bars represent mean RQ + RQ max; *p<0.05, **p<0.01, ***p<0.00, **** p<0.0001. Student's t-test comparing time matched unstimulated controls, n=3.

5.4.3 MiR-214 expression in an *in vitro* model of rat renal fibroblasts

MiR-214 expression was then examined in an *in vitro* model of renal fibroblasts. Rat renal fibroblasts (NRK 49F) were cultured and stimulated with TGF-β for 72 and 96 hours. Fibroblasts are integral to promoting fibrosis in multiple *in vitro* and *in vivo* models of renal fibrosis under the influence of TGF-β. *In vitro* TGF-β induced activation of fibroblasts has been shown to induce α-SMA expression which is hallmark of fibroblast to myofibroblast differentiation.

Stimulation of fibroblasts with TGF-β resulted in phenotypic changes seen in activated fibroblasts including alterations in cellular structure. **Figure 5.25** shows the normal projections seen in fibroblasts becoming more spindle-like in appearance. There was also evidence of increased PDGFR-β staining on immunohistochemistry together with upregulation of α-SMA at both 72- and 96-hours post injury compared to time matched unstimulated controls. Gene expression also demonstrated a significant upregulation of α-SMA in keeping with myofibroblast differentiation (**Figure 5.26**).

Following stimulation, there was a 3-fold and 3.7-fold increase in levels of miR-214 at 72 and 96 hours respectively demonstrating a potential role of miR-214 in facilitating fibroblast to myofibroblast differentiation (**Figure 5.27**). Although miR-21 has previously been shown to be upregulated in activated fibroblasts, there was no significant difference in miR-21 expression; however, there was a 60% reduction in miR-29c expression.

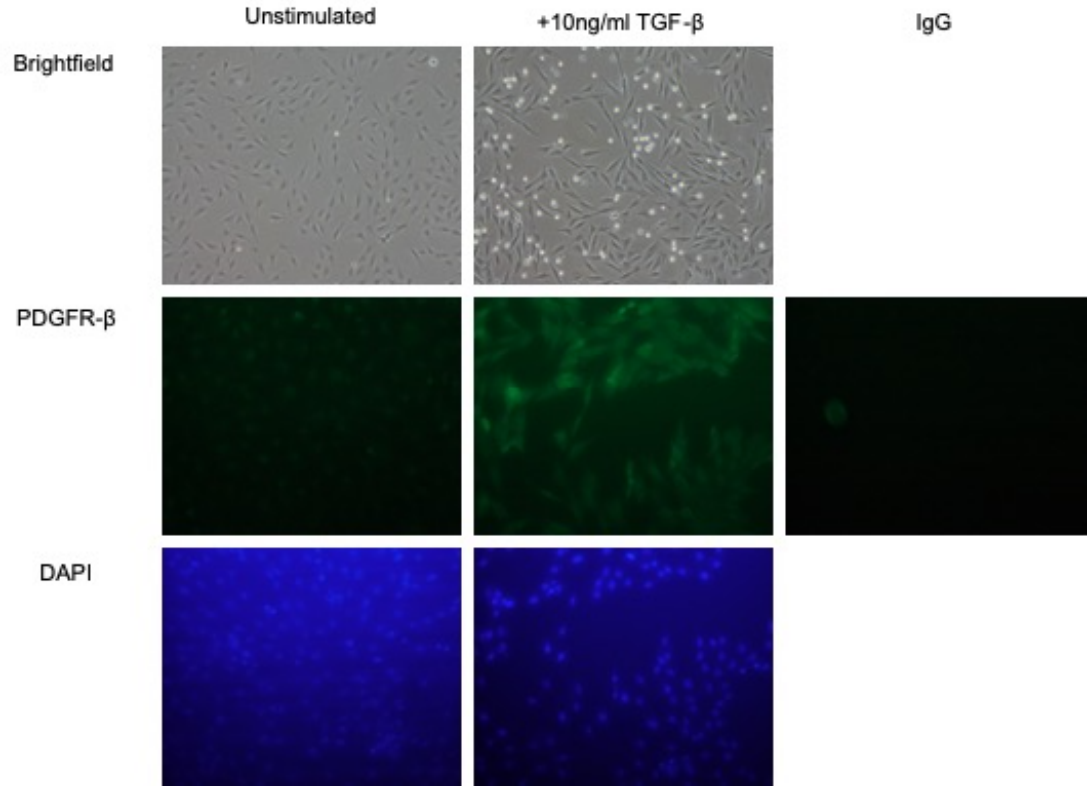

Figure 5.25 NRK-49F stimulated with TGF-β. Representative pictures of rat renal fibroblasts (NRK-49F) cells stimulated with TGF-β and stained for PDGFR-β. Species specific IgG used as control.

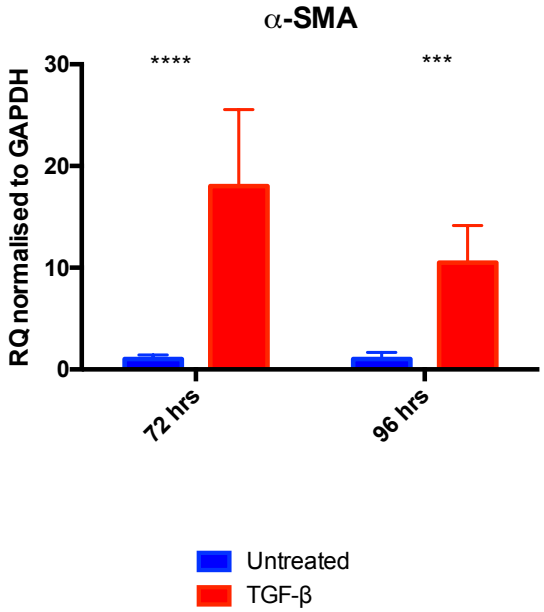

Figure 5.26 Validation of NRK-49F model of renal injury. Rat tubular fibroblasts were stimulated with 10ng/ml TGF-β and RNA extracted at 72 and 96 hours and gene expression quantified. cDNA synthesised and expression determined by Taqman qRT-PCR using specific gene primers and normalised to species specific GAPDH. Bars represent mean RQ + RQ max; **p<0.01, ***p<0.001, **** p<0.0001. Student's t-test comparing time matched unstimulated controls, n=3.

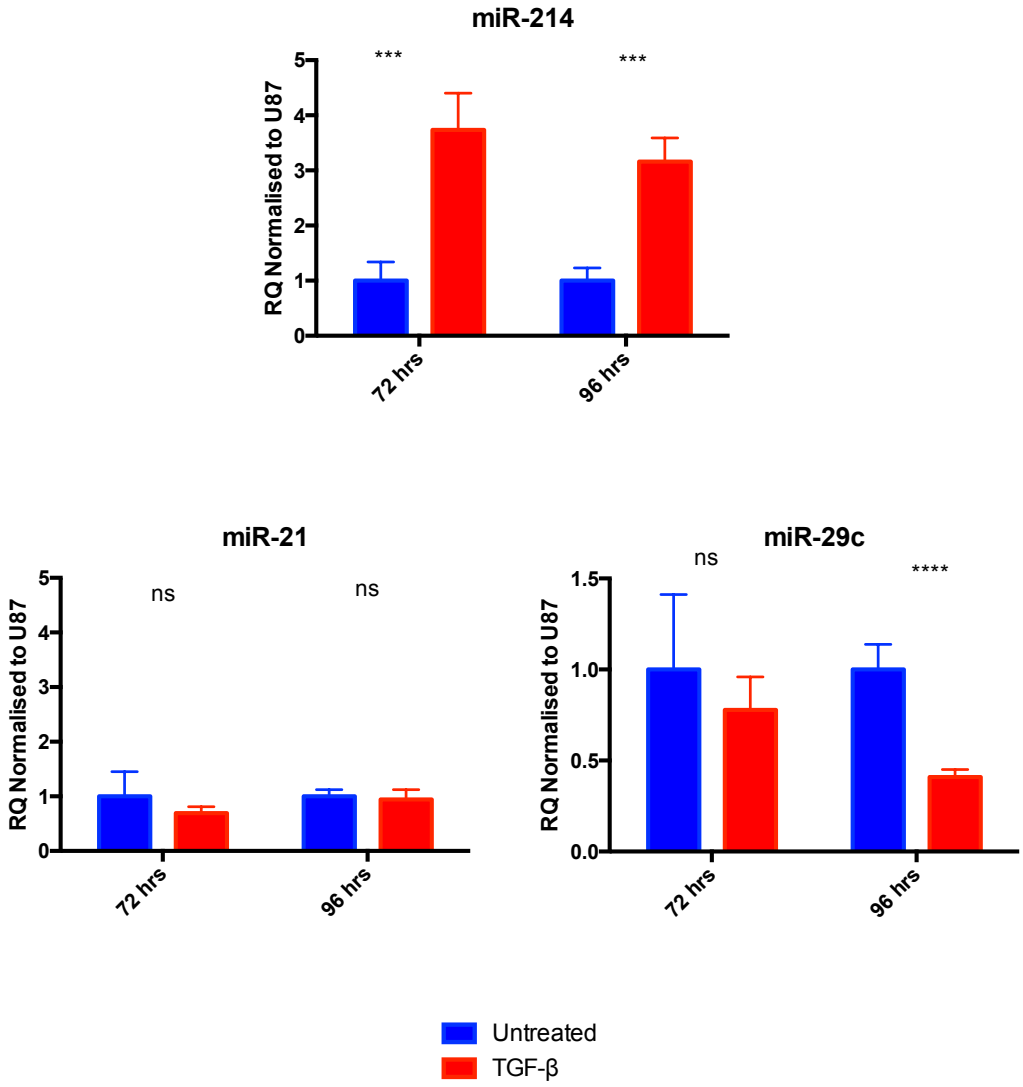

Figure 5.27 MiR expression in an NRK-49F model of renal injury. Rat renal fibroblasts were stimulated with 10ng/ml TGF-β and RNA extracted at 72 and 96 hours and gene expression quantified. MiR expression was quantified using reverse transcription and expression determined by Taqman qRT-PCR using specific miR primers. Data normalised to U87. Bars represent mean RQ + RQ max; *p<0.05, **p<0.01, ***p<0.001, **** p<0.0001. Student's t-test comparing time matched unstimulated controls, n=3.

5.5 The effect of miR-214 deletion on early injury and fibrosis

Having demonstrated that miR-214 was significantly upregulated in early injury and fibrosis, IRI was performed in a miR-214 knockout model in order to test the hypothesis that miR-214 ablation ameliorates early injury and fibrosis following IRI.

MIR-214 was shown to peak at 21 days when there was both histological and transcriptomic changes in keeping with significant fibrosis. Elevation in miR-214 as early as 2 days is a novel finding in the context of IRI and, given these findings, IRI was performed in miR-214$^{-/-}$ mice at 2 and 21 days.

IRI was performed in miR-214$^{-/-}$ and miR-214$^{+/+}$ male mice and compared to outcomes in sham operated miR-214 $^{-/-}$ and miR-214$^{+/+}$ mice.

5.5.1 Phenotypic differences when comparing miR-214$^{-/-}$ and miR-214$^{+/+}$ mice

5.5.1.1 MiR-214 is knocked out successfully in miR-214$^{-/-}$ mice

MiR-214 expression was assessed from whole kidney in order to demonstrate successful knock out. **Figure 5.28** shows that miR-214 is successfully knocked out in all miR-214 $^{-/-}$ animals when compared to WT sham operated controls.

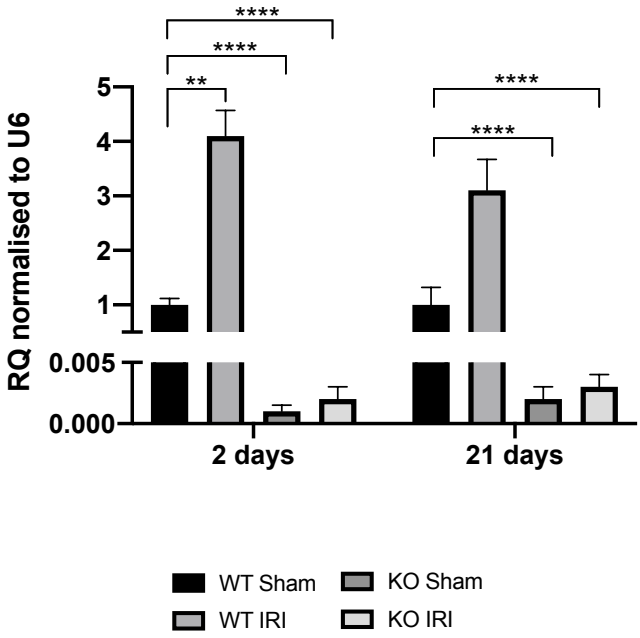

Figure 5.28 MiR-214 expression at 2 and 21 days. Male C57bl/6 miR-214$^{+/+}$ and miR-214$^{-/-}$ mice were subjected to 18 minutes unilateral renal IRI and culled at 2 and 21 days (n=5/6) compared to sham operated controls (n=3). MiR expression quantified from total kidney RNA, reverse transcription performed, and expression determined by Taqman qRT-PCR using specific miR primers. Data and normalised to U6. Bars represent mean RQ + RQ max **p<0.01, **** p<0.001. One-way ANOVA with Tukey's adjustment for multiple comparison.

5.5.1.2 There is a significant difference in body weight in miR-214$^{-/-}$ and miR-214$^{+/+}$ mice

Mice were weighed pre-operatively and routinely for 3 days post-operatively followed by twice weekly up to 21 days. MiR-214$^{-/-}$ male mice weighed significantly less than miR-214$^{+/+}$ male mice at baseline and at all time points following surgery (**Figure 5.29**). **Figure 5.30** shows there was no significant difference in percentage weight gain when comparing all groups in the 21-day experiment.

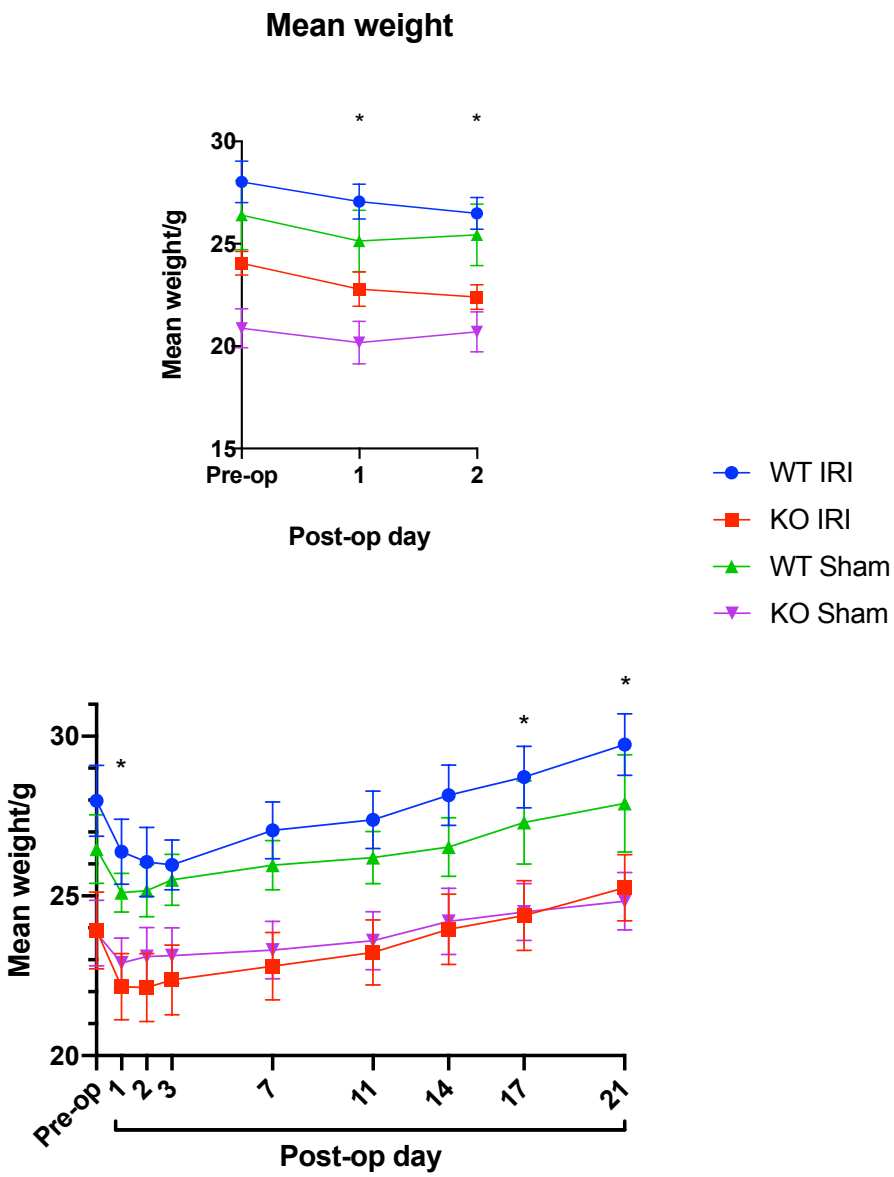

Figure 5.29 Pre-operative and post-operative mean body weight. Male C57bl/6 miR-214$^{+/+}$ and miR-214$^{-/-}$ mice were subjected to 18 minutes unilateral renal IRI for 18 minutes and culled at 2 and 21 days (n=5-6) compared to sham operated controls (n=3). **Top**: mice culled at 2 days. **Bottom**: mice culled at 21 days. * p<0.05, KO IRI vs WT IRI; one-way ANOVA with Tukey's adjustment for multiple comparisons.

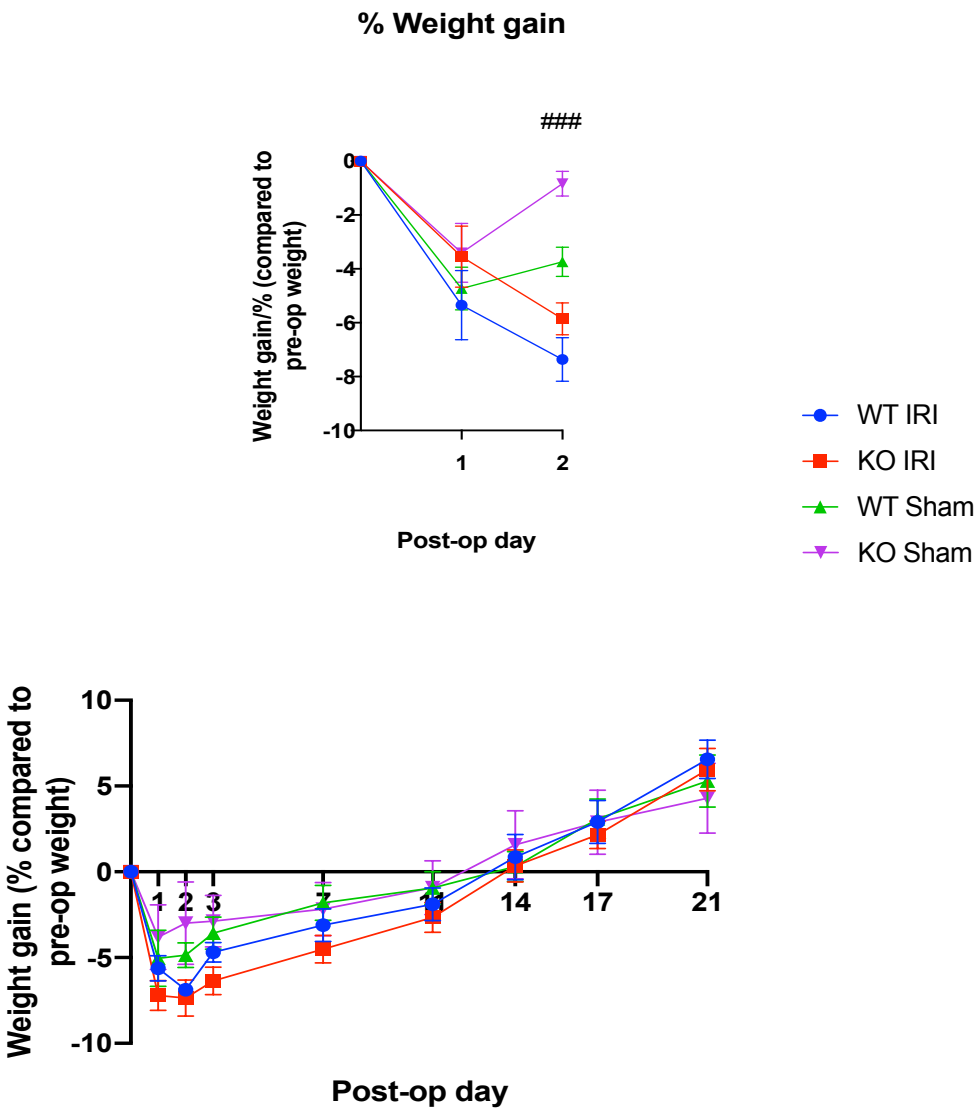

Figure 5.30 Pre-operative and post-operative mean percentage change in body weight. Male C57bl/6 miR-214$^{+/+}$ and miR-214$^{-/-}$ mice were subjected to 18 minutes unilateral renal IRI for 18 minutes and culled at 2 and 21 days (n=5-6) compared to sham operated controls (n=3). **Top**: mice culled at 2 days. **Bottom**: mice culled at 21 days. ### p<0.001, KO sham versus KO IRI; one-way ANOVA with Tukey's adjustment for multiple comparisons.

5.5.2 The effect of miR-214$^{-/-}$ on outcome at 2 days following IRI

5.5.2.1 There was a significant increase in kidney weight in miR-214$^{-/-}$ mice at 2 days following IRI

Examination of kidney weight following IRI at 2 days demonstrated a significant increase in kidney weight in the miR-214$^{-/-}$ IRI group compared to miR-214$^{-/-}$ sham-operated control but no significant increase in miR-214$^{+/+}$ kidney weights when comparing IRI and sham (**Figure 5.31**). The increase in weight in the knockout group suggests that the knockout IRI kidney is potentially more oedematous than the wildtype kidney following injury.

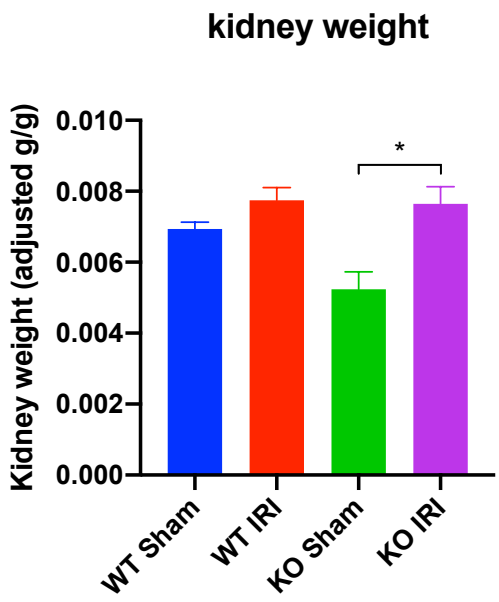

Figure 5.31 Comparison of kidney weights from miR-214$^{-/-}$ and miR-214$^{+/+}$ at 2 days. The right kidney from animals undergoing 18 minutes unilateral IRI (n=5-6 per group) was compared against time-matched sham-operated controls (n=3 per group) at 2 days. Kidney weight adjusted for body weight g/g. Bars represent group mean + SEM *p<0.05. One-way ANOVA with Tukey's adjustment for multiple comparison.

5.5.2.2 There was no significant difference in tubular damage in miR-214$^{-/-}$ mice at 2 days

There was no significant difference in ATN scores when comparing miR-214$^{-/-}$ and miR-214$^{+/+}$ IRI groups (52% vs 65% miR-214$^{-/-}$ vs miR-214$^{+/+}$ respectively, one-way Anova with Tukey's correction, **Figure 5.32**). On lower power magnification, there was evidence of widespread tubular necrosis and disorganised structure within the outer stripe of the outer medulla whilst the cortex was spared from injury. On higher power, debris and casts are seen within grossly necrotic tubules. Furthermore, there is evidence of cellular infiltrates within the interstitium. Sham-operated controls had intact kidney structure with no evidence of tubular necrosis within the OSOM.

Following on from histological analysis, KIM-1 gene expression was assessed from whole kidney tissue. KIM-1 expression was elevated in both miR-214$^{+/+}$ and miR-214$^{-/-}$ IRI groups compared to their respective controls (**Figure 5.33**). There was no significant difference when comparing miR-214$^{+/+}$ and miR-214$^{-/-}$ IRI groups suggesting miR-214$^{-/-}$ does not confer significant protection from tubular damage in the immediate period following IRI.

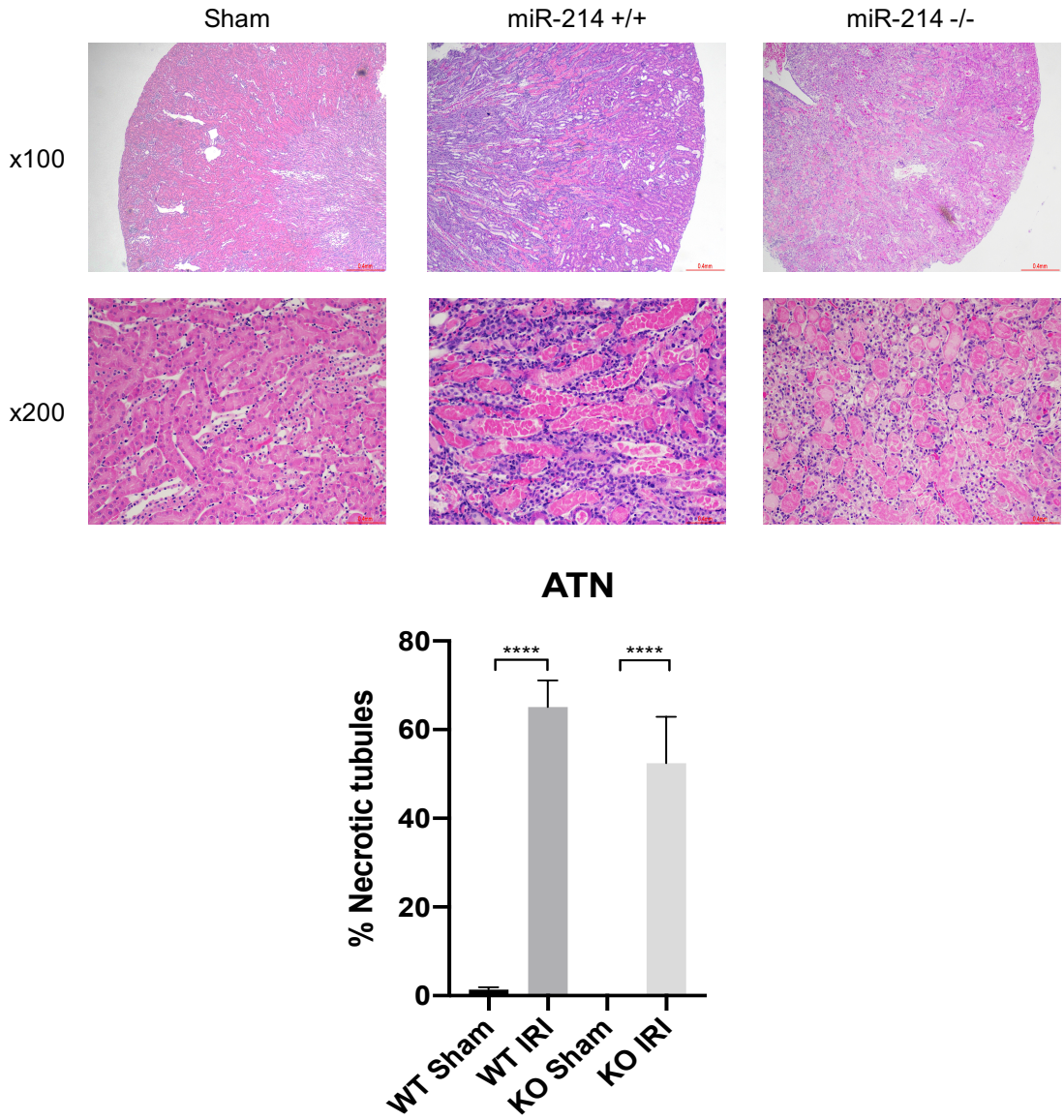

Figure 5.32 Structural injury at 2 days in miR-214$^{+/+}$ and miR-214$^{-/-}$ mice undergoing 18 minutes IRI or sham. Male C57Bl/6 miR-214$^{+/+}$ or miR-214$^{-/-}$ mice either underwent 18 minutes of unilateral IRI (n=5/6) or sham laparotomy (n=3) and sacrificed at 2 days **Top** Haemotoxylin and eosin stains of a sham kidney (left), miR-214$^{+/+}$ (middle) and miR-214$^{-/-}$ (right) kidney undergoing IRI **Bottom** Quantification of ATN in miR-214$^{+/+}$ or miR-214$^{-/-}$ animals undergoing renal IRI (n=5/6), and sham (n=3), represented as mean ± SEM, One way Anova with Tukey's adjustment **** p<0.0001.

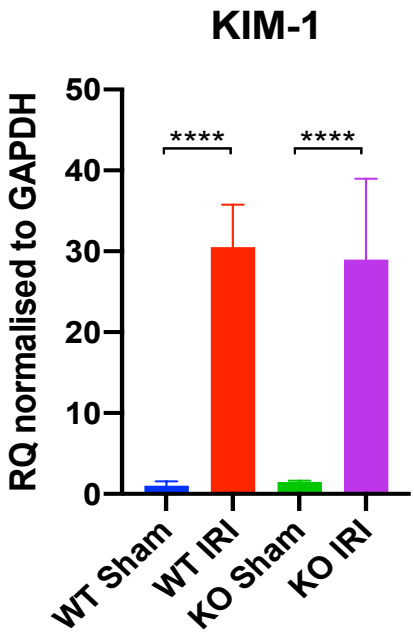

Figure 5.33 KIM-1 expression at 2 days in miR-214$^{+/+}$ or miR-214$^{-/-}$ mice undergoing IRI or sham. Male C57bl/6 mice were subjected to 18 minutes unilateral renal IRI and culled at 2 days (n=5/6) minutes compared to sham operated controls (n=3). Gene expression quantified from total kidney RNA. cDNA synthesised and expression determined by Taqman qRT-PCR using specific gene primers and normalised to GAPDH. Bars represent mean RQ + RQ max; **p<0.01, ***p<0.001, **** p<0.0001. One-way Anova withTukey's adjustment for multiple comparisons.

5.5.2.3 There was significant reduction in pro-inflammatory gene expression in miR-214$^{-/-}$ mice

The same panel of genes as previously described were assessed from whole kidney tissue from all groups. Results demonstrate that there was a significant reduction in pro-inflammatory gene expression in the kidney despite there being no improvement in tubular injury markers in kidneys of miR-214$^{-/-}$ mice following IRI. The greatest reduction in expression was seen in IL-1β were there was a 76% reduction in miR-214$^{-/-}$ mice compared to miR-214$^{+/+}$ mice (9.3-fold versus 40-fold increase respectively). There was also a significant reduction in TNF-α expression (5.4 vs 15.3-fold increase respectively) and IL-6 expression (2.7 vs 6-fold increase respectively) in miR-214$^{-/-}$ mice compared to miR-214$^{+/+}$ mice.

IL-10 was also assessed however expression in the kidneys from miR-214$^{-/-}$ mice was undetectable.

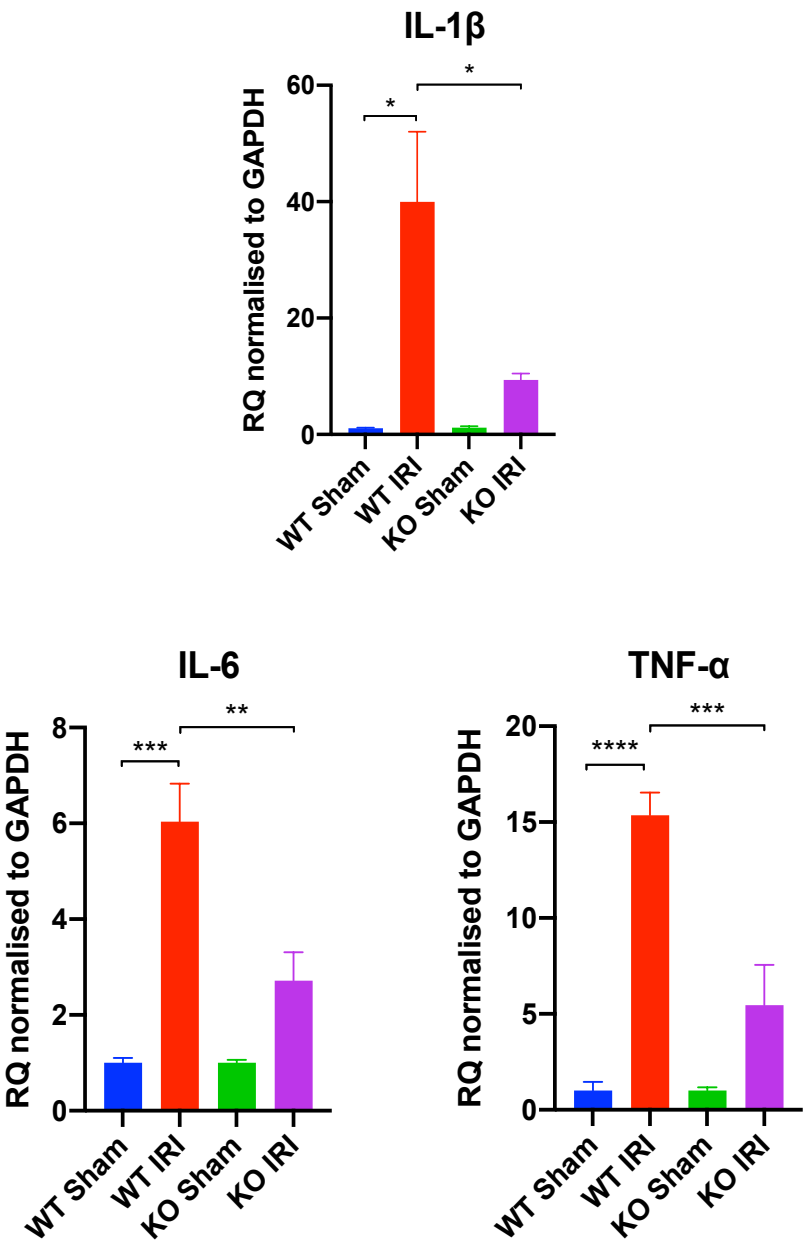

Figure 5.34 Pro-inflammatory expression at 2 days in miR-214$^{+/+}$ or miR-214$^{-/-}$ mice undergoing IRI or sham. Male C57bl/6 mice were subjected to 18 minutes unilateral renal IRI and culled at 2 days (n=5/6) minutes compared to sham operated controls (n=3). Gene expression quantified from total kidney RNA. cDNA synthesised and expression determined by Taqman qRT-PCR using specific gene primers and normalised to GAPDH. Bars represent mean RQ + RQ max;*p<0.05, **p<0.01, ***p<0.001, **** p<0.0001. One-way Anova with Tukey's adjustment for multiple comparisons.

CD3e and CD68 were also examined as markers of T cells and macrophages respectively (**Figure 5.35**). Interestingly, there was no significant difference in CD68 expression when comparing miR-214$^{-/-}$ mice with miR-214$^{+/+}$ mice (6.4-fold versus 12.6-fold increase respectively). There was also no significant difference in expression when comparing miR-214$^{-/-}$ sham and miR-214$^{-/-}$ IRI groups.

There was significant upregulation of CD3e in miR-214$^{+/+}$ kidneys undergoing IRI compared to sham-operated controls (7.6-fold increase in expression, one way-ANOVA p=0.0001). There was no difference in expression when comparing the same groups in the miR-214$^{-/-}$ kidneys which was almost at baseline expression (1.4-fold increase, p=0.14). When comparing CD3e expression in miR-214$^{-/-}$ and miR-214$^{+/+}$ IRI groups, there was 82% relative reduction in CD3e mRNA ($p<0.05$, one-way ANOVA with Tukey's adjustment).

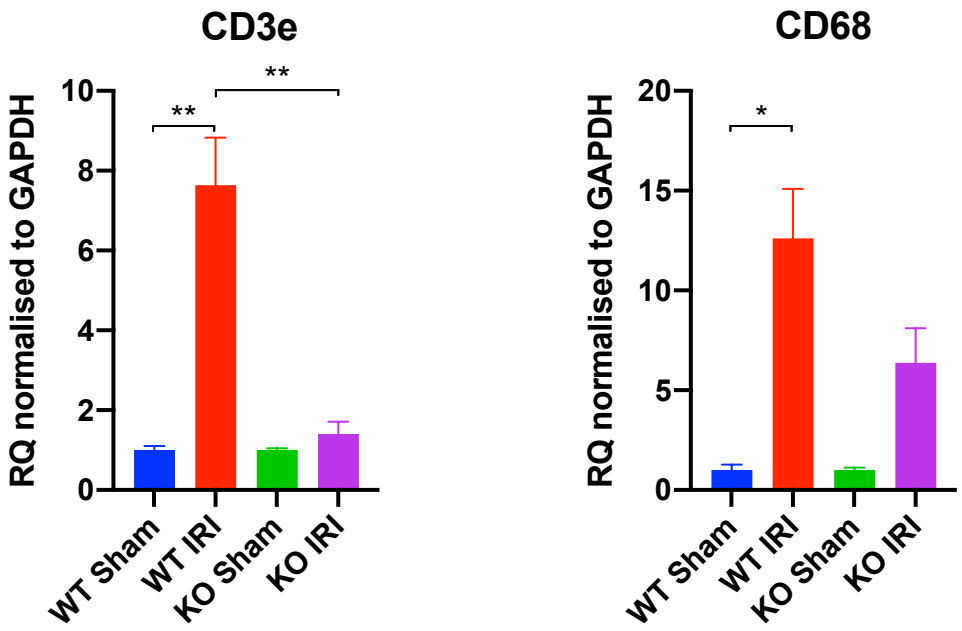

Figure 5.35 CD3 and CD68 expression at 2 days in miR-214$^{+/+}$ or miR-214$^{-/-}$ mice undergoing IRI or sham. Male C57bl/6 mice were subjected to 18 minutes unilateral renal IRI and culled at 2 days (n=5/6) minutes compared to sham operated controls (n=3). Gene expression quantified from total kidney RNA. cDNA synthesised and expression determined by Taqman qRT-PCR using specific gene primers and normalised to GAPDH. Bars represent mean RQ + RQ max; *p<0.05 **p<0.01. One-way Anova with Tukey's adjustment for multiple comparisons.

5.5.2.4 There is a significant reduction in serum cytokines at 2 days in miR-214$^{-/-}$ mice subjected to IRI

The serum of animals was assessed for cytokine expression using LEGENDplex™ bead assay (Biolegend) to assess the potential effects of miR-214 deletion on the systemic inflammatory response following IRI.

Results show there was a significant increase in IL-6 protein in the serum of miR-214$^{+/+}$ mice undergoing IRI compared to the respective shams (**Figure 5.36**). Protein

levels were significantly reduced in the serum of miR-214$^{-/-}$ mice undergoing IRI suggesting an attenuation in the systemic inflammatory response in this group.

There was also a significant reduction in MCP-1 serum protein levels between IRI groups however there was no difference in concentration when comparing each group to their respective shams (**Figure 5.36**). Interestingly, there was a reduction in protein levels between the sham groups, potentially suggesting a dampened response to sham surgery in the miR-214$^{-/-}$ animals. There was no significant difference in TNF-α or IL-1α concentrations.

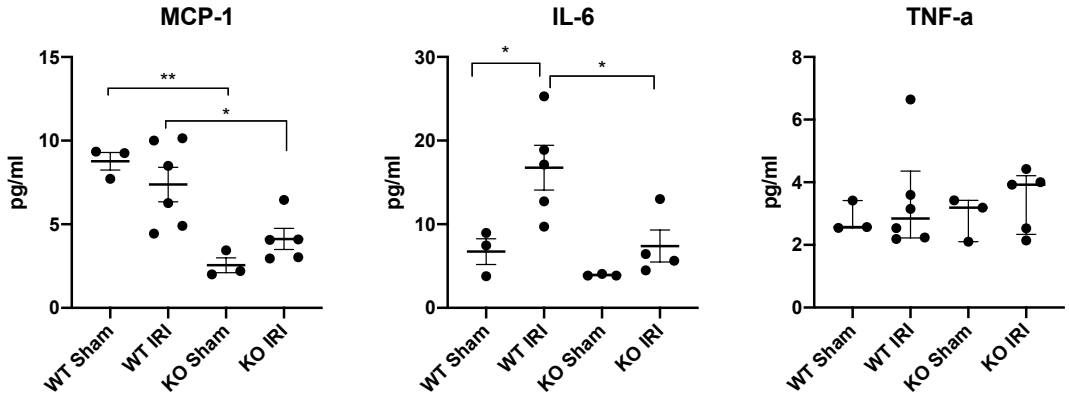

Figure 5.36 Serum cytokine expression at 2 days in miR-214$^{+/+}$ or miR-214$^{-/-}$ mice undergoing IRI or sham. Male C57bl/6 mice were subjected to 18 minutes unilateral renal IRI and culled at 2 days (n=5/6) minutes compared to sham operated controls (n=3). 25μl serum was assessed for cytokine expression using LEGENDplex™ bead assay (Biolegend) according to manufacturer's instructions. Concentrations were normalised to standard curve and presented in pg/ml. *p<0.05, **p<0.01, One-way Anova with Tukey's adjustment for multiple comparisons.

5.5.3 The effect of miR-214$^{-/-}$ on outcomes at 21 days following IRI

5.5.3.1 There is less tubular damage in miR-214$^{-/-}$ mice at 21 days following IRI

Results show a significant reduction in KIM-1 expression when comparing miR-214$^{-/-}$ and miR-214$^{+/+}$ IRI experimental groups (**Figure 5.37**). There was also a significant increase in expression when comparing miR-214$^{+/+}$ shams versus IRI but no significant difference between miR-214$^{-/-}$ sham and IRI groups suggesting that miR-214 knockout may protect tubules against ongoing injury.

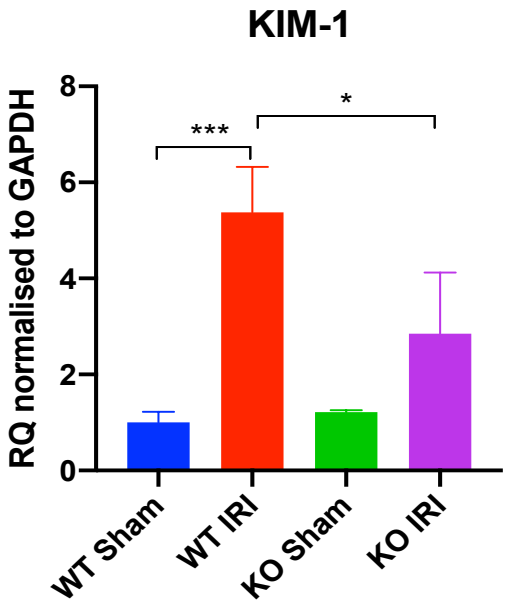

Figure 5.37 KIM-1 expression at 21 days in miR-214$^{+/+}$ or miR-214$^{-/-}$ mice undergoing IRI or sham. Male C57bl/6 mice were subjected to 18 minutes unilateral renal IRI and culled at 21 days (n=5/6) compared to sham (n=3). Gene expression quantified from total kidney RNA. cDNA synthesised and expression determined by Taqman qRT-PCR using specific gene primers and normalised to GAPDH. Bars represent mean RQ + RQ max; **p<0.01, ***p<0.001. One-way Anova with Tukey's adjustment for multiple comparisons.

Histology demonstrated an improvement in appearances of kidney sections following H&E staining. Whilst there is evidence of some tubular damage in the miR-214$^{-/-}$ group, it is less than that seen in the wildtype group where there was interstitial expansion and tubular atrophy in keeping with ongoing kidney damage (**Figure 5.38**).

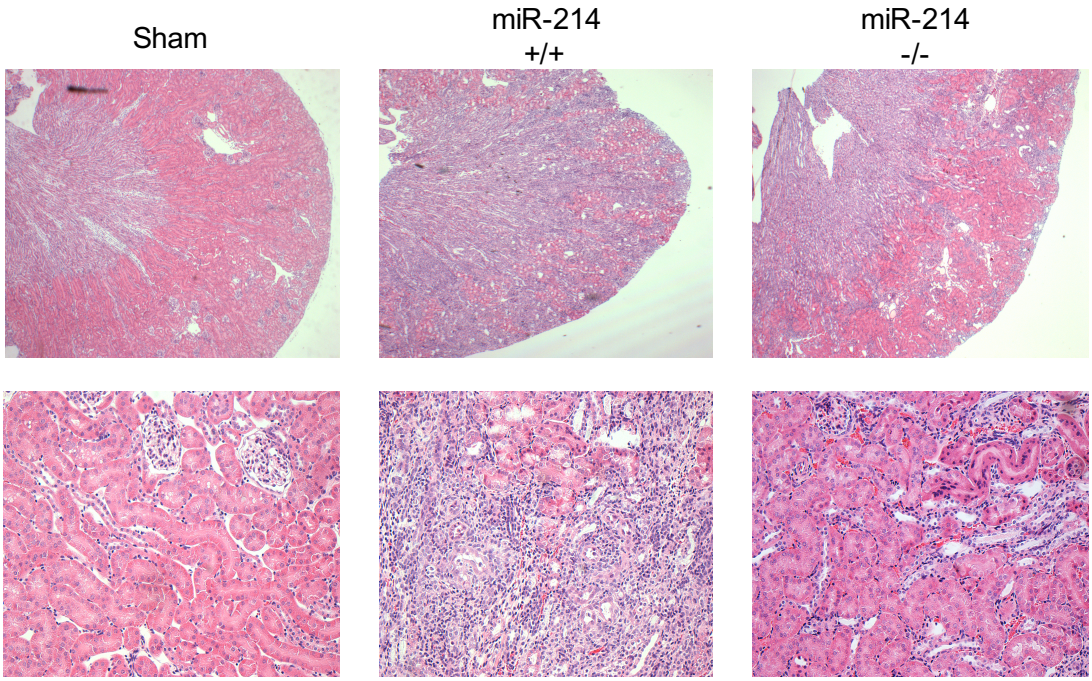

Figure 5.38 Structural injury at 2 days in miR-214$^{+/+}$ and miR-214$^{-/-}$ mice undergoing 18 minutes IRI or sham. Male C57Bl/6 miR-214$^{+/+}$ or miR-214$^{-/-}$ mice either underwent 18 minutes of unilateral IRI (n=5/6) or sham laparotomy (n=3) and were sacrificed at 21 days. Haemotoxylin and eosin stains of a sham kidney (left), miR-214$^{+/+}$ (middle) and miR-214$^{-/-}$ (right) kidney undergoing IRI.

5.5.3.2 There is significant reduction in pro-inflammatory gene expression in miR-214$^{-/-}$ mice at 21 days

Qrt-PCR was performed for the panel of pro-inflammatory gene expression markers that were examined as part of the time-course expression analysis.

Figure 5.39 show there was a reduction in pro-inflammatory gene expression in all examined markers when compared to both the miR-214$^{+/+}$ IRI group as well as sham operated controls in IL-1, IL-6 and TNF-α. The greatest reduction in expression was a 69% reduction in TNF-α between miR-214$^{+/+}$ IRI and miR-214$^{-/-}$ IRI groups (relative quantification 10.6 vs 3.2 respectively, $p<0.001$ one-way Anova). There was no significant difference in expression between miR-214$^{-/-}$ IRI and sham groups. There was a 58% reduction in expression in IL-1 between miR-214$^{+/+}$ and miR-214$^{-/-}$ IRI respectively with no significant difference between miR-214$^{-/-}$ IRI and sham groups. IL-6 was significantly upregulated in both miR-214$^{+/+}$ and miR-214$^{-/-}$ groups compared to their respective sham groups but there was no significant difference in expression between miR-214$^{+/+}$ and miR-214$^{-/-}$ IRI groups.

IL-10 was also assessed and whilst there was no significant difference between IRI groups, there was a significant difference in IL-10 expression when comparing miR-214$^{+/+}$ sham and IRI groups. There was no difference in mRNA levels between miR-214$^{-/-}$ IRI and control groups.

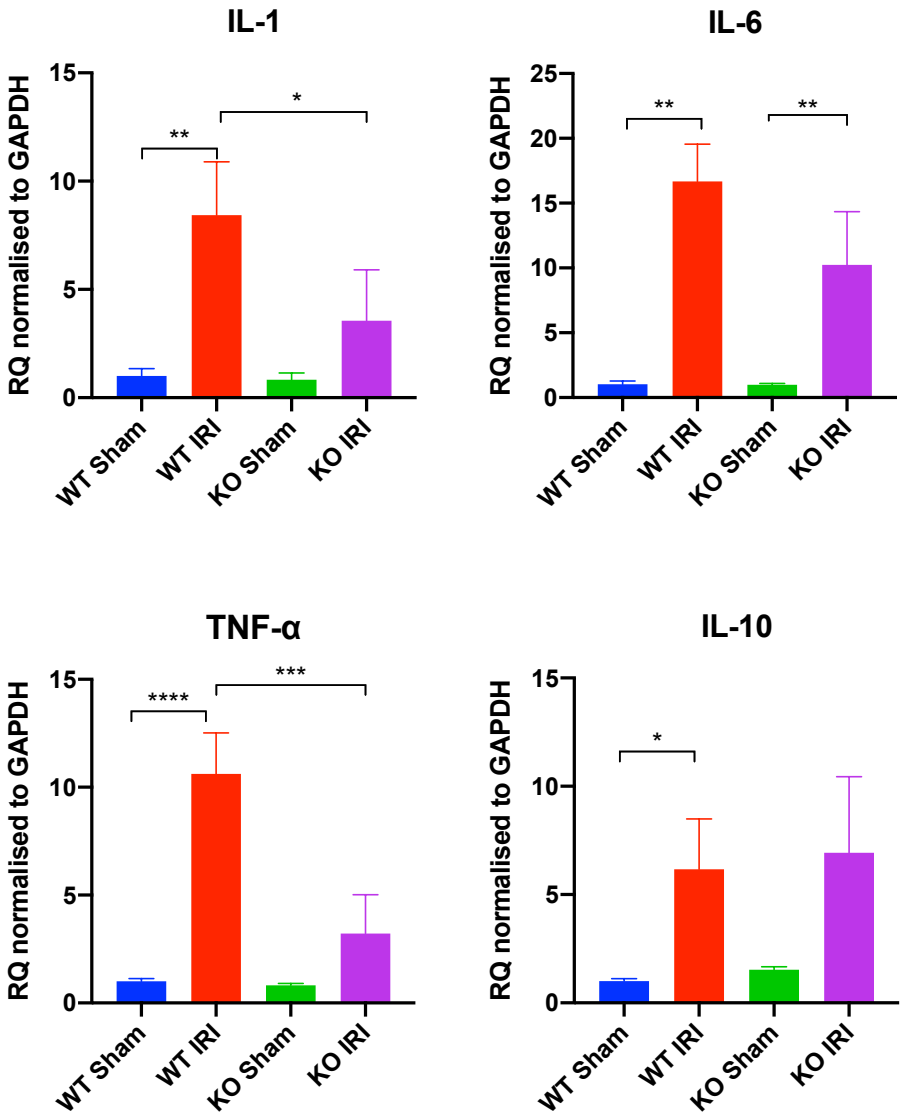

Figure 5.39 Inflammatory cytokine gene **expression at 21 days in miR-214$^{+/+}$ or miR-214$^{-/-}$ mice undergoing IRI or sham.** Male C57bl/6 mice were subjected to 18 minutes unilateral renal IRI and culled at 21 days (n=5-6) compared to sham operated controls (n=3). Gene expression quantified from total kidney RNA. cDNA synthesised and expression determined by Taqman qRT-PCR using specific gene primers and normalised to GAPDH. Bars represent mean RQ + RQ max; **p<0.01, ***p<0.001, **** p<0.0001. One-way Anova with Tukey's adjustment for multiple comparisons.

5.5.3.3 There is an increase in IL-10 in serum of miR-214$^{-/-}$ mice at 21 days

The LEGENDplex™ bead assay (Biolegend) was also used to assess serum cytokine expression at 21 days. **Figure 5.40** demonstrates a significant increase in IL-10 in miR-214$^{-/-}$ mice compared to miR-214$^{-/-}$ sham operated controls and to miR-214$^{+/+}$ IRI mice. There was no significant difference in MCP-1 or TNF-α levels when comparing any of the groups.

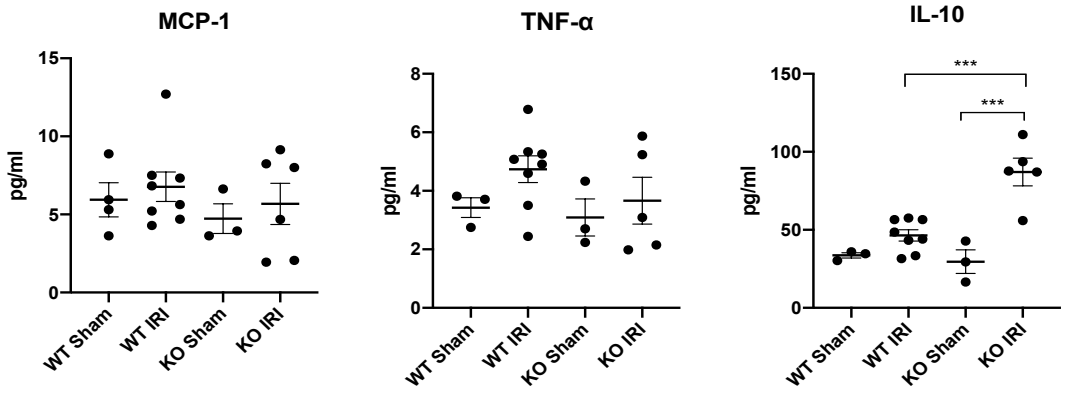

Figure 5.40 Serum cytokine expression at 2 days in miR-214$^{+/+}$ or miR-214$^{-/-}$ mice undergoing IRI or sham. Male C57bl/6 mice were subjected to 18 minutes unilateral renal IRI and culled at 2 days (n=5/6) compared to sham operated controls (n=3). 25μl serum was assessed for cytokine expression using LEGENDplex™ bead assay (Biolegend) according to manufacturer's instructions. Concentrations were normalised to standard curve and presented in pg/ml. ***p<0.001, One-way Anova with Tukey's adjustment for multiple comparisons.

5.5.3.4 MiR-214 knockout results in significantly less fibrosis at 21 days following IRI

Kidneys were weighed immediately following animal sacrifice to determine loss of kidney volume which is a marker of fibrosis as demonstrated previously. There was

a 32% reduction in kidney mass following IRI in miR-214$^{+/+}$ compared to respective sham-operated controls (mean adjusted weight 0.004061 versus 0.005928 respectively, $p<0.05$ One Way Anova with Tukey's adjustment, **Figure 5.41**). There was no significant decrease in adjusted weight when comparing miR-214$^{-/-}$ sham and IRI groups (0.0058g/g versus 0.0055g/g respectively). There was a significant increase in kidney weight in the miR-214$^{-/-}$ IRI group compared to miR-214$^{+/+}$ IRI group (0.0054g/g versus 0.0041g/g respectively, $p<0.05$ one-way ANOVA with Tukey's adjustment).

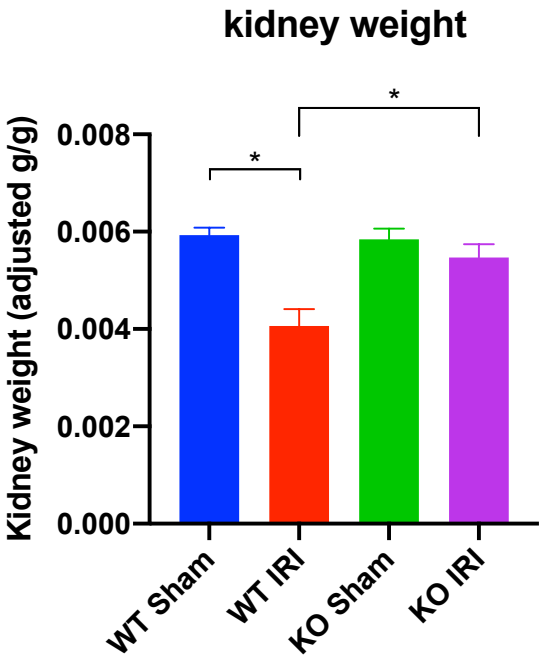

Figure 5.41 Comparison of kidney weights from miR-214$^{-/-}$ and miR-214$^{+/+}$ mice undergoing IRI or sham. The right kidney from animals undergoing 18 minutes unilateral IRI (n=5-6 per group) is compared against time-matched sham-operated controls (n=3 per group) at 21 days. Kidney weight adjusted for body weight g/g. Bars represent group mean + SEM *p<0.05, **p<0.01, ***p<0.001, ****p<0.0001, One-way Anova with Tukey's adjustment for multiple comparisons.

When comparing the experimental right kidney with the contralateral left kidney, there is a significant difference in the adjusted weights in the miR-214$^{+/+}$ IRI group as seen previously in mice with significant renal fibrosis (**Figure 5.42**). This was not demonstrated in the weights of kidneys from miR-214$^{-/-}$ mice undergoing IRI. These results suggest there is less fibrosis in the kidneys from miR-214$^{-/-}$ mice undergoing IRI compared to wildtype animals.

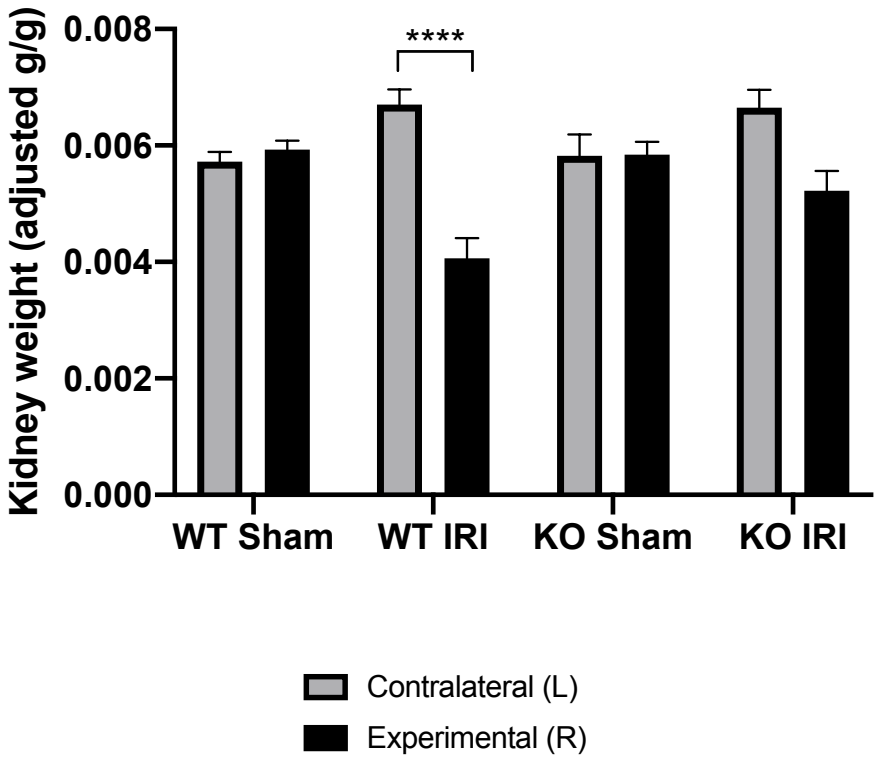

Figure 5.42 Comparison of weights of experimental (right) kidney vs contralateral (left) kidney. Male miR-214$^{-/-}$ and miR-214$^{+/+}$ mice ether underwent 18 minutes unilateral IRI (right kidney, n=5/6 per group) or sham laparotomy as control (n=3 per group) and sacrificed at 21 days. Kidney weight adjusted for body weight g/g. Bars represent group mean + SEM **p<0.01, Paired t-test

Histological assessment of fibrosis demonstrated significant increase in collagen deposition in kidneys from miR-214$^{+/+}$ mice undergoing IRI compared to respective shams (**Figure 5.43**). There is also evidence of interstitial expansion and tubular atrophy in these sections. There was a concurrent increase in pro-fibrotic gene expression compared to shams with significant upregulation in *Col3a* (20-fold, $p<0.001$), *Col4a* (3.4-fold, $p<0.001$), and *PDGFR-β* (3-fold, $p<0.001$, all one way ANOVA with Tukey's adjustment).

There was no significant increase in kidney fibrosis in miR-214$^{-/-}$ IRI compared to the respective sham-operated group. Absence of miR-214 resulted in a 79% relative reduction in fibrosis as demonstrated on histology (1.9% versus 9.1%, $p<0.01$, one-way ANOVA). As might be expected following these findings, there was a significant reduction in pro-fibrotic gene expression in this group compared to wildtype counterparts (**Figure 5.44**) with a 62% reduction in *Col3a* (7.9 fold versus 19.9 fold increase, $p<0.01$) and 29% reduction in *Col4a* expression (2.5 fold versus 3.4 fold increase, $p<0.05$). There was no significant reduction in *PDGFR-β* expression.

These results demonstrate that miR-214 contributes towards fibrosis and deletion confers significant protection from cortical fibrosis in the kidney.

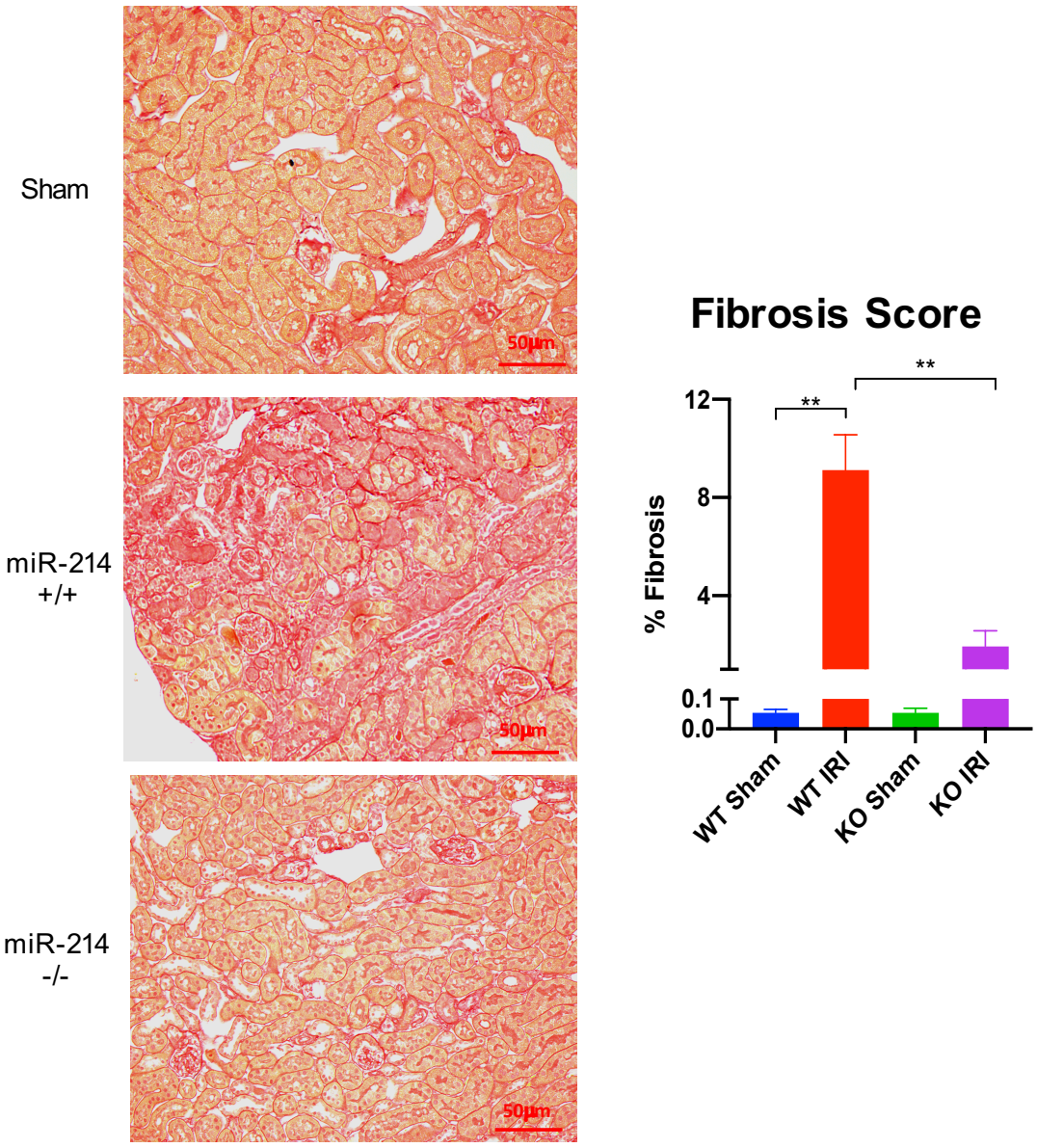

Figure 5.43 Fibrosis in male miR-214$^{+/+}$ and miR-214$^{-/-}$ mice 21 days after 18 minutes unilateral renal IRI. Male C57bl/6 mice underwent 18 minutes IRI or sham laparotomy and were sacrificed at 21 days. Formalin fixed and paraffin embedded kidney were cut into 3µm sections. Picrosirius red stain of sham kidneys (n=3) and IRI kidneys in miR-214$^{+/+}$ and miR-214$^{-/-}$ (n=5/6) mice 21 days post injury. Corresponding fibrosis score quantified in a blinded manner using Image-J. **p<0.01, One way Anova with Tukey's adjustment.

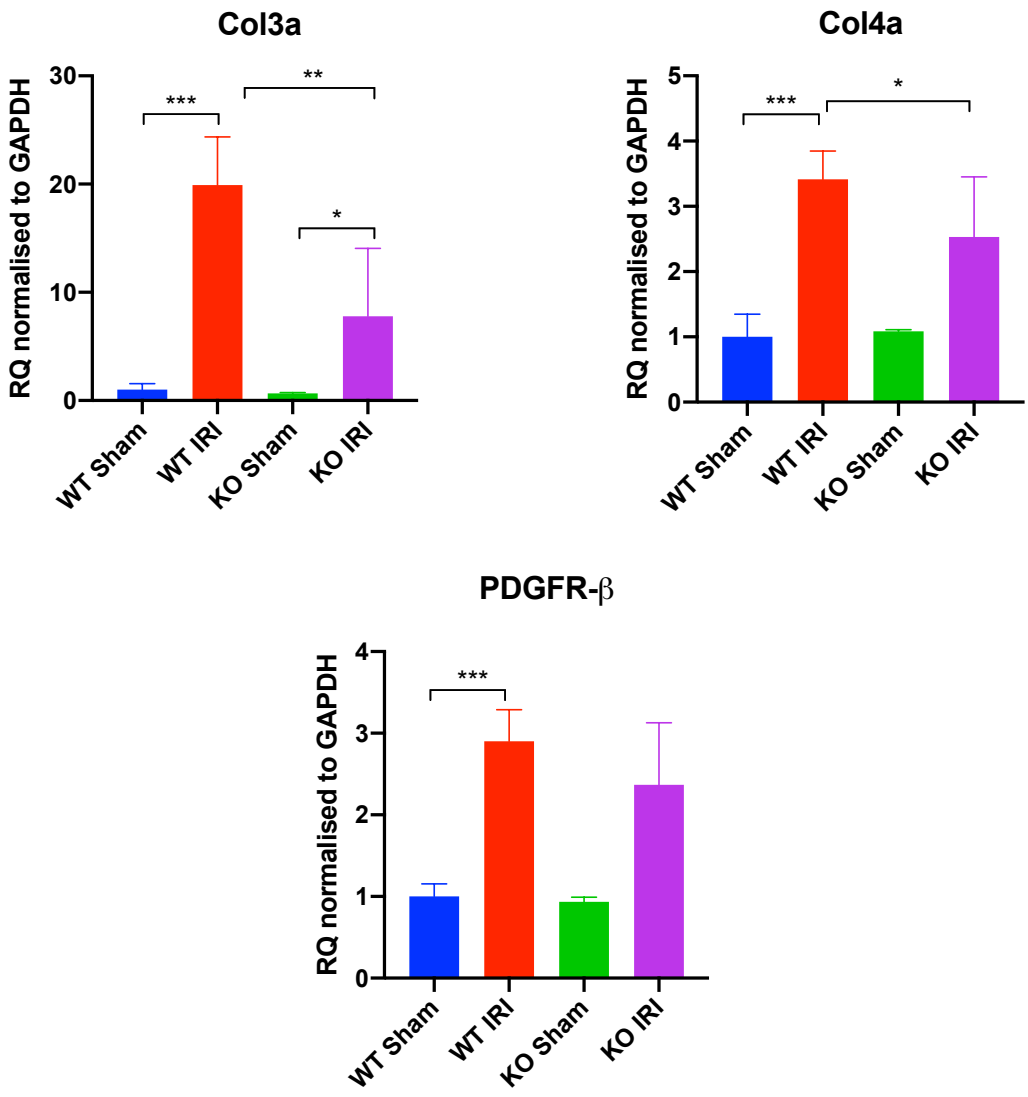

Figure 5.44 Pro-fibrotic gene expression in miR-214$^{+/+}$ and miR-214$^{-/-}$ mice 21 days after 18 minutes unilateral renal IRI. Male C57bl/6 mice underwent 18 minutes IRI (n=5/6) or sham laparotomy (n=3) and were sacrificed at 21 days, pro-fibrotic gene expression quantified from total kidney RNA. cDNA synthesised and expression determined by Taqman qRT-PCR using specific gene primers and normalised to GAPDH. Bars represent mean RQ + RQ max; *p<0.05 **p<0.01, ***p<0.001. One-way Anova with Tukey's adjustment for multiple comparisons.

5.5.3.5 There was no difference in miR-214 target PTEN between miR-214$^{+/+}$ and miR-214$^{-/-}$ mice

Phosphatase and tensin homolog (PTEN) is a validated target of miR-214 in multiple disease conditions and its expression was assessed in whole kidney tissue at 21 days following IRI. Results show there was no difference in expression when comparing either miR-214$^{+/+}$ and miR-214$^{-/-}$ IRI groups to their respective shams nor was there a difference when comparing IRI groups to each other (**Figure 5.45**).

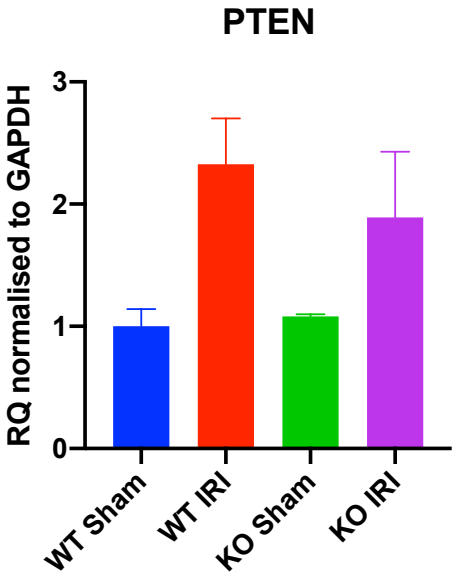

Figure 5.45 PTEN gene expression in miR-214$^{+/+}$ and miR-214$^{-/-}$ mice at 21 days. Male C57bl/6 mice underwent 18 minutes IRI (n=5/6) or sham laparotomy (n=3) and were sacrificed at 21 days, pro-fibrotic gene expression quantified from total kidney RNA. cDNA synthesised and expression determined by Taqman qRT-PCR using specific gene primers and normalised to GAPDH. Bars represent mean RQ + RQ max. One-way Anova with Tukey's adjustment for multiple comparisons.

5.5.4 Mechanism of miR-214$^{-/-}$ protection in the kidney following IRI

5.5.4.1 Fibrosis in miR-214$^{+/+}$ mice is potentially mediated via CD4^{+} T cells

Flow cytometry was performed on kidney segments using a T cell panel. This was based on increasing evidence from the literature that miR-214 is involved in T cell modulation, and previous results that showed miR-214 upregulation in CD3^{+} populations at 7 days following IRI in FACS populations.

Results show that there is no significant difference in CD3^{+} populations when comparing IRI in miR-214$^{-/-}$ and miR-214$^{+/+}$ mice at 2 or 21 days (**Figure 5.46 and Figure 5.47**). Analysis of CD3^{+} subpopulations demonstrated a reduction in percentage of CD4^{+} cells in miR-214$^{-/-}$ mice undergoing IRI compared to miR-214$^{+/+}$ mice at 21 days but not 2 days. There was no significant difference in CD8^{+} populations at either time point. Unfortunately, there were too few cells to examine CD4^{+} subpopulations or CD4^{+} and CD8^{+} effector phenotypes (naïve, effector, memory) profiles but this could be considered if this were repeated using a larger volume of tissue.

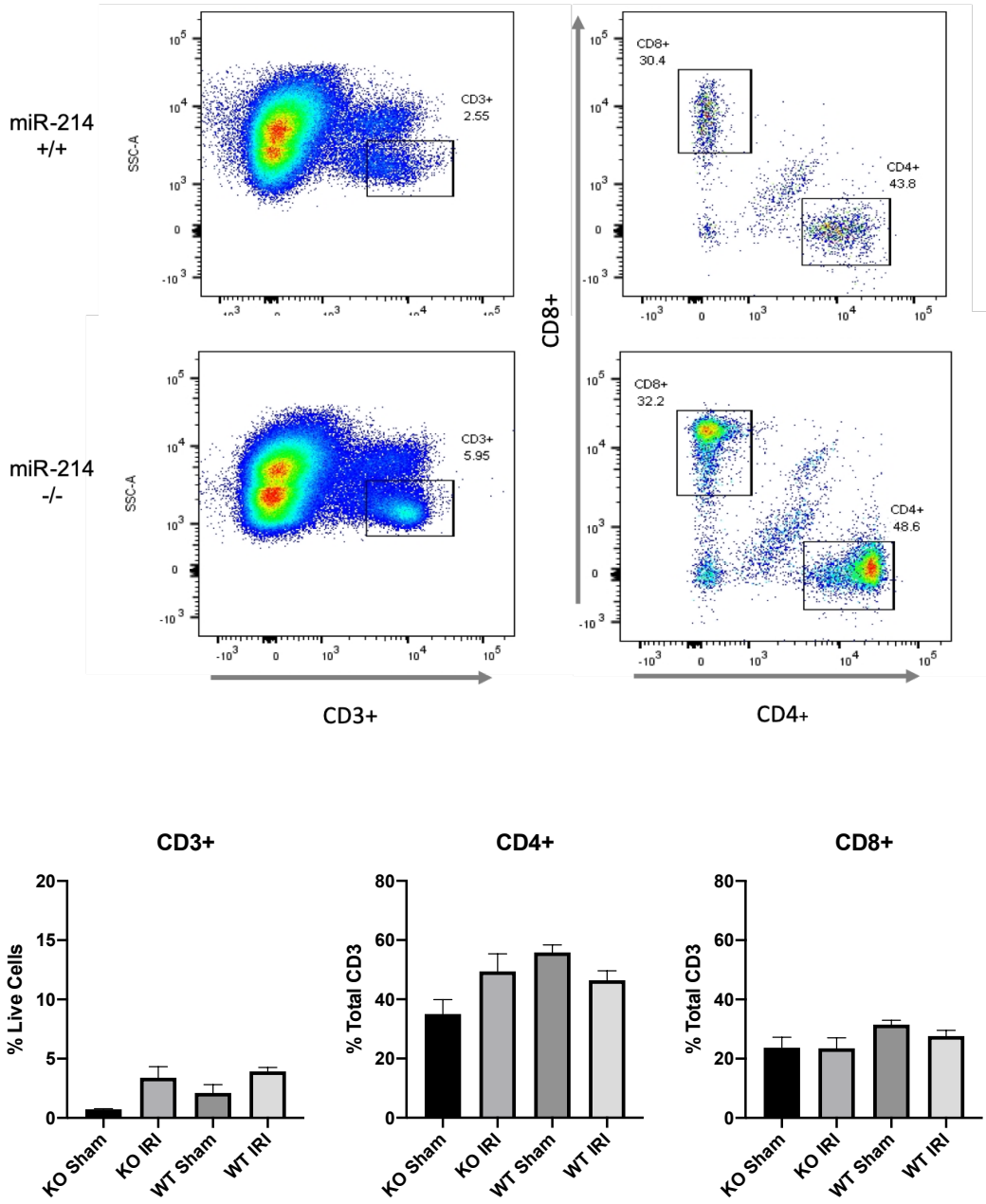

Figure 5.46 T cell populations from kidneys of male miR-214$^{+/+}$ and miR-214$^{-/-}$ mice 2 days after 18 minutes unilateral renal IRI. Kidney sections were digested into single cell suspension and stained with CD3^{+}, CD4^{+} and CD8^{+} antibodies. After staining, samples were washed and analysed using 5 LSR Fortessa. **Top:** Representative examples of CD3^{+}, CD4^{+} and CD8^{+} populations. **Bottom:** quantification of T cell populations; n=5/6 per IRI group, n=3 per sham group. Bars represent mean + SEM. One-way ANOVA with Tukey's adjustment for multiple comparison.

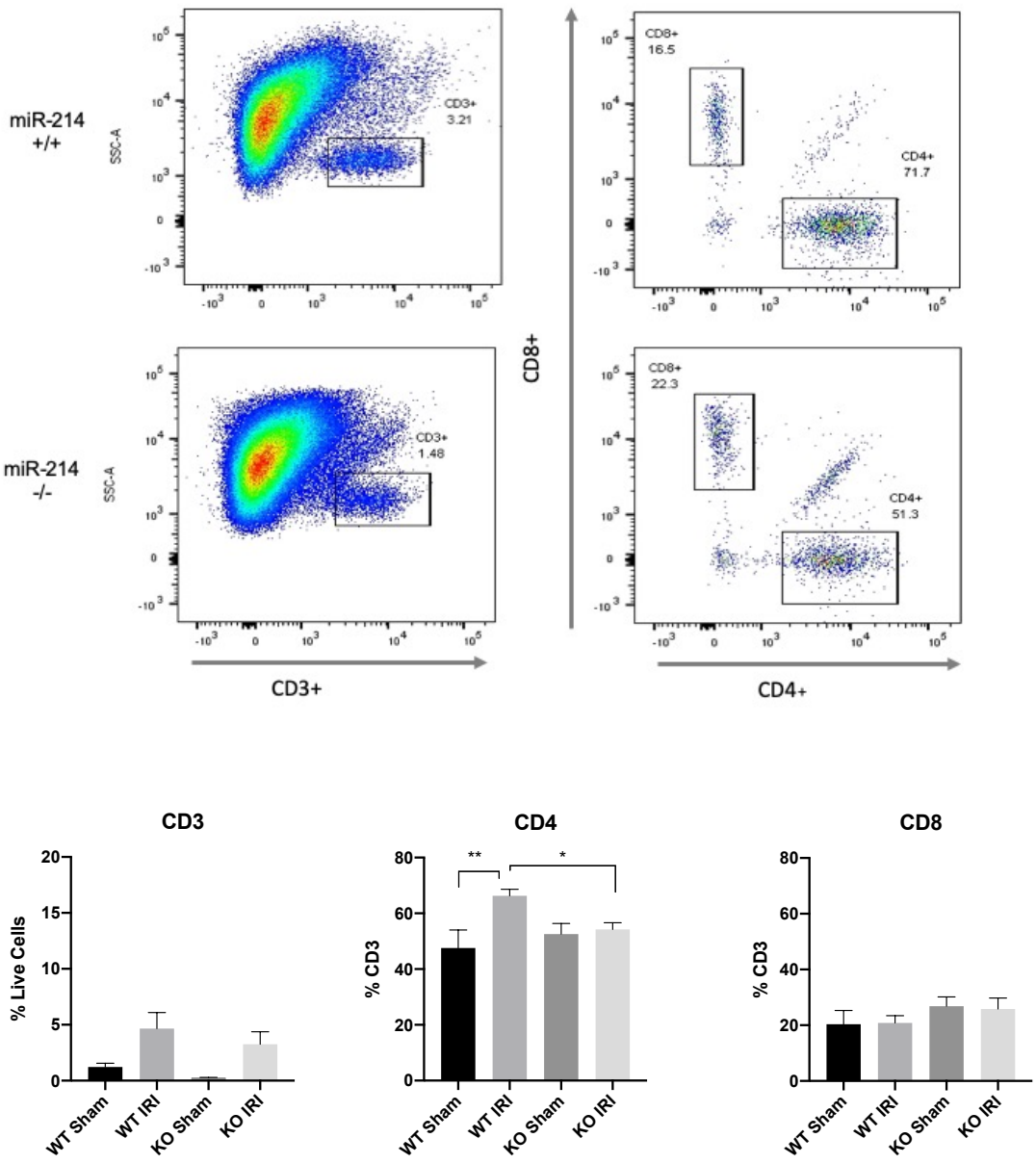

Figure 5.47 T cell populations from kidneys of male miR-214$^{+/+}$ and miR-214$^{-/-}$ mice 21 days after 18 minutes unilateral renal IRI. Kidney sections were digested into single cell suspension and stained with CD3^{+}, CD4^{+} and CD8^{+} antibodies. After staining, samples were washed and analysed using 5 LSR Fortessa. **Top:** Representative examples of CD3^{+}, CD4^{+} and CD8^{+} populations. **Bottom:** quantification of T cell populations; n=5/6 per IRI group, n=3 per sham group. Bars represent mean + SEM. $p<0.05$, $^{**}p<0.01$. One-way ANOVA with Tukey's adjustment for multiple comparison.

5.5.4.2 There are no differences in $CD4^+$ T cell populations in the spleen

Spleens were harvested at the time of cull and stained for the same T cell panel used in the kidney. Examination of splenocytes demonstrated no significant difference in $CD3^+$, $CD4^+$ or $CD8^+$ populations when comparing miR-$214^{-/-}$ and miR-$214^{+/+}$ mice subjected to IRI or sham operations at either time point (**Figures 5.48 and 5.49**).

Given that miR-214 has a potential role in Treg modulation, T cells were stained for the transcription factor FOXP3 along with other $CD4^+$ sub-populations. Again, there was no significant difference in FOXP3 positive cells when comparing groups at 2 and 21 days.

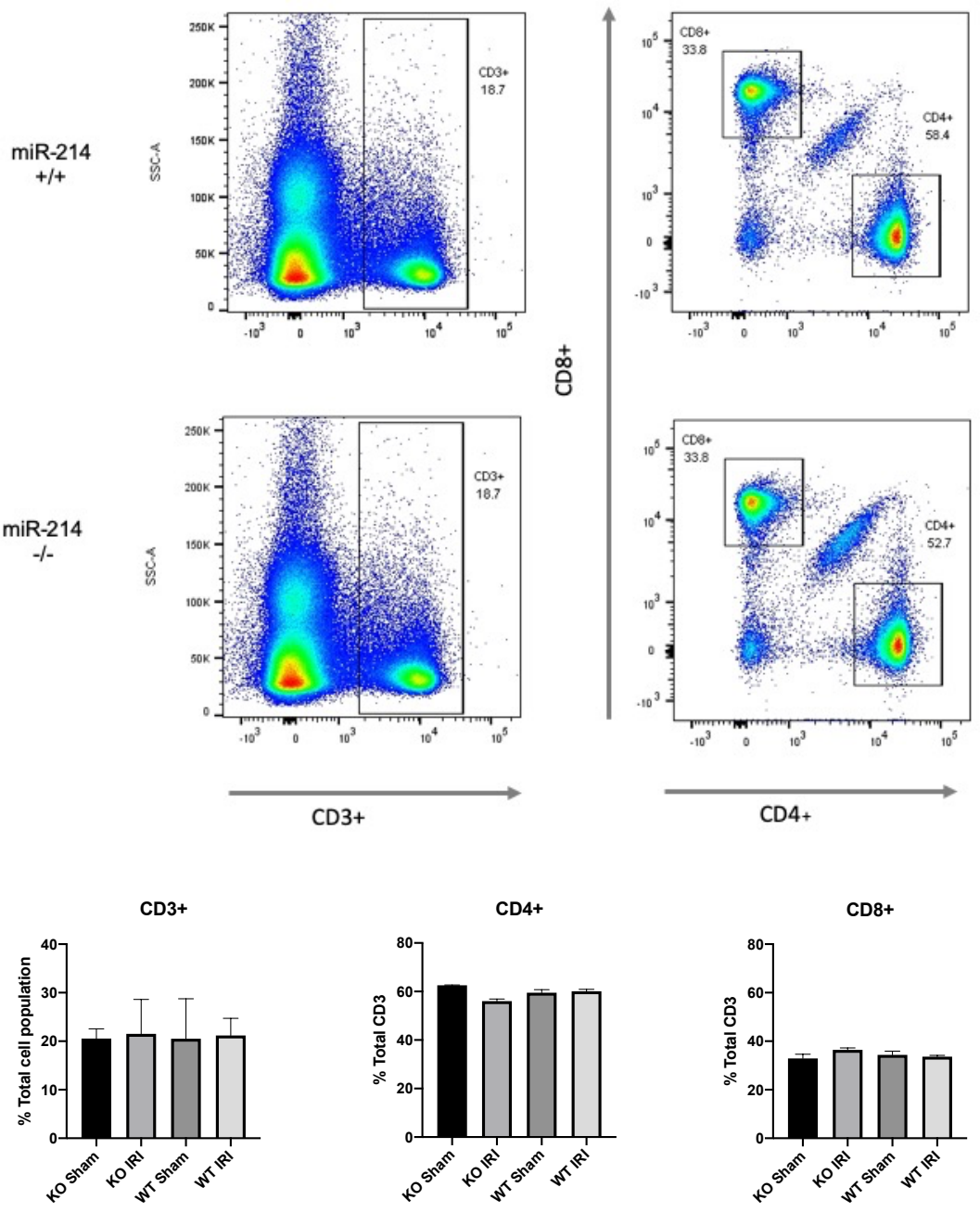

Figure 5.48 T cell populations from spleens of male miR-214$^{+/+}$ and miR-214$^{-/-}$ mice 2 days after 18 minutes unilateral renal IRI. Spleens were prepared into single cell suspension and stained with T cell panel antibodies. After staining, samples were washed and analysed using 5 LSR Fortessa. **Top:** Representative examples of CD3^{+}, CD4^{+} and CD8^{+} populations; n=5/6 per IRI group, n=3 per sham group. **Bottom:** quantification of T cell populations. Bars represent mean +SEM. One-way ANOVA with Tukey's adjustment for multiple comparison.

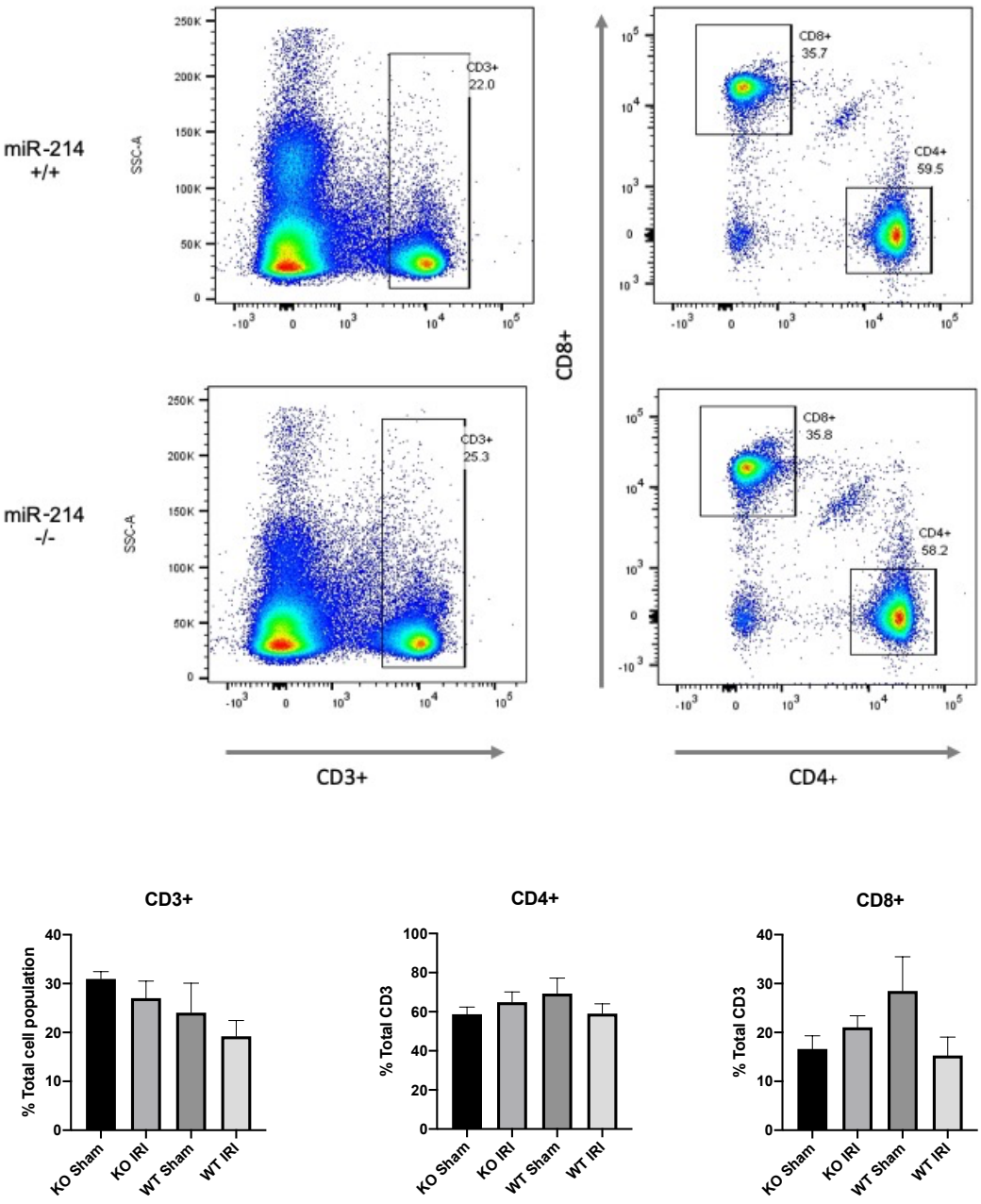

Figure 5.49 T cell populations from spleens of male miR-214$^{+/+}$ and miR-214$^{-/-}$ mice 21 days after 18 minutes unilateral renal IRI. Spleens were prepared into single cell suspension and stained with T cell panel antibodies. After staining, samples were washed and analysed using 5 LSR Fortessa. **Top:** Representative examples of CD3^{+}, CD4^{+} and CD8^{+} populations; n=5/6 per IRI group, n=3 per sham groupv. **Bottom:** quantification of T cell populations. Bars represent mean +SEM. One-way ANOVA with Tukey's adjustment for multiple comparison.

5.5.4.3 There are differences in $CD4^+$ activation profiles in the spleen at 2 days but not 21 days

Examination of T cell activation markers CD44 and CD62L revealed a difference in $CD4^+$ memory cells ($CD44^+$ $CD62L^+$) when comparing miR-$214^{-/-}$ and miR-$214^{+/+}$ mice subjected to IRI at 2 days (**Figure 5.50**). There was also a significant increase in this population when comparing IRI and sham in miR-$214^{+/+}$ mice. There was no significant difference at 21 days.

There was a significant reduction in naïve $CD4^+$ T cells ($CD44^-$ $CD62L^+$) in miR-$214^{+/+}$ mice subjected to IRI compared to shams at 2 days (**Figure 5.50**) but not 21 days (**Figure 5.51**) suggesting there is a potential systemic T cell response to IRI at 2 days but not at 21 days.

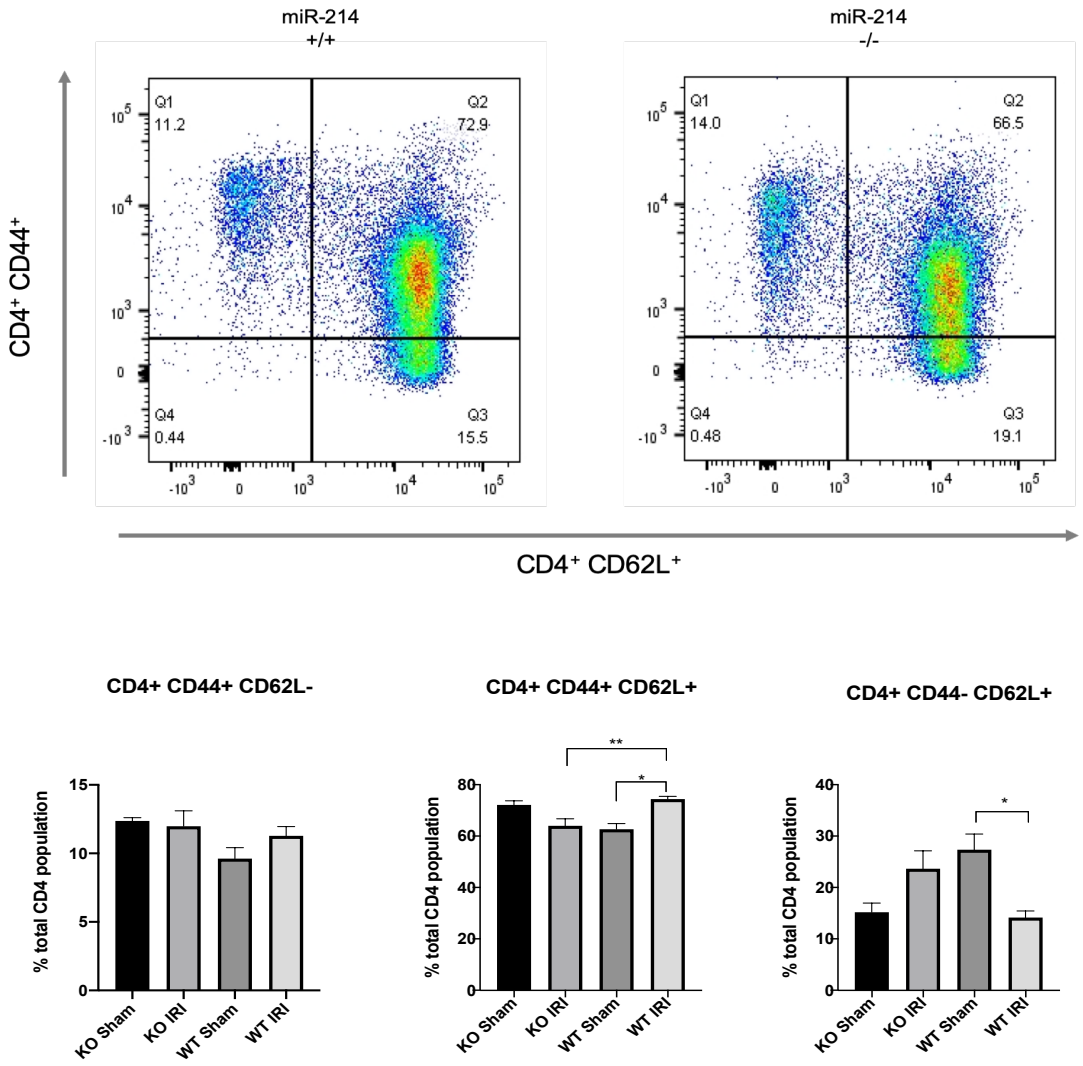

Figure 5.50 CD4^{+} T cell populations from spleens of male miR-214$^{+/+}$ and miR-214$^{-/-}$ mice 2 days after 18 minutes unilateral renal IRI. Spleens were prepared into single cell suspension and stained with T cell activation antibodies including CD44 and CD62L as part of T cell panel. After staining, samples were washed and analysed using 5 LSR Fortessa. **Top:** Representative examples of CD4^{+} activation markers. **Bottom:** quantification of CD4^{+} T cell populations; n=5/6 per IRI group, n=3 per sham group. Bars represent mean +SEM. *p<0.05, **p<0.01. One-way ANOVA with Tukey's adjustment for multiple comparison.

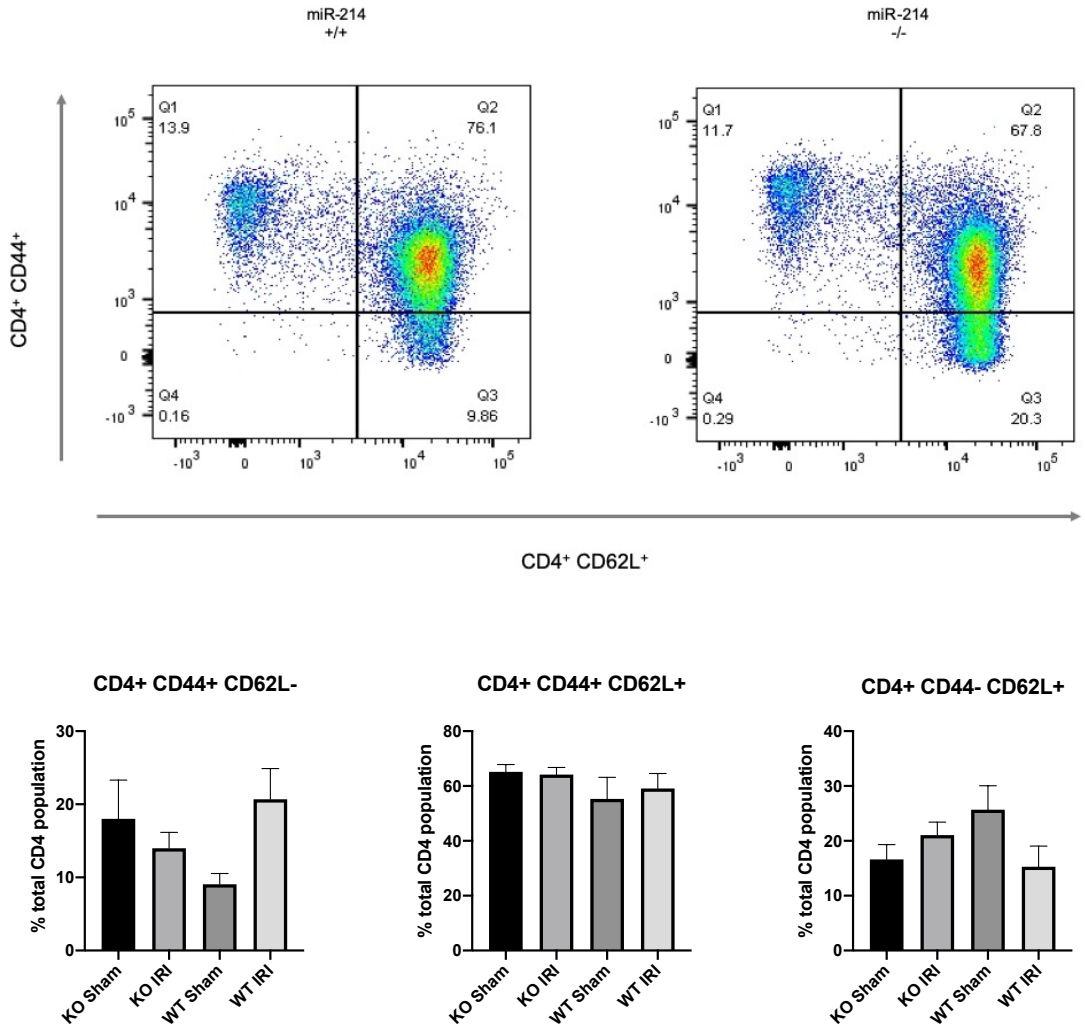

Figure 5.51 CD4^{+} T cell populations from spleens of male miR-214$^{+/+}$ and miR-214$^{-/-}$ mice after 18 minutes unilateral renal IRI and culled at 21 days. Spleens were prepared into single cell suspension and stained with T cell activation antibodies including CD44 and CD62L as part of T cell panel. After staining, samples were washed and analysed using 5 LSR Fortessa. **Top:** Representative examples of CD4^{+} activation markers. **Bottom:** quantification of CD4^{+} T cell populations; n=5/6 per IRI group, n=3 per sham group. Bars represent mean +SEM. One-way ANOVA with Tukey's adjustment for multiple comparison.

5.6 Discussion

In order to test the hypothesis that miR-214 is upregulated following ischaemia and reperfusion injury and the subsequent development of fibrosis, the effect of 18 minutes of IRI was examined at various time points following injury. Results show that 18 minutes of unilateral ischaemia resulted in significant early injury in the affected kidney as demonstrated by an ATN score of 67% at 2 days, and similar to that seen in the bilateral model. Alongside this, there was rapid upregulation of KIM-1 suggesting a significant tubular injury within the surviving tubules. Progression of injury continued beyond the early phase and, although there was partial resolution of ATN at 7 days, there was ongoing injury within the kidney involving gradual tubular atrophy and expansion of the interstitium. Indeed, KIM-1 levels never returned to normal and remained significantly elevated throughout the time-course, suggesting ongoing tubular injury. This is in contrast to rodent IRI studies where KIM-1 levels were transiently elevated in the early phase of injury and returned to basal expression at one week[316]. This could be explained by differences in the models; this group used a recoverable bilateral model of ischaemia which, as discussed previously, is potentially less severe than a unilateral model due to reduced post-ischaemic vasoconstriction within the outer medulla.

There was increased collagen deposition in keeping with fibrosis as early as 14 days and this was confirmed by significant upregulation of pro-fibrotic gene expression from whole kidney samples including *col1a* and *col3a*, peaking at 21 days. Fibrosis scores also demonstrated significant cortical fibrosis from 14 days onwards, reaching 7.9% at 21 days. Interestingly, there was significant upregulation of pro-fibrotic gene expression as early as 2 days in all genes examined, which preceded histological evidence of collagen deposition at day 14. Others have shown significant early

upregulation of collagens following renal IRI including *Col1a*, *Col3a* and *Col4a* potentially from activated myofibroblasts within the interstitium particularly as there is concurrent upregulation of α-SMA. Deposition of collagen proteins in the early phases of injury however are inhibited by matrix metalloproteinase (MMP) activity secreted by pro-inflammatory macrophages resulting in greater turnover of the extracellular matrix. Two independent studies have shown that there is significant upregulation of the genes encoding matrix-gla protein (*Mglap*) and cathepsin S (*Css*) involved in continuous extracellular matrix remodeling from 2-3 days in rodents following IRI[317,318]. Over time, activation of MMPs are inhibited by TIMPs[319] and collagen deposition accumulates due to an imbalance of synthesis and degradation[320].

MiR-214 was significantly elevated at all time points following injury. To date, miR-214 has not been shown to be elevated earlier than three days in this model and therefore significant upregulation at 2 days is a novel finding following renal injury. Studies have demonstrated that miR-214 has a potential role in modulation of inflammatory cells which may explain its role in early injury in this context. Indeed, miR-214 has been shown to be upregulated in macrophages in an *ex-vivo* model of CKD[210] and to promote TNF-α and IL-6 secretion in bone-marrow derived macrophages by targeting the anti-inflammatory receptor adenosine A_{2A} receptor[211]. Results from this study demonstrate upregulation of miR-214 in kidney macrophages at 2, 7 and 21 days, suggesting a potential role for macrophage activity in different stages of kidney injury and repair. There was no significant increase in miR-214 expression in an *ex-vivo* model of human macrophages derived from healthy donor PBMCs, suggesting that miR-214 may only act on tissue macrophages.

MiR-214 remained upregulated beyond the early phase of injury as the kidney demonstrated progression towards fibrosis, peaking at 21 days, corresponding to histological evidence of significant fibrosis *in vivo*. It was also upregulated in two *in vitro* models of renal injury including rodent renal fibroblasts and tubular epithelial cells in keeping with pro-fibrotic response to TGF-β stimulation. Furthermore, fluorescence activated cell sorting demonstrated significant upregulation of miR-214 in PDGFR-β positive cells at 7 and 21 days. Fibroblasts are critical in promoting fibrosis by differentiating into myofibroblasts and producing ECM components. Previous results from our group have suggested that there was a limited role for miR-214 in tubular epithelial cells in an *in vivo* renal fibrosis model; however, miR-214 was found to be upregulated in cell populations stained for the proximal tubular epithelial LTL marker at 2 and 21 days following IRI. TECs undergo cell arrest when injured before potential redifferentiation but are known to secrete pro-inflammatory cytokines during growth arrest, thereby promoting ongoing injury. MiR-214 has been shown to be upregulated in human and murine tubular epithelial cells *in vitro*[1,19] in which there is a subsequent reduction in E-cadherin in keeping with tubular cell dedifferentiation. Liu *et al* claimed that miR-214 results in proximal tubular cell epithelial to mesenchymal transition (EMT) *in vivo*[227] however there is mounting evidence to suggest that EMT plays a limited role in renal fibrosis[140,145,153]. Therefore, the role of miR-214 in tubular epithelial cells could be to promote ongoing inflammation or differentiation of nearby fibroblasts and/or pericytes.

Examination of the potential role of miR-214 in early injury and fibrosis was examined using a miR-214 knockout mouse. Whilst miR-214$^{-/-}$ did not confer protection against tubular injury at 2 days, there was a significant reduction in pro-inflammatory gene expression from whole kidney tissue compared to miR-214$^{+/+}$ mice undergoing IRI at this time point. This was reflected in the serum of miR-214$^{-/-}$ animals where there was

a concurrent reduction in the chemokine MCP-1 and pro-inflammatory cytokine IL-6. MCP-1 (also known as CCL2) attracts monocytes following ischaemia[321] and is secreted by TECs and mesangial cells following injury[322]. *In vivo* studies have demonstrated accumulation of macrophages and T cells near cells secreting MCP-1 in the kidney[323,324] and blockade of its receptor CCR2 results in protection against ischaemia[325,326]. IL-6 is also secreted by TECs in response to ischaemia[327] and blockade reduces fibrosis by reducing collagen 1 synthesis[328]. IL-6 modulates monocyte and T cell differentiation[329] and it may have an indirect role in reducing the inflammatory response in miR-214$^{-/-}$ mice. Attenuation of the inflammatory response was also seen in the kidney at day 21 with upregulation of the anti-inflammatory cytokine IL-10 in serum of knockout mice. IL-10 is secreted by multiple immune cells including macrophages, T cells (Th cells and Tregs), DCs and TECs in following injury[330,331]; its upregulation in this context likely represents a secondary effect of the dampened pro-inflammatory response. Although there is evidence of a dampened immune response at the transcriptomic and protein levels, the immunological phenotype is not well described in the miR-214$^{-/-}$ mouse. There were no observed differences in wound healing or complications (including susceptibility to infection) following surgery between wildtype and knockout mice.

Alongside the differences in immune response between groups, there was a reduction in KIM-1 expression in knockout mice and less tubular atrophy on histology, suggesting that miR-214 knockout is potentially beneficial to tubular recovery. These results are similar to a study by Bai *et al* who showed enhanced tubular recovery in a conditional PTEC miR-214 knockout mice subjected to IRI, UUO and albumin overload[225]. They also demonstrated a reduction in pro-inflammatory gene expression within the kidney, again supporting the suggestion that miR-214 is involved in the inflammatory response.

Overall there was a 79% reduction in cortical fibrosis in miR-214$^{-/-}$ mice compared to wildtype, which is similar to that seen after UUO by Denby et al[223]. Classically, miR-214 is described as a 'fibro-miR' and is associated with multiple *in vivo* models of renal injury and fibrosis including UUO, diabetic nephropathy, and IRI[222,223,225,227,293,332]. The evidence behind its role on fibrosis points to its action on different cells populations within the kidney. As inflammation and fibrosis are intricately linked, its role in fibrosis could be partly explained by perpetuating a pro-inflammatory response triggered by a transient insult. T cells are important mediators of injury that act to promote inflammation following IRI and are integral to the alloimmune response following renal transplantation. Examination of CD3^{+} subsets using flow cytometry demonstrated a significant reduction in the percentage of CD4^{+} T cells in the kidney of knockout mice at day 21 following injury. There was also a reduction in naïve CD4^{+} T cells from the spleens of miR-214$^{+/+}$ mice undergoing IRI compared to miR-214$^{+/+}$ shams but no difference in the miR-214$^{-/-}$ groups suggesting a potentially dampened systemic response to ischaemia in the knockout group at 2 days. There was also a reduction in memory T cells in the knockout group compared to wildtype at 2 days. The differences in CD4^{+} memory T cells populations in wildtype and knockout groups suggest that miR-214 may play a role in T cell differentiation during the acute inflammatory response which is no longer present once the systemic response has subsided. Jindra et al have previously shown that miR-214 was elevated in memory CD4^{+} T cells and this was significantly greater than expression in naïve T cells at the same timepoint[215]. Other miRs have been shown to be differentially expressed in T helper cell populations and can affect memory, effector and naïve T cell differentiation[333]. Alternatively, the T cell responses observed could be secondary to attenuation of the inflammatory response seen in the miR-214$^{-/-}$ mice. Further investigation of the potential role of miR-214 in T cells is required to make firm conclusions about its role in renal fibrosis.

Overall, these results suggest a multi-faceted role for miR-214 following kidney injury where miR-214 appears to promote tubular injury, inflammation and fibrosis through multiple different cell populations. The precise mechanism remains unclear however its role may be through mediating inflammation through damaged TECs and T cell responses. MiR-214 remains an attractive target in renal injury and blockade has potential therapeutic benefit to take forward to future studies.

Chapter 6: Final discussion

6.1 Discussion

Renal transplantation has significant benefit in terms of quality of life and its length and is the gold standard treatment for patients with end-stage renal failure. However, despite the increase in the number of transplants being performed, a proportion fail over time secondary to chronic allograft damage, which is the leading cause late graft failure[5]. Length of ischaemia and in particular, a prolonged cold ischaemia time (CIT) is an independent risk factor for poor short- and long-term graft function and higher rates of graft attrition. Whilst improvements in reducing CIT are achievable, the inherent logistical challenge associated with organ transportation from donor to recipient site means that the impact of ischaemia cannot be entirely removed from clinical practice. Thus improvements in understanding the pathways triggered by early injury, manifested by ischaemia reperfusion injury (IRI) may result in novel therapeutic targets and future therapies.

The main focus of the research has been on the impact of renal ischaemia for the purposes of transplantation and the role miR-214 plays in the pathogenesis of ischaemia related injury and fibrosis. In order to mimic IRI observed in transplantation, initial studies performed revealed that 18 minutes of ischaemia was sufficient to induce significant fibrosis at 28 days. This was accompanied by upregulation of pro-inflammatory gene expression, suggesting that a modest 18 minutes of ischaemia resulted in a persistent and non-recoverable cycle of inflammation and fibrosis.

Critically the IRI studies found that miR-214 was significantly upregulated in the kidneys of mice undergoing IRI at all time points following injury. The finding of an early rise in miR-214 expression was novel, as its role in early injury had not been explored previously in the literature. By day 21, miR-214 expression had peaked at

5.5-fold increase compared to time-matched controls. Its mechanism of action was explored using miR-214 knockout studies which demonstrated attenuation of the inflammatory response and a 79% reduction in fibrosis in knockout mice. In addition, there was evidence of tubular recovery at 21 days despite there being no difference in ATN between miR-214$^{+/+}$ and miR-214$^{-/-}$IRI groups at 2 days. Given the severity of ischaemic injury, it is not unexpected that miR-214 ablation did not protect the kidney against acute tubular necrosis, but it is encouraging is that, despite this, there was protection against ongoing injury and reduction in fibrosis. The translational potential of miR-214 reduction strategies means that anti-miR-214 could still be given after injury and potentially promote repair even in the presence of established necrosis.

The findings of this study have the potential to impact short- and long-term clinical outcomes related to ischaemia in renal grafts. Dampening of the immune response may impact on rates of acute rejection where there is a proportional relationship between length of ischaemia and the alloimmune response. Enhanced tubular recovery may result in better graft function and, together with reduced rates of AR, lead to a reduction in CAD and graft loss.

Anti-miR-214 oligonucleotides have been shown to result in a significant reduction in fibrosis following UUO in mice with no evidence of harmful off-target effects[310]. In this study, there was a concurrent dampening of the immune response during the early and late phases of injury which was accompanied by a reduction in fibrosis following miR-214 ablation. Although there was no difference in early injury markers (ATN and KIM-1 expression), anti-miR-214 treatment may be beneficial at the time or even before transplantation to reduce the immune response to ischaemia. Fibrosis is often diagnosed late, and reserving treatment to when there is evidence of CAD on biopsy may reduce the efficacy of treatment.

Anti-miR-214 strategies can be delivered to the graft by several methods. Unlike in native renal ischaemic injury, renal transplant is relatively well controlled and anti-miR-214 could be given to recipients up to several hours before transplantation. Alternatively, there is increasing research into the development of normothermic machine perfusion strategies that could be used to deliver drugs to kidney, lung and liver grafts prior to implantation. So far, results are promising as multiple studies have demonstrated improved organ function and sufficient drug delivery[334]. The majority of studies have delivered therapies via the perfusate[334,335] whereas some researchers have used nanoparticles[336]. One study by Sewpaul *et al* has shown that anti-miR-24 antisense oligonucleotide delivered via perfusate is rapidly taken up by human kidneys and was observed in proximal tubules and endothelium. Importantly, there was upregulation of miR-24 targets HO-1 and sphingosine 1-phosphate receptor-1 (S1PR1) which regulated immune cell function[337]. This study highlights the potential of combining anti-miR therapies with normothermic machine perfusion. There is scope to introduce anti-miR-214 via this method although at present, studies are primarily focused on improving discarded or poorly perfused DCD kidneys and so there will be a delay before this can be utilised clinically. In addition, it is likely that machine perfusion will be utilised in grafts that meet certain criteria such as marginal kidneys from DCD donors. Therefore, not all grafts will be subjected to machine perfusion techniques prior to implantation and alternatively strategies maybe required to address DBD grafts.

MiR-214 has been shown to have deleterious effects following cardiac ischaemia[233]. Although Denby *et al* demonstrated that the mechanism of action in cardiomyocytes was not a target in the kidney[310], there is some concern regarding off target effects in transplant recipients. Patients with ESRD are high risk for cardiovascular disease[338], particularly those with diabetes and managing cardiac risk is an important

consideration in anti-miR-214 therapy. Denby *et al* also demonstrated that anti-miR-214 was preferentially taken up by the kidney, thereby reducing potential off-target side effect profile[310]. Another benefit of using normothermic machine perfusion is avoidance of systemic therapy; the drug is delivered to the organ directly and there can be a 'washout' period prior to implantation to reduce systemic delivery. Nevertheless, cardiac complications may be a limiting factor in anti-miR-214 treatment. One criticism of this study is that the heart was not examined for signs of injury but should be factored into any future experimental studies examining the effect of anti-miR-214 in IRI.

6.2 Strengths and limitations of the study

There are inherent limitations to this project which are centred around the animal models used. An advantage of animal models is that they allow researchers to perform and replicate invasive procedures that are not possible in humans. Furthermore, *in vivo* experiments can be altered using genetic manipulation, and cells can be readily extracted for *ex vivo* experiments more readily than in humans.

Given that the project focused on the impact of ischaemia on transplant outcomes, an ideal model would be a model of transplantation where there is an allogenic response to a single class II mismatch resulting in histological findings of CAD[122,280,282], which is more reflective of the process observed in human renal transplantation. Whilst this model is superior to non-transplant models, **Chapter 3** explored the difficulty in establishing this model which is technically challenging with a considerable learning curve. Despite several adaptations and improvements in anastomotic times, there was inconsistency in outcomes which meant the model was unsustainable in the

timeframe of the project. One option would have been to use a larger rat model which has been used by other groups[287,288], however this would have resulted in further delay to the project. A potential advantage of using a non-allogenic model of IRI is that the specific mechanisms relating to ischaemia can be explored in isolation from the allogenic response following transplantation. It can be used to model AKI and fibrosis and in certain circumstances one kidney can be used as a control, thereby negating the requirement for sham animals. The IRI model is less technically challenging and results in higher throughput of procedures and data in a relatively short timeframe. The model is easily reproducible, and animals recover quickly with little mortality and few post-procedure complications.

However, despite the benefits of the IRI model, there are also limitations associated with it. The group routinely utilises a unilateral model of renal IRI which allows the animal to progress beyond the early phase of injury and renal failure. Alternatively, the uninjured kidney can be used as control tissue, negating the requirement for sham animals in experiments with short-term endpoints[239]. Unilateral IRI is beneficial in allowing the animal to survive beyond the phase of acute renal failure but ultimately results in an accelerated progression towards fibrosis due to prolonged vasoconstriction in the immediate post-ischaemic phase. Unilateral IRI in the presence of a normal kidney does not reflect what is seen following human renal transplantation where the graft functions in isolation, without the support of functioning native kidneys. Similarly, in native renal injury, ischaemic AKI commonly affects both kidneys as severe hypovolaemia results in an acute decline in renal perfusion. Following unilateral IRI, the uninjured kidney hypertrophies in compensation for the reduced renal mass as shown in **Chapters 4** and **5**. At a transcriptomic level, there was a significant increase in miR-214 levels compared to sham controls suggesting that there may be underlying injury, potentially reflecting the sequalae of a

haemodynamic imbalance across the two kidneys. These results demonstrate that the uninjured kidney is not a suitable control and sham groups are required for comparison.

In addition, the model does not reflect the local and systemic effects of ESRD and uraemia seen clinically. Studies have shown that renal failure can impact the inflammatory response[339] and the presence of a functioning kidney may impact on the immune cell milieu present systemically in the injured kidney. Evidence suggests that ESRD alters the turnover of T cells and depletes naïve and memory $CD4^+$ and $CD8^+$ T cells[340,341]. The exact mechanism behind this remains poorly understood.

The presence of the uninjured kidney means that function of the injured kidney cannot be easily assessed using standard biochemical measurements and therefore there is an assumption that fibrosis reflects poor function. Many publications use renal fibrosis and not renal function as a primary endpoint, particularly in other unilateral renal injury models such as UUO. Ideally renal function would have been quantified alongside assessment of structural injury however this would have involved utilising inulin clearance which, although is the gold standard for assessing renal function *in vivo*[342], is time consuming and can be cumbersome. Assessment of inulin clearance was considered prior to commencing the final knockout studies however it would not have been achievable to perform inulin clearance alongside flow cytometry in the same experimental animals. Therefore, a decision was made to prioritise flow cytometry over functional assessment as it yielded information about the potential mechanism of miR-214, particularly as structural injury was examined using histology. An alternative strategy would have been to adopt the use of transdermal measurement of GFR which measures excretion of exogenous tracer FITC-conjugated sinistrin which is an inulin analogue[343,344] and has been validated against standard measurements of renal function. Even though some reports have shown inter-strain

variability with reduced GFR in C57Bl/6 with age compared to BALB/c mice[345], it is a validated tool that can used as an alternative to traditional inulin clearance. This technique could have allowed measurement of renal function *in vivo* prior to animal sacrifice and would have been beneficial to ascertain whether there was quicker recovery of renal function in miR-214$^{-/-}$ mice.

A bilateral IRI model is advantageous in that it is a better reflection of human pathophysiology, but there is a high morbidity associated with this model. An alternative to this would involve performing a nephrectomy of the uninjured kidney once fibrosis has become established in order to model the systemic effects of ESRD[346], but this in itself poses extra challenges to the model such as timing of nephrectomy and requirement for an additional procedure. Studies have shown that performing a nephrectomy can induce a pre-conditioning event which is protective in the injured kidney[256,257]. Therefore, modelling progressive ESRD using IRI poses challenges that would require further refinements to model effectively.

6.3 Future directions

Further work is required to understand the precise targets of miR-214 in renal injury and fibrosis. The difficulty in understanding its precise role is partially due to the wide spectrum of targets presented in the literature and variety of disease pathways it has been shown to be involved in. MiRs are inherently small and can have matching seed sequences in a multitude of mRNA targets. Indeed, results from this study demonstrated that miR-214 is upregulated in multiple different cell types within the kidney; therefore, it has the potential to act on different targets within each population. Further assessment of potential targets could be assessed using RNA sequencing

but this is costly and has been performed by the group in other models of renal injury and fibrosis.

Another avenue to explore would be to perform IRI in immune cell-depleted mice and reconstitute T cells using adoptive transfer from miR-214$^{+/+}$ or miR-214$^{-/-}$ mice to examine if miR-214 depletion in T cells is beneficial in protecting against kidney injury. An inherent difficulty in examining T cells in the kidney *in vivo* is that the heterogeneity of the kidney makes it more challenging to examine them using flow cytometry. Evidence using adoptive transfer would be a more direct way of examining the role of miR-214 on T cells *in vivo* as Nosalski et al demonstrated in mice with perivascular fibrosis[312].

The next logical step following demonstration that miR-214 blockade abrogates injury is to examine whether this can be replicated using an anti-sense oligonucleotide to miR-214. Anti-sense oligonucleotides or anti-miRs have been shown to improve fibrosis following renal injury[223,293,347] and have strong potential as a future therapy[347,348]. Unlike in patients with native renal disease who often present after significant fibrosis has already occurred, renal transplantation is more controlled and pharmacological agents can be administered to the recipient prior to transplantation. In addition, with an ever-increasing interest in *ex vivo* perfusion, novel therapies could be delivered to a graft prior to implantation[349] resulting in targeted multi-modal therapy.

A small pilot study examining non-invasive early diagnostic markers of CAD was performed as part of these studies. Due to time constraints, this section of the study was not completed but initial images of renal transplants and native kidneys demonstrated that MR elastography could be performed in renal transplant recipients and healthy volunteers safely at the University of Edinburgh's Clinical Research

Imaging Centre. In addition, miR-214 was shown to be upregulated in patients with mild to moderate fibrosis on allograft biopsy which in encourages further examination of its role as a potential biomarker. A further study examining the role of imaging in combination with biomarkers of fibrosis would be beneficial in discovering novel non-invasive diagnostic markers of CAD.

References

1. Tonelli M, Wiebe N, Knoll G, et al. Systematic review: Kidney transplantation compared with dialysis in clinically relevant outcomes. *Am J Transplant*. 2011;11(10):2093-2109. doi:10.1111/j.1600-6143.2011.03686.x

2. Hariharan S, Johnson CP, Bresnahan BA, Taranto SE, McIntosh MJ, Stablein D. Improved Graft Survival after Renal Transplantation in the United States, 1988 to 1996. *N Engl J Med*. 2000;342(9):605-612. doi:10.1056/NEJM200003023420901

3. Webb L, Casula A, Ravanan R, Tomson CRV. Chapter 5: Demographic and Biochemistry Profile of Kidney Transplant Recipients in the UK in 2008: national and centre-specific analyses. *Nephron Clin Pract*. 2010;115(1):c69-c102. doi:10.1159/000301160

4. Chapman JR, O'connell PJ, Nankivell BJ. Chronic Renal Allograft Dysfunction. *J Am Soc Nephrol*. 2005;16:3015-3026. doi:10.1681/ASN.2005050463

5. Ponticelli C, Villa M, Cesana B, Montagnino G, Tarantino A. Risk factors for late kidney allograft failure. *Kidney Int*. 2002;62(5):1848-1854. doi:10.1046/j.1523-1755.2003.00952.x

6. Waiser J, Schreiber M, Budde K, et al. Age-matching in renal transplantation. *Nephrol Dial Transplant*. 2000;15(5):696-700. doi:10.1093/ndt/15.5.696

7. Van Ittersum FJ, Hemke AC, Dekker FW, et al. Increased risk of graft failure and mortality in Dutch recipients receiving an expanded criteria donor kidney transplant. *Transpl Int*. 2017;30:14-28. doi:10.1111/tri.12863

8. El Ene Querard A-H, Foucher Y, Combescure C, et al. Comparison of survival outcomes between Expanded Criteria Donor and Standard Criteria Donor kidney transplant recipients: a systematic review and meta-analysis. *Transpl Int*. 2016;29:403-415. doi:10.1111/tri.12736

9. Robinson BM, Zhang J, Morgenstern H, et al. Worldwide, mortality risk is high soon after initiation of hemodialysis. *Kidney Int*. 2014;85(1):158-165. doi:10.1038/ki.2013.252

10. Hosgood SA, Saeb-Parsy K, Hamed MO, Nicholson ML. Successful Transplantation of Human Kidneys Deemed Untransplantable but Resuscitated by Ex Vivo Normothermic Machine Perfusion. *Am J Transplant*. 2016;16(11):3282-3285. doi:10.1111/ajt.13906

11. Hosgood SA, Thompson E, Moore T, Wilson CH, Nicholson ML. Normothermic machine perfusion for the assessment and transplantation of declined human kidneys from donation after circulatory death donors. *Br J Surg*. 105(4):388-394. doi:10.1002/bjs.10733

12. Hosgood SA, Nicholson ML. An Assessment of Urinary Biomarkers in a Series

of Declined Human Kidneys Measured During Ex Vivo Normothermic Kidney Perfusion. *Transplantation*. 2017;101(9):2120-2125. doi:10.1097/TP.0000000000001504

13. Kaths JM, Echeverri J, Chun YM, et al. Continuous Normothermic Ex Vivo Kidney Perfusion Improves Graft Function in Donation After Circulatory Death Pig Kidney Transplantation. *Transplantation*. 2017;101(4):754-763. doi:10.1097/TP.0000000000001343

14. Hosgood SA, Saeb-Parsy K, Wilson C, Callaghan C, Collett D, Nicholson ML. Protocol of a randomised controlled, open-label trial of ex vivo normothermic perfusion versus static cold storage in donation after circulatory death renal transplantation. doi:10.1136/bmjopen-2016

15. Pearson R, Geddes C, Clancy M AJ. A Single Non-Retrieval Centre Experience. *Am J Transplant*. 2019;19(Suppl 3). https://atcmeetingabstracts.com/abstract/normothermic-regional-perfusion-of-kidneys-a-single-non-retrieval-centre-experience/.

16. Thomas RAB, Czopek A, Bellamy COC, McNally SJ, Kluth DC, Marson LP. Hemin preconditioning upregulates heme oxygenase-1 in deceased donor renal transplant recipients: A randomized, controlled, phase IIB Trial. *Transplantation*. 2016;100(1):176-183. doi:10.1097/TP.0000000000000770

17. Barker CF, Markmann JF. Historical overview of transplantation. *Cold Spring Harb Perspect Med*. 2013;3(4):1-18. doi:10.1101/cshperspect.a014977

18. Otterbein LE, Fan Z, Koulmanda M, Thronley T, Strom TB. Innate immunity for better or worse govern the allograft response. *Curr Opin Organ Transplant*. 2015;20(1):8-12. doi:10.1097/MOT.0000000000000152

19. Sert I, Colak H, Tugmen C, Dogan S, Karaca C. The effect of cold ischemia time on delayed graft function and acute rejection in kidney transplantation. *Saudi J Kidney Dis Transplant*. 2014;25(5):960. doi:10.4103/1319-2442.139865

20. Yarlagadda SG, Coca SG, Garg AX, et al. Marked variation in the definition and diagnosis of delayed graft function: a systematic review. *Nephrol Dial Transpl*. 2008;23:2995-3003. doi:10.1093/ndt/gfn158

21. Perico N, Cattaneo D, Sayegh MH, Remuzzi G. Delayed graft function in kidney transplantation. *Lancet*. 2004;364(9447):1814-1827. doi:10.1016/S0140-6736(04)17406-0

22. McLaren A, Jassem W, Gray D, Fuggle S, Welsh K, Morris P. Delayed graft function: risk factors and the relative effects of early function and acute rejection on long-term survival in cadaveric renal transplantation. *Clin Transplant*. 1999;13(3):266-272. doi:10.1034/j.1399-0012.1999.130308.x

23. Transplantation Society. AOWHP. *Transplantation.* Vol 63. Williams & Wilkins Co; 1997. https://insights.ovid.com/crossref?an=00007890-199704150-00011. Accessed June 27, 2019.

24. Giblin L, O'kelly P, Little D, et al. A Comparison of Long-Term Graft Survival Rates Between the First and Second Donor Kidney Transplanted-The Effect of a Longer Cold Ischaemic Time for the Second Kidney. *Am J Transplant*. 2005;5:1071-1075. doi:10.1111/j.1600-6143.2005.00798.x

25. Quiroga I, Mcshane P, Koo DDH, et al. Major effects of delayed graft function and cold ischaemia time on renal allograft survival. *Nephrol Dial Transpl*. 2006;21:1689-1696. doi:10.1093/ndt/gfl042

26. Kayler LK, Magliocca J, Zendejas I, Srinivas TR, Schold JD. Impact of cold ischemia time on graft survival among ecd transplant recipients: A paired kidney analysis. *Am J Transplant*. 2011;11(12):2647-2656. doi:10.1111/j.1600-6143.2011.03741.x

27. Kayler L, Yu X, Cortes C, Lubetzky M, Friedmann P. Impact of Cold Ischemia Time in Kidney Transplants From Donation After Circulatory Death Donors. *Transplant Direct*. 2017;3(7):e177. doi:10.1097/txd.0000000000000680

28. Shoskes DA, Cecka JM. Deleterious effects of delayed graft function in cadaveric renal transplant recipients independent of acute rejection. *Transplantation*. 1998;66(12):1697-1701. http://www.ncbi.nlm.nih.gov/pubmed/9884262. Accessed June 28, 2019.

29. Salahudeen AK, Haider N, May W. *Cold Ischemia and the Reduced Long-Term Survival of Cadaveric Renal Allografts*. Vol 65.; 2004. doi:10.1111/j.1523-1755.2004.00416.x

30. Krishnan AR, Wong G, Chapman JR, et al. Prolonged Ischemic Time, Delayed Graft Function, and Graft and Patient Outcomes in Live Donor Kidney Transplant Recipients. 2016. doi:10.1111/ajt.13817

31. Redfield RR, Scalea JR, Zens TJ, et al. Predictors and outcomes of delayed graft function after living-donor kidney transplantation. *Transpl Int*. 2016;29(1):81-87. doi:10.1111/tri.12696

32. Troppmann C, Gillingham KJ, Benedetti E, et al. Delayed graft function, acute rejection, and outcome after cadaver renal transplantation. The multivariate analysis. *Transplantation*. 1995;59(7):962-968. http://www.ncbi.nlm.nih.gov/pubmed/7709456. Accessed June 28, 2019.

33. Troppmann C, Gillingham KJ, Gruessner RW, et al. Delayed graft function in the absence of rejection has no long-term impact. A study of cadaver kidney recipients with good graft function at 1 year after transplantation. *Transplantation*. 1996;61(9):1331-1337. http://www.ncbi.nlm.nih.gov/pubmed/8629292. Accessed June 28, 2019.

34. Chaumont M, Racapé J, Broeders N, et al. Delayed Graft Function in Kidney Transplants: Time Evolution, Role of Acute Rejection, Risk Factors, and Impact on Patient and Graft Outcome. *J Transplant*. 2015;2015:1-9. doi:10.1155/2015/163757

35. Qureshi F, Rabb H, Kasiske BL. Silent acute rejection during prolonged delayed graft function reduces kidney allograft survival. *Transplantation*.

2002;74(10):1400-1404. doi:10.1097/00007890-200211270-00010

36. Gjertson DW. Impact of delayed graft function and acute rejection on kidney graft survival. *Clin Transpl*. 2000:467-480. http://www.ncbi.nlm.nih.gov/pubmed/11512359. Accessed June 29, 2019.

37. Lu CY, Penfield JG, Kielar ML, Vazquez MA, Rohan D. *Hypothesis: Is Renal Allograft Rejection Initiated by the Response to Injury Sustained during the Transplant Process? Hypothesis: Is Renal Allograft Rejection Initiated by the Response*. Vol 55.; 1999. doi:10.1046/j.1523-1755.1999.00491.x

38. Bryan CF, Luger AM, Martinez J, et al. Cold ischemia time: an independent predictor of increased HLA class I antibody production after rejection of a primary cadaveric renal allograft. *Transplantation*. 2001;71(7):875-879. http://www.ncbi.nlm.nih.gov/pubmed/11349719. Accessed June 28, 2019.

39. Mikhalski D, Wissing KM, Ghisdal L, et al. Cold Ischemia is a Major Determinant of Acute Rejection and Renal Graft Survival in the Modern Era of Immunosuppression. *Transplantation*. 2008;85(Supplement):S3-S9. doi:10.1097/TP.0b013e318169c29e

40. Postalcioglu M, Kaze AD, Byun BC, et al. Association of Cold Ischemia Time with Acute Renal Transplant Rejection. *Transplantation*. 2018;102(7):1188-1194. doi:10.1097/TP.0000000000002106

41. Wu WK, Famure O, Li Y, Kim SJ. Delayed graft function and the risk of acute rejection in the modern era of kidney transplantation. *Kidney Int*. 2015;88(4):851-858. doi:10.1038/ki.2015.190

42. Lo LJ, Go AS, Chertow GM, et al. Dialysis-requiring acute renal failure increases the risk of progressive chronic kidney disease. *Kidney Int*. 2009;76(8):893-899. doi:10.1038/ki.2009.289

43. Heung M, Chawla LS. Acute Kidney Injury: Gateway to Chronic Kidney Disease. *Nephron Clin Pr*. 2014;127:30-34. doi:10.1159/000363675

44. Roodnat JI, Mulder PGH, van Riemsdijk IC, IJzermans JNM, van Gelder T, Weimar W. Ischemia times and donor serum creatinine in relation to renal graft failure. *Transplantation*. 2003;75(6):799-804. doi:10.1097/01.TP.0000056632.00848.8D

45. Pérez Valdivia MA, Gentil MA, Toro M, et al. Impact of Cold Ischemia Time on Initial Graft Function and Survival Rates in Renal Transplants From Deceased Donors Performed in Andalusia. *Transplant Proc*. 2011;43(6):2174-2176. doi:10.1016/J.TRANSPROCEED.2011.06.047

46. Racusen LC, Solez K, Colvin RB, et al. *The Banff 97 Working Classification of Renal Allograft Pathology Standardization of Renal Allograft Biopsy Interpreta-Tion and Reporting Is Necessary to Guide Therapy in Trans*. Vol 55.; 1999. doi:10.1046/j.1523-1755.1999.00299.x

47. Nankivell B, Borrows R, Fung C, O'connell P, Allen R, Chapman J. The natural history of chronic allograft nephropathy. *N Engl J Med*. 2003;349:2326-2333.

48. Matas AJ, Gillingham KJ, Payne WD, Najarian JS. The impact of an acute rejection episode on long-term renal allograft survival (t1/2). *Transplantation*. 1994;57(6):857-859.

49. Troppmann C, Gillingham KJ, Benedetti E, et al. Delayed graft function, acute rejection, and outcome after cadaver renal transplantation. The multivariate analysis. *Transplantation*. 1995;59(7):962-968. http://www.ncbi.nlm.nih.gov/pubmed/7709456.

50. Cosio FG, Grande JP, Wadei H, Larson TS, Griffin MD, Stegall MD. Predicting Subsequent Decline in Kidney Allograft Function from Early Surveillance Biopsies. *Am J Transplant*. 2005;5(10):2464-2472. doi:10.1111/j.1600-6143.2005.01050.x

51. Stegall MD, Park WD, Larson TS, et al. The Histology of Solitary Renal Allografts at 1 and 5 Years After Transplantation. *Am J Transplant*. 2011;11(4):698-707. doi:10.1111/j.1600-6143.2010.03312.x

52. Mannon RB, Matas AJ, Grande J, et al. Inflammation in Areas of Tubular Atrophy in Kidney Allograft Biopsies: A Potent Predictor of Allograft Failure. *Am J Transplant*. 2010;10(9):2066-2073. doi:10.1111/j.1600-6143.2010.03240.x

53. Moreso F, Ibernon M, Gomà M, et al. Subclinical Rejection Associated with Chronic Allograft Nephropathy in Protocol Biopsies as a Risk Factor for Late Graft Loss. *Am J Transplant*. 2006;6:747-752. doi:10.1111/j.1600-6143.2005.01230.x

54. Ávila C, Líbano L, Rojas I, Rodrigo R. Role of ischemia-reperfusion in oxidative stress-mediated injury during kidney transplantation. *Clin Res Trials*. 2019;5(3). doi:10.15761/crt.1000260

55. Kosieradzki M, Rowiński W. Ischemia/Reperfusion Injury in Kidney Transplantation: Mechanisms and Prevention. *Transplant Proc*. 2008;40(10):3279-3288. doi:10.1016/j.transproceed.2008.10.004

56. Li C, Jackson RM. Reactive species mechanisms of cellular hypoxia-reoxygenation injury. *Am J Physiol Physiol*. 2002;282(2):C227-C241. doi:10.1152/ajpcell.00112.2001

57. Tabriziani H, Lipkowitz MS, Vuong N. Chronic kidney disease, kidney transplantation and oxidative stress: A new look to successful kidney transplantation. *Clin Kidney J*. 2018;11(1):130-135. doi:10.1093/ckj/sfx091

58. Fonseca I, Reguengo H, Almeida M, et al. Oxidative stress in kidney transplantation: Malondialdehyde is an early predictive marker of graft dysfunction. *Transplantation*. 2014;97(10):1058-1065. doi:10.1097/01.TP.0000438626.91095.50

59. Azmandian J, Mohamadifar M, Rahmanian-Koshkaki S, et al. Study of the association between the donors and recipients angiotensin-converting enzyme insertion/deletion gene polymorphism and the acute renal allograft rejection. *J Nephropathol*. 2015;4(3):62-68. doi:10.12860/jnp.2015.13

60. Antolini F, Valente F, Ricciardi D, Fagugli RM. Normalization of oxidative stress parameters after kidney transplant is secondary to full recovery of renal function. *Clin Nephrol*. 2004;62(2):131-137. doi:10.5414/cnp62131

61. Long C, Yang J, Yang H, Li X, Wang G. Attenuation of renal ischemia/reperfusion injury by oleanolic acid preconditioning via its antioxidant, anti-inflammatory, and anti-apoptotic activities. *Mol Med Rep*. 2016;13(6):4697-4704. doi:10.3892/mmr.2016.5128

62. Liu Y, Shi B, Li Y, Zhang H. Protective effect of luteolin against renal ischemia/reperfusion injury via modulation of pro-inflammatory cytokines, oxidative stress and apoptosis for possible benefit in kidney transplant. *Med Sci Monit*. 2017;23:5720-5727. doi:10.12659/MSM.903253

63. Cusumano G, Romagnoli J, Liuzzo G, et al. N-Acetylcysteine and High-Dose Atorvastatin Reduce Oxidative Stress in an Ischemia-Reperfusion Model in the Rat Kidney. *Transplant Proc*. 2015;47(9):2757-2762. doi:10.1016/j.transproceed.2015.09.035

64. Danilovic A, Lucon AM, Srougi M, et al. Protective effect of N-acetylcysteine on early outcomes of deceased renal transplantation. *Transplant Proc*. 2011;43(5):1443-1449. doi:10.1016/j.transproceed.2011.02.020

65. Morales-Buenrostro LE, Ortega-Trejo JA, Pérez-Villalva R, et al. Spironolactone reduces oxidative stress in living donor kidney transplantation: A randomized controlled trial. *Am J Physiol - Ren Physiol*. 2019;317(3):F519-F528. doi:10.1152/ajprenal.00606.2018

66. Land WG, Agostinis P, Gasser S, Garg AD, Linkermann A. Transplantation and Damage-Associated Molecular Patterns (DAMPs). *Am J Transplant*. 2016;16(12):3338-3361. doi:10.1111/ajt.13963

67. Brezis M, Rosen S. Hypoxia of the Renal Medulla — Its Implications for Disease. Epstein FH, ed. *N Engl J Med*. 1995;332(10):647-655. doi:10.1056/NEJM199503093321006

68. Conger J. Hemodynamic factors in acute renal failure. *Adv Ren Replace Ther*. 1997;4(2 Suppl 1):25-37. http://www.ncbi.nlm.nih.gov/pubmed/9113238. Accessed June 11, 2018.

69. Kelly KJ, Williams WW, Colvin RB, et al. Intercellular adhesion molecule-1-deficient mice are protected against ischemic renal injury. *J Clin Invest*. 1996;97(4):1056-1063. doi:10.1172/JCI118498

70. Basile DP. The endothelial cell in ischemic acute kidney injury: Implications for acute and chronic function. *Kidney Int*. 2007;72(2):151-156. doi:10.1038/sj.ki.5002312

71. Kezić A, Stajic N, Thaiss F. Innate Immune Response in Kidney Ischemia/Reperfusion Injury: Potential Target for Therapy. 2017. doi:10.1155/2017/6305439

72. Sutton TA, Fisher CJ, Molitoris BA. Microvascular endothelial injury and

dysfunction during ischemic acute renal failure. *Kidney Int*. 2002;62(5):1539-1549. doi:10.1046/j.1523-1755.2002.00631.x

73. Regner KR, Roman RJ. Role of medullary blood flow in the pathogenesis of renal ischemia-reperfusion injury. *Curr Opin Nephrol Hypertens*. 2012;21(1):33-38. doi:10.1097/MNH.0b013e32834d085a

74. Tewes S, Gueler F, Chen R, et al. Functional MRI for characterization of renal perfusion impairment and edema formation due to acute kidney injury in different mouse strains. *PLoS One*. 2017;12(3). doi:10.1371/journal.pone.0173248

75. Aderem A, Ulevitch RJ. Toll-like receptors in the induction of the innate immune response. *Nature*. 2000;406(6797):782-787. doi:10.1038/35021228

76. Tsan M-F, Gao B. Endogenous ligands of Toll-like receptors. *J Leukoc Biol*. 2004;76(3):514-519. doi:10.1189/jlb.0304127

77. Takeuchi O, Akira S. Pattern Recognition Receptors and Inflammation. *Cell*. 2010;140(6):805-820. doi:10.1016/j.cell.2010.01.022

78. Bonventre J V. Dedifferentiation and Proliferation of Surviving Epithelial Cells in Acute Renal Failure. 2003. doi:10.1097/01.ASN.0000067652.51441.21

79. Kruger B, Krick S, Dhillon N, et al. Donor Toll-like receptor 4 contributes to ischemia and reperfusion injury following human kidney transplantation. *Proc Natl Acad Sci*. 2009;106(9):3390-3395. doi:10.1073/pnas.0810169106

80. Wu H, Chen G, Wyburn KR, et al. TLR4 activation mediates kidney ischemia/reperfusion injury. *J Clin Invest*. 2007;117(10):2847-2859. doi:10.1172/JCI31008

81. Zhang L-M, Liu J-H, Xue C-B, et al. Pharmacological inhibition of MyD88 homodimerization counteracts renal ischemia reperfusion-induced progressive renal injury in vivo and in vitro. *Sci Rep*. 2016;6(1):26954. doi:10.1038/srep26954

82. Bonventre J. Cellular pathophysiology of ischemic acute kidney injury. *J Clin Invest*. 2011;121(11):4210-4221. doi:10.1172/JCI45161.The

83. Goldstein DR, Tesar BM, Akira S, Lakkis FG. Critical role of the Toll-like receptor signal adaptor protein MyD88 in acute allograft rejection. *J Clin Invest*. 2003;111(10):1571-1578. doi:10.1172/JCI17573

84. Damman J, Schuurs TA, Ploeg RJ, Seelen MA. Complement and Renal Transplantation: From Donor to Recipient. *Transplantation*. 2008;85(7):923-927. doi:10.1097/TP.0b013e3181683cf5

85. Danobeitia JS, Djamali A, Fernandez LA. The role of complement in the pathogenesis of renal ischemia-reperfusion injury and fibrosis. *Fibrogenes Tissue Repair*. 2014;7(1):1-11. doi:10.1186/1755-1536-7-16

86. Peng Q, Li K, Smyth LA, et al. C3a and C5a Promote Renal Ischemia-

Reperfusion Injury. *J Am Soc Nephrol*. 2012;23:1474-1485. doi:10.1681/ASN.2011111072

87. Thurman JM, Scott Lucia M, Ljubanovic D, Michael Holers V. Acute tubular necrosis is characterized by activation of the alternative pathway of complement. *Kidney Int*. 2005;67(2):524-530. doi:10.1111/j.1523-1755.2005.67109.x

88. Naesens M, Li L, Ying L, et al. Expression of Complement Components Differs Between Kidney Allografts from Living and Deceased Donors. *J Am Soc Nephrol*. 2009;20(8):1839-1851. doi:10.1681/ASN.2008111145

89. Awad AS, Rouse M, Huang L, et al. Compartmentalization of neutrophils in the kidney and lung following acute ischemic kidney injury. *Kidney Int*. 2009;75(7):689-698. doi:10.1038/ki.2008.648

90. Kelly KJ, Williams WW, Colvint RB, Bonventre J V. *Antibody to Intercellular Adhesion Molecule 1 Protects the Kidney against Ischemic Injury (Acute Renal Faflure/Ischemia-Reperfusion Injury/Adhesion Molecule Receptors/Integrins)*. Vol 91.; 1994. https://www.pnas.org/content/pnas/91/2/812.full.pdf. Accessed July 6, 2019.

91. Tang PM-K, Nikolic-Paterson DJ, Lan H-Y. Macrophages: versatile players in renal inflammation and fibrosis. *Nat Rev Nephrol*. 2019;15(3):144-158. doi:10.1038/s41581-019-0110-2

92. Lu Sarah Faubel Zhibin He Ana Andres Hernando Alkesh Jani Ross Kedl Charles Edelstein LL. Depletion of Macrophages and Dendritic Cells in Ischemic Acute Kidney Injury. *Am J Nephrol*. 2012;35:181-190. doi:10.1159/000335582

93. Steinman RM, Hemmi H. Dendritic cells: Translating innate to adaptive immunity. *Curr Top Microbiol Immunol*. 2006;311:17-58. doi:10.1007/3-540-32636-7_2

94. Friedewald JJ, Rabb H. Inflammatory cells in ischemic acute renal failure. In: *Kidney International*. Vol 66. ; 2004:486-491. doi:10.1111/j.1523-1755.2004.761_3.x

95. Rabb H. Immune Modulation of Acute Kidney Injury. *J Am Soc Nephrol*. 2006;17(3):604-606. doi:10.1681/ASN.2006010060

96. Lai LW, Yong KC, Igarashi S, Lien YHH. A sphingosine-1-phosphate type 1 receptor agonist inhibits the early T-cell transient following renal ischemia-reperfusion injury. *Kidney Int*. 2007;71(12):1223-1231. doi:10.1038/sj.ki.5002203

97. Kinsey GR, Okusa MD. Expanding role of T cells in acute kidney injury. *Curr Opin Nephrol Hypertens*. 2014;23(1):9-16. doi:10.1097/01.mnh.0000436695.29173.de

98. Zwacka RM, Dudus L, Engelhardt JF, et al. CD4(+) T-lymphocytes mediate ischemia/reperfusion-induced inflammatory responses in mouse liver. CD4 T-

Lymphocytes Mediate Ischemia/Reperfusion-induced Inflammatory Responses in Mouse Liver. *J Clin Invest*. 1997;100(2):279-289. doi:10.1172/JCI119533

99. Le Moine O, Louis H, Demols A, et al. Cold liver ischemia-reperfusion injury critically depends on liver T cells and is improved by donor pretreatment with interleukin 10 in mice. *Hepatology*. 2000;31(6):1266-1274. doi:10.1053/jhep.2000.7881

100. Horie Y, Chervenak RP, Wolf R, et al. Lymphocytes mediate TNF-alpha-induced endothelial cell adhesion molecule expression: studies on SCID and RAG-1 mutant mice. *J Immunol*. 1997;159(10):5053-5062. http://www.ncbi.nlm.nih.gov/pubmed/9366433.

101. Linfert D, Chowdhry T, Rabb H. Lymphocytes and ischemia-reperfusion injury. *Transplant Rev*. 2009;23(1):1-10. doi:10.1016/j.trre.2008.08.003

102. Rabb H, Daniels F, O'Donnell M, et al. Pathophysiological role of T lymphocytes in renal ischemia-reperfusion injury in mice. *Am J Physiol - Ren Physiol*. 2000;279(3 48-3):F525-F531. doi:10.1152/ajprenal.2000.279.3.f525

103. Burne MJ, Daniels F, El Ghandour A, et al. Identification of the CD4+ T cell as a major pathogenic factor in ischemic acute renal failure. *J Clin Invest*. 2001;108(9):1283-1290. doi:10.1172/jci12080

104. Yokota N, Daniels F, Crosson J, Rabb H. Protective effect of T cell depletion in murine renal ischemia-reperfusion injury. *Transplantation*. 2002;74(6):759-763. doi:10.1097/00007890-200209270-00005

105. Huang Y, Rabb H, Womer KL. Ischemia–reperfusion and immediate T cell responses. *Cell Immunol*. 2007;248(1):4-11. doi:10.1016/j.cellimm.2007.03.009

106. Day Y-J, Huang L, Ye H, Li L, Linden J, Okusa MD. Renal Ischemia-Reperfusion Injury and Adenosine 2A Receptor-Mediated Tissue Protection: The Role of CD4 + T Cells and IFN-γ . *J Immunol*. 2006;176(5):3108-3114. doi:10.4049/jimmunol.176.5.3108

107. Roussey-Kesler G, Giral M, Moreau A, et al. Clinical operational tolerance after kidney transplantation. *Am J Transplant*. 2006;6(4):736-746. doi:10.1111/j.1600-6143.2006.01280.x

108. Kinsey GR, Sharma R, Huang L, et al. Regulatory T cells suppress innate immunity in kidney ischemia-reperfusion injury. *J Am Soc Nephrol*. 2009;20(8):1744-1753. doi:10.1681/ASN.2008111160

109. Gandolfo MT, Jang HR, Bagnasco SM, et al. Foxp3+ regulatory T cells participate in repair of ischemic acute kidney injury. *Kidney Int*. 2009;76(7):717-729. doi:10.1038/ki.2009.259

110. Jun C, Qingshu L, Ke W, et al. Protective Effect of CXCR3 + CD4 + CD25 + Foxp3 + Regulatory T Cells in Renal Ischemia-Reperfusion Injury. *Mediators Inflamm*. 2015;2015:1-8. doi:10.1155/2015/360973

111. Kinsey GR, Sharma R, Okusa MD. Regulatory T cells in AKI. *J Am Soc Nephrol*. 2013;24(11):1720-1726. doi:10.1681/ASN.2013050502

112. Kim M-G, Koo TY, Yan J-J, et al. IL-2/Anti-IL-2 Complex Attenuates Renal Ischemia-Reperfusion Injury through Expansion of Regulatory T Cells. *J Am Soc Nephrol*. 2013;24(10):1529-1536. doi:10.1681/ASN.2012080784

113. Hu J, Zhang L, Wang N, et al. Mesenchymal stem cells attenuate ischemic acute kidney injury by inducing regulatory T cells through splenocyte interactions. *Kidney Int*. 2013;84(3):521-531. doi:10.1038/ki.2013.114

114. Lai L-W, Yong K-C, Lien Y-HH. Pharmacologic recruitment of regulatory T cells as a therapy for ischemic acute kidney injury. *Kidney Int*. 2012;81(10):983-992. doi:10.1038/ki.2011.412

115. Garris CS, Blaho VA, Hla T, Han MH. Sphingosine-1-phosphate receptor 1 signalling in T cells: Trafficking and beyond. *Immunology*. 2014;142(3):347-353. doi:10.1111/imm.12272

116. Liu G, Burns S, Huang G, et al. The receptor S1P1 overrides regulatory T cell–mediated immune suppression through Akt-mTOR. *Nat Immunol*. 2009;10(7):769-777. doi:10.1038/ni.1743

117. Karahan GE, Claas FHJ, Heidt S. B cell immunity in solid organ transplantation. *Front Immunol*. 2017;7(JAN):1-11. doi:10.3389/fimmu.2016.00686

118. Kissmeyer-Nielsen F, Olsen S, Petersen VP, Fjeldborg O. HYPERACUTE REJECTION OF KIDNEY ALLOGRAFTS, ASSOCIATED WITH PRE-EXISTING HUMORAL ANTIBODIES AGAINST DONOR CELLS. *Lancet*. 1966;288(7465):662-665. doi:10.1016/S0140-6736(66)92829-7

119. TERASAKI PI, McCLELLAND JD. Microdroplet Assay of Human Serum Cytotoxins. *Nature*. 1964;204(4962):998-1000. doi:10.1038/204998b0

120. Patel R, Terasaki PI. Significance of the Positive Crossmatch Test in Kidney Transplantation. *N Engl J Med*. 1969;280(14):735-739. doi:10.1056/NEJM196904032801401

121. Lund FE. Cytokine-producing B lymphocytes - key regulators of immunity. *Curr Opin Immunol*. 2008;20(3):332-338. doi:10.1016/j.coi.2008.03.003

122. Tse GH, Johnston CJC, Kluth D, et al. Intrarenal B cell cytokines promote transplant fibrosis and tubular atrophy. *Am J Transplant*. 2015;15(12):3067-3080. doi:10.1111/ajt.13393

123. Clatworthy MR, Watson CJE, Plotnek G, et al. B-Cell–Depleting Induction Therapy and Acute Cellular Rejection. *N Engl J Med*. 2009;360(25):2683-2685. doi:10.1056/NEJMc0808481

124. Rogers NJ, Lechler RI, Lechler RI. Allorecognition. *Am J Transplant*. 2001;1:97-102.

125. Marino J, Paster J, Benichou G. Allorecognition by T Lymphocytes and

Allograft Rejection. *Front Immunol*. 2016;7. doi:10.3389/fimmu.2016.00582

126. Siu JHY, Surendrakumar V, Richards JA, Pettigrew GJ. T cell Allorecognition Pathways in Solid Organ Transplantation. *Front Immunol*. 2018;9. doi:10.3389/fimmu.2018.02548

127. Yang Z-F, David W-Y, Ho A, Chu C-Y, Wang Y-Q, Fan S-T. Linking Inflammation to Acute Rejection in Small-For-Size Liver Allografts: The Potential Role of Early Macrophage Activation. *Am J Transplant*. 2003;4:196-209. doi:10.1046/j.1600-6143.2003.00313.x

128. Kreisel D, Sugimoto S, Zhu J, et al. Emergency granulopoiesis promotes neutrophil-dendritic cell encounters that prevent mouse lung allograft acceptance. 2011. doi:10.1182/blood-2011-04-347823

129. Xiao B, Xia W, Zhang J, Liu B, Guo S. Prolonged Cold Ischemic Time Results in Increased Acute Rejection in a Rat Allotransplantation Model. *J Surg Res*. 2010;164(2):e299-e304. doi:10.1016/j.jss.2010.08.012

130. Kakuta Y, Okumi M, Miyagawa S, et al. Blocking of CCR5 and CXCR3 Suppresses the Infiltration of Macrophages in Acute Renal Allograft Rejection. *Transplantation*. 2012;93(1):24-31. doi:10.1097/TP.0b013e31823aa585

131. Goto R, Issa F, Heidt S, Taggart D, Wood KJ. Ischemia-reperfusion injury accelerates human antibody-mediated transplant vasculopathy. *Transplantation*. 2013;96(2):139-145. doi:10.1097/TP.0b013e318295ee32

132. Chun N, Fairchild RL, Li Y, et al. Complement Dependence of Murine Costimulatory Blockade-Resistant Cellular Cardiac Allograft Rejection. 2017. doi:10.1111/ajt.14328

133. Uehara M, Solhjou Z, Banouni N, et al. Ischemia augments alloimmune injury through IL-6-driven CD4+ alloreactivity. *Sci Rep*. 2018;8(1). doi:10.1038/s41598-018-20858-4

134. Su CA, Iida S, Abe T, Fairchild RL. Endogenous memory CD8 T cells directly mediate cardiac allograft rejection. *Am J Transplant*. 2014;14(3):568-579. doi:10.1111/ajt.12605

135. Shrestha BM, Haylor J. Biological pathways and potential targets for prevention and therapy of chronic allograft nephropathy. *Biomed Res Int*. 2014;2014. doi:10.1155/2014/482438

136. Liu Y. Cellular and molecular mechanisms of renal fibrosis. *Nat Rev Nephrol*. 2011;7(12):684-696. doi:10.1038/nrneph.2011.149

137. Tapmeier TT, Fearn A, Brown K, et al. Pivotal role of CD4+ T cells in renal fibrosis following ureteric obstruction. *Kidney Int*. 2010;78(4):351-362. doi:10.1038/ki.2010.177

138. Liu L, Kou P, Zeng Q, et al. CD4+ T lymphocytes, especially Th2 cells, contribute to the progress of renal fibrosis. *Am J Nephrol*. 2012;36(4):386-396. doi:10.1159/000343283

139. Meng XM, Nikolic-Paterson DJ, Lan HY. Inflammatory processes in renal fibrosis. *Nat Rev Nephrol*. 2014;10(9):493-503. doi:10.1038/nrneph.2014.114

140. Humphreys BD, Valerius MT, Kobayashi A, et al. Cell Stem Cell Intrinsic Epithelial Cells Repair the Kidney after Injury. doi:10.1016/j.stem.2008.01.014

141. Venkatachalam MA, Weinberg JM, Kriz W, Bidani AK. Failed Tubule Recovery, AKI-CKD Transition, and Kidney Disease Progression. *J Am Soc Nephrol*. 2015;26:1765-1776. doi:10.1681/ASN.2015010006

142. Suzuki T, Kimura M, Asano M, Fujigaki Y, Hishida A. Role of atrophic tubules in development of interstitial fibrosis in microembolism-induced renal failure in rat. *Am J Pathol*. 2001;158(1):75-85. doi:10.1016/S0002-9440(10)63946-6

143. Klingberg F, Hinz B, White ES. The myofibroblast matrix: implications for tissue repair and fibrosis. *J Pathol*. 2013;229(2):298-309. doi:10.1002/path.4104

144. Zeisberg M, Duffield JS. Resolved: EMT produces fibroblasts in the kidney. *J Am Soc Nephrol*. 2010;21(8):1247-1253. doi:10.1681/ASN.2010060616

145. Lin SL, Kisseleva T, Brenner DA, Duffield JS. Pericytes and perivascular fibroblasts are the primary source of collagen-producing cells in obstructive fibrosis of the kidney. *Am J Pathol*. 2008;173(6):1617-1627. doi:10.2353/ajpath.2008.080433

146. Kaissling B, Le Hir M. The renal cortical interstitium: morphological and functional aspects. *Histochem Cell Biol*. 2008;130:247-262. doi:10.1007/s00418-008-0452-5

147. Mack M, Yanagita M. Origin of myofibroblasts and cellular events triggering fibrosis. *Kidney Int*. 2015;87(2):297-307. doi:10.1038/ki.2014.287

148. Boor P, Floege J. Chronic kidney disease growth factors in renal fibrosis. *Clin Exp Pharmacol Physiol*. 2011;38(7):441-450. doi:10.1111/j.1440-1681.2011.05487.x

149. Floege J, Eitner F, Alpers CE. A New Look at Platelet-Derived Growth Factor in Renal Disease. *J Am Soc Nephrol*. 2008;19(1):12-23. doi:10.1681/ASN.2007050532

150. Paliege A, Rosenberger C, Bondke A, et al. Hypoxia-inducible factor-2α-expressing interstitial fibroblasts are the only renal cells that express erythropoietin under hypoxia-inducible factor stabilization. *Kidney Int*. 2010;77(4):312-318. doi:10.1038/ki.2009.460

151. Lebleu VS, Taduri G, O'Connell J, et al. Origin and function of myofibroblasts in kidney fibrosis. *Nat Med*. 2013;19(8):1047-1053. doi:10.1038/nm.3218

152. Asada N, Takase M, Nakamura J, et al. Dysfunction of fibroblasts of extrarenal origin underlies renal fibrosis and renal anemia in mice. *J Clin Invest*. 2011;121. doi:10.1172/JCI57301

153. Humphreys BD, Lin SL, Kobayashi A, et al. Fate tracing reveals the pericyte

and not epithelial origin of myofibroblasts in kidney fibrosis. *Am J Pathol*. 2010;176(1):85-97. doi:10.2353/ajpath.2010.090517

154. Lin S-L, Chang F-C, Schrimpf C, et al. Targeting Endothelium-Pericyte Cross Talk by Inhibiting VEGF Receptor Signaling Attenuates Kidney Microvascular Rarefaction and Fibrosis. *Am J Pathol*. 2011;178(2):911-923. doi:10.1016/j.ajpath.2010.10.012

155. Kida Y, Duffield JS. Frontiers in Research: Chronic Kidney Diseases: The pivotal role of pericytes in kidney fibrosis. doi:10.1111/j.1440-1681.2011.05531.x

156. Tyler JR, Robertson H, Booth TA, Burt AD, Kirby JA. Chronic Allograft Nephropathy: Intraepithelial Signals Generated by Transforming Growth Factor-beta and Bone Morphogenetic Protein-7. *Am J Transplant*. 2006;6(6):1367-1376. doi:10.1111/j.1600-6143.2006.01339.x

157. Park S, Dimaio TA, Liu W, Wang S, Sorenson CM, Sheibani N. Endoglin regulates the activation and quiescence of endothelium by participating in canonical and non-canonical TGF-β signaling pathways. *J Cell Sci*. 2013;126(Pt 6):1392-1405. doi:10.1242/jcs.117275

158. Bülow RD, Boor P. Extracellular Matrix in Kidney Fibrosis: More Than Just a Scaffold. *J Histochem Cytochem*. 2019;67(9):643-661. doi:10.1369/0022155419849388

159. Chen S, Birk DE. The regulatory roles of small leucine-rich proteoglycans in extracellular matrix assembly. *FEBS J*. 2013;280(10):2120-2137. doi:10.1111/febs.12136

160. Lin CHS, Chen J, Zhang Z, et al. Endostatin and transglutaminase 2 are involved in fibrosis of the aging kidney. *Kidney Int*. 2016;89(6):1281-1292. doi:10.1016/j.kint.2016.01.030

161. Eddy AA. Progression in Chronic Kidney Disease. *Adv Chronic Kidney Dis*. 2005;12(4):353-365. doi:10.1053/j.ackd.2005.07.011

162. Abo-Zenah H, Katsoudas S, de Takats D, et al. Early progressive interstitial fibrosis in human renal allografts. *Clin Nephrol*. 2002;57(1):9-18. doi:10.5414/cnp57009

163. Henderson NC, Arnold TD, Katamura Y, et al. Targeting of αv integrin identifies a core molecular pathway that regulates fibrosis in several organs. *Nat Med*. 2013;19(12):1617-1624. doi:10.1038/nm.3282

164. Chang Y, Lau WL, Jo H, et al. Pharmacologic Blockade of αvβ1 Integrin Ameliorates Renal Failure and Fibrosis In Vivo. *J Am Soc Nephrol*. 2017;28(7):1998-2005. doi:10.1681/ASN.2015050585

165. Poluzzi C, Nastase MV, Zeng-Brouwers J, et al. Biglycan evokes autophagy in macrophages via a novel CD44/Toll-like receptor 4 signaling axis in ischemia/reperfusion injury. *Kidney Int*. 2019;95(3):540-562. doi:10.1016/j.kint.2018.10.037

166. Goldfarb M, Rosenberger C, Abassi Z, et al. Acute-on-chronic renal failure in the rat: Functional compensation and hypoxia tolerance. *Am J Nephrol*. 2006;26(1):22-33. doi:10.1159/000091783

167. Kang D-H, Kanellis J, Hugo C, et al. Role of the microvascular endothelium in progressive renal disease. *J Am Soc Nephrol*. 2002;13(3):806-816.

168. Zhang P, Wu W, Chen Q, Chen M. Non-Coding RNAs and their Integrated Networks. *J Integr Bioinform*. 2019;16(3). doi:10.1515/jib-2019-0027

169. Eddy SR. Non-coding RNA genes and the modern RNA world. *Nat Rev Genet*. 2001;2(12):919-929. doi:10.1038/35103511

170. Uchida S, Adams JC. Physiological roles of non-coding RNAs. *Am J Physiol Physiol*. 2019;317(1):C1-C2. doi:10.1152/ajpcell.00114.2019

171. Schimmel P. RNA Processing and Modifications: The emerging complexity of the tRNA world: Mammalian tRNAs beyond protein synthesis. *Nat Rev Mol Cell Biol*. 2018;19(1):45-58. doi:10.1038/nrm.2017.77

172. Ma L, Bajic VB, Zhang Z. On the classification of long non-coding RNAs. *RNA Biol*. 2013;10(6):924-933. doi:10.4161/rna.24604

173. Kornienko AE, Guenzl PM, Barlow DP, Pauler FM. Gene regulation by the act of long non-coding RNA transcription. *BMC Biol*. 2013;11(1):59. doi:10.1186/1741-7007-11-59

174. Salzman J, Gawad C, Wang PL, Lacayo N, Brown PO. Circular RNAs are the predominant transcript isoform from hundreds of human genes in diverse cell types. Preiss T, ed. *PLoS One*. 2012;7(2):e30733. doi:10.1371/journal.pone.0030733

175. Salzman J. Circular RNA Expression: Its Potential Regulation and Function. *Trends Genet*. 2016;32(5):309-316. doi:10.1016/j.tig.2016.03.002

176. Sun X, Liu J, Xu C, Tang S-C, Ren H. The insights of Let-7 miRNAs in oncogenesis and stem cell potency. *J Cell Mol Med*. 2016;20(9):1779-1788. doi:10.1111/jcmm.12861

177. Kumar M, DeVaux RS, Herschkowitz JI. Molecular and Cellular Changes in Breast Cancer and New Roles of lncRNAs in Breast Cancer Initiation and Progression. In: *Progress in Molecular Biology and Translational Science*. Vol 144. ; 2016:563-586. doi:10.1016/bs.pmbts.2016.09.011

178. Ha M, Kim VN. Regulation of microRNA biogenesis. *Nat Rev Mol Cell Biol*. 2014;15(8):509-524. doi:10.1038/nrm3838

179. Nankivell BJ. microRNA in Transplantation. *Transplantation*. 2015;99(9):1. doi:10.1097/TP.0000000000000807

180. Fan PC, Chen CC, Chen YC, Chang YS, Chu PH. MicroRNAs in acute kidney injury. *Hum Genomics*. 2016;10(1):29. doi:10.1186/s40246-016-0085-z

181. Wei Q, Bhatt K, He HZ, Mi QS, Haase VH, Dong Z. Targeted Deletion of Dicer from Proximal Tubules Protects against Renal Ischemia-Reperfusion Injury. *J Am Soc Nephrol*. 2010;21(5):756-761. doi:10.1681/ASN.2009070718

182. Godwin JG, Ge X, Stephan K, Jurisch A, Tullius SG, Iacomini J. Identification of a microRNA signature of renal ischemia reperfusion injury. *Proc Natl Acad Sci U S A*. 2010;107(32):14339-14344. doi:10.1073/pnas.0912701107

183. Shapiro MD, Bagley J, Latz J, et al. Microrna expression data reveals a signature of kidney damage following Ischemia reperfusion injury. *PLoS One*. 2011;6(8). doi:10.1371/journal.pone.0023011

184. Banaei S. Novel role of microRNAs in renal ischemia reperfusion injury. *Ren Fail*. 2015;37(7):1073-1079. doi:10.3109/0886022X.2015.1055697

185. Ferenbach DA, Ramdas V, Spencer N, et al. Macrophages expressing heme oxygenase-1 improve renal function in ischemia/reperfusion injury. *Mol Ther*. 2010;18(9):1706-1713. doi:10.1038/mt.2010.100

186. Ferenbach DA, Nkejabega NCJ, McKay J, et al. The induction of macrophage hemeoxygenase-1 is protective during acute kidney injury in aging mice. *Kidney Int*. 2011;79(9):966-976. doi:10.1038/ki.2010.535

187. Lorenzen JM, Kaucsar T, Schauerte C, et al. MicroRNA-24 antagonism prevents renal ischemia reperfusion injury. *J Am Soc Nephrol*. 2014;25(12):2717-2729. doi:10.1681/ASN.2013121329

188. Lan Y-F, Chen H-H, Lai P-F, et al. MicroRNA-494 Reduces ATF3 Expression and Promotes AKI. *J Am Soc Nephrol*. 2012;23(12):2012-2023. doi:10.1681/ASN.2012050438

189. Xiaohong Wang, MD1,#, Xiaowei Zhang, PhD1,#, Xiao-Ping Ren, MD1, Jing Chen, PhD2, Hongzhu Liu, MD3, Junqi Yang, MD, PhD3, Mario Medvedovic, PhD2, Zhuowei Hu, PhD4, and Guo-Chang Fan P. MicroRNA-494 Targeting both Pro-apoptotic and Anti-apoptotic Proteins Protects against Ischemia/Reperfusion-Induced Cardiac Injury. *Circulation*. 2010;122(13):1308-1318. doi:doi:10.1161/CIRCULATIONAHA.

190. Khalid U, Newbury LJ, Simpson K, et al. A urinary microRNA panel that is an early predictive biomarker of delayed graft function following kidney transplantation. *Sci Rep*. 2019;9(1):1-11. doi:10.1038/s41598-019-38642-3

191. Wilflingseder J, Reindl-schwaighofer R, Sunzenauer J. MicroRNAs in Kidney Transplantation. *Nephrol Dial Transplant*. 2015;30(6):910-917. doi:10.1093/ndt/gfu280.microRNAs

192. Wilflingseder J, Jelencsics K, Bergmeister H, et al. miR-182-5p Inhibition Ameliorates Ischemic Acute Kidney Injury. *Am J Pathol*. 2017;187(1):70-79. doi:10.1016/j.ajpath.2016.09.011

193. Lorenzen JM, Volkmann I, Fiedler J, et al. Urinary miR-210 as a Mediator of Acute T-Cell Mediated Rejection in Renal Allograft Recipients. *Am J Transplant*. 2011;11(10):2221-2227. doi:10.1111/j.1600-6143.2011.03679.x

194. Anglicheau D, Sharma VK, Ding R, et al. MicroRNA expression profiles predictive of human renal allograft status. *Proc Natl Acad Sci*. 2009;106(13):5330-5335. doi:10.1073/pnas.0813121106

195. Sui W, Dai Y, Huang Y, Lan H, Yan Q, Huang H. Microarray analysis of MicroRNA expression in acute rejection after renal transplantation. *Transpl Immunol*. 2008;19(1):81-85. doi:10.1016/j.trim.2008.01.007

196. Wilflingseder J, Regele H, Perco P, et al. MiRNA profiling discriminates types of rejection and injury in human renal allografts. *Transplantation*. 2013;95(6):835-841. doi:10.1097/TP.0b013e318280b385

197. Ledeganck KJ, Gielis EM, Abramowicz D, Van Craenenbroeck AH, Stenvinkel P, Shiels PG. MicroRNAs in AKI and kidney transplantation. *Clin J Am Soc Nephrol*. 2019;14(3):454-468. doi:10.2215/CJN.08020718

198. Scian MJ, Maluf DG, David KG, et al. MicroRNA profiles in allograft tissues and paired urines associate with chronic allograft dysfunction with IF/TA. *Am J Transplant*. 2011;11(10):2110-2122. doi:10.1111/j.1600-6143.2011.03666.x

199. Scian MJM. MicroRNA profiles in allograft tissues and paired urines associate with chronic allograft dysfunction with IF/TA. *Am J Transplant*. 2011;11(10):2110-2122. doi:doi:10.1111/j.1600-6143.2011.03666.x

200. Ben-Dov I, Muthukumar T, Morozov P. MicroRNA sequence profiles of human kidney allogarft with or without tubulointerstitial fibrosis. *Transplantation*. 2012;94(11). doi:10.1097/TP.0b013e3182751efd.MicroRNA

201. Glowacki F, Savary G, Gnemmi V, et al. Increased Circulating miR-21 Levels Are Associated with Kidney Fibrosis. *PLoS One*. 2013;8(2):1-11. doi:10.1371/journal.pone.0058014

202. Schauerte C, Hübner A, Rong S, et al. Antagonism of profibrotic microRNA-21 improves outcome of murine chronic renal allograft dysfunction. *Kidney Int*. 2017;92(3):646-656. doi:10.1016/j.kint.2017.02.012

203. Loebel DAFF, Tsoi B, Wong N, Tam PPLL. A conserved noncoding intronic transcript at the mouse Dnm3 locus. *Genomics*. 2005;85(6):782-789. doi:10.1016/j.ygeno.2005.02.001

204. Watanabe T, Sato T, Amano T, et al. Dnm3os, a non-coding RNA, is required for normal growth and skeletal development in mice. *Dev Dyn*. 2008;237(12):3738-3748. doi:10.1002/dvdy.21787

205. Lee YB, Bantounas I, Lee DY, Phylactou L, Caldwell MA, Uney JB. Twist-1 regulates the miR-199a/214 cluster during development. *Nucleic Acids Res*. 2009;37(1):123-128. doi:10.1093/nar/gkn920

206. Polytarchou C, Hommes DW, Palumbo T, et al. MicroRNA214 Is Associated With Progression of Ulcerative Colitis, and Inhibition Reduces Development of Colitis and Colitis-Associated Cancer in Mice. *Gastroenterology*. 2015;149(4):981-992. doi:10.1053/j.gastro.2015.05.057

207. Che M, Shi T, Feng S, et al. The MicroRNA-199a/214 Cluster Targets E-Cadherin and Claudin-2 and Promotes High Glucose-Induced Peritoneal Fibrosis. *J Am Soc Nephrol*. 2017;28(8):2459-2471. doi:10.1681/ASN.2016060663

208. Wang X, Guo B, Li Q, et al. MiR-214 targets ATF4 to inhibit bone formation. *Nat Med*. 2013;19(1):93-100. doi:10.1038/nm.3026

209. Roberto VP, Gavaia P, Nunes MJ, Rodrigues E, Cancela ML, Tiago DM. Evidences for a New Role of miR-214 in Chondrogenesis. *Sci Rep*. 2018;8(1):3704. doi:10.1038/s41598-018-21735-w

210. Li L-M, Hou D-X, Guo Y-L, et al. Role of microRNA-214-targeting phosphatase and tensin homolog in advanced glycation end product-induced apoptosis delay in monocytes. *J Immunol*. 2011;186:2552-2560. doi:10.4049/jimmunol.1001633

211. Zhao L, Liu YW, Yang T, et al. The mutual regulation between miR-214 and A2AR signaling plays an important role in inflammatory response. *Cell Signal*. 2015;27(10):2026-2034. doi:10.1016/j.cellsig.2015.07.007

212. Lakhia R, Yheskel M, Flaten A, et al. Interstitial microRNA miR-214 attenuates inflammation and polycystic kidney disease progression. *JCI Insight*. 2020;5(7). doi:10.1172/jci.insight.133785

213. Cobb BS, Hertweck A, Smith J, et al. A role for Dicer in immune regulation. *J Exp Med*. 2006;203(11):2519-2527. doi:10.1084/jem.20061692

214. Zhou X, Jeker LT, Fife BT, et al. Selective miRNA disruption in T reg cells leads to uncontrolled autoimmunity. *J Exp Med*. 2008;205(9):1983-1991. doi:10.1084/jem.20080707

215. Jindra PT, Bagley J, Godwin JG, Iacomini J. Costimulation-Dependent Expression of MicroRNA-214 Increases the Ability of T Cells To Proliferate by Targeting Pten. *J Immunol*. 2010;185(2):990-997. doi:10.4049/jimmunol.1000793

216. Chen L, Ma H, Hu H, et al. Special role of Foxp3 for the specifically altered microRNAs in Regulatory T cells of HCC patients. *BMC Cancer*. 2014;14(1):1-10. doi:10.1186/1471-2407-14-489

217. Yin Y, Cai X, Chen X, et al. Tumor-secreted miR-214 induces regulatory T cells: a major link between immune evasion and tumor growth. *Nat Publ Gr*. 2014;24:1164-1180. doi:10.1038/cr.2014.121

218. Buckler JL, Liu X, Turka LA. Regulation of T-cell responses by PTEN. *Immunol Rev*. 2008;224(1):239-248. doi:10.1111/j.1600-065X.2008.00650.x

219. Junker A, Krumbholz M, Eisele S, et al. MicroRNA profiling of multiple sclerosis lesions identifies modulators of the regulatory protein CD47. *Brain*. 2009;132(12):3342-3352. doi:10.1093/brain/awp300

220. Qiu YY, Zhang YW, Qian XF, Bian T. MiR-371, miR-138, miR-544, miR-145,

and miR-214 could modulate Th1/Th2 balance in asthma through the combinatorial regulation of Runx3. *Am J Transl Res*. 2017;9(7):3184-3199.

221. Wong WF, Kohu K, Chiba T, Sato T, Satake M. Interplay of transcription factors in T-cell differentiation and function: The role of Runx. *Immunology*. 2011;132(2):157-164. doi:10.1111/j.1365-2567.2010.03381.x

222. Denby L, Ramdas V, McBride MW, et al. MiR-21 and miR-214 are consistently modulated during renal injury in rodent models. *Am J Pathol*. 2011;179(2):661-672. doi:10.1016/j.ajpath.2011.04.021

223. Denby L, Ramdas V, Lu R, et al. MicroRNA-214 Antagonism Protects against Renal Fibrosis. *J Am Soc Nephrol*. 2014;25(1):65-80. doi:10.1681/ASN.2013010072

224. Liu M, Liu L, Bai M, et al. Hypoxia-induced activation of Twist/miR-214/E-cadherin axis promotes renal tubular epithelial cell mesenchymal transition and renal fibrosis. *Biochem Biophys Res Commun*. 2018;495(3):2324-2330. doi:10.1016/j.bbrc.2017.12.130

225. Bai M, Chen H, Ding D, et al. MicroRNA-214 promotes chronic kidney disease by disrupting mitochondrial oxidative phosphorylation. *Kidney Int*. 2019;95(6):1389-1404. doi:10.1016/j.kint.2018.12.028

226. Wang X, Shen E, Wang Y, et al. Cross talk between miR-214 and PTEN attenuates glomerular hypertrophy under diabetic conditions. *Sci Rep*. 2016;6(1):31506. doi:10.1038/srep31506

227. Liu Y, Usa K, Wang F, et al. MicroRNA-214-3p in the kidney contributes to the development of hypertension. *J Am Soc Nephrol*. 2018;29(10):2518-2528. doi:10.1681/ASN.2018020117

228. Schwartzbauer G, Robbins J. The Tumor Suppressor Gene *PTEN* Can Regulate Cardiac Hypertrophy and Survival. *J Biol Chem*. 2001;276(38):35786-35793. doi:10.1074/jbc.M102479200

229. Wijesekara N, Konrad D, Eweida M, et al. Muscle-Specific Pten Deletion Protects against Insulin Resistance and Diabetes. *Mol Cell Biol*. 2005;25(3):1135-1145. doi:10.1128/MCB.25.3.1135-1145.2005

230. Zhu X, Li W, Li H. miR-214 ameliorates acute kidney injury via targeting DKK3 and activating of Wnt/ β-catenin signaling pathway. *Biol Res*. 2018;51(1):1-10. doi:10.1186/s40659-018-0179-2

231. Savary G, Dewaeles E, Diazzi S, et al. The Long Non-Coding RNA DNM3OS is a Reservoir of FibromiRs with Major Functions in Lung Fibroblast Response to TGF-β and Pulmonary Fibrosis. *Am J Respir Crit Care Med*. 2019;200:rccm.201807-1237OC. doi:10.1164/rccm.201807-1237OC

232. Hennino MF, Buob D, Van Der Hauwaert C, et al. MiR-21-5p renal expression is associated with fibrosis and renal survival in patients with IgA nephropathy. *Sci Rep*. 2016;6:1-9. doi:10.1038/srep27209

233. Aurora AB, Mahmoud AI, Luo X, et al. MicroRNA-214 protects the mouse heart from ischemic injury by controlling Ca 2+ overload and cell death. *J Clin Invest*. 2012;122(4):1222-1232. doi:10.1172/JCI59327

234. Stevens HC, Deng L, Grant JS, et al. Regulation and Function of miR-214 in Pulmonary Arterial Hypertension. *Pulm Circ*. 2016;6(1):109-117. doi:10.1086/685079

235. van Rooij E, Sutherland LB, Liu N, et al. A signature pattern of stress-responsive microRNAs that can evoke cardiac hypertrophy and heart failure. *Proc Natl Acad Sci U S A*. 2006;103(48):18255-18260. doi:10.1073/pnas.0608791103

236. Reddy S, Zhao M, Hu D-Q, et al. Dynamic microRNA expression during the transition from right ventricular hypertrophy to failure. *Physiol Genomics*. 2012;44(10):562-575. doi:10.1152/physiolgenomics.00163.2011

237. El Azzouzi H, Leptidis S, Dirkx E, et al. The Hypoxia-Inducible MicroRNA Cluster miR-199a~214 targets myocardial PPARδ and impairs mitochondrial fatty acid oxidation. *Cell Metab*. 2013;18(3):341-354. doi:10.1016/j.cmet.2013.08.009

238. SHOSKES DA, PARFREY NA, HALLORAN PF. INCREASED MAJOR HISTOCOMPATIBILITY COMPLEX ANTIGEN EXPRESSION IN UNILATERAL ISCHEMIC ACUTE TUBULAR NECROSIS IN THE MOUSE. *Transplantation*. 1990;49(1):201-207. doi:10.1097/00007890-199001000-00045

239. Hesketh EE, Czopek A, Clay M, et al. Renal Ischaemia Reperfusion Injury: A Mouse Model of Injury and Regeneration. *J Vis Exp*. 2014;(88):1-8. doi:10.3791/51816

240. Jablonski P, Howden BO, Rae DA, Birrell CS, Marshall VC, Tange J. An experimental model for assessment of renal recovery from warm ischemia. *Transplantation*. 1983;35(3):198-204. doi:10.1097/00007890-198303000-00002

241. Wei Q, Dong Z. Mouse model of ischemic acute kidney injury: technical notes and tricks. *Am J Physiol Physiol*. 2012;303(11):F1487-F1494. doi:10.1152/ajprenal.00352.2012

242. Delbridge MS, Shrestha BM, Raftery AT, El Nahas AM, Haylor JL. The Effect of Body Temperature in a Rat Model of Renal Ischemia-Reperfusion Injury. *Transplant Proc*. 2007;39(10):2983-2985. doi:10.1016/j.transproceed.2007.04.028

243. Skrypnyk NI, Harris RC, de Caestecker MP. Ischemia-reperfusion model of acute kidney injury and post injury fibrosis in mice. *J Vis Exp*. 2013;(78). doi:10.3791/50495

244. Spurgeon-Pechman KR, Donohoe DL, Mattson DL, Lund H, James L, Basile DP. Recovery from acute renal failure predisposes hypertension and secondary renal disease in response to elevated sodium. *Am J Physiol Physiol*.

2007;293(1):F269-F278. doi:10.1152/ajprenal.00279.2006

245. KOLETSKY S. Effects of temporary interruption of renal circulation in rats. *AMA Arch Pathol*. 1954;58(6):592-603. http://www.ncbi.nlm.nih.gov/pubmed/13217575.

246. Finn WF, Chevalier RL. *Recovery from Postischemic Acute Renal Failure in the Rat*. Vol 16.; 1979. doi:10.1038/ki.1979.112

247. Finn WF. *Enhanced Recovery from Postischemic Acute Renal Failure Micropuncture Studies in the Rat*. Vol 46.; 1980. http://ahajournals.org. Accessed August 15, 2019.

248. Eisenbach GM, Steinhausen M. *Micropuncture Studies after Temporary Ischemia of Rat Kidneys**. Vol 343. Springer-Verlag; 1973. https://link.springer.com/content/pdf/10.1007%2FBF00586571.pdf. Accessed August 15, 2019.

249. Zager RA, Johnson ACM, Becker K. Acute unilateral ischemic renal injury induces progressive renal inflammation, lipid accumulation, histone modification, and "end-stage" kidney disease. *Am J Physiol Ren Physiol*. 2011;301:1334-1345. doi:10.1152/ajprenal.00431.2011.-There

250. Le Clef N, Verhulst A, D'haese PC, et al. Unilateral Renal Ischemia-Reperfusion as a Robust Model for Acute to Chronic Kidney Injury in Mice. Chatziantoniou C, ed. *PLoS One*. 2016;11(3):e0152153. doi:10.1371/journal.pone.0152153

251. Hueper K, Schmidbauer M, Thorenz A, et al. Longitudinal evaluation of perfusion changes in acute and chronic renal allograft rejection using arterial spin labeling in translational mouse models. *J Magn Reson Imaging*. 2017;46(6):1664-1672. doi:10.1002/jmri.25713

252. Hueper K, Peperhove M, Rong S, et al. T1-mapping for assessment of ischemia-induced acute kidney injury and prediction of chronic kidney disease in mice. *Eur Radiol*. 2014;24(9):2252-2260. doi:10.1007/s00330-014-3250-6

253. Hueper K, Rong S, Gutberlet M, et al. T2 Relaxation Time and Apparent Diffusion Coefficient for Noninvasive Assessment of Renal Pathology After Acute Kidney Injury in Mice. *Invest Radiol*. 2013;48(12):834-842. doi:10.1097/RLI.0b013e31829d0414

254. Ferenbach DA, Ramdas V, Spencer N, et al. Macrophages Expressing Heme Oxygenase-1 Improve Renal Function in Ischemia/Reperfusion Injury. *Mol Ther*. 2010;18(9):1706-1713. doi:10.1038/mt.2010.100

255. Fernandez-Repollet, E. and WFF. Effect of contralateral nephrectomy on the initial phase of postischemic acute renal failure. *Acute Ren Fail*. 1982:262-266.

256. Paula Jablonski, B. Howden, D. Rae, G. Rigol, C. Birrell, V. Marshall, J. Tange. The influence of the contralateral kidney upon recovery from unilateral warm renal ischemia. *Pathology*. 1985;17(4):623-627. doi:doi.org/10.3109/00313028509084764.

257. Fried TA, Hishida A, Barnes JL, Stein JH. Ischemic acute renal failure in the rat: Protective effect of uninephrectomy. *Am J Physiol - Ren Fluid Electrolyte Physiol*. 1984;16(4). doi:10.1152/ajprenal.1984.247.4.f568

258. Krohn AG, Peng BBK, Antell HI, Stein S, Waterhouse K. Compensatory Renal Hypertrophy: The Role of Immediate Vascular Changes in its Production. *J Urol*. 1970;103(5):564-568. doi:10.1016/S0022-5347(17)62003-2

259. Kato A, Hishida A, Nakajima T. Role of thromboxane A2 and prostacyclin in uninephrectomy-induced attenuation of ischemic renal injury. *Kidney Int*. 1995;48(5):1577-1583. doi:10.1038/ki.1995.450

260. Kato A, Hishida A, Tanaka I, Komatsu K. Unmephrectomy Prevents the Ischemia-Induced Increase in Renin Activity. *Nephron*. 1997;75(1):72-76. doi:10.1159/000189502

261. Nakajima T, Miyaji T, Kato A, Ikegaya N, Yamamoto T, Hishida A. Uninephrectomy reduces apoptotic cell death and enhances renal tubular cell regeneration in ischemic ARF in rats. *Am J Physiol Physiol*. 1996;271(4):F846-F853. doi:10.1152/ajprenal.1996.271.4.F846

262. Fong D, Denton KM, Moritz KM, Evans R, Singh RR. Compensatory responses to nephron deficiency: Adaptive or maladaptive? *Nephrology*. 2014;19(3):119-128. doi:10.1111/nep.12198

263. Hauser P, Kainz A, Perco P, et al. Transcriptional response in the unaffected kidney after contralateral hydronephrosis or nephrectomy. *Kidney Int*. 2005;68(6):2497-2507. doi:10.1111/J.1523-1755.2005.00725.X

264. FAGIN JA, MELMED S. Relative Increase in Insulin-Like Growth Factor I Messenger Ribonucleic Acid Levels in Compensatory Renal Hypertrophy*. *Endocrinology*. 1987;120(2):718-724. doi:10.1210/endo-120-2-718

265. Flyvbjerg A, Bennett WF, Rasch R, et al. Compensatory renal growth in uninephrectomized adult mice is growth hormone dependent. *Kidney Int*. 1999;56(6):2048-2054. doi:10.1046/j.1523-1755.1999.00776.x

266. Cingel-Ristić V, Flyvbjerg A, Drop SLS. The physiological and pathophysiological roles of the GH/IGF-axis in the kidney: Lessons from experimental rodent models. *Growth Horm IGF Res*. 2004;14(6):418-430. doi:10.1016/j.ghir.2004.06.003

267. Kierulf-Lassen C, Nielsen PM, Qi H, et al. Unilateral nephrectomy diminishes ischemic acute kidney injury through enhanced perfusion and reduced pro-inflammatory and pro-fibrotic responses. Joles JA, ed. *PLoS One*. 2017;12(12):e0190009. doi:10.1371/journal.pone.0190009

268. De Rosa S, Antonelli M, Ronco C. Hypothermia and kidney: A focus on ischaemia-reperfusion injury. *Nephrol Dial Transplant*. 2017;32(2):241-247. doi:10.1093/ndt/gfw038

269. Lee CY, Mangino MJ. Preservation methods for kidney and liver. *Organogenesis*. 2009;5(3):105-112. doi:10.4161/org.5.3.9582

270. Carattino MD, Cueva F, Zuccollo A, Monti JL, Navarro M, Catanzaro OL. Renal ischemia-induced increase in vascular permeability is limited by hypothermia. *Immunopharmacology*. 1999;43(2-3):241-248. doi:10.1016/S0162-3109(99)00095-8

271. Santos EB dos, Koff WJ, Grezzana Filho T de JM, et al. Oxidative stress evaluation of ischemia and reperfusion in kidneys under various degrees of hypothermia in rats. *Acta Cir Bras*. 2013;28(8):568-573. doi:10.1590/S0102-86502013000800003

272. Laing RW, Mergental H, Yap C, et al. Viability testing and transplantation of marginal livers (VITTAL) using normothermic machine perfusion: Study protocol for an open-label, non-randomised, prospective, single-arm trial. *BMJ Open*. 2017;7(11). doi:10.1136/bmjopen-2017-017733

273. Nasralla D, Coussios CC, Mergental H, et al. A randomized trial of normothermic preservation in liver transplantation. *Nature*. 2018;557(7703):50-56. doi:10.1038/s41586-018-0047-9

274. Jayant K, Reccia I, Virdis F, Shapiro AMJ. The Role of Normothermic Perfusion in Liver Transplantation (TRaNsIT Study): A Systematic Review of Preliminary Studies. *HPB Surg*. 2018;2018:1-14. doi:10.1155/2018/6360423

275. Watson CJE, Hunt F, Messer S, et al. In situ normothermic perfusion of livers in controlled circulatory death donation may prevent ischemic cholangiopathy and improve graft survival. *Am J Transplant*. 2019;19(6):1745-1758. doi:10.1111/ajt.15241

276. Zager RA, Altschuld R. Body temperature: an important determinant of severity of ischemic renal injury. *Am J Physiol Physiol*. 1986;251(1):F87-F93. doi:10.1152/ajprenal.1986.251.1.F87

277. Zager RA, Gmur DJ, Bredl CR, Eng MJ. Degree and time sequence of hypothermic protection against experimental ischemic acute renal failure. *Circ Res*. 1989;65(5):1263-1269. doi:10.1161/01.RES.65.5.1263

278. Zager RA, Gmur DJ, Bredl CR, Eng MJ. Temperature effects on ischemic and hypoxic renal proximal tubular injury. *Lab Invest*. 1991;64(6):766-776. http://www.ncbi.nlm.nih.gov/pubmed/2046328.

279. del Moral RMG, Gómez-Morales M, Hernández-Cortés P, et al. PARP Inhibition Attenuates Histopathological Lesion in Ischemia/Reperfusion Renal Mouse Model after Cold Prolonged Ischemia. *Sci World J*. 2013;2013:1-8. doi:10.1155/2013/486574

280. Tse GH, Heskth EE, Clay M, Borthwick G, Hughes J, Marson LP. Mouse kidney transplantation: Models of allograft rejection. *J Vis Exp*. 2014;(92):e52163. doi:10.3791/52163

281. Win TS, Rehakova S, Negus MC, et al. Donor CD4 T Cells Contribute to Cardiac Allograft Vasculopathy by Providing Help for Autoantibody Production. *Circ Hear Fail*. 2009;2(4):361-369. doi:10.1161/CIRCHEARTFAILURE.108.827139

282. Dang Z, MacKinnon A, Marson LP, Sethi T. Tubular atrophy and interstitial fibrosis after renal transplantation is dependent on galectin-3. *Transplantation*. 2012;93(5):477-484. doi:10.1097/TP.0b013e318242f40a

283. Skoskiewicz M, Chase C, Winn HJ, Russell PS. Kidney transplants between mice of graded immunogenetic diversity. *Transplant Proc*. 1973;5(1):721-725. http://www.ncbi.nlm.nih.gov/pubmed/4121181. Accessed May 12, 2019.

284. Tse GH, Hughes J, Marson LP. Systematic review of mouse kidney transplantation. *Transpl Int*. 2013;26(12):1149-1160. doi:10.1111/tri.12129

285. Martins PN. Learning curve, surgical results and operative complications for kidney transplantation in mice. *Microsurgery*. 2006;26(8):590-593. doi:10.1002/micr.20292

286. Zarjou A, Guo L, Sanders PW, Mannon RB, Agarwal A, George JF. A reproducible mouse model of chronic allograft nephropathy with vasculopathy. *Kidney Int*. 2012;82(11):1231-1235. doi:10.1038/ki.2012.277

287. Schumacher M, Van Vliet BN, Ferrari P. Kidney transplantation in rats: An appraisal of surgical techniques and outcome. *Microsurgery*. 2003;23(4):387-394. doi:10.1002/micr.10139

288. Karatzas T, Santiago S, Xanthos T, De Faria W, Gandia C, Kostakis A. An easy and safe model of kidney transplantation in rats. *Microsurgery*. 2007;27(8):668-672. doi:10.1002/micr.20429

289. Black LM, Lever JM, Agarwal A. Renal Inflammation and Fibrosis: A Double-edged Sword. *J Histochem Cytochem*. 2019;67(9):663-681. doi:10.1369/0022155419852932

290. Fine LG, Norman JT. Chronic hypoxia as a mechanism of progression of chronic kidney diseases: From hypothesis to novel therapeutics. *Kidney Int*. 2008;74(7):867-872. doi:10.1038/ki.2008.350

291. Mimura I, Nangaku M. The suffocating kidney: Tubulointerstitial hypoxia in end-stage renal disease. *Nat Rev Nephrol*. 2010;6(11):667-678. doi:10.1038/nrneph.2010.124

292. Havasi A, Borkan SC. Apoptosis and acute kidney injury. *Kidney Int*. 2011;80(1):29-40. doi:10.1038/ki.2011.120

293. Chau BN, Xin C, Hartner J, et al. MicroRNA-21 promotes fibrosis of the kidney by silencing metabolic pathways. *Sci Transl Med*. 2012;4(121). doi:10.1126/scitranslmed.3003205

294. Hultström M, Becirovic-Agic M, Jönsson S. Comparison of acute kidney injury of different etiology reveals in-common mechanisms of tissue damage. *Physiol Genomics*. 2018;50(3):127-141. doi:10.1152/physiolgenomics.00037.2017

295. Regner KR, Roman RJ. ROLE OF MEDULLARY BLOOD FLOW IN THE PATHOGENESIS OF RENAL ISCHEMIA-REPERFUSION INJURY. doi:10.1097/MNH.0b013e32834d085a

296. Ichimura T, Bonventre J V, Bailly V, et al. Kidney injury molecule-1 (KIM-1), a putative epithelial cell adhesion molecule containing a novel immunoglobulin domain, is up-regulated in renal cells after injury. *J Biol Chem*. 1998;273(7):4135-4142. doi:10.1074/jbc.273.7.4135

297. Van Timmeren MM, Vaidya VS, Van Ree RM, et al. High urinary excretion of kidney injury molecule-1 is an independent predictor of graft loss in renal transplant recipients. *Transplantation*. 2007;84(12):1625-1630. doi:10.1097/01.tp.0000295982.78039.ef

298. van Timmeren MM, van den Heuvel MC, Bailly V, Bakker SJL, van Goor H, Stegeman CA. Tubular kidney injury molecule-1 (KIM-1) in human renal disease. *J Pathol*. 2007;212(2):209-217. doi:10.1002/path.2175

299. Waanders F, Van Timmeren MM, Stegeman CA, Bakker SJL, Van Goor H. Kidney injury molecule-1 in renal disease. *J Pathol*. 2010;220(1):7-16. doi:10.1002/path.2642

300. Yin C, Wang N. Kidney injury molecule-1 in kidney disease. *Ren Fail*. 2016;38(10):1567-1573. doi:10.1080/0886022X.2016.1193816

301. Humphreys BD, Xu F, Sabbisetti V, et al. Chronic epithelial kidney injury molecule-1 expression causes murine kidney fibrosis. *J Clin Invest*. 2013;123(9):4023-4035. doi:10.1172/JCI45361

302. Rabb H, Griffin MD, McKay DiB, et al. Inflammation in AKI: Current understanding, key questions, and knowledge gaps. *J Am Soc Nephrol*. 2016;27(2):371-379. doi:10.1681/ASN.2015030261

303. Stroo I, Stokman G, Teske GJD, et al. Chemokine expression in renal ischemia/reperfusion injury is most profound during the reparative phase. *Int Immunol*. 2010;22(6):433-442. doi:10.1093/intimm/dxq025

304. Zager RA. Progression from acute kidney injury to chronic kidney disease: Clinical and experimental insights and queries. In: *Nephron - Clinical Practice*. Vol 127. ; 2014:46-50. doi:10.1159/000363726

305. Chung ACKK, Lan HY. MicroRNAs in renal fibrosis. *Front Physiol*. 2015;6(FEB):1-9. doi:10.3389/fphys.2015.00050

306. Petrillo F, Iervolino A, Zacchia M, et al. MicroRNAs in Renal Diseases: A Potential Novel Therapeutic Target. *Kidney Dis*. 2017;3(3):111-119. doi:10.1159/000481730

307. Wang B, Komers R, Carew R, et al. Suppression of microRNA-29 expression by TGF-β1 promotes collagen expression and renal fibrosis. *J Am Soc Nephrol*. 2012;23(2):252-265. doi:10.1681/ASN.2011010055

308. Wang G, Kwan BCH, Lai FMM, Chow KM, Li PKT, Szeto CC. Urinary miR-21, miR-29, and miR-93: Novel biomarkers of fibrosis. *Am J Nephrol*. 2012;36(5):412-418. doi:10.1159/000343452

309. Chen HY, Zhong X, Huang XR, et al. MicroRNA-29b inhibits diabetic

nephropathy in db/db mice. *Mol Ther*. 2014;22(4):842-853. doi:10.1038/mt.2013.235

310. Denby L, Ramdas V, Lu R, et al. MicroRNA-214 Antagonism Protects against Renal Fibrosis. *J Am Soc Nephrol*. 2014;25(1):65-80. doi:10.1681/ASN.2013010072

311. Ahmadian-Elmi M, Bidmeshki Pour A, Naghavian R, et al. miR-27a and miR-214 exert opposite regulatory roles in Th17 differentiation via mediating different signaling pathways in peripheral blood CD4+ T lymphocytes of patients with relapsing–remitting multiple sclerosis. *Immunogenetics*. 2016;68(1):43-54. doi:10.1007/s00251-015-0881-y

312. Nosalski R, Siedlinski M, Denby L, et al. T-cell-derived miRNA-214 mediates perivascular fibrosis in hypertension. *Circ Res*. 2020;44(0):988-1003. doi:10.1161/CIRCRESAHA.119.315428

313. Kinsey GR, Okusa MD. Expanding role of T cells in acute kidney injury. *Curr Opin Nephrol Hypertens*. 2014;23(1):9-16. doi:10.1097/01.mnh.0000436695.29173.de

314. Kumar S, Liu J, McMahon AP. Defining the acute kidney injury and repair transcriptome. *Semin Nephrol*. 2014;34(4):404-417. doi:10.1016/j.semnephrol.2014.06.007

315. Chuang T-D, Pearce WJ, Khorram O. miR-29c induction contributes to downregulation of vascular extracellular matrix proteins by glucocorticoids. *Am J Physiol Physiol*. 2015;309(2):C117-C125. doi:10.1152/ajpcell.00254.2014

316. Liu J, Kumar S, Dolzhenko E, et al. Molecular characterization of the transition from acute to chronic kidney injury following ischemia/reperfusion. *JCI insight*. 2017;2(18). doi:10.1172/jci.insight.94716

317. Riss J, Khanna C, Koo S, et al. Cancers as wounds that do not heal: Differences and similarities between renal regeneration/repair and renal cell carcinoma. *Cancer Res*. 2006;66(14):7216-7224. doi:10.1158/0008-5472.CAN-06-0040

318. Ko GJ, Boo CS, Jo SK, Cho WY, Kim HK. Macrophages contribute to the development of renal fibrosis following ischaemia/reperfusion-induced acute kidney injury. *Nephrol Dial Transplant*. 2008;23(3):842-852. doi:10.1093/ndt/gfm694

319. Johnson TS, Haylor JL, Thomas GL, Fisher M, El Nahas AM. Matrix Metalloproteinases and Their Inhibitions in Experimental Renal Scarring. *Nephron Exp Nephrol*. 2002;10(3):182-195. doi:10.1159/000058345

320. Boor P, Floege J. Comprehensive Review Renal Allograft Fibrosis: Biology and Therapeutic Targets. 2015. doi:10.1111/ajt.13180

321. Rice JC, Spence JS, Yetman DL, Safirstein RL. Monocyte chemoattractant protein-1 expression correlates with monocyte infiltration in the post-ischemic kidney. *Ren Fail*. 2002;24(6):703-723. doi:10.1081/JDI-120015673

322. Segerer S, Nelson PJ, Schlöndorff D. Chemokines, chemokine receptors, and renal disease: From basic science to pathophysiologic and therapeutic studies. *J Am Soc Nephrol*. 2000;11(1):152-176.

323. Anders HJ, Vielhauer V, Schlöndorff D. Chemokines and chemokine receptors are involved in the resolution or progression of renal disease. *Kidney Int*. 2003;63(2):401-415. doi:10.1046/j.1523-1755.2003.00750.x

324. Lai KN, Leung JCK, Chan LYY, Guo H, Tang SCW. Interaction between proximal tubular epithelial cells and infiltrating monocytes/T cells in the proteinuric state. *Kidney Int*. 2007;71(6):526-538. doi:10.1038/sj.ki.5002091

325. Furuichi K, Wada T, Iwata Y, et al. CCR2 signaling contributes to ischemia-reperfusion injury in kidney. *J Am Soc Nephrol*. 2003;14(10):2503-2515. doi:10.1097/01.ASN.0000089563.63641.A8

326. Furuichi K, Wada T, Iwata Y, et al. Gene therapy expressing amino-terminal truncated monocyte chemoattractant protein-1 prevents renal ischemia-reperfusion injury. *J Am Soc Nephrol*. 2003;14(4):1066-1071. doi:10.1097/01.ASN.0000059339.14780.E4

327. Kielar ML, John R, Bennett M, et al. Maladaptive Role of IL-6 in Ischemic Acute Renal Failure Materials and Methods Animals and Surgical Protocols. *J Am Soc Nephrol*. 2005;16:3315-3325. doi:10.1681/ASN.2003090757

328. Ranganathan P, Jayakumar C, Ramesh G. Proximal tubule-specific overexpression of netrin-1 suppresses acute kidney injury-induced interstitial fibrosis and glomerulosclerosis through suppression of IL-6/STAT3 signaling. *Am J Physiol Physiol*. 2013;304(8):F1054-F1065. doi:10.1152/ajprenal.00650.2012

329. Su H, Lei CT, Zhang C. Interleukin-6 signaling pathway and its role in kidney disease: An update. *Front Immunol*. 2017;8(APR). doi:10.3389/fimmu.2017.00405

330. Saraiva M, O'Garra A. The regulation of IL-10 production by immune cells. *Nat Rev Immunol*. 2010;10(3):170-181. doi:10.1038/nri2711

331. Singh P, Castillo A, Majid DSA. Decrease in IL-10 and increase in TNF- α levels in renal tissues during systemic inhibition of nitric oxide in anesthetized mice. *Physiol Rep*. 2014;2(2):e00228. doi:10.1002/phy2.228

332. Wang X, Shen E, Wang Y, et al. Cross talk between miR-214 and PTEN attenuates glomerular hypertrophy under diabetic conditions. *Nat Sci Reports*. 2016;6(August):31506. doi:10.1038/srep31506

333. Baumjohann D, Mark Ansel K. MicroRNA Regulation of T Helper Cell Differentiation and Plasticity. doi:10.1038/nri3494

334. Griffiths C, Scott WE, Ali S, Fisher AJ. Maximizing organs for donation: the potential for ex situ normothermic machine perfusion. *QJM An Int J Med*. 2020;(October 2019):1-6. doi:10.1093/qjmed/hcz321

335. Hameed AM, Lu DB, Burns H, et al. Pharmacologic targeting of renal ischemia-reperfusion injury using a normothermic machine perfusion platform. *Sci Rep*. 2020;10(1):6930. doi:10.1038/s41598-020-63687-0

336. Tietjen GT, Hosgood SA, DiRito J, et al. Nanoparticle targeting to the endothelium during normothermic machine perfusion of human kidneys. *Sci Transl Med*. 2017;9(418):eaam6764. doi:10.1126/scitranslmed.aam6764

337. Sewpaul A, Figueiredo RS, Bates L, et al. Modifying Renal Gene Expression by Anti-Sense Oligonucleotide Delivery during Normothermic Machine Perfusion. *Transplantation*. 2018;102:S728. doi:10.1097/01.tp.0000543708.68424.93

338. Gansevoort RT, Correa-Rotter R, Hemmelgarn BR, et al. Chronic kidney disease and cardiovascular risk: epidemiology, mechanisms, and prevention. *Lancet*. 2013;382(9889):339-352. doi:10.1016/S0140-6736(13)60595-4

339. Vaziri ND, Pahl M V., Crum A, Norris K. Effect of Uremia on Structure and Function of Immune System. *J Ren Nutr*. 2012;22(1):149-156. doi:10.1053/j.jrn.2011.10.020

340. Moser B, Roth G, Brunner M, et al. Aberrant T cell activation and heightened apoptotic turnover in end-stage renal failure patients: A comparative evaluation between non-dialysis, haemodialysis, and peritoneal dialysis. *Biochem Biophys Res Commun*. 2003;308(3):581-585. doi:10.1016/S0006-291X(03)01389-5

341. Yoon JW, Gollapudi S, Pahl M V., Vaziri ND. Naïve and central memory T-cell lymphopenia in end-stage renal disease. *Kidney Int*. 2006;70(2):371-376. doi:10.1038/sj.ki.5001550

342. Konikowski T, Haynie TP, Farr LE. Inulin Clearance in Mice as a Standard for Radiopharmaceutical Bioassay. *Proc Soc Exp Biol Med*. 1970;135(2):320-324. doi:10.3181/00379727-135-35044

343. Schreiber A, Shulhevich Y, Geraci S, et al. Transcutaneous measurement of renal function in conscious mice. *Am J Physiol - Ren Physiol*. 2012;303(5):F783-F788. doi:10.1152/ajprenal.00279.2012

344. Scarfe L, Schock-Kusch D, Ressel L, et al. Transdermal measurement of glomerular filtration rate in mice. *J Vis Exp*. 2018;2018(140). doi:10.3791/58520

345. Schock-Kusch D, Geraci S, Ermeling E, et al. Reliability of transcutaneous measurement of renal function in various strains of conscious mice. Remuzzi G, ed. *PLoS One*. 2013;8(8):e71519. doi:10.1371/journal.pone.0071519

346. Basile DP, Leonard EC, Tonade D, Friedrich JL, Goenka S. Distinct effects on long-term function of injured and contralateral kidneys following unilateral renal ischemia-reperfusion. *Am J Physiol - Ren Physiol*. 2012;302(5):F625-F635. doi:10.1152/ajprenal.00562.2011

347. Gomez IG, MacKenna DA, Johnson BG, et al. Anti-microRNA-21

oligonucleotides prevent Alport nephropathy progression by stimulating metabolic pathways. *J Clin Invest*. 2015;125(1):141-156. doi:10.1172/JCI75852

348. Geary RS, Norris D, Yu R, Bennett CF. Pharmacokinetics, biodistribution and cell uptake of antisense oligonucleotides. *Adv Drug Deliv Rev*. 2015;87:46-51. doi:10.1016/j.addr.2015.01.008

349. Hameed A, Rogers N, Pleass H, Lu B, Miraziz R, Hawthorne W. Intra-Renal Delivery of Drugs Targeting Ischemia-Reperfusion Injury of the Kidney using Normothermic Machine Perfusion. *Transplantation*. 2018;102:S700. doi:10.1097/01.tp.0000543660.39716.78

Appendices

Appendix 1: Funding received

Table A1-1 Funding received for PhD

Funding body	**Amount (£)**
Royal College of Surgeons of Edinburgh Small Pump Priming Grant	10,000
Kidney Research UK Training Fellowship, Grant no TF_003_20161125	173,229.22
Transplant Endowment Fund	2316.24
British Transplantation Society Educational Bursary	500

Appendix 2: Presentations and Prizes

Oral Presentations

Banwell V, Denby L, Marson L. MicroRNA-214 is up-regulated following renal ischaemia reperfusion injury and subsequent fibrosis. KRUK Fellow's Day, Leicester September 2019.

Banwell V, Denby L, Marson L. MicroRNA-214 is up-regulated following renal ischaemia reperfusion injury and subsequent fibrosis. Presented at Congress of the European Society of Organ Transplantation, Copenhagen September 2019. **Transplant International 2019, 32(S2) 178-179**

V Banwell, J O'Sullivan, S Finnie, C Cairns, L Denby, L Marson. The role of miR-214 in renal ischaemia reperfusion induced injury and fibrosis. Chiene Medal Sessions, Department of Surgery, University of Edinburgh, November 2019.

V Banwell, J O'Sullivan, S Finnie, C Cairns, L Denby, L Marson. The role of miR-214 in renal ischaemia reperfusion injury and fibrosis. British Transplantation Society, Belfast March 2020.

Prizes

Runner up in Chiene Medal (£200), University of Edinburgh

Appendix 3: Surgical instruments and consumables

Table A3-1 Surgical Instruments used in mouse models

Instrument	Company	Cat no	Model
Toothed forceps 1x2 teeth	Fine Science Tools	11027-12	Transplant/IRI
Blunt tissue scissors 11.5cm	Fine Science Tools	14072-10	Transplant/IRI
Spring scissors-vannas 2.5 mm	Fine Science Tools	15000-08	Transplant
Dumont 5/45 angled forceps	Fine Science Tools	11251-35	Transplant/IRI
Moira ultra-fine tipped forceps	Fine Science Tools	11370-40	Transplant
Colibri 3cm wire retractor	Fine Science Tools	17000-02	Transplant/IRI
Clips-micro serrefine, spring width 2mm, jaw length 4mm	Fine Science Tools	18055-02	Transplant/IRI
Clip applicator-with lock	Fine Science Tools	18056-14	Transplant/IRI
Halsey mico needle holder-Tungsten carbide	Fine Science Tools	12500-12	Transplant/IRI
7mm Wound Clips	Fine Science Tools	12032-07	Transplant/IRI
Wound clip applicator	Fine Science Tools	12031-07	Transplant/IRI

Table A3-2 Sutures used in mouse models

Instrument	Company	Cat no	Model
7-O silk suture	Pearsill	30514	Transplant
10-O Nylon double ended suture	Ethicon	W2801	Transplant
5-O vicryl rapide	Ethicon	W9915	Transplant/IRI

Table A3-3: Consumables used in mouse models

Instrument	Company	Cat no	Model
2ml Syringe	Becton, Dickinson &Co	300185	Transplant/IRI
5ml Syringe	Becton, Dickinson &Co	302187	Transplant/IRI
21G bevel needle	Becton, Dickinson &Co	305175	Transplant
29G insulin needle/syringe 1ml	Becton, Dickinson &Co	324826	Transplant/IRI
30G insulin needle/syringe 0.3ml	Becton, Dickinson &Co	324826	Transplant/IRI
Cotton wool buds	Johnson and Johnson		Transplant/IRI
Surgical Drapes	Guardian	CB03	Transplant/IRI